AD-A056 285 PRATT AND WHITNEY AIRCRAFT GROUP EAST HARTFORD CONN F/G 21/5
INVESTIGATION OF A HIGHLY LOADED TWO-STAGE FAN-DRIVE TURBINE, V--ETC(U)
DEC 69 H WELNA, D E DAHLBERG, W H HEISER F33615-68-C-1208
UNCLASSIFIED PWA-3827 AFAPL-TR-69-92-VOL-4 NL

1 OF 3
AD
A056 285

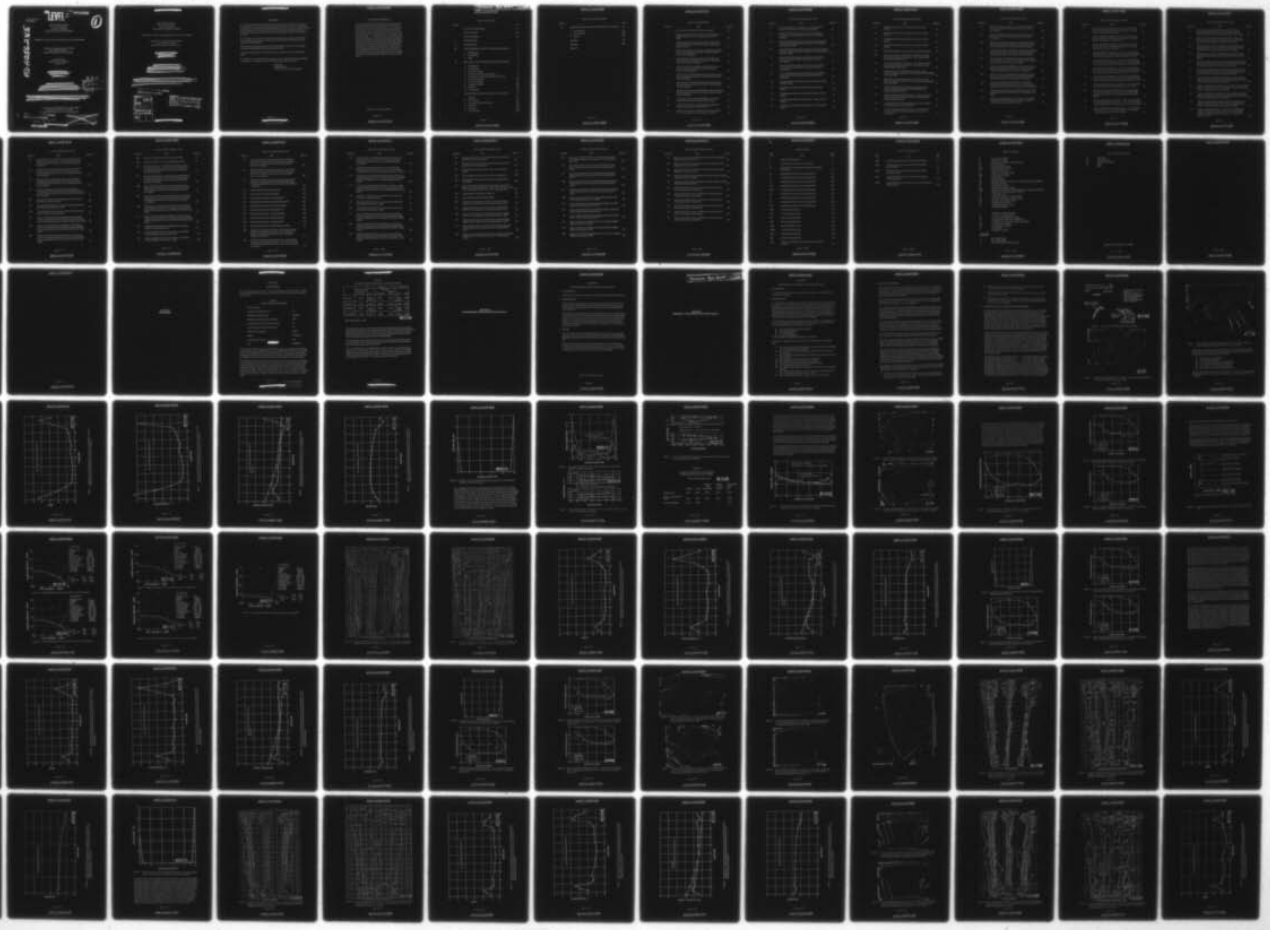

AFAPL-TR-69-92
VOLUME IV

(UNCLASSIFIED TITLE)
INVESTIGATION OF A HIGHLY LOADED TWO-STAGE FAN-DRIVE TURBINE

VOLUME IV. Phase II, End Wall Boundary Layer Control Evaluation

H. Welna, D. E. Dahlberg and W. H. Heiser
Pratt & Whitney Aircraft
Division of United Aircraft Corporation

Technical Report
AFAPL-TR-69-92 Volume IV
December 1969

AIR FORCE AERO PROPULSION LABORATORY
AIR FORCE SYSTEMS COMMAND
WRIGHT-PATTERSON AIR FORCE BASE, OHIO

[redacted]

(UNCLASSIFIED TITLE)
INVESTIGATION OF
A HIGHLY LOADED
TWO-STAGE FAN-DRIVE TURBINE

VOLUME IV. Phase II, End Wall Boundary Layer Control Evaluation

H. Welna, D. E. Dahlberg and W. H. Heiser
Pratt & Whitney Aircraft
Division of United Aircraft Corporation

[redacted]
Downgraded at 3 Year Intervals;
Declassified after 12 Years,
DOD DIR. 5200.10

[redacted]
SPECIAL HANDLING REQUIRED
NOT RELEASABLE TO FOREIGN NATIONALS
The information contained in this document will not be disclosed to foreign nationals or their representatives.

[redacted]
This document contains information affecting the national defense of the United States within the meaning of the Espionage Laws, Its transmission or the revelation of its contents in any manner to an unauthorized person is prohibited by law.

Approved for public release;
distribution unlimited

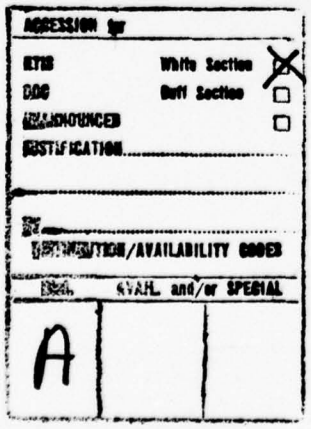

Classified by
SUBJECT TO GENERAL DECLASSIFICATION
SCHEDULE OF EXECUTIVE ORDER 11652
AUTOMATICALLY DOWNGRADED AT TWO
YEAR INTERVALS
DECLASSIFIED ON DECEMBER 31 75

[redacted]

FOREWORD

(U) This Interim Technical Status Report (Contractors Reference No. PWA 3827) was prepared by Pratt & Whitney Aircraft, Division of United Aircraft Corporation, East Hartford, Connecticut, as the fourth Semiannual Report under United States Air Force Contract F33615-68-C-1208, Project No. 3066, Task No. 306606. This report was submitted by the Contractor on 31 December 1969, and covers the report period from 1 July 1969 to 31 December 1969.

(U) The findings and conclusions of this report are not deemed as final by the Contractor. They are subject to verification or revision in the Final Report to be published upon the completion of this Contract.

(U) The Air Force Program Monitor is Mr. Wayne Tall, APTC, Air Force Aero Propulsion Laboratory, Wright-Patterson Air Force Base, Ohio, 45433.

(U) This report contains no Classified information extracted from other Classified documents.

(U) Publication of this report does not constitute Air Force approval of the report's findings or conclusions. It is published only for the exchange and stimulation of ideas.

Wayne Tall
Project Engineer
Air Force Aero Propulsion Laboratory

UNCLASSIFIED ABSTRACT

(U) A comprehensive, four-phase, three-year program is in progress to investigate methods of improving the performance of fan-drive turbines. The goals of this program are to develop turbine design procedures and aerodynamic techniques for high work, efficient, low-pressure turbines. The first phase effort of defining the preliminary turbine design has been completed and the results were reported (Reference 1). The second phase consists of an experimental evaluation which includes establishment of both two-dimensional loss levels and three-dimensional flow behavior for the baseline airfoils and for airfoils utilizing various boundary layer control methods. The design of the baseline cascade packs was reported in the Reference 2 Report, and the three-dimensional performance of the baseline airfoils was reported in the Reference 3 Report. The test results of the baseline airfoil boundary layer control methods and the performance of the decreased solidity annular cascades are presented in this report.

(The reverse of this page is blank)

TABLE OF CONTENTS

TABLE OF CONTENTS (Cont'd)

LIST OF ILLUSTRATIONS

LIST OF ILLUSTRATIONS (Cont'd)

LIST OF ILLUSTRATIONS (Cont'd)

LIST OF ILLUSTRATIONS (Cont'd)

LIST OF ILLUSTRATIONS (Cont'd)

LIST OF ILLUSTRATIONS (Cont'd)

LIST OF ILLUSTRATIONS (Cont'd)

LIST OF ILLUSTRATIONS (Cont'd)

LIST OF ILLUSTRATIONS (Cont'd)

LIST OF ILLUSTRATIONS (Cont'd)

LIST OF ILLUSTRATIONS (Cont'd)

LIST OF ILLUSTRATIONS (Cont'd)

LIST OF ILLUSTRATIONS (Cont'd)

LIST OF ILLUSTRATIONS (Cont'd)

LIST OF ILLUSTRATIONS (Cont'd)

LIST OF TABLES

LIST OF TABLES (Cont'd)

LIST OF SYMBOLS

A	- area, square inches
B	- axial chord, inches
C	- absolute gas velocity, feet per second
C_F	- drag coefficient
C_L	- Zwiefel load coefficient
C_L*	- load coefficient, $\Delta Cu/U$
E	- diffusion parameter
H	- boundary layer shape factor
ΔH	- work, Btu per pound
M	- Mach number
P	- pressure, psia
ΔP	- pressure rise from minimum to exit value on suction surface
Q	- exit dynamic head
R	- fillet radius, inches
R_C	- radius of curvature, inches
Re_θ	- Reynolds number based on boundary layer momentum thickness
S	- distance along airfoil surface, inches
T	- temperature, °R
u	- tangential velocity, feet per second
W	- relative gas velocity, feet per second
Wg	- gas flow, pounds per second
X	- axial distance, inches
Y	- tangential distance, inches
Z	- number of airfoils

α	- absolute gas angle, degrees
β	- relative gas angle degrees
δ	- boundary layer thickness, inches
δ*	- boundary layer displacement thickness
θ	- boundary layer momentum thickness, inches
θ_b	- blade camber, degrees
θ_v	- vane camber, degrees
τ	- gap, inches
η	- efficiency, percent

Subscripts

0	inlet to first vane
1	inlet to first blade
2	exit from stage or airfoil section

LIST OF SYMBOLS (Cont'd)

G	gage point
ws	wetted surface
ms	mainstream surface
S	static
T	total

(The reverse of this page is blank)

SECTION I
INTRODUCTION

SECTION I

INTRODUCTION

(U) Design analysis and optimization studies of aircraft jet engines involve a trade between component efficiencies and engine size and weight. Advanced mission studies show that the bypass turbofan engine, which has seen increased use in recent military aircraft applications, will continue to be of primary interest. One characteristic of the turbofan is that fuel economy increases with bypass ratio. Higher bypass ratios require increased fan power to be supplied by the fan drive or low-pressure turbine. However, the increased turbine power requirements must be met without a turbine efficiency decrement.

(U) The efficiency of a turbine is determined by the turbine diameter, rotational speed, number of stages and airfoil loading. In particular, fan-drive turbine design is constrained by several other requirements. The rotational speed of the turbine must be limited in order that the fan tip Mach number does not exceed the limit for acceptable losses. For higher bypass ratios, where larger fan diameters are required, this problem is further aggravated. Applying conventional aerodynamics, at fixed rotational speed, increased work can only be realized by a further increase in the number of stages and/or the turbine diameter. Reduction of the turbine diameter or airfoil solidity results in a lighter turbine, but also leads to a sacrifice in efficiency due to losses associated with increased airfoil loading. If the turbine diameter and solidity can be reduced without a penalty in turbine efficiency, considerable gains can be realized by the engine. Therefore, the promise of turbofan engines depends to a large extent on improved fan-drive turbine technology.

(U) The objective of the work done under this contract is to analyze and test concepts which will increase the fan-drive turbine loading while maintaining or increasing the efficiency level. The goals of this program are to develop design procedures and turbine aerodynamic techniques for efficient high-work, low-pressure turbines by means of analytical studies and cascade testing, and to demonstrate the effectiveness of the techniques by designing and testing a two-stage turbine that meets or exceeds the Contract stage-work and efficiency goals.

(U) The complete program is being conducted in four phases over a three year period which commenced on 1 January 1968. Phase I defined the basic turbine design and an analysis of promising increased loading concepts was completed. The results of the Phase I study were reported in the Reference 1 Report. Phases II and III consist of experimental testing to verify and extend the turbine aerodynamic techniques and design procedures for high loading levels. The design details of the baseline cascade test airfoils for both the annular segment and plane cascade rig were reported in the Reference 2 Report. The results of the annular cascade testing of the four baseline airfoils were reported in the Reference 3 Report. Phase IV will subject the aerodynamic techniques and design procedure to a two-stage rotating rig test.

(U) Work on the Contract during this report period proceeded on Phase II and the design and fabrication effort of Phase III. Design work was initiated on Phase IV. The results of the boundary layer control technique evaluations and the medium solidity baseline tests are described in this Report. The status of the remaining Phase II tasks is also presented.

(The reverse of this page is blank)

SECTION II
BACKGROUND

SECTION II

BACKGROUND

(U) The objective of Phase I study was to select a preliminary turbine design that is capable of meeting the performance requirements of this Contract. These requirements are summarized in Table I.

TABLE I
TURBINE DESIGN PARAMETERS

Number of Stages	2
Average Load Coefficient, C_L*	2.2
First Blade Tip Wheel Speed	1000 fps
First Blade Inlet Hub–Tip Diameter Ratio	$\leqslant 0.8$
Exit Swirl Angle–Without Exit Guide Vanes	20°
Exit Swirl Angle–With Exit Guide Vanes	0°
Turbine Inlet Temperature	1450°F
Airflow	$\geqslant$ 50 lbs/sec
Average Stage Efficiency	91%
Life [redacted]	10,000 hrs

(U) The Phase I analysis has been completed and the results were reported in the Reference 1 Report. These analyses included the consideration of flowpath, reaction level, load coefficient level, and variations in work distribution for which velocity triangles were generated. Futhermore, as part of Phase I, preliminary airfoil contours were defined for the same velocity triangles at three levels of reaction and three levels of solidity for the resulting stages.

(U) The medium-reaction, normal solidity airfoils were selected for the Phase II and III baseline evaluations. These airfoil sections were then subjected to additional refinement, which included evaluation of the two-dimensional boundary layer behavior. The baseline airfoil contours, for the first and second vanes and the first and second blades, were described in the Reference 2 Report. All of the baseline airfoils were fabricated and evaluated in an annular segment cascade. These results were presented in the Reference 3 Report. A summary of the test results is shown in Table II, where the measured loss coefficients ($1-\phi^2$) are tabulated.

TABLE II

MEASURED LOSS VS PREDICTED – BASELINE AIRFOILS

	Turbine Design Midspan Exit Mach. No.	Midspan			Overall	
			Predicted			
		Test	Correlation	Boundary Layer	Test	Pred.
First Vane	0.854	0.017 0.023*	0.031	0.032	0.034 0.032*	0.049
First Blade	0.780	0.0266	0.036	0.049	0.040	0.054
Second Vane	0.869	0.021 0.028*	0.036	0.046	0.030 0.034*	0.050
Second Blade	0.904	0.028	0.030	0.044	0.038	0.042

UNCLASSIFIED

*With inlet turbulence screen

(U) The baseline second vane was chosen for further end wall loss study by the process of elimination. The first-stage vane and blade inside diameter end-wall extensions indicated some separation beyond the test cascade which could influence probe readings near this wall in future tests if it became more severe. The short second stage blade chord makes the fabrication of end-wall boundary layer control techniques difficult.

(U) Four boundary layer control techniques were selected for application to the second vane airfoil. These airfoil variations were fabricated and the results of tests conducted on the four variations are presented in this report.

(U) As part of Phase II, lower solidity airfoils were also designed. These airfoils were designed for a 15 percent increase in Zweifel load coefficient and are referred to as medium solidity airfoils in reports under this Contract. The airfoil section and fabrication coordinates were reported in the Reference 3 Report. These airfoils were fabricated and evaluated during this report period. The results are presented in this report.

SECTION III
TWO-DIMENSIONAL DESIGN VERIFICATION (TASK IIa)

SECTION III

TWO-DIMENSIONAL DESIGN VERIFICATION (TASK IIa)

1. RFP OBJECTIVE

(U) Provide an experimental verification of the two-dimensional design characteristics.

2. TASK OBJECTIVE

(U) The purpose of this Task is to conduct plane cascade tests in order to verify the aerodynamic concepts applied to the turbine design during the Phase I Program, and to establish the two-dimensional loss levels for the chosen turbine airfoil profiles at design conditions.

(U) The plane cascade tests will serve two equally important purposes. First, the measured profile losses will be compared with those contained in the existing design procedures in order to verify their accuracy. Secondly, the total pressure and flow angle profiles at the exit plane will indicate whether or not the surface boundary layer has separated. Each airfoil has been designed so that such two-dimensional separation should not occur, and these tests will constitute a verification of the entire airfoil section design procedure.

3. STATUS

(U) Six medium-reaction normal-solidity airfoil section cascades were designed and fabricated. The design details of the airfoil sections, including the airfoil coordinates and fabrication details of the cascade test packs, were presented in the Reference 2 Report.

(U) Three of the cascade packs have been tested and the fourth is currently being evaluated. Data analysis is proceeding on the tested airfoils. However, for completeness, the results of the plane cascade testing will be reported in the next Interim Technical Report, when the results of all six cascade tests will be available.

(The reverse of this page is blank)

SECTION IV
BOUNDARY LAYER CONTROL EVALUATION (TAKS IIc)

SECTION IV

BOUNDARY LAYER CONTROL EVALUATION (TASK IIc)

1. RFP OBJECTIVE

(U) Determine the effects of the most promising boundary layer control techniques on corner flow separation.

2. TASK OBJECTIVE

(U) The RFP objective indicates that methods to eliminate corner flow separation will be considered. Subsequent baseline tests indicated that the end-wall problem for these airfoils was not corner boundary layer separation, but rather the secondary flow of the end-wall boundary layer across the channel. This can be seen in the baseline tests as high loss regions in all suction surface corners. These regions probably originate on the end-wall, but migrate from pressure surface to suction surface and accumulate in the corners. Therefore, the boundary layer control methods that apply to the baseline airfoils are those that reduce the secondary flow at the end-walls.

(U) Four boundary layer control methods were selected and these were applied to one airfoil. The chosen airfoil was the second vane, for reasons given in Section II. The selected methods that were experimentally evaluated are:

- flow fences and increased surface roughness
- local airfoil recontouring
- end-wall contouring
- local airfoil recambering

The results of these tests will be presented in the above order.

(U) These task objectives were met, and the task was completed by the following steps:

- Application of four methods of boundary layer control techniques indicating the best potential for lowering end loss
- Measurement of all important aerodynamic properties at the cascade inlet and exit planes
- Measurement at design Reynolds Number and design incidence for three exit Mach numbers
- Reconstruction of the entire exit plane loss distribution
- Reconstruction of the entire exit plane flow pattern
- Flow visualization of the airfoil and end-wall flow patterns
- Careful analysis of all data and visual clues
- Measurement of the airfoil surface static pressure distributions at three radial locations
- Evaluation of the effectiveness of each boundary layer control method, relative to each other and to the baseline test results
- Selection of best boundary layer control technique for optimization

3. CASCADE PACK DESIGN

(U) The cascade pack chosen for the boundary layer control technique evaluation was the second vane. The design of the baseline second vane cascade pack was presented in the Reference 2 Report. The boundary layer techniques were applied to this cascade, and the hardware variations for each test will be discussed in the section devoted to each of the boundary layer techniques.

(U) As in the baseline evaluation, airfoil surface static pressure taps were distributed around each cascade test airfoil at the root, mean and tip section. The details of the tap locations were given in the Reference 3 Report.

(U) A single cone probe was used for simultaneously measuring local exit plane total pressure static pressure, and exit gas flow angle. Details of the probe design were presented in the Reference 2 Report. The probe was calibrated to determine total and static pressure errors due to the pitch angle over the test Mach number range. Based on this calibration and the theoretical pitch angle, corrections were provided for the data reduction program.

(U) A total pressure probe was also installed just upstream of the test airfoils in order to measure the losses of the turning vanes. The total pressure loss measured for the inlet turning vanes was used to determine the local inlet total pressure profile upstream of the test airfoils. Turning vane losses are used to define the test airfoil inlet conditions in the data reduction program which calculates the test airfoil performance.

(U) The inlet flow angle approaching the test airfoils was also measured for the cascade. The value of the incidence angle was determined from this measurement.

(U) The experimental accuracy of the loss coefficient ($1-\phi^2$) is estimated to be ±0.003. Values that will be given during the discussion of the data are to three significant digits. The purpose for doing this is for identification only, since sometimes it is easier to identify a particular test by loss level rather than its physical description.

(U) Data for all tests were taken at the airfoil design Mach number and Reynolds Number, as well as at two other Mach number levels where the Reynolds Number was no longer matched. As the airfoil exit Mach number increases, the Reynolds Number also increases. The general tendency is for the loss level to decrease as Mach number and Reynolds Number increase. This is true until Mach numbers approach and exceed sonic values, causing shocks. Then, in this case, the loss level increases with increasing Mach number and Reynolds Number.

(U) During the course of this investigation, a great number of flow visualization photographs using oil and graphite tracers were taken. These photographs have a number of items in common which should be noted, including

- Profile flow patterns which always indicate transition on the trailing portion of the suction side, a condition found in turbines (with possible exception observed during flow fence/increased roughness test)

- No flow separation observed on the airfoil profile, verifying the validity of the airfoil surface static pressure distribution program
- Attached flow on the cascade end-wall extensions which substantiates use of the second vane for these tests
- Indication of a strong corner or secondary flow effect in the suction surface and end-wall corners, with no sign of separation, implying that the important thing to do is to decrease the cross-flow.

4. FLOW FENCE AND INCREASED SURFACE ROUGHNESS

(U) Even though there was considerable doubt about their effectiveness in controlling secondary flows, two methods that were given some consideration were the use of a flow fence and increased surface roughness. The intention of the flow fence was to block or impede channel cross-flows at the end walls, while the intention of the increased surface roughness was to force the boundary layer to be turbulent and, consequently, as thin as possible. These tests were carried out in spite of the lack of promise largely because they were easily added on to the primary test program, and because it was felt that they would add to our understanding of secondary flows. It was also possible to do this testing without interfering with the primary test schedule. Both methods were, in fact, simultaneously tested on opposite walls of the same cascade.

(U) The design of the flow fence was described in the Reference 3 Report, and is shown in Figure 1 for convenience. This fence was applied to the second vane outside diameter wall and its height was obtained from the suction surface secondary flow patterns that were observed in the baseline tests reported in the Reference 3 Report. Those patterns indicated a radially inward movement of the boundary layer at the airfoil trailing edge, extending approximately 0.5 inch from the wall surface. Allowing for the growth of the corner vortex size from inside the passage to the exit plane, the fence height required to significantly reduce the end wall cross-flow was estimated to be one-half the trailing edge size, or 0.3 percent of the span. The fence was mounted in four passages midway between airfoil surfaces and extended the full passage length from loading edge to trailing edge (see Figure 2).

(U) Roughening of the inside diameter wall was accomplished by attaching emery cloth to the end-wall region in four passages. Calculations of the wall boundary layer indicated that the boundary layer would be transitional in the region between the inlet guide vanes and test airfoils. Since this calculation involved approximation of the pressure gradient through the rig, it was decided to increase the surface roughness in case the boundary layer had not transitioned. The calculated boundary layer thickness prior to transition was 0.20 inch. A No. 50 grit emery cloth with a roughness height of 0.013 inch was used. This height is greater than the computed critical value required for boundary layer transition. The emery cloth was cemented to the inside diameter end-wall and to the leading edges of the airfoils adjacent to the inside diameter wall (See Figure 3).

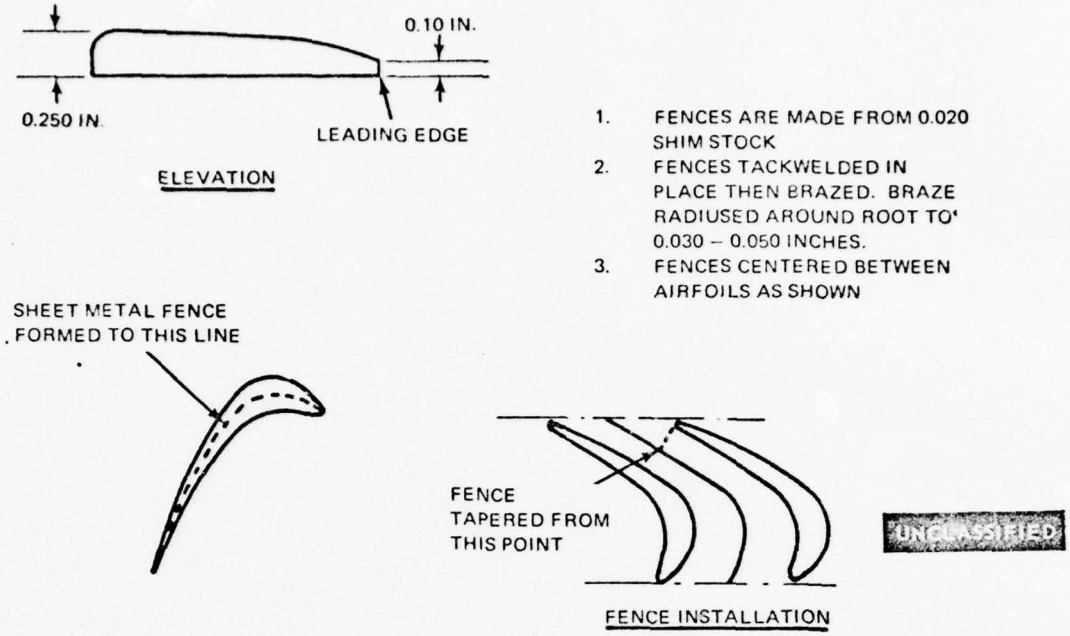

Figure 1 Second Vane O. D. Shroud Flow Fence Installation

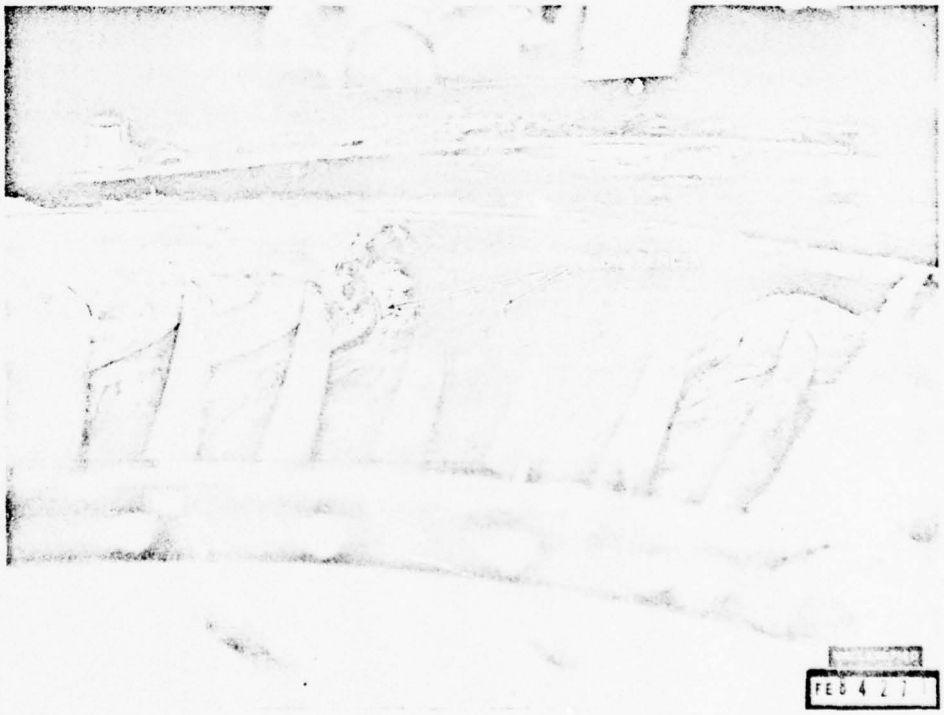

Figure 2 Oil and Graphite Flow Patterns–Second Vane with View of Outside Diameter Flow Fences; Midspan Exit Mach No. =0.903

Figure 3 Oil and Graphite Flow Patterns–Second Vane with View of Inside Diameter Increased Surface Roughness; Midspan Exit Mach No. =0.903

(U) Plots of the important aerodynamic quantities based on the inlet and exit plane measurements for each test will always be presented in the following order and will be simply referred to as performance data in this Report:

- total pressure loss contour plots
- exit gas angle contour plots
- average spanwise total pressure loss distribution
- average spanwise loss coefficient distribution
- average spanwise exit flow angle distribution
- average spanwise exit Mach number distribution.

The performance data for the flow fence and increased surface roughness test are shown in Figures 4 through 9. Also, a plot of the inlet guide vane and duct loss is shown in Figure 10.

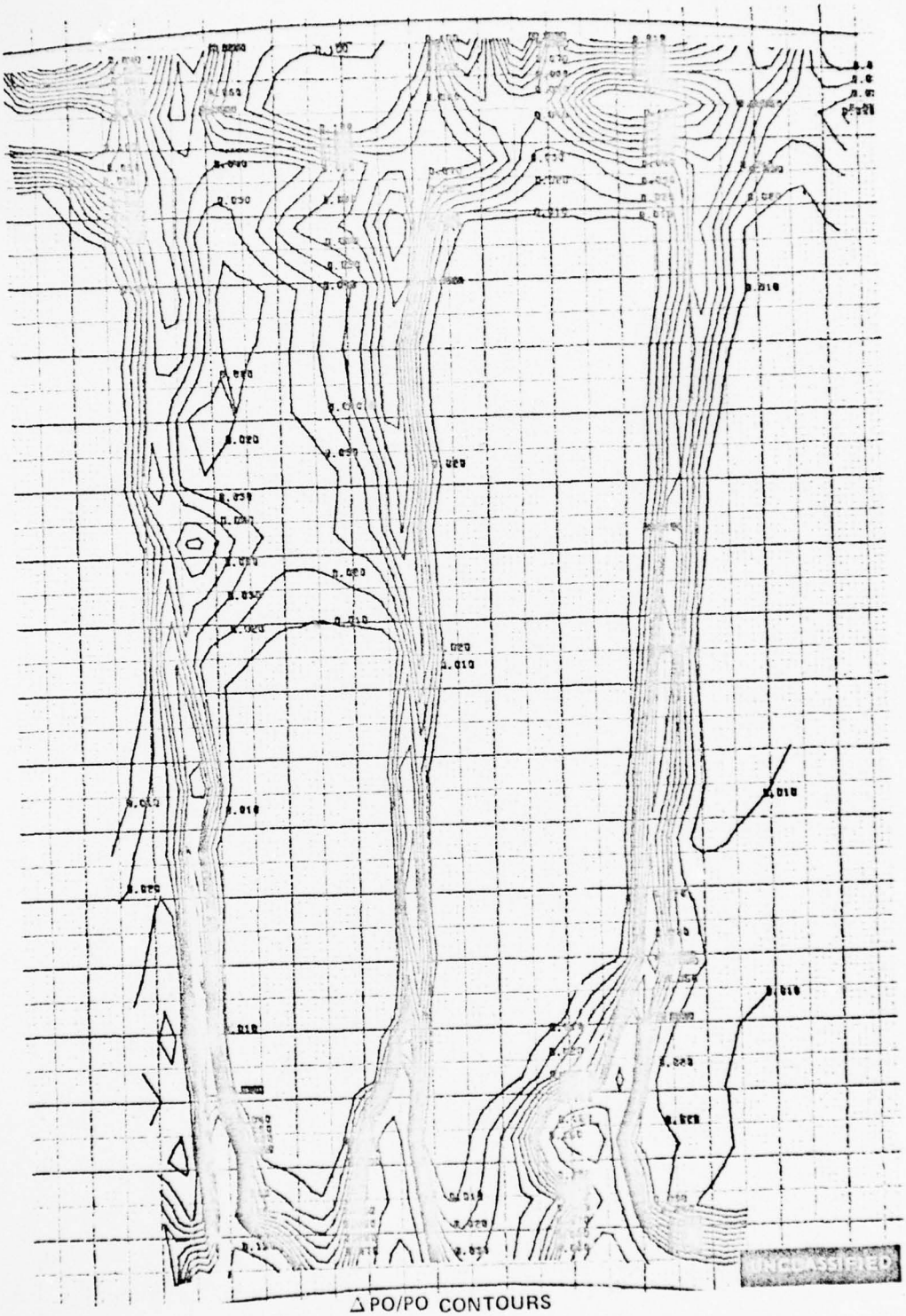

Figure 4 Pressure Loss Contours, Second Vane - Screen Removed, Three Flow Passages, Midspan Exit Mach No. = 0.903, O. D. Flow Fences and I. D. Roughness

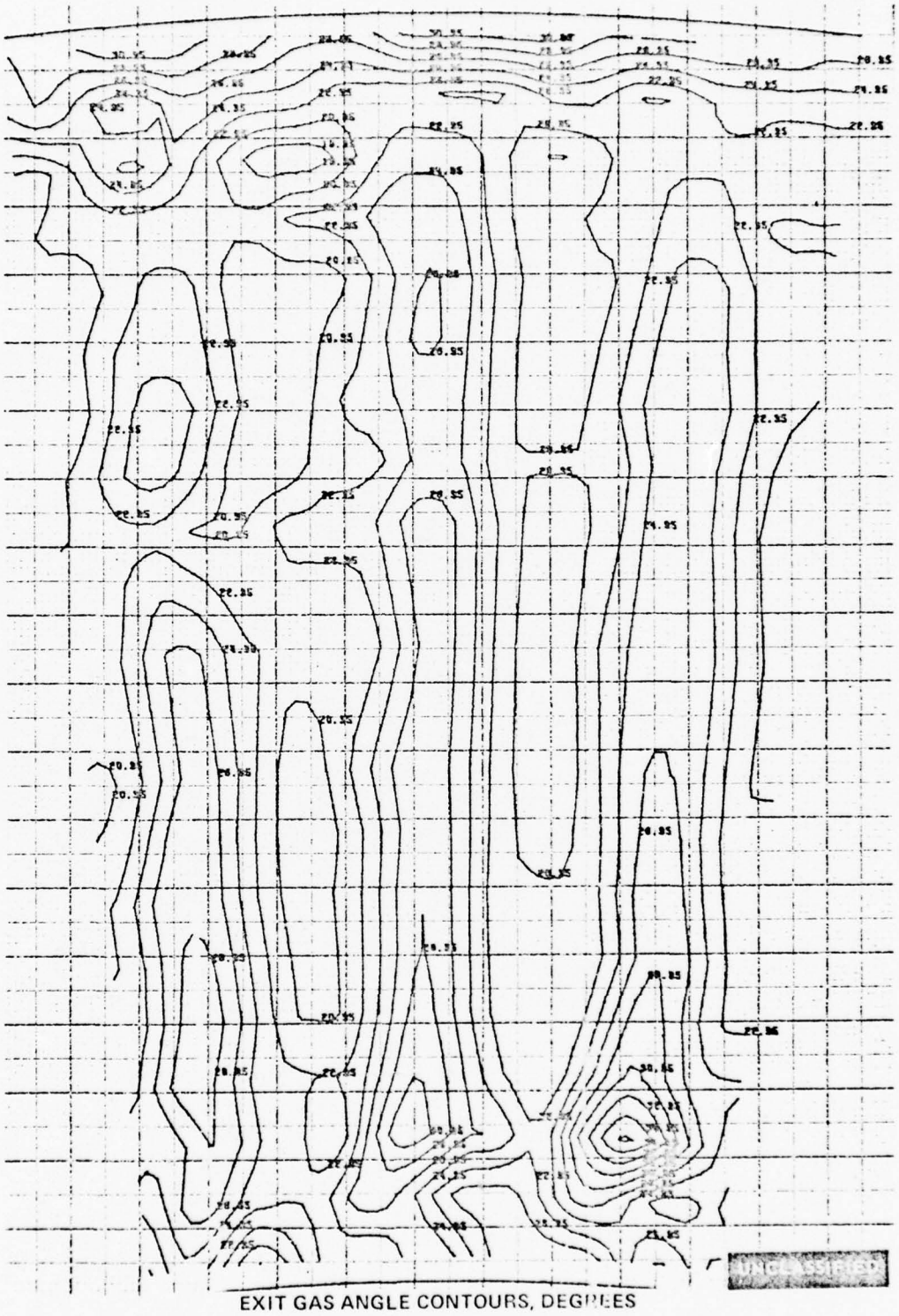

Figure 5 Exit Gas Angle Contours, Second Vane - Screen Removed, Three Flow Passages, Midspan Exit Mach No. = 0.903, O. D. Flow Fences and I. D. Roughness

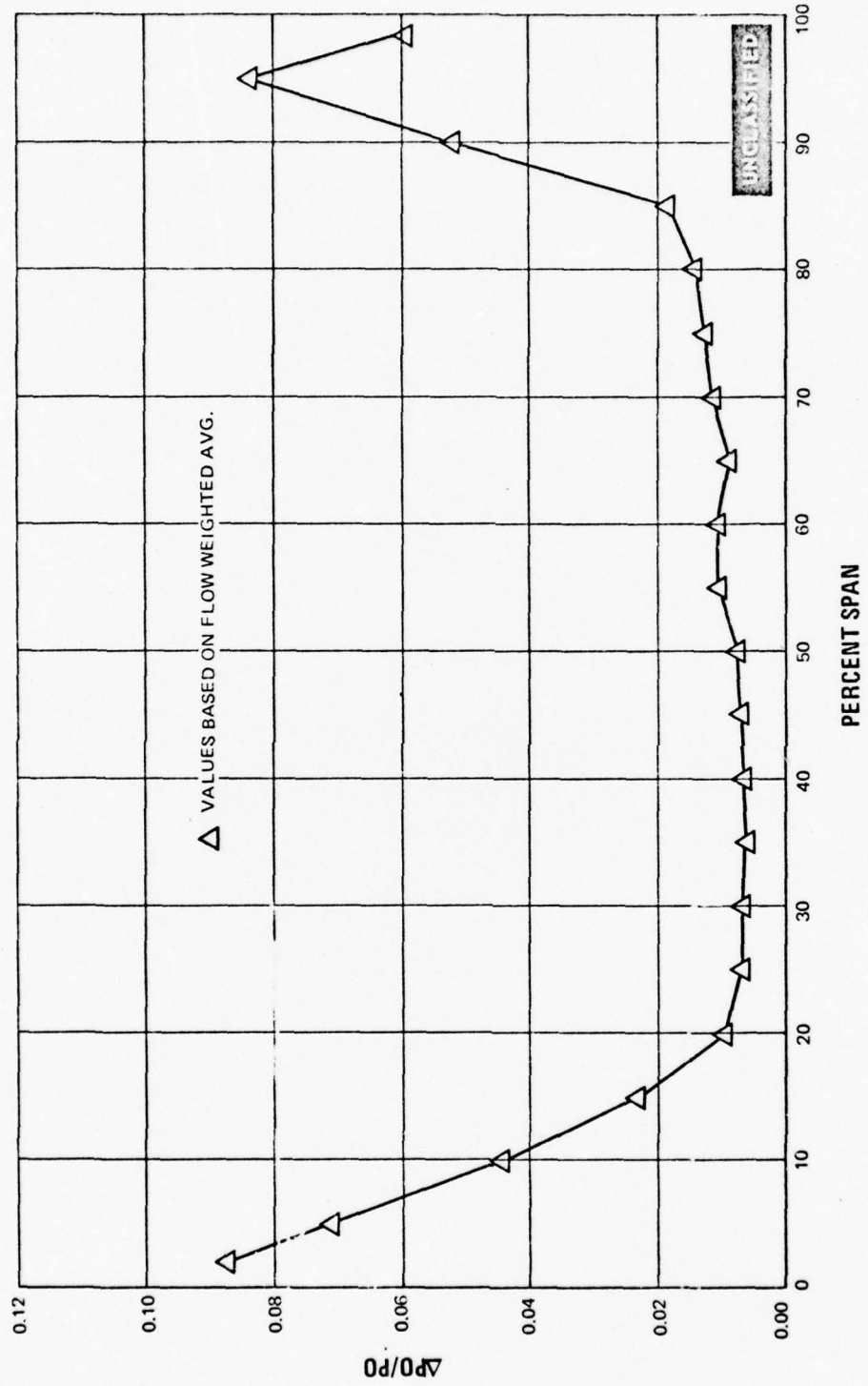

Figure 6 Spanwise Pressure Loss Distribution, Second Vane - Screen Removed, Midspan Exit Mach No. = 0.903, O. D. Flow Fences and I. D. Roughness

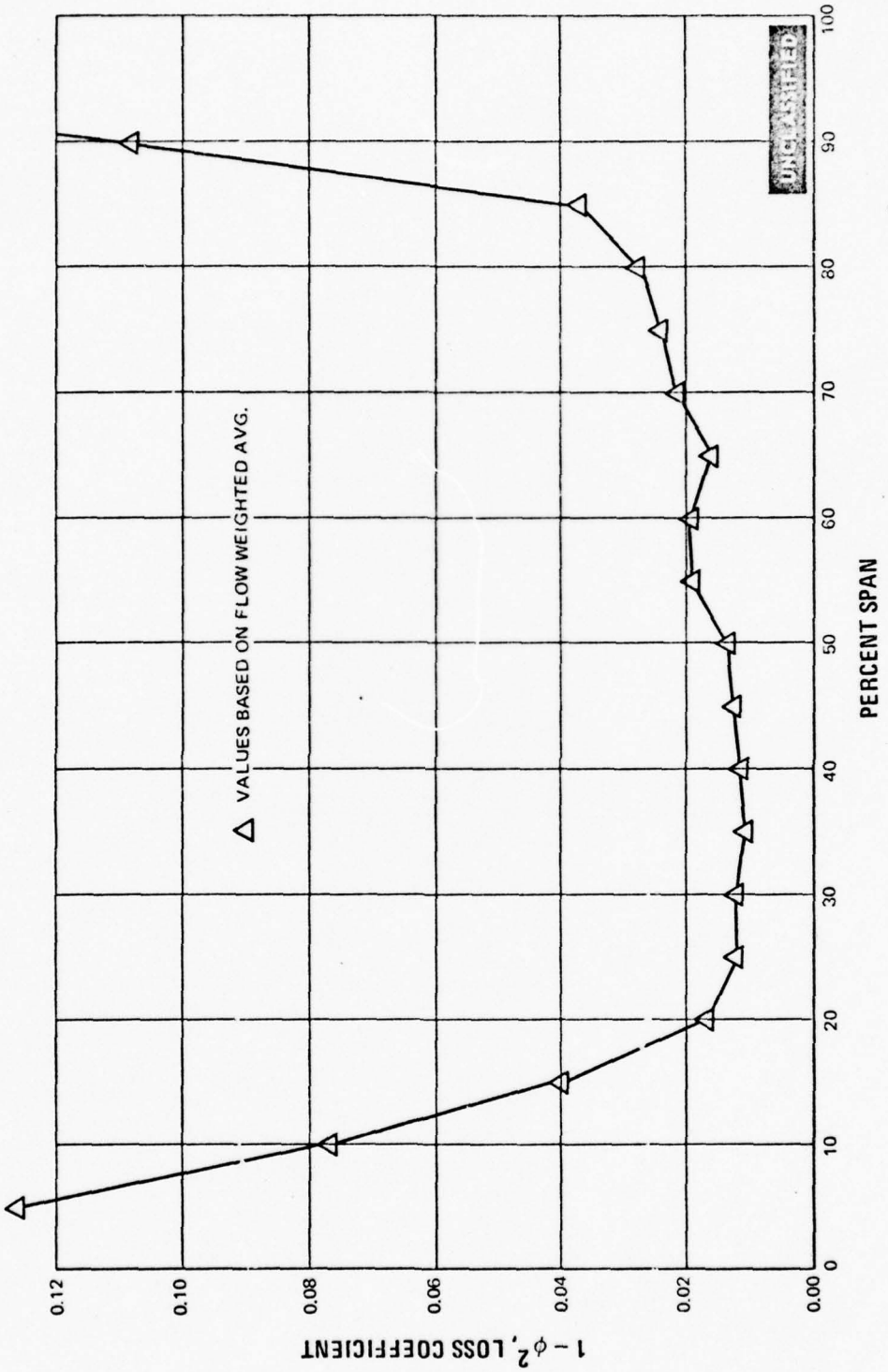

Figure 7 Spanwise Loss Coefficient Distribution, Second Vane - Screen Removed, Mid-span Exit Mach No. = 0.903, O. D. Flow Fences and I. D. Roughness

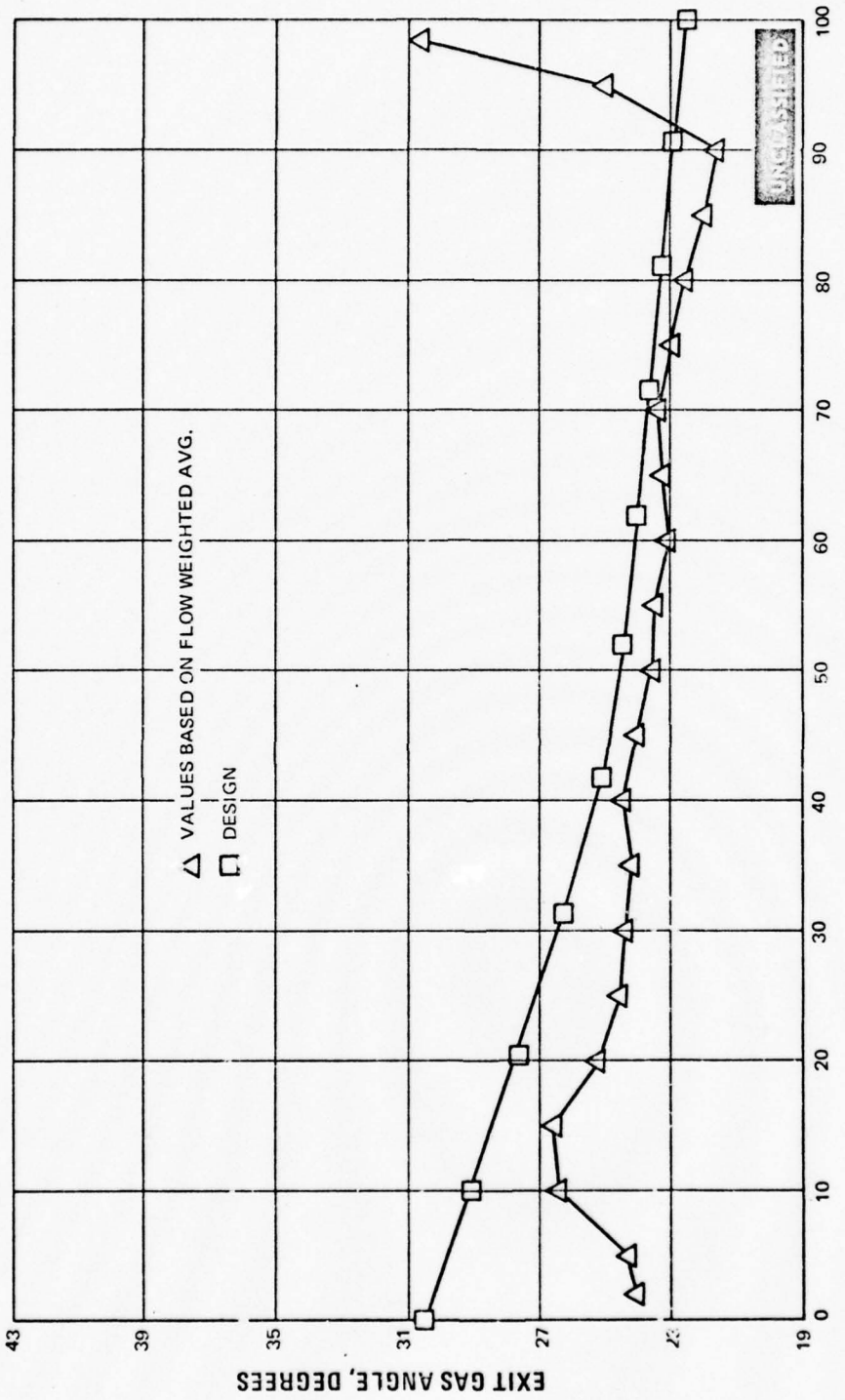

Figure 8 Spanwise Exit Gas Angle Distribution, Second Vane - Screen Removed, Mid-span Exit Mach No. = 0.903, O. D. Flow Fences and I. D. Roughness

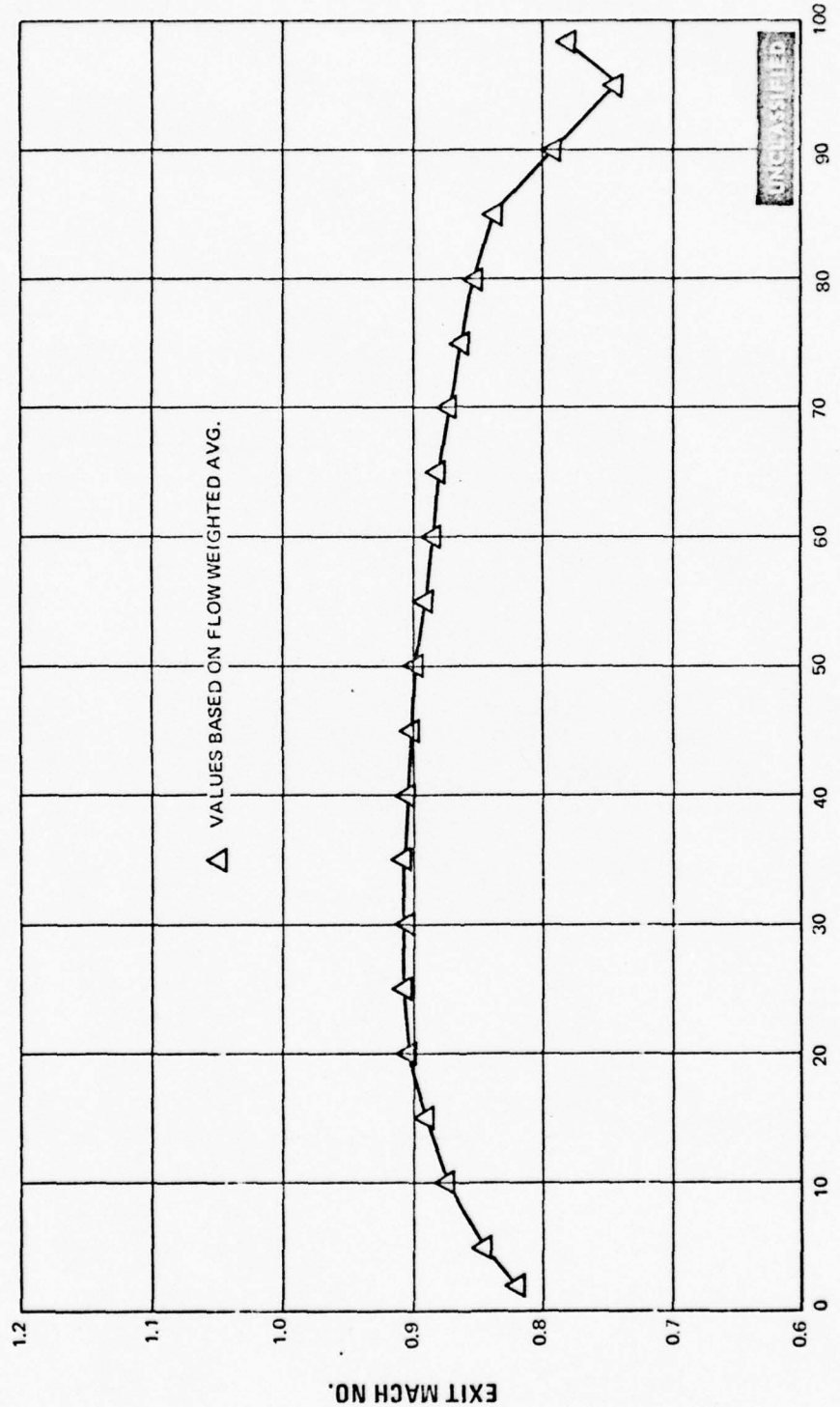

Figure 9 Spanwise Exit Mach Number Distribution, Second Vane - Screen Removed, Midspan Exit Mach No. = 0.903, O. D. Flow Fences and I. D. Roughness

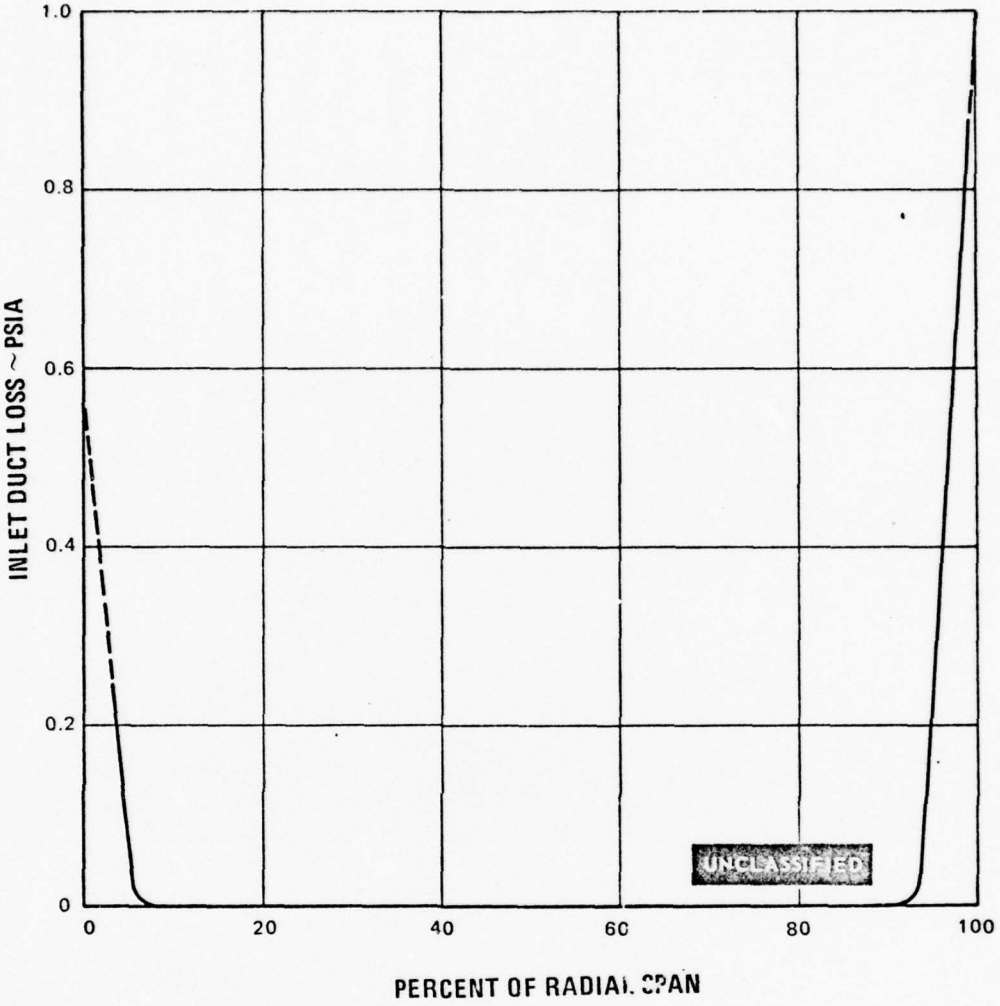

Figure 10 Inlet Duct Loss Versus Percent Radial Span–Second Vane Cascade With I.D. Roughness and O.D. Flow Fences

(U) A comparison plot of the average spanwise loss variation for the flow fence and increased roughness, versus baseline loss coefficients, is shown in Figure 11 at approximately the same Mach number. The variation of the loss coefficient with Mach number can be seen to be very slight from the data of Figure 12. The contribution of each end to the overall loss is shown separately in Figure 13, in order to evaluate the effect of each end-wall treatment. A summary of these results is tabulated in Table III, where the loss values are compared with the baseline test values. Both treatments resulted in increased end-wall losses, although an unexpected improvement was observed in the midspan region. The low midspan values appear inconsistent, but since the end losses were considerably higher than the baseline values, it was not worthwhile to pursue the flow fence and increased surface roughness techniques.

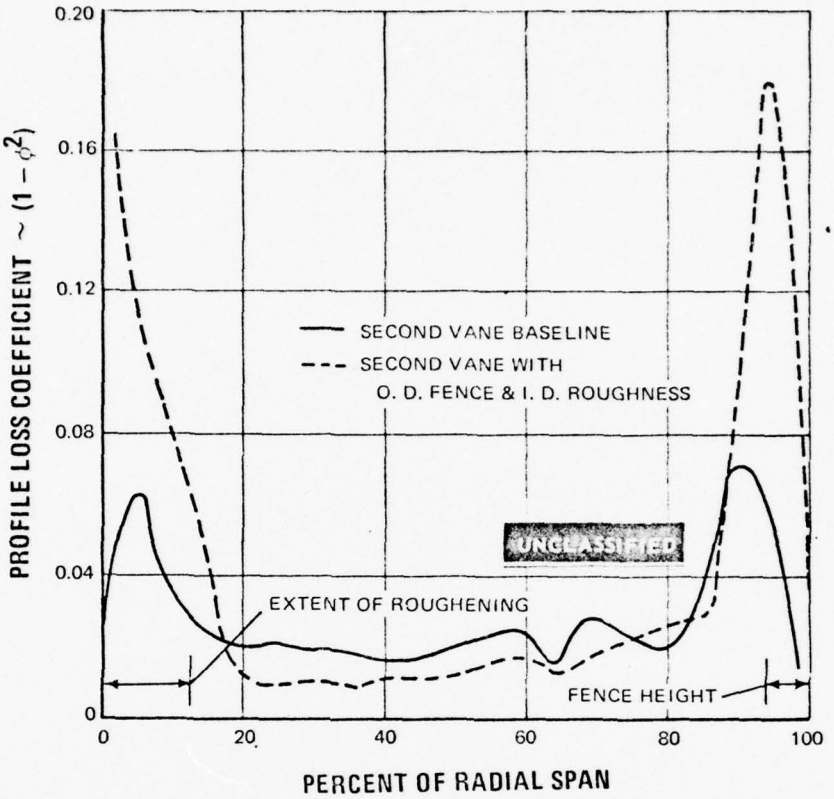

Figure 11 Comparison of O. D. Flow Fence and I. D. Roughness Loss Coefficient Distribution with Baseline Values

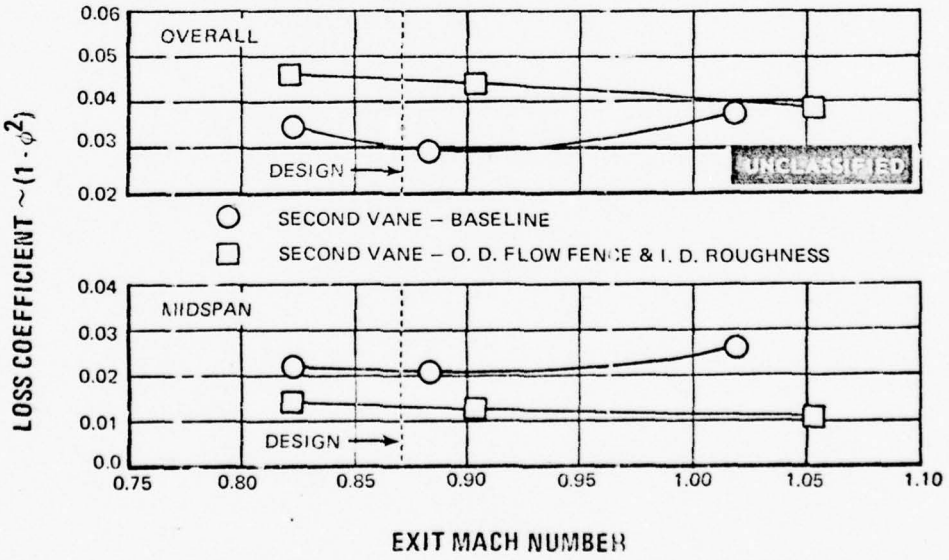

Figure 12 Effect of Mach Number on Profile Loss Coefficient for O. D. Flow Fence and I. D. Increased Roughness Evaluation

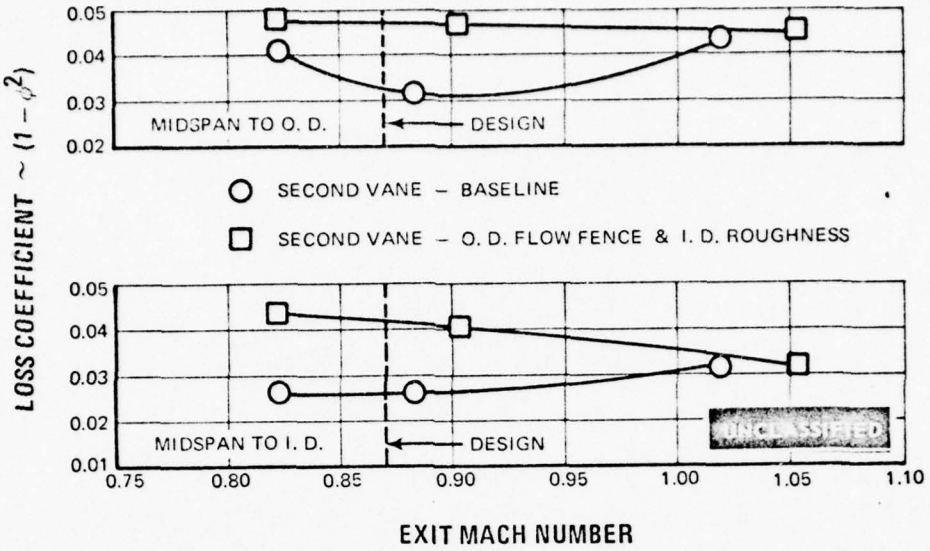

Figure 13 Effect of Mach Number on Profile Loss Coefficient for O. D. Flow Fence and I. D. Increased Roughness Evaluation

TABLE III

EFFECT OF FLOW FENCES AND SURFACE ROUGHNESS ON SECOND VANE LOSSES

Profile Loss Coefficients $(1-\phi^2)$

UNCLASSIFIED

	Midspan	Overall	Midspan to I.D. (Roughness)	Midspan to O. D. (Fences)	Midspan Exit Mach No.
Baseline (Test)	0.021	0.030	0.026	0.033	0.883
Boundary Layer Control (Test)	0.013	0.045	0.042	0.047	0.903
Baseline (Predicted)	0.036	0.050	-	-	0.870

(U) The shift in position of the maximum circumferentially integrated loss from 90 to 94 percent span (See Figure 11) corresponds to a shift in the center of the suction corner vortex from 84 to 94 percent span, indicating the reduced migration effect with reduced secondary flow. However, the peak loss at the vortex center increased from about 7 percent for the baseline to 18 percent by the fences. The inside wall loss indicated a continuous increase toward the wall due to the surface roughening, without the decrease shown in the baseline data. Apparently, the end wall boundary layer had in fact transitioned to turbulent flow and the rougher surface merely increased the frictional drag.

(U) Comparison of the baseline gas exit angle spanwise distribution with the flow fence /increased surface roughness exit gas angles is shown in Figure 14. The discharge angle was not affected by the end-wall treatments except at the outside wall, where the anticipated reduction in overturning due to reduced secondary flow is indicated.

(U) To provide additional clues as to the behavior of the flow in the cascade, a mixture of oil and graphite was painted on the airfoils. Figures 2 and 3, and Figures 15 and 16 show the location of the flow fences on the outside wall and the emery cloth on the inside wall. The patterns indicated that the corner flow remained attached, although the end-wall losses are high.

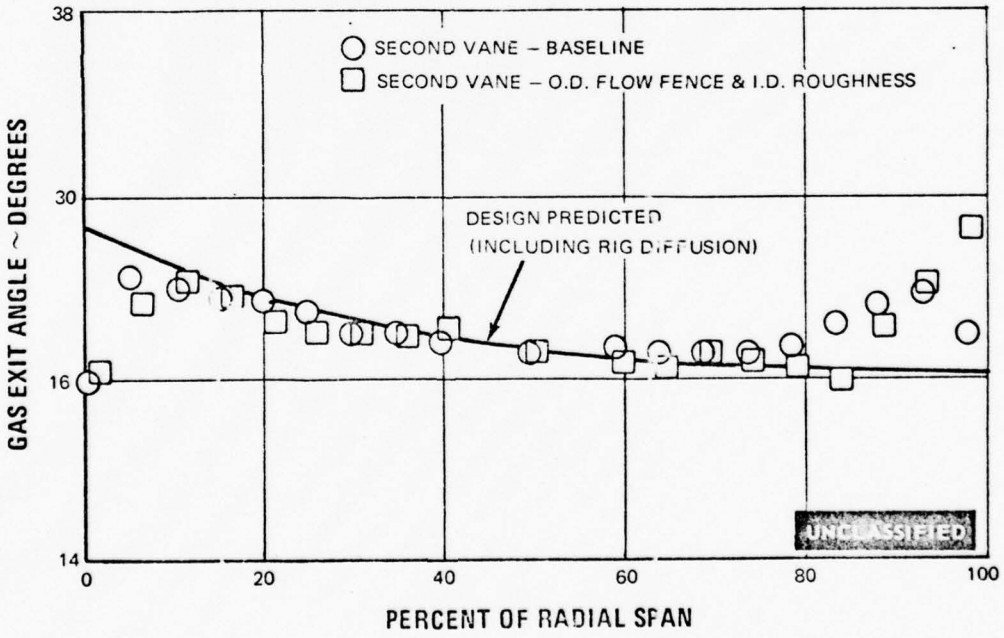

Figure 14 Comparison of Spanwise Averaged Exit Gas Angle Baseline Distribution and Angles Measured with Flow Fences/Surface Roughness.

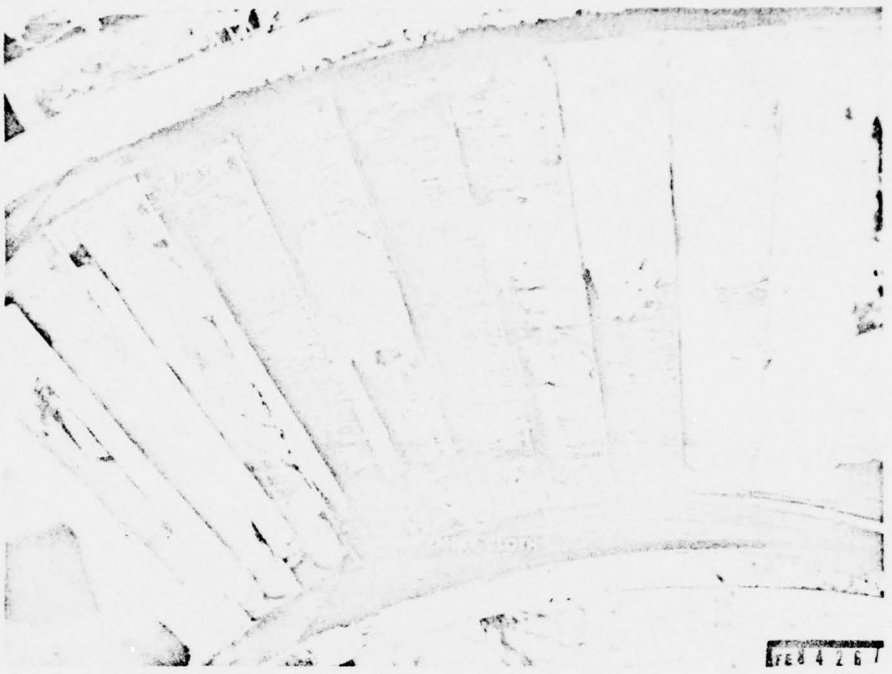

Figure 15 Oil and Graphite Flow Patterns–Second Vane with View of Both Flow Fence and Increased Surface Roughness Effects; Midspan Exit Mach No. =0.903

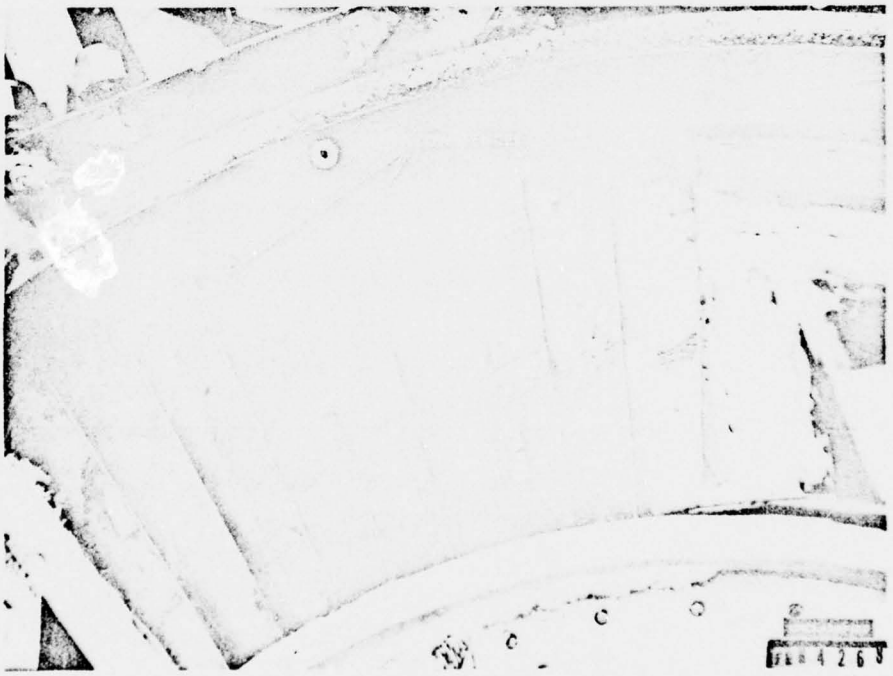

Figure 16 Oil and Graphite Flow Patterns–Second Vane with View of Both Flow Fence and Increased Surface Roughness Effects; Midspan Exit Mach No. =0.903

(U) The airfoil surface static pressure distribution at the root, mean and tip are shown in Figures 17 through 19, respectively. The measured loading in the midspan region was almost identical to the desired value. The loading at the root and tip sections does not correspond to the design values, primarily due to the exit-plane effect explained in detail in the Reference 3 Report. This is primarily due to the fundamental difference between the annular segment cascade and rotating rig, since the limited extension of the inside and outside diameter walls tends to make the exit plane static pressure uniform and atmospheric, rather than reproducing the radially increasing static pressure of the axisymmetric rotating flow. Therefore, the airfoil roots are slightly less loaded, and the airfoil tips are slightly more loaded, than the complete turbine required. The situation is further complicated by the fact that the root and tip are both unloaded because they must turn fluid having a lower than average velocity.

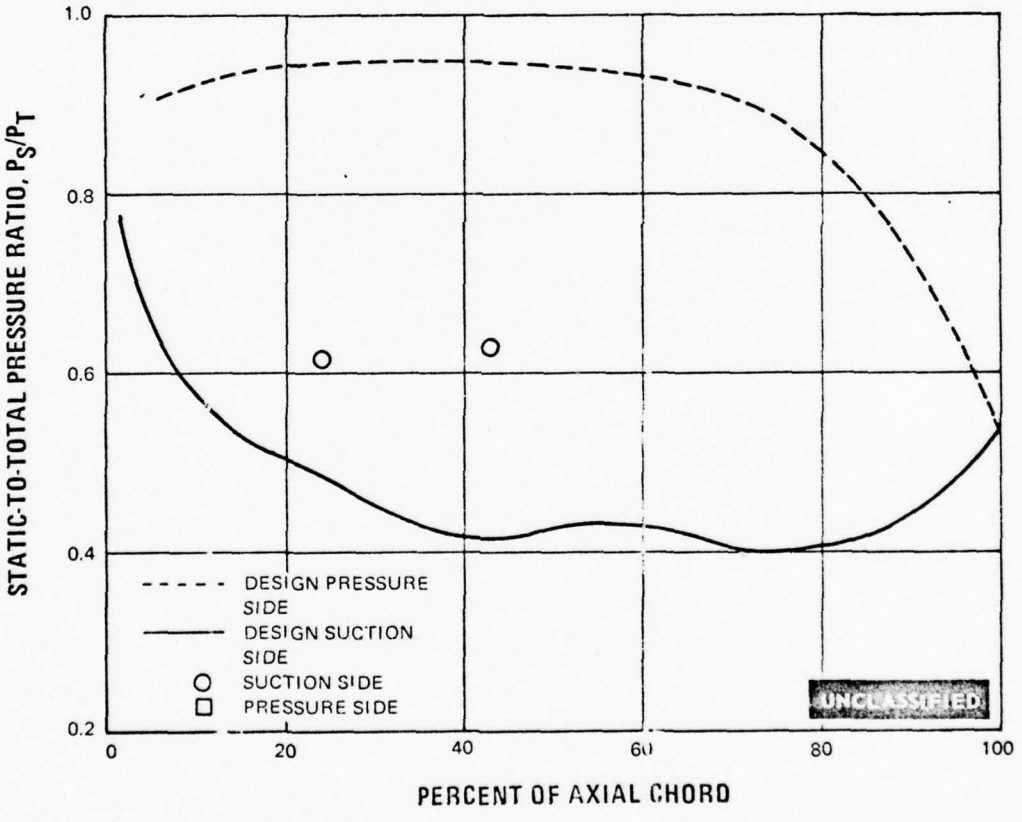

Figure 17 Static-to-Total Pressure Ratio Versus Percent of Axial Chord, Second Vane With I.D. Roughness and O.D. Flow Fences–Root Section

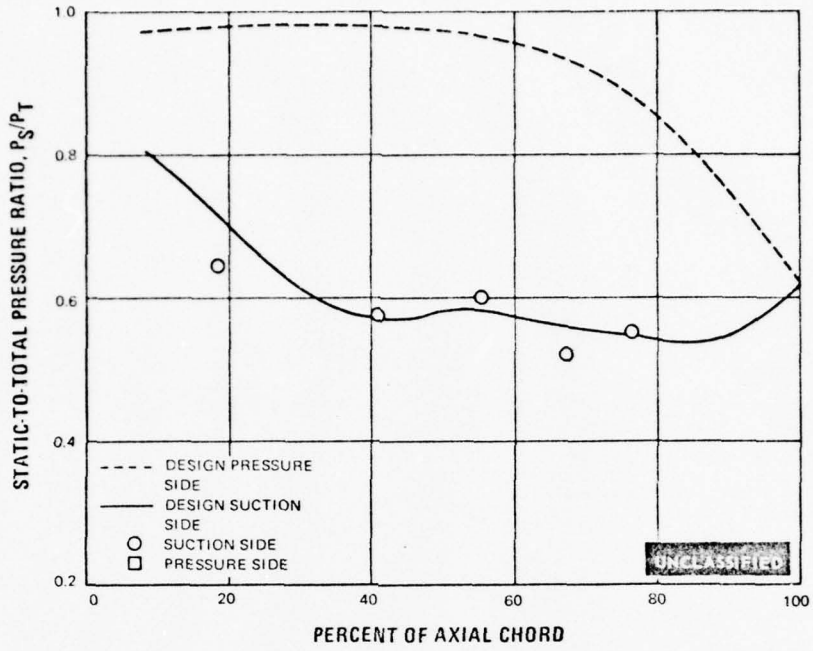

Figure 18 Static-to-Total Pressure Ratio Versus Percent of Axial Chord, Second Vane With I.D. Roughness and O.D. Flow Fences–Mean Section

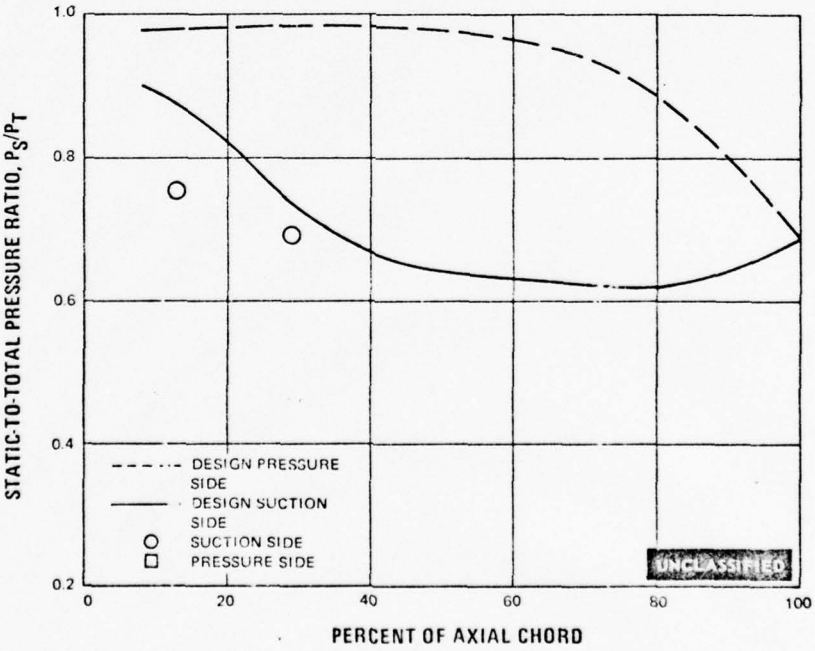

Figure 19 Static-to-Total Pressure Ratio Versus Percent of Axial Chord, Second Vane With I.D. Roughness and O.D. Flow Fences–Tip Section

5. BASELINE RETEST WITH REDESIGNED INLET GUIDE VANES

(U) The baseline second vane was retested with redesigned inlet guide vanes. This was necessary since the diagonal wakes from the original inlet guide vanes were interfering with the test airfoil exit plane measurements, as reported in the Reference 3 Report. The elevation and location of each section of the redesigned inlet guide vane is shown in Figure 20, and the sections are presented in Figures 21 through 29. The fabrication coordinates for each section are tabulated in Tables IV through XII in the Appendix.

(U) The performance data for the second vane, normal solidity baseline retest with the redesigned inlet guide vanes are presented in Figures 30 through 35. The inlet guide vane and duct loss is shown in Figure 36. Airfoil surface static pressure distributions at root, mean and tip sections are shown in Figures 37 through 39.

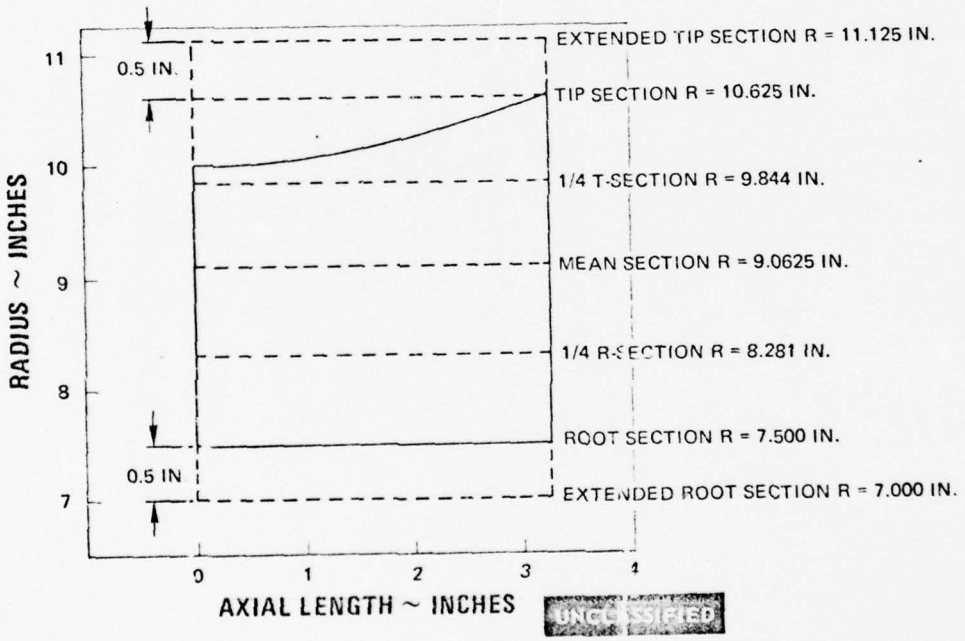

NOTE: SOLID BOUNDARY DEFINES TURNING VANE AIRFLOW PATH

Figure 20 Elevation and Section Location of the Redesigned Second Vane Inlet Guide Vane

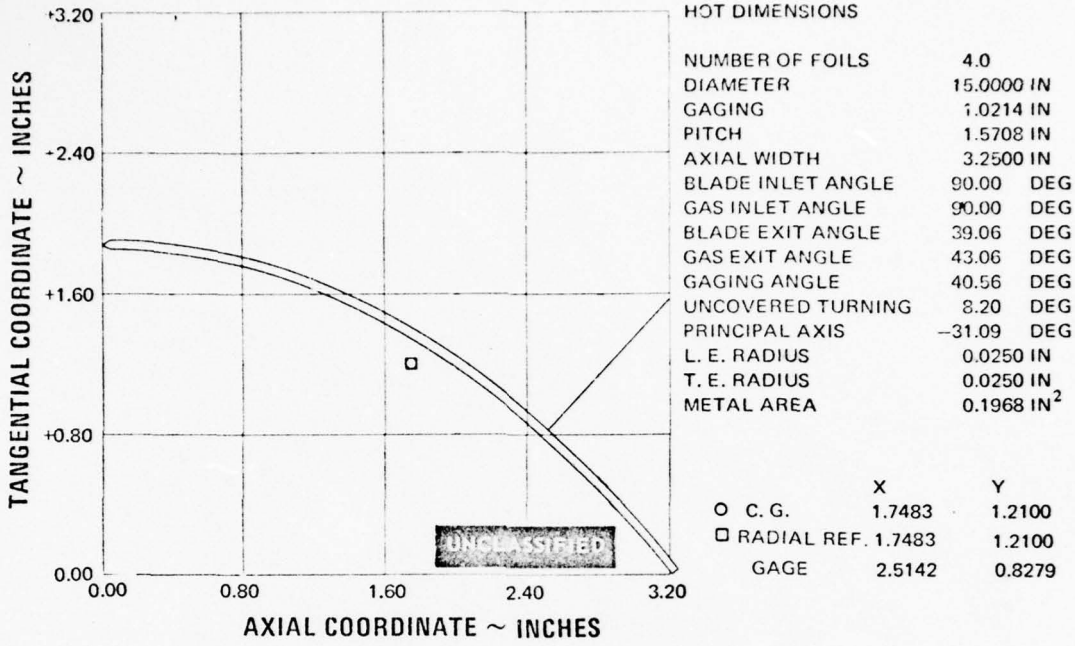

Figure 21 Redesigned Inlet Guide Vane, Second Vane Cascade, Root Section

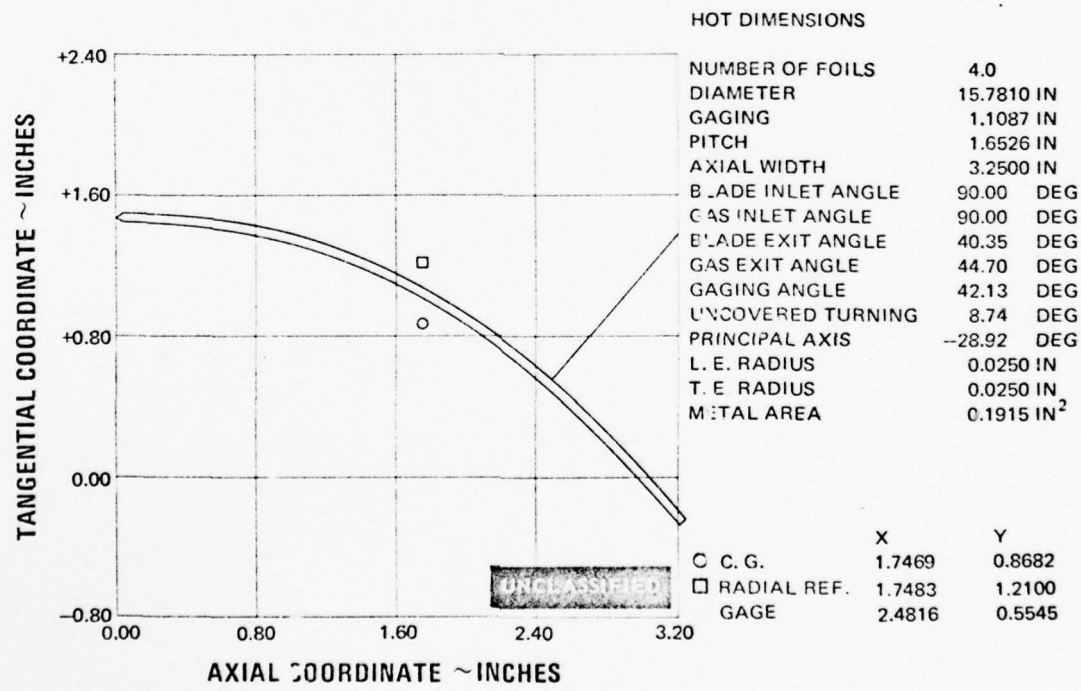

Figure 22 Redesigned Inlet Guide Vane, Second Vane Cascade, 1/8 Root Section

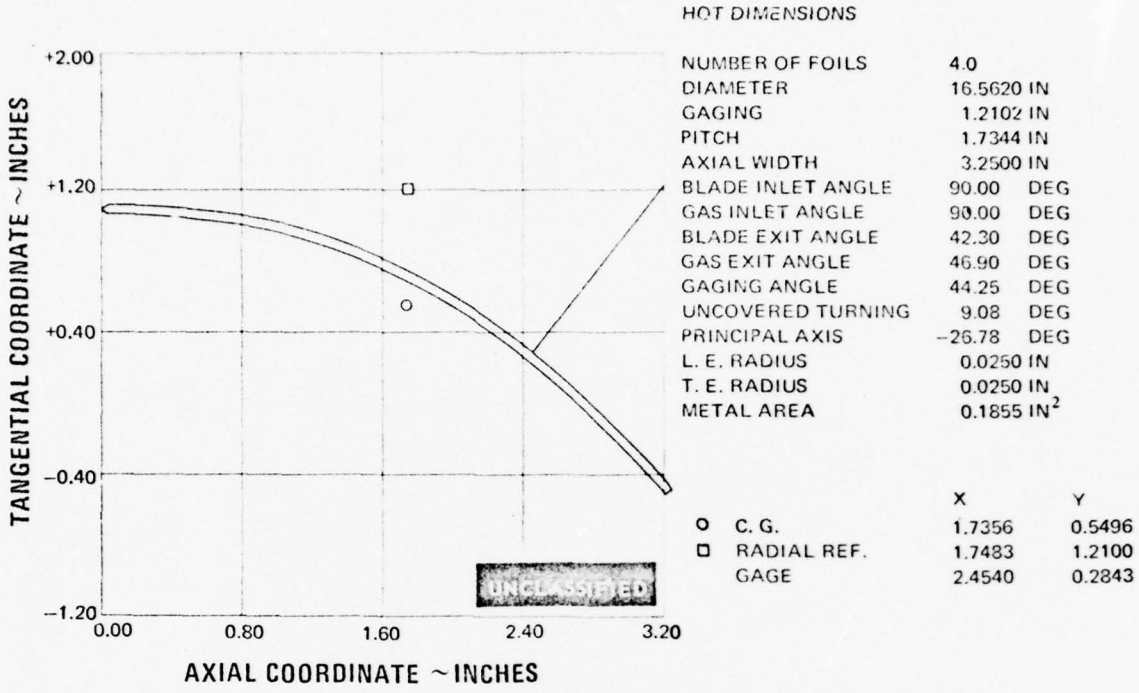

Figure 23 Redesigned Inlet Guide Vane, Second Vane Cascade, ¼ Root Section

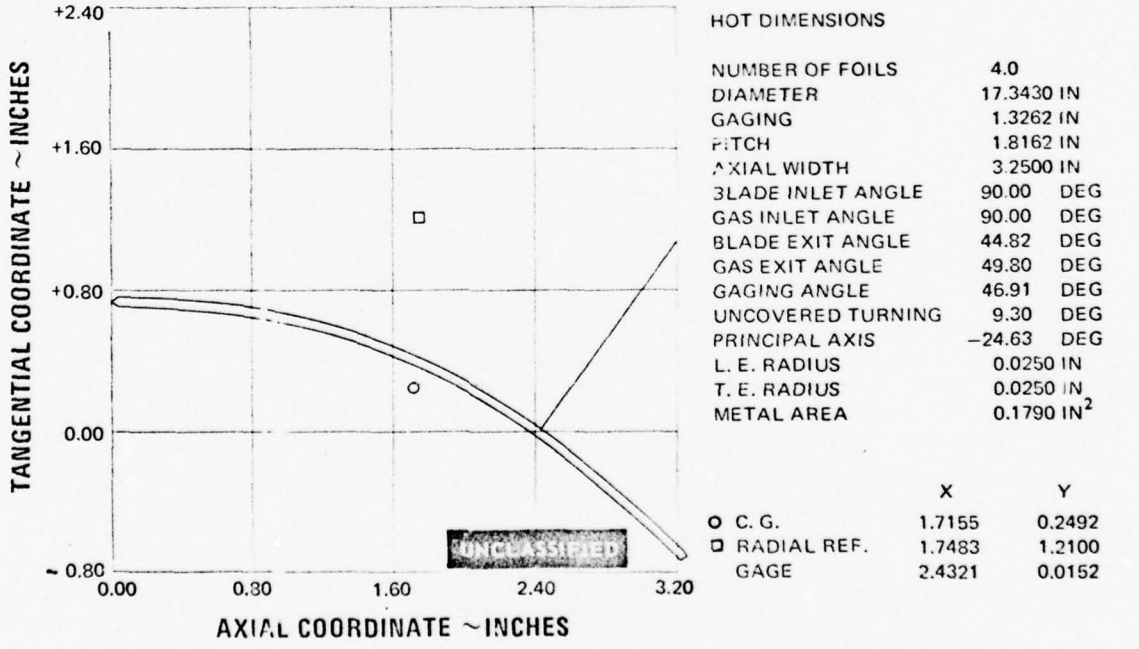

Figure 24 Redesigned Inlet Guide Vane, Second Vane Cascade, 3/8 Root Section

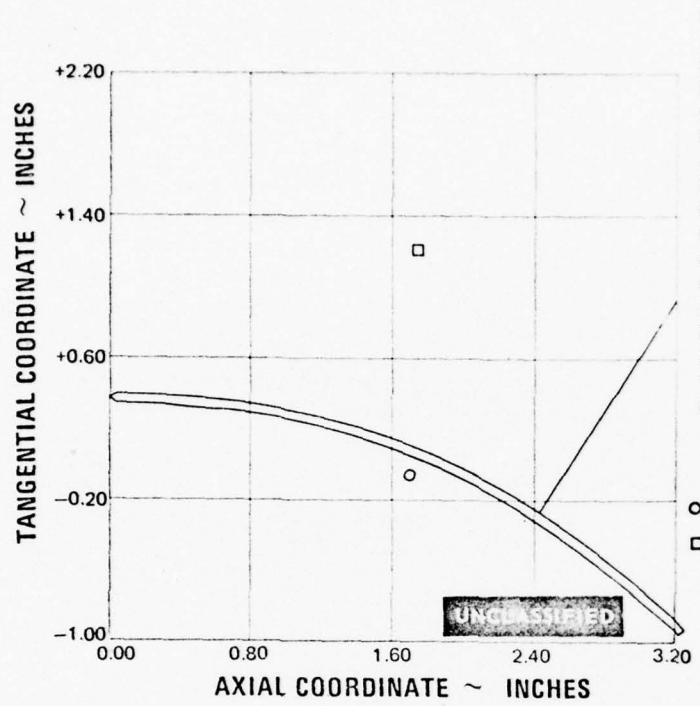

HOT DIMENSIONS

NUMBER OF FOILS	4.0	
DIAMETER	18.1250	IN.
GAGING	1.4514	IN.
PITCH	1.8980	IN.
AXIAL WIDTH	3.2500	IN.
BLADE INLET ANGLE	90.00	DEG.
GAS INLET ANGLE	90.00	DEG.
BLADE EXIT ANGLE	47.55	DEG.
GAS EXIT ANGLE	53.00	DEG.
GAGING ANGLE	49.00	DEG.
UNCOVERED TURNING	9.65	DEG.
PRINCIPAL AXIS	−22.19	DEG.
L. E. RADIUS	0.0250	IN.
T. E. RADIUS	0.0250	IN.
METAL AREA	0.1736	IN.^{2}

	X	Y
○ C. G.	1.6977	−0.0585
□ RADIAL REF.	1.7483	1.2100
GAGE	2.4249	−0.2678

Figure 25 Redesigned Inlet Guide Vane, Second Vane Cascade, Mean Section

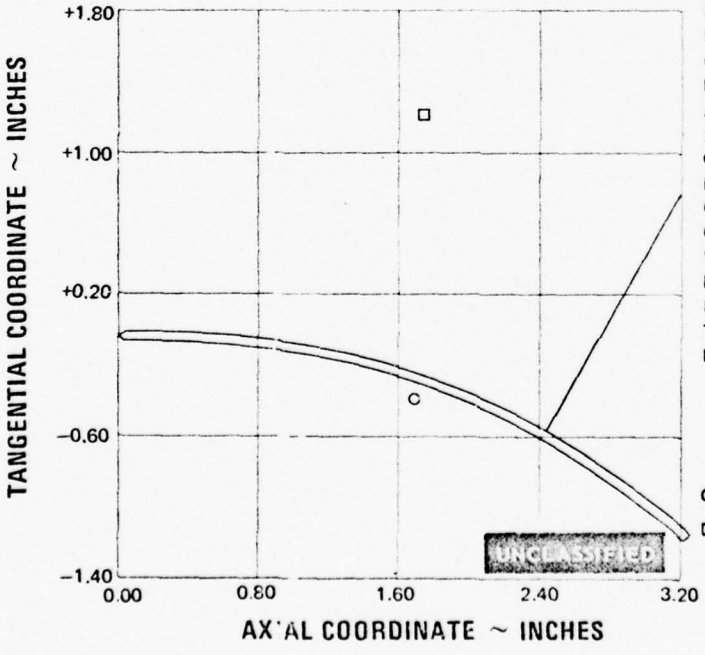

HOT DIMENSIONS

NUMBER OF FOILS	4.0	
DIAMETER	18.9062	IN.
GAGING	1.5786	IN.
PITCH	1.9799	IN.
AXIAL WIDTH	3.2500	IN.
BLADE INLET ANGLE	90.00	DEG.
GAS INLET ANGLE	90.00	DEG.
BLADE EXIT ANGLE	50.13	DEG.
GAS EXIT ANGLE	56.10	DEG.
GAGING ANGLE	52.88	DEG.
UNCOVERED TURNING	10.41	DEG.
PRINCIPAL AXIS	−19.10	DEG.
L. E. RADIUS	0.0250	IN.
T. E. RADIUS	0.0250	IN.
METAL AREA	0.1704	IN.^{2}

	X	Y
○ C. G.	1.6908	−0.3909
□ RADIAL REF.	1.7483	1.2100
GAGE	2.4368	−0.5699

Figure 26 Redesigned Inlet Guide Vane, Second Vane Cascade, 1/8 Tip Section

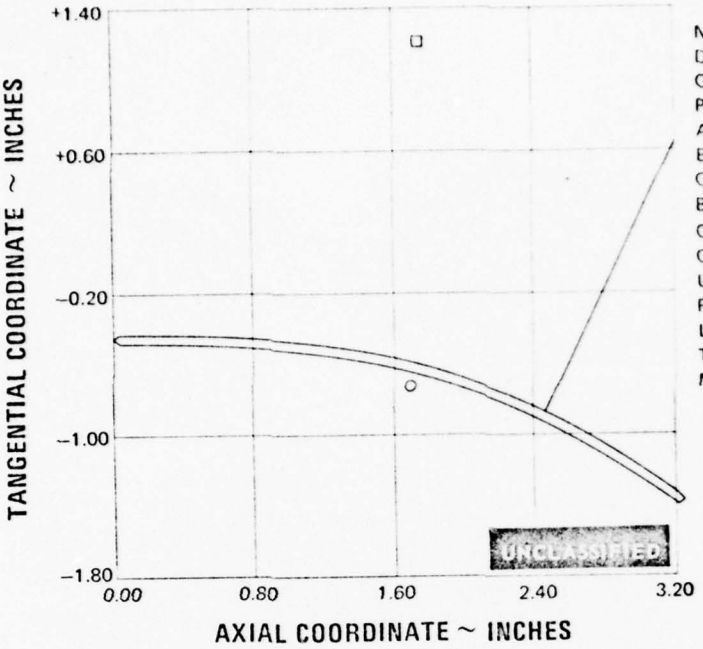

HOT DIMENSIONS

NUMBER OF FOILS	4.0
DIAMETER	19.6874 IN.
GAGING	1.7072 IN.
PITCH	2.0617 IN.
AXIAL WIDTH	3.2500 IN.
BLADE INLET ANGLE	90.00 DEG.
GAS INLET ANGLE	90.00 DEG.
BLADE EXIT ANGLE	52.63 DEG.
GAS EXIT ANGLE	58.90 DEG.
GAGING ANGLE	55.90 DEG.
UNCOVERED TURNING	11.26 DEG
PRINCIPAL AXIS	-15.60 DEG.
L. E. RADIUS	0.0250 IN.
T. E. RADIUS	0.0250 IN.
METAL AREA	0.1685 IN.^{2}

	X	Y
○ C. G.	1.6891	-0.7293
□ RADIAL REF.	1.7483	1.2100
GAGE	2.4622	-0.8735

Figure 27 Redesigned Inlet Guide Vane, Second Vane Cascade, ¼ Tip Section

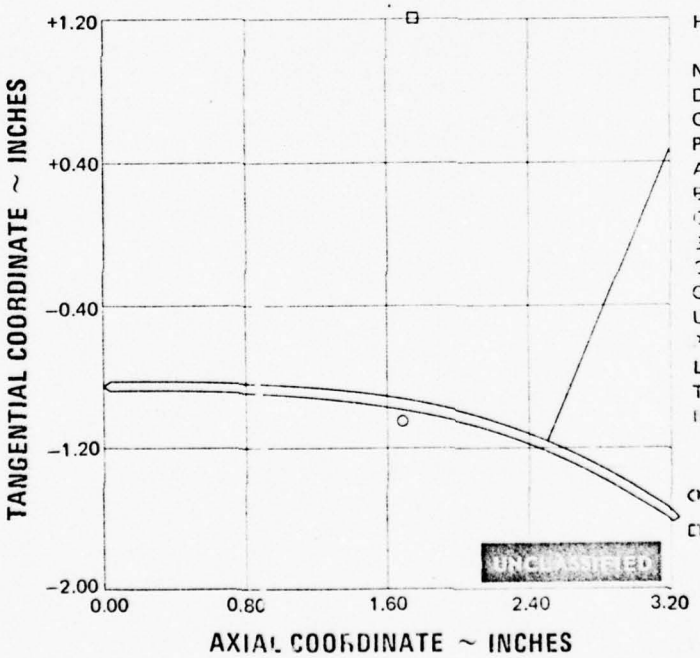

HOT DIMENSIONS

NUMBER OF FOILS	4.0
DIAMETER	20.4687 IN.
GAGING	1.8386 IN.
PITCH	2.1435 IN.
AXIAL WIDTH	3.2500 IN.
BLADE INLET ANGLE	90.00 DEG.
GAS INLET ANGLE	90.00 DEG.
BLADE EXIT ANGLE	55.17 DEG.
GAS EXIT ANGLE	61.80 DEG.
GAGING ANGLE	59.07 DEG.
UNCOVERED TURNING	11.84 DEG.
PRINCIPAL AXIS	-12.08 DEG.
L. E. RADIUS	0.0250 IN.
T. E. RADIUS	0.0250 IN.
METAL AREA	0.1670 IN.^{2}

	X	Y
○ C. G.	1.6842	-1.0507
□ RADIAL REF.	1.7483	1.2100
GAGE	2.4970	-1.1620

Figure 28 Redesigned Inlet Guide Vane, Second Vane Cascade, 3/8 Tip Section

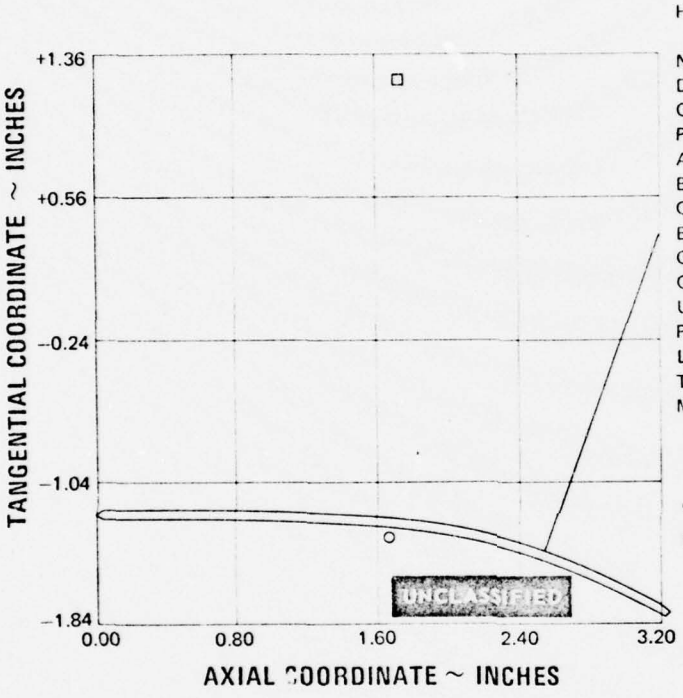

HOT DIMENSIONS

NUMBER OF FOILS	4.0
DIAMETER	21.2500 IN.
GAGING	1.9724 IN.
PITCH	2.2253 IN.
AXIAL WIDTH	3.2500 IN.
BLADE INLET ANGLE	90.00 DEG.
GAS INLET ANGLE	90.00 DEG.
BLADE EXIT ANGLE	57.79 DEG.
GAS EXIT ANGLE	64.89 DEG.
GAGING ANGLE	62.42 DEG.
UNCOVERED TURNING	12.14 DEG.
PRINCIPAL AXIS	− 8.65 DEG.
L. E. RADIUS	0.0250 IN.
T. E. RADIUS	0.0250 IN.
METAL AREA	0.1654 IN.^{2}

	X	Y
○ C. G.	1.6735	−1.3508
□ RADIAL REF.	1.7483	1.2100
GAGE	2.5401	−1.4311

Figure 29 Redesigned Inlet Guide Vane, Second Vane Cascade, Tip Section

Figure 30 Pressure Loss Contours, Second Vane - Screen Removed, Three Flow Passages, Midspan Exit Mach No. = 0.912, Baseline With Redesigned Inlet Guide Vanes

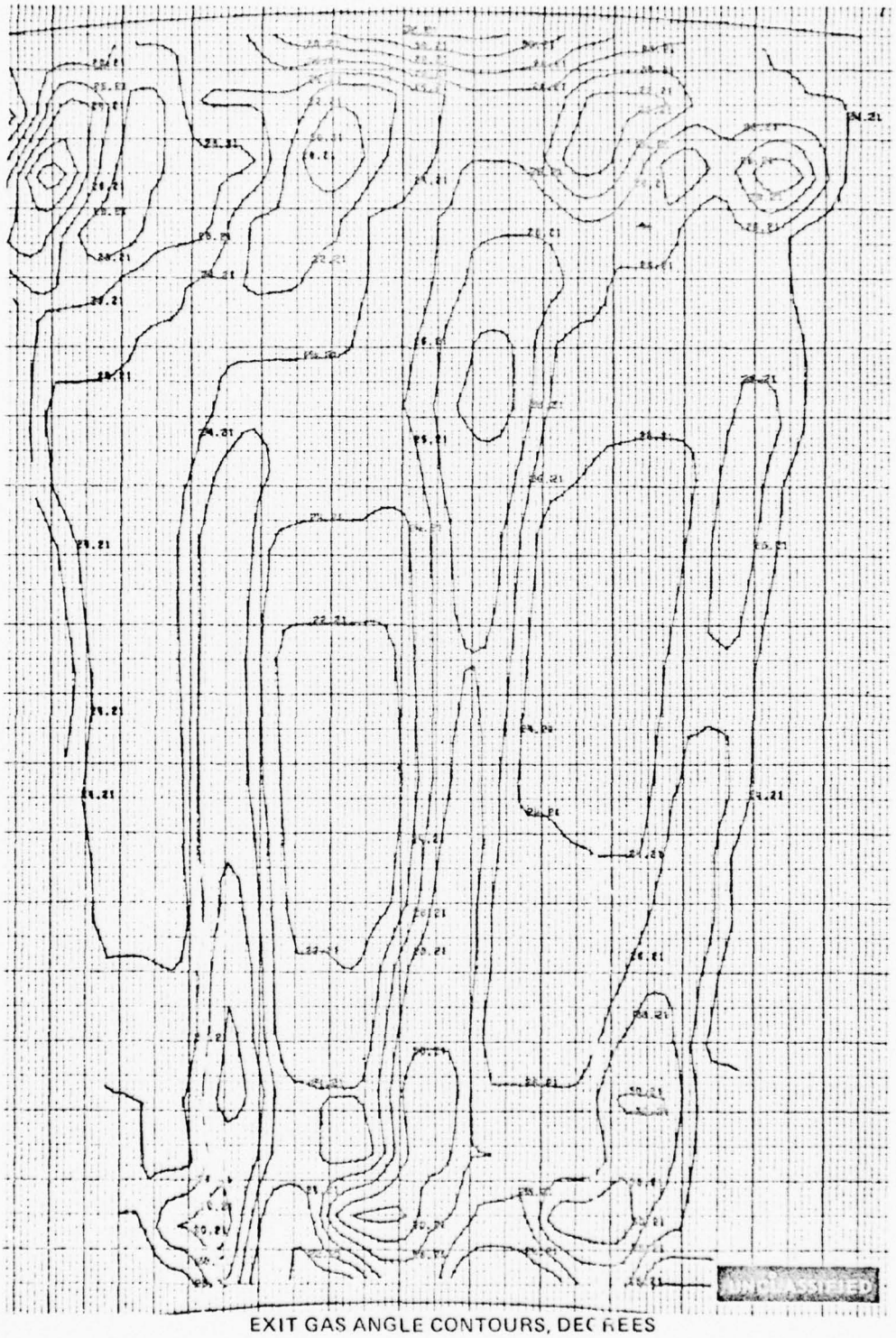

Figure 31 Exit Gas Angle Contours, Second Vane - Screen Removed, Three Flow Passages, Midspan Exit Mach No. = 0.912, Baseline With Redesigned Inlet Guide Vanes

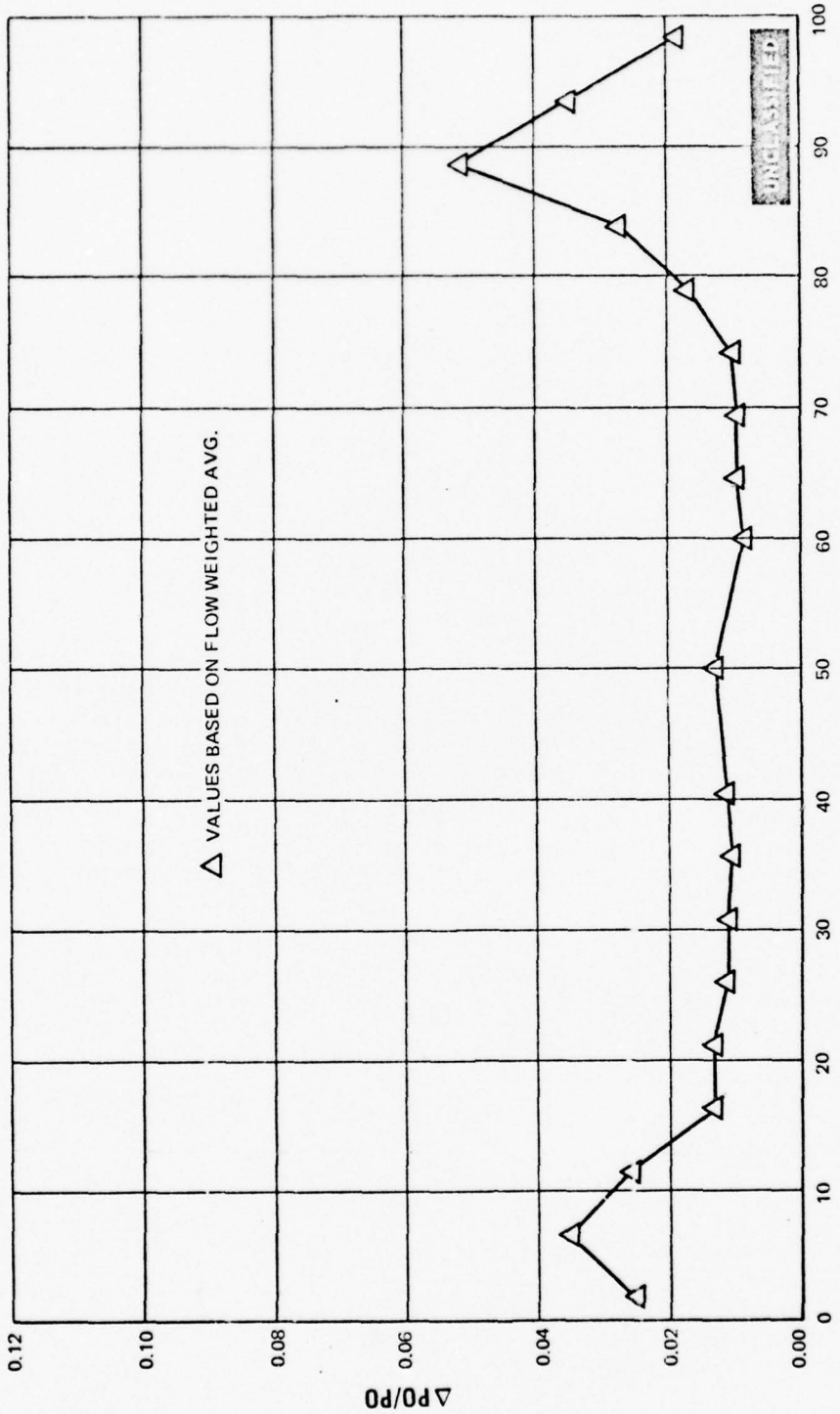

Figure 32 Spanwise Pressure Loss Distribution, Second Vane - Screen Removed, Midspan Exit Mach No. = 0.912, Baseline With Redesigned Inlet Guide Vanes

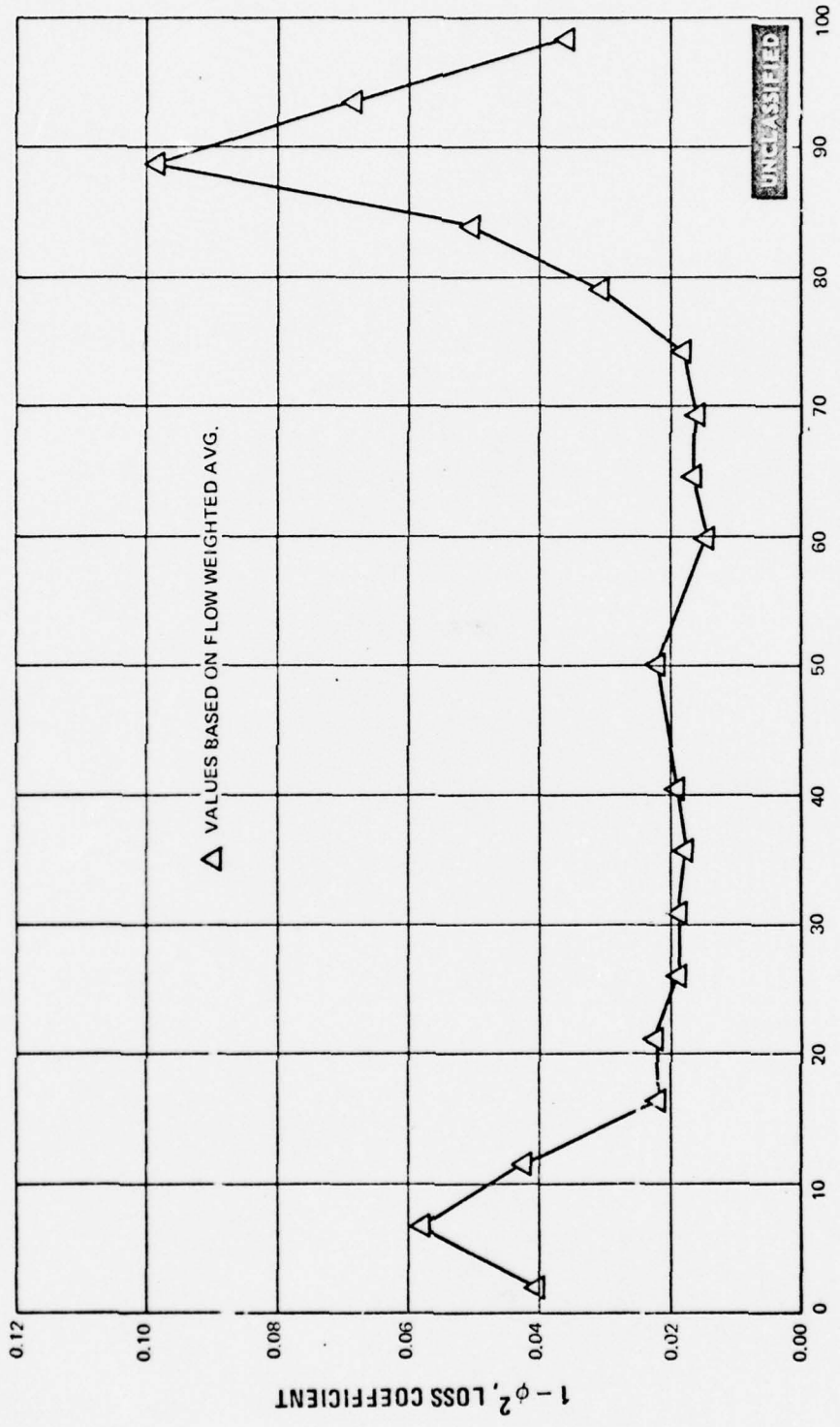

Figure 33 Spanwise Loss Coefficient Distribution, Second Vane - Screen Removed, Mid-span Exit Mach No. = 0.912, Baseline With Redesigned Inlet Guide Vanes

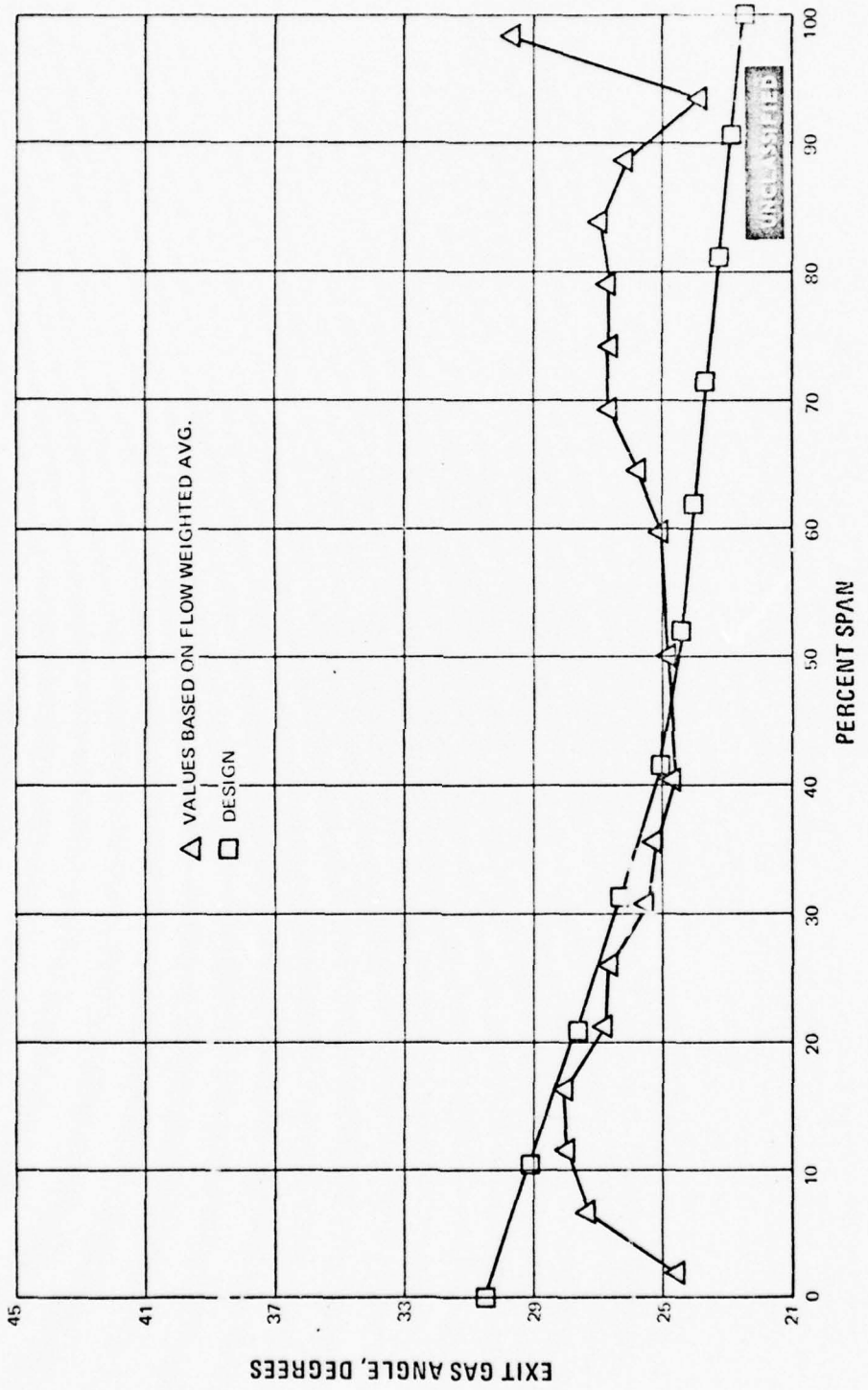

Figure 34 Spanwise Exit Gas Angle Distribution, Second Vane - Screen Removed, Mid-span Exit Mach No. = 0.912, Baseline With Redesigned Inlet Guide Vanes

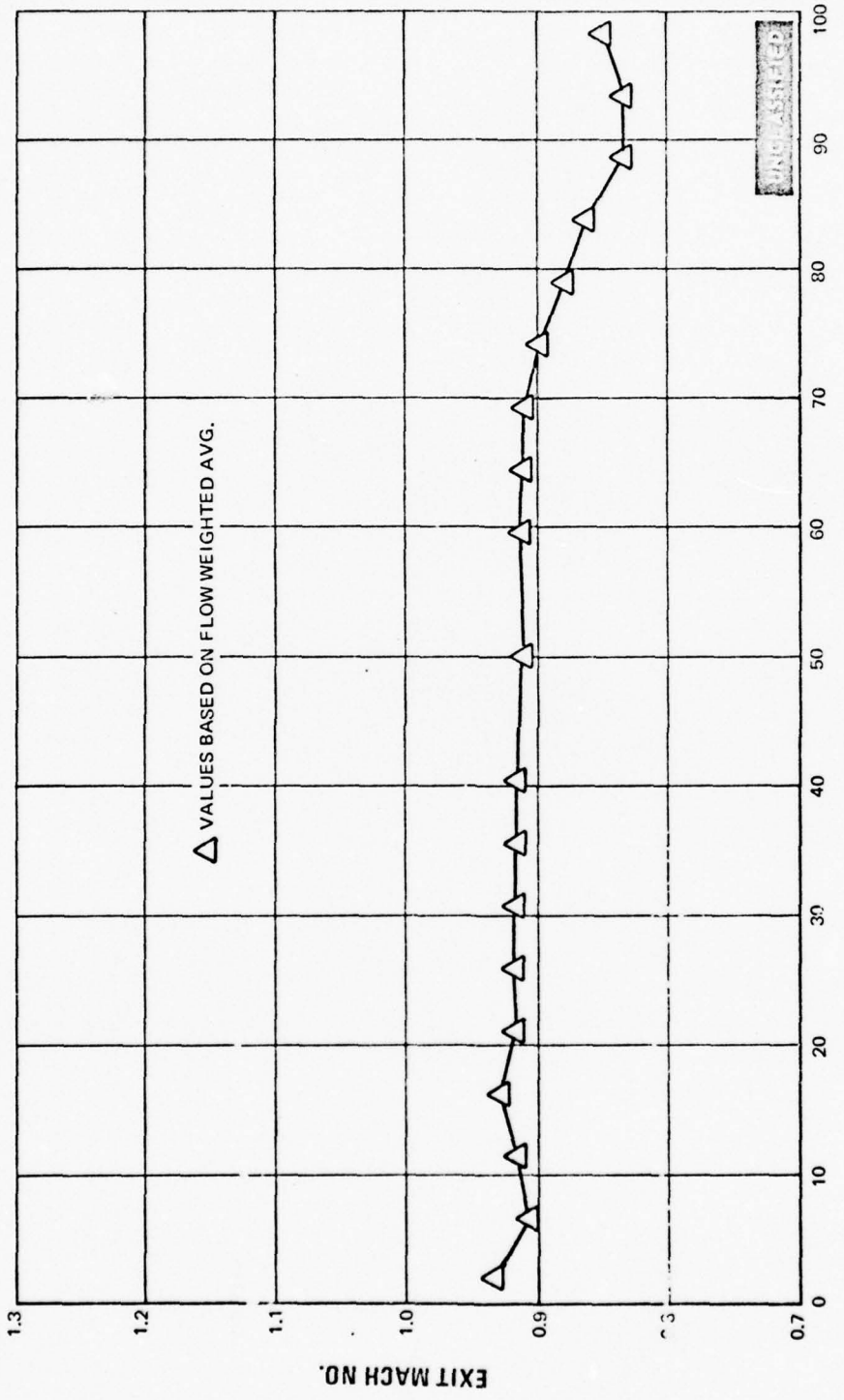

Figure 35 Spanwise Exit Mach Number Distribution, Second Vane - Screen Removed, Midspan Exit Mach No. = 0.912, Baseline With Redesigned Inlet Guide Vanes

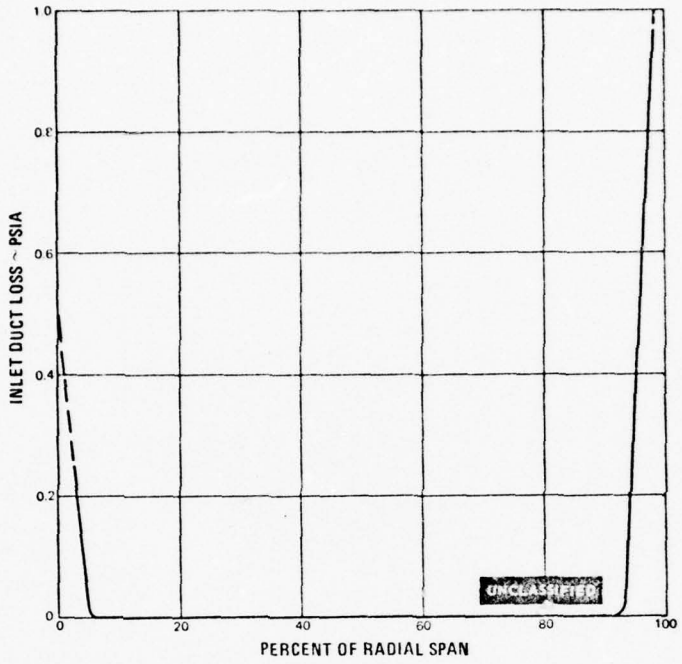

Figure 36 Inlet Duct Loss Versus Percent Radial Span–Second Vane Baseline With Redesigned Inlet Guide Vanes

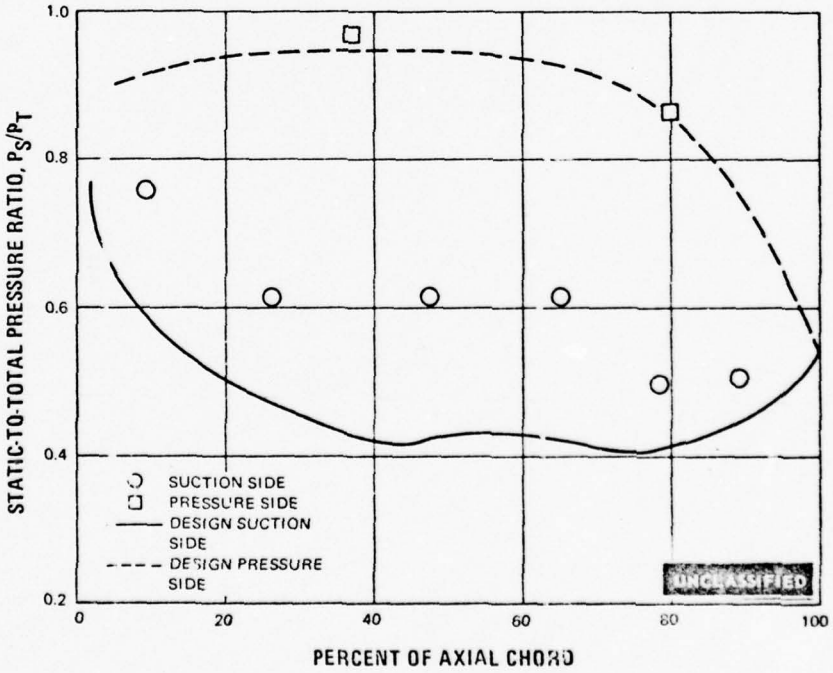

Figure 37 Static-to-Total Pressure Ratio Versus Percent of Axial Chord, Second Vane Baseline With Redesigned Inlet Guide Vanes--Root Section

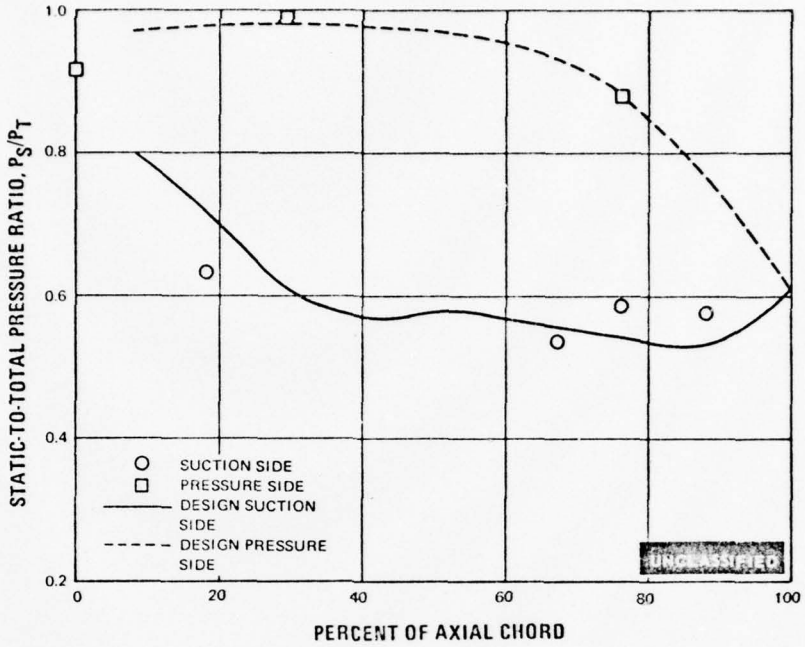

Figure 38 Static-to-Total Pressure Ratio Versus Percent of Axial Chord, Second Vane Baseline With Redesigned Inlet Guide Vanes–Mean Section

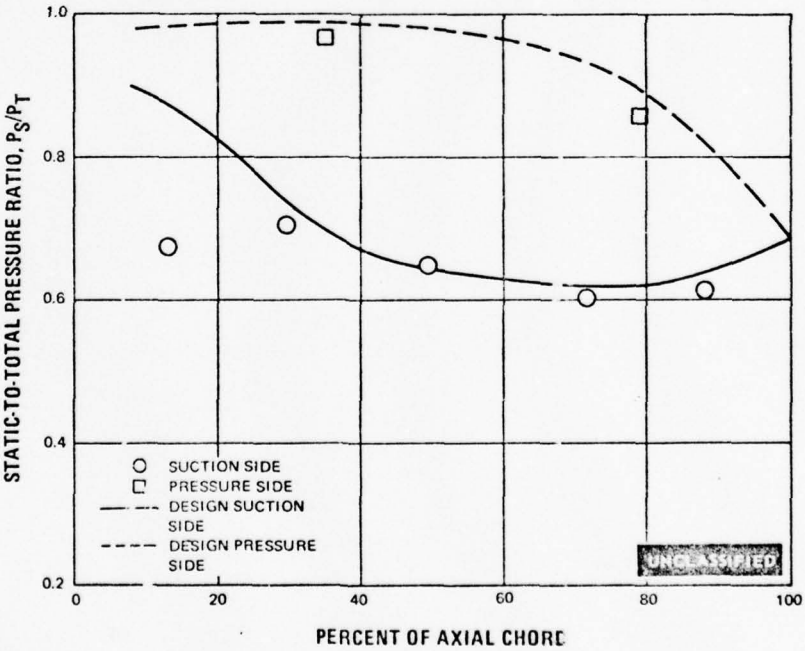

Figure 39 Static-to-Total Pressure Ratio Versus Percent of Axial Chord, Second Vane Baseline With Redesigned Inlet Guide Vanes–Tip Section

(U) Analysis of this data indicated that excessive inlet boundary losses were migrating into the test passage due to outside diameter corner boundary layer separation and secondary flow currents within the inlet guide vane channels. This can be clearly seen on the total pressure loss contour maps (Figure 30), where pockets of large losses are seen at the outside portion of the test airfoil channel. To correct this, boundary layer bleed slots were cut into the inlet guide vane pack inside-diameter and outside-diameter walls. The slots were cut close to the inlet guide vane, along the full length of the chord, on the acute angle side of the passage. Initially, a 0.125 inch wide slot was cut at the outside-diameter, and a 0.094 inch slot at the inside-diameter.

(U) This baseline second vane cascade, with the redesigned inlet guide vanes and the boundary layer bleeds was tested in the annular segment cascade. The performance data is presented in Figures 40 through 45. The inlet duct loss with the boundary layer bleeds is indicated in Figure 46. The airfoil surface statics are shown in Figures 47 through 49. Analysis of this data with the boundary layer bleeds showed significant improvement of the pressure loss contours at the end-walls, especially at the tip section. The cascade was free of inlet guide vane wakes and end-wall losses over all of the span with the exception of a small region at the inside diameter wall, which had a slight disturbance. Furthermore, oil and graphite flow visualization tests were made on the test airfoils and these are shown in Figures 50 through 53. These indicate attached flow over the airfoil with some radial inflow at the endwalls.

(U) A photograph of the patterns on the inlet guide vane suction surface is shown in Figure 54. It can be observed from this photograph that there was a strong tendency for radial flow toward the bleed slots along the guide vanes. Consequently, a program to minimize the boundary layer bleed slots, in order to maintain the lowest bleed flow and still prevent the accumulation of losses due to the inlet duct boundary layer separation, was undertaken.

(U) As a result of this program, it was found that the outside diameter boundary layer bleeds could be reduced from 0.125 to 0.047 inch in width and still prevent inlet duct boundary layer effects on the test airfoils. The inside diameter slots were not changed. The performance data of the baseline cascade with these "optimum" bleeds are shown in Figures 55 through 60. The inlet guide vane and duct loss with the optimum bleeds is shown in Figure 61. Analysis of these data indicated a shift of the baseline loss coefficients to a slightly lower level, compared to the original baseline data without bleeds. Extremely thorough checks of hardware, instrumentation and data did not resolve the data shift. To verify the accuracy of the optimum bleed test, this test was rerun and the lower loss level was repeated. The reason for the lower loss level is probably due to a lower turbulence intensity of the flow as seen by the test airfoil; this lower turbulence resulting from the bleeding of inlet boundary layer.

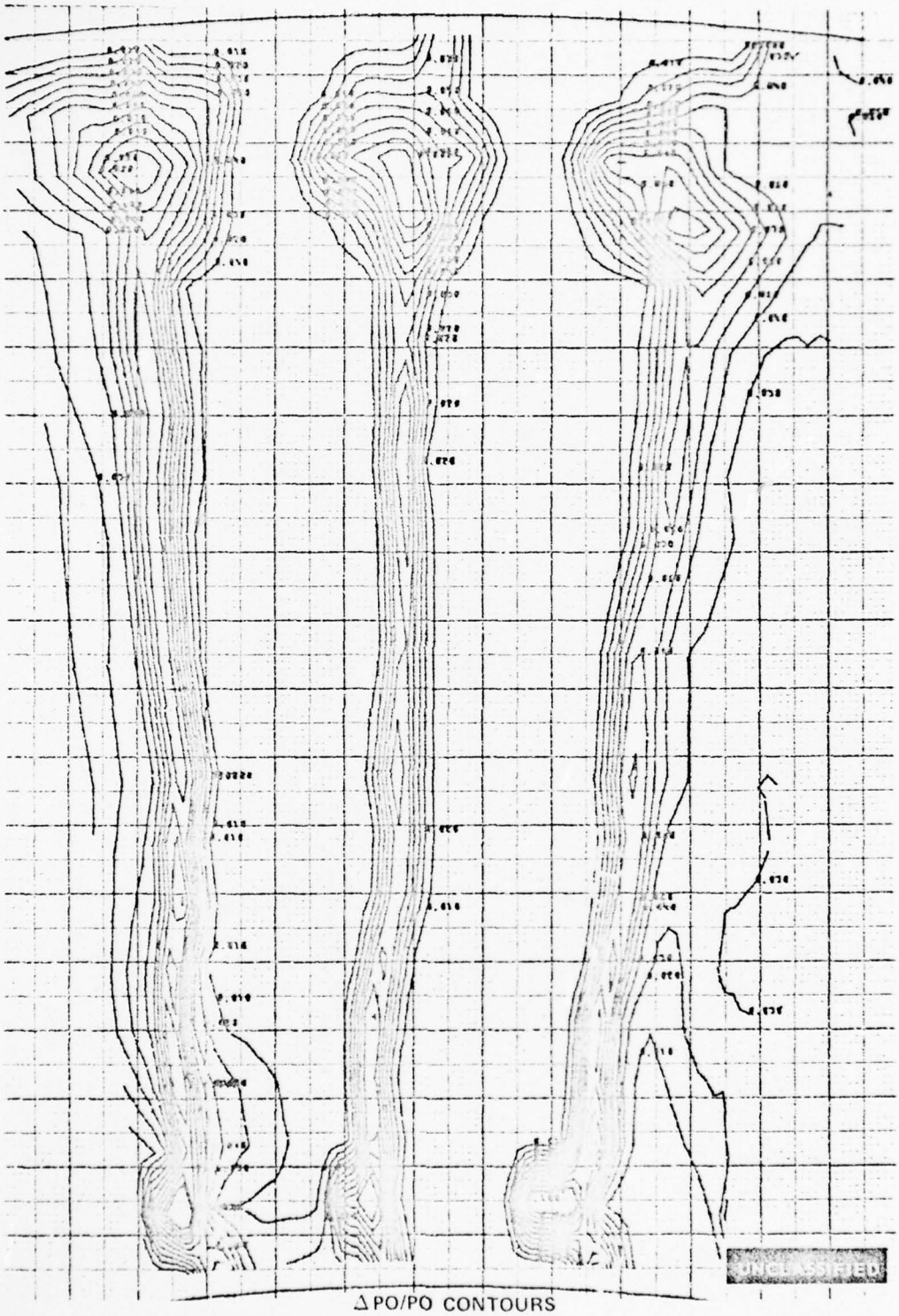

Figure 40 Pressure Loss Contours, Second Vane - Screen Removed, Three Flow Passages, Midspan Exit Mach No. = 0.869, Baseline With Redesigned Inlet Guide Vanes and Boundary Layer Bleeds

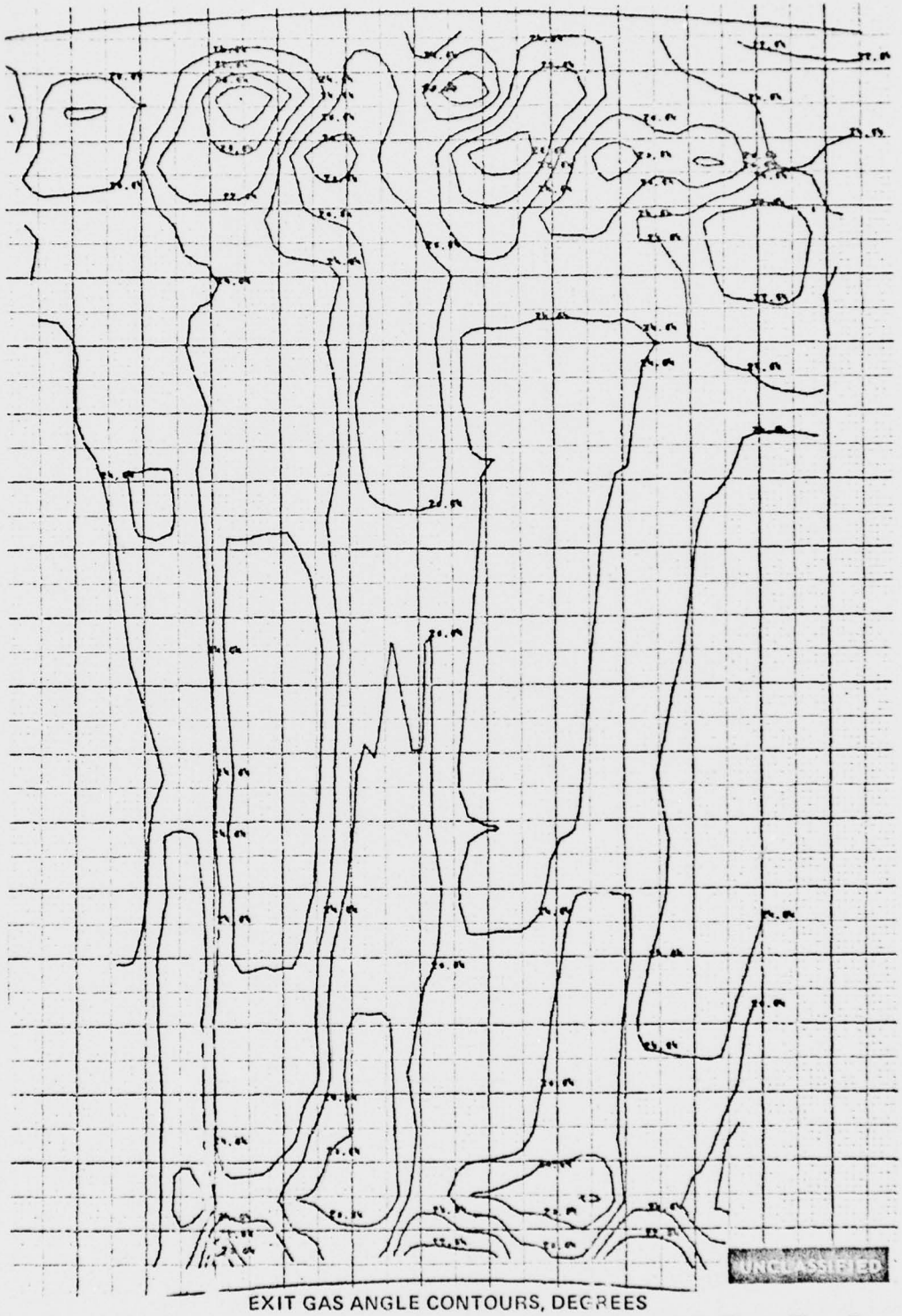

Figure 41 Exit Gas Angle Contours, Second Vane - Screen Removed, Three Flow Passages, Midspan Exit Mach No. = 0.869, Baseline With Redesigned Inlet Guide Vanes and Boundary Layer Bleeds

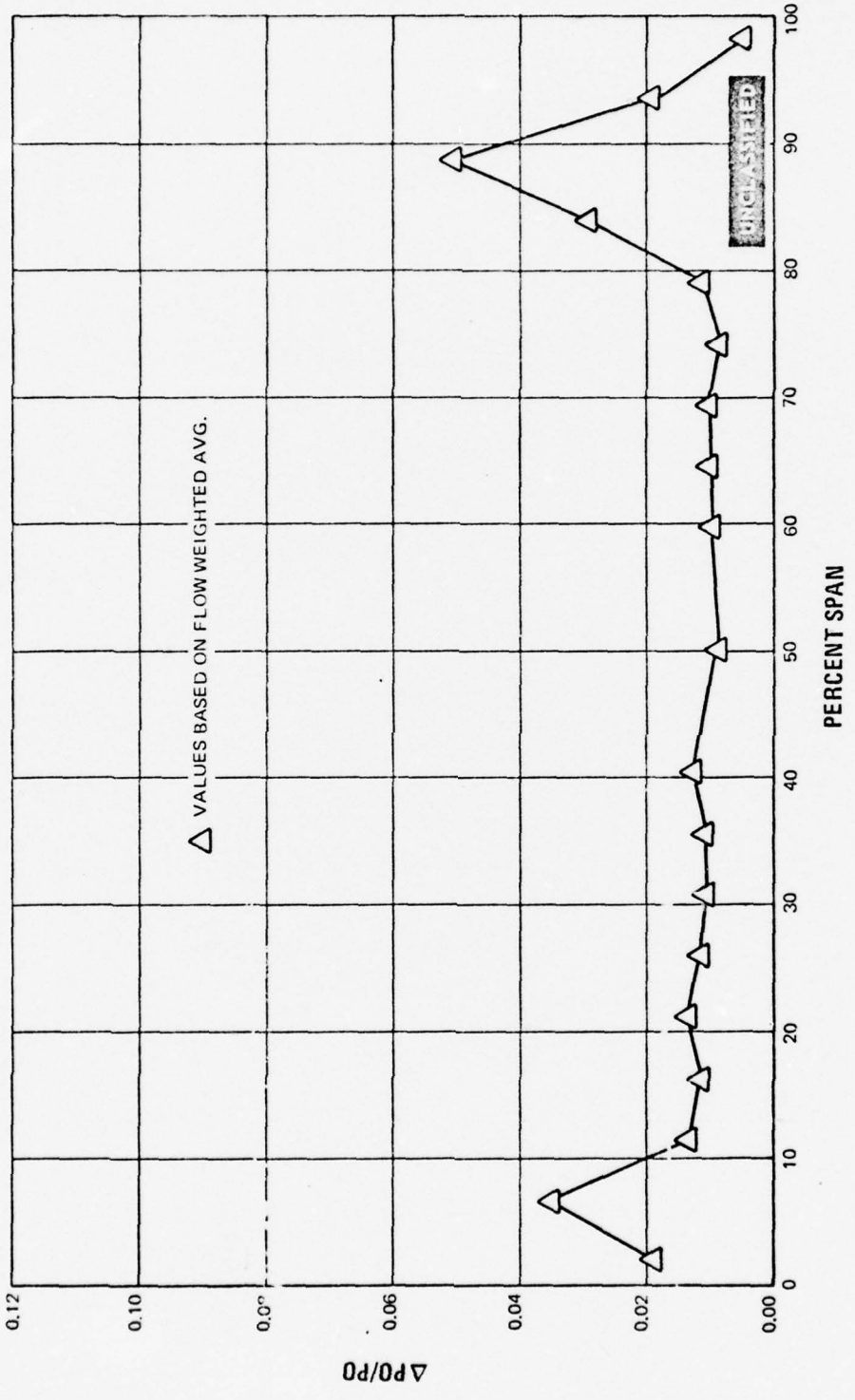

Figure 42 Spanwise Pressure Loss Distribution, Second Vane - Screen Removed, Midspan Exit Mach No. = 0.869, Baseline With Redesigned Inlet Guide Vanes and Boundary Layer Bleeds

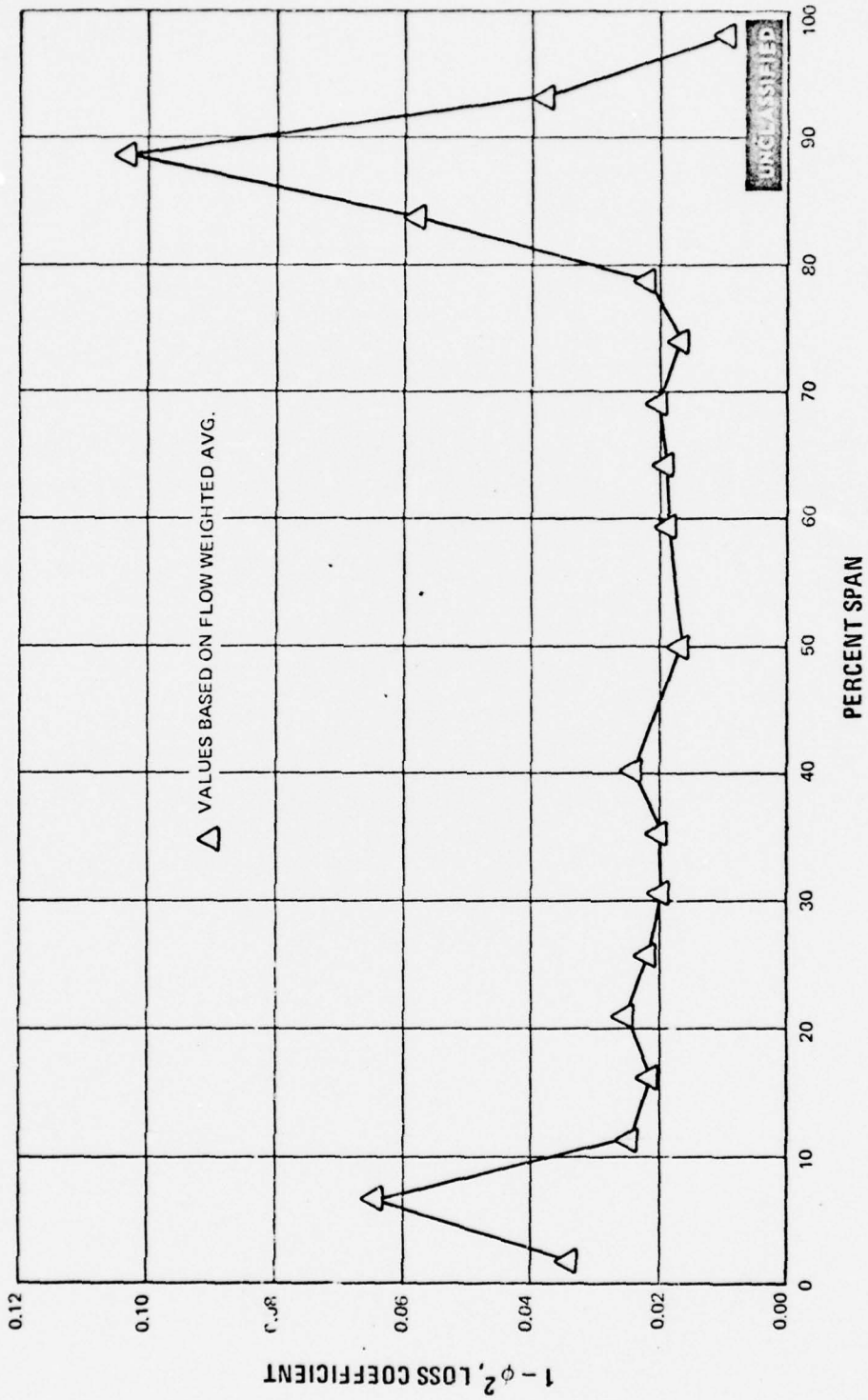

Figure 43 Spanwise Loss Coefficient Distribution, Second Vane - Screen Removed, Mid-span Exit Mach No. = 0.869, Baseline With Redesigned Inlet Guide Vanes and Boundary Layer Bleeds

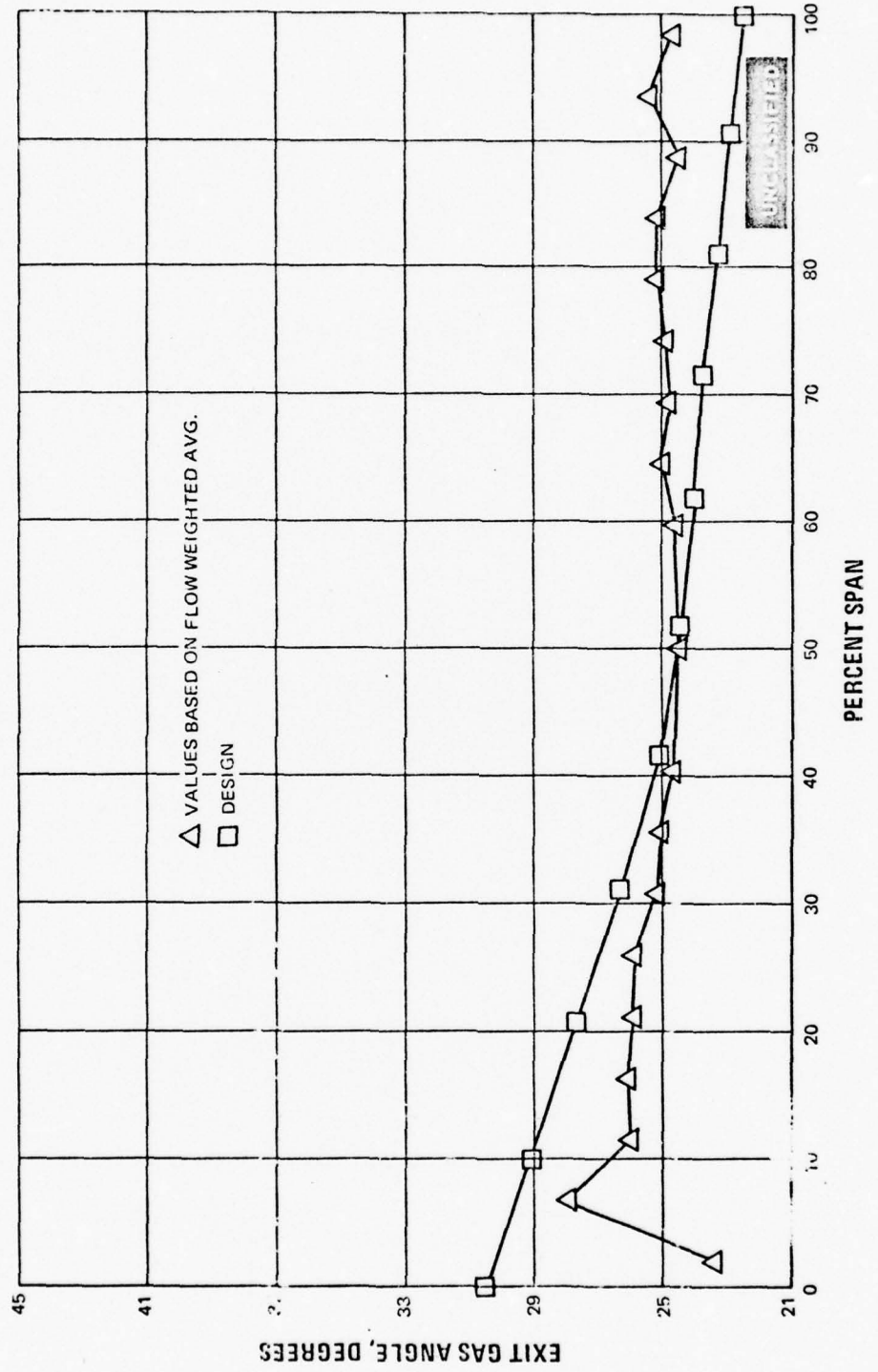

Figure 44 Spanwise Exit Gas Angle Distribution, Second Vane - Screen Removed, Mid-span Exit Mach No. = 0.869, Baseline With Redesigned Inlet Guide Vanes and Boundary Layer Bleeds

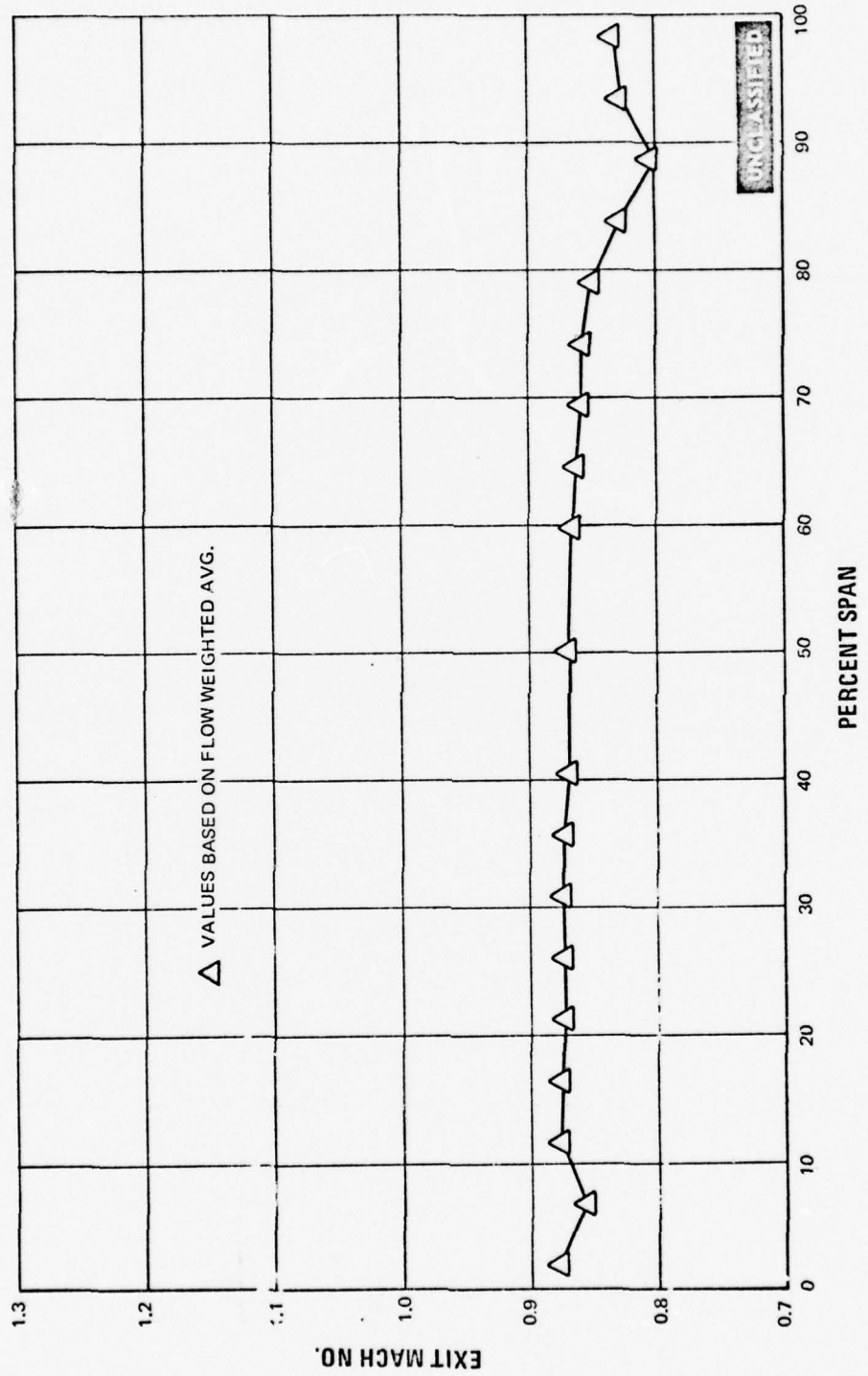

Figure 45 Spanwise Exit Mach Number Distribution, Second Vane - Screen Removed, Midspan Exit Mach No. = 0.869, Baseline With Redesigned Inlet Guide Vanes and Boundary Layer Bleeds

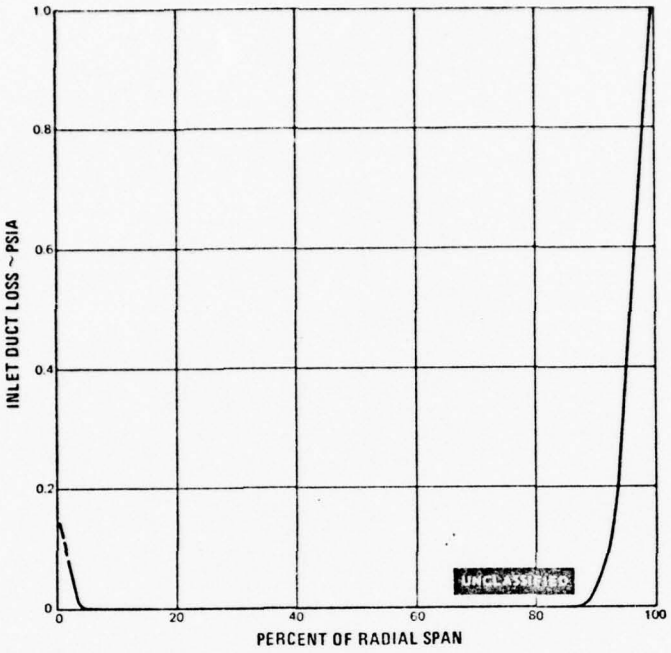

Figure 46 Inlet Duct Loss Versus Percent Radial Span—Second Vane Cascade With Redesigned Inlet Guide Vanes and Boundary Layer Bleeds

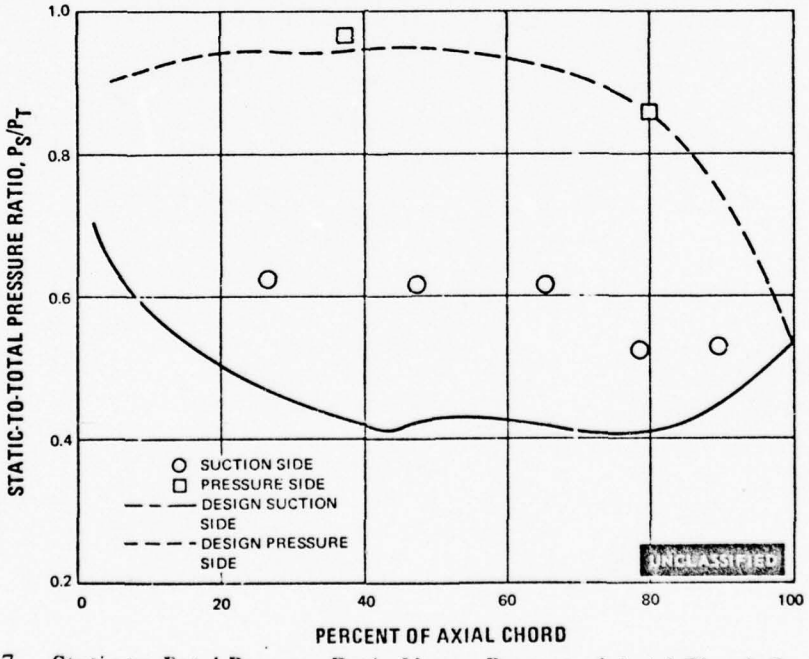

Figure 47 Static-to-Total Pressure Ratio Versus Percent of Axial Chord, Second Vane Baseline With Redesigned Inlet Guide Vanes and Boundary Layer Bleeds—Root Section

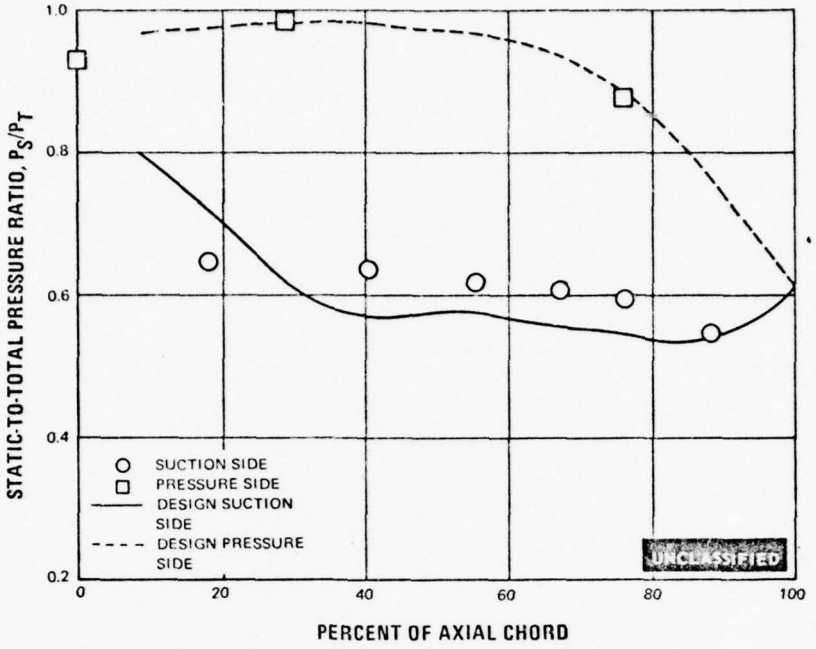

Figure 48 Static-to-Total Pressure Ratio Versus Percent of Axial Chord, Second Vane Baseline With Redesigned Inlet Guide Vanes and Boundary Layer Bleeds– Mean Section

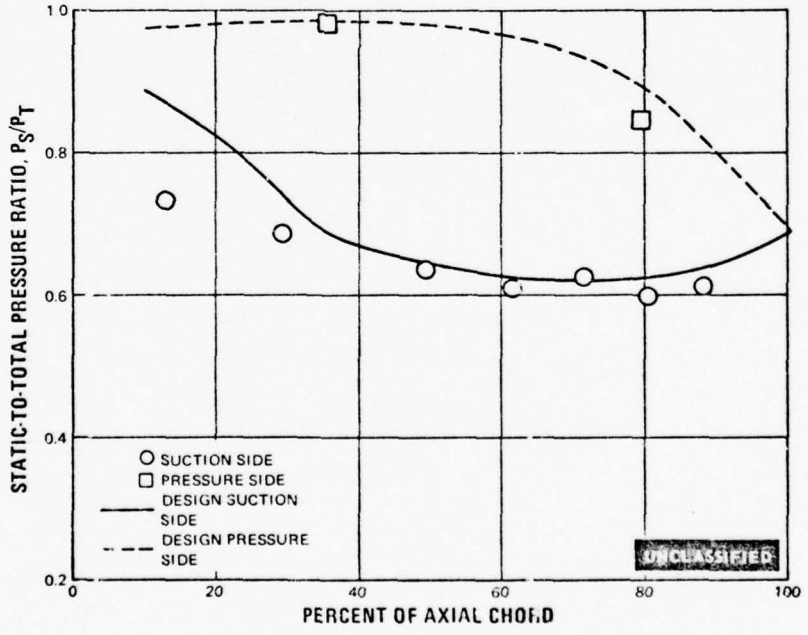

Figure 49 Static-to-Total Pressure Ratio Versus Percent of Axial Chord, Second Vane Baseline With Redesigned Inlet Guide Vanes and Boundary Layer Bleeds– Tip Section

Figure 50 Oil and Graphite Flow Patterns–Second Vane with Redesigned Inlet Guide Vanes and Original Boundary Layer Bleed Slots; View of Upstream Inside Diameter; Midspan Exit Mach No. =0.87

Figure 51 Oil and Graphite Flow Patterns–Second Vane with Redesigned Inlet Guide Vanes and Original Boundary Layer Bleed Slots; View of Downstream Outside Diameter; Midspan Exit Mach No. =0.87

Figure 52 Oil and Graphite Flow Patterns–Second Vane with Redesigned Inlet Guide Vanes and Original Boundary Layer Bleed Slots; View of Downstream Inside Diameter; Midspan Exit Mach No. =0.87

Figure 53 Oil and Graphite Flow Patterns–Second Vane with Redesigned Inlet Guide Vanes and Original Boundary Layer Bleed Slots; View of Downstream Outside Diameter; Midspan Exit Mach No. =0.87

Figure 54 Oil and Graphite Flow Patterns Inlet Guide Vane with Original Boundary Layer Bleed Slots; Midspan Exit Mach No. =0.87

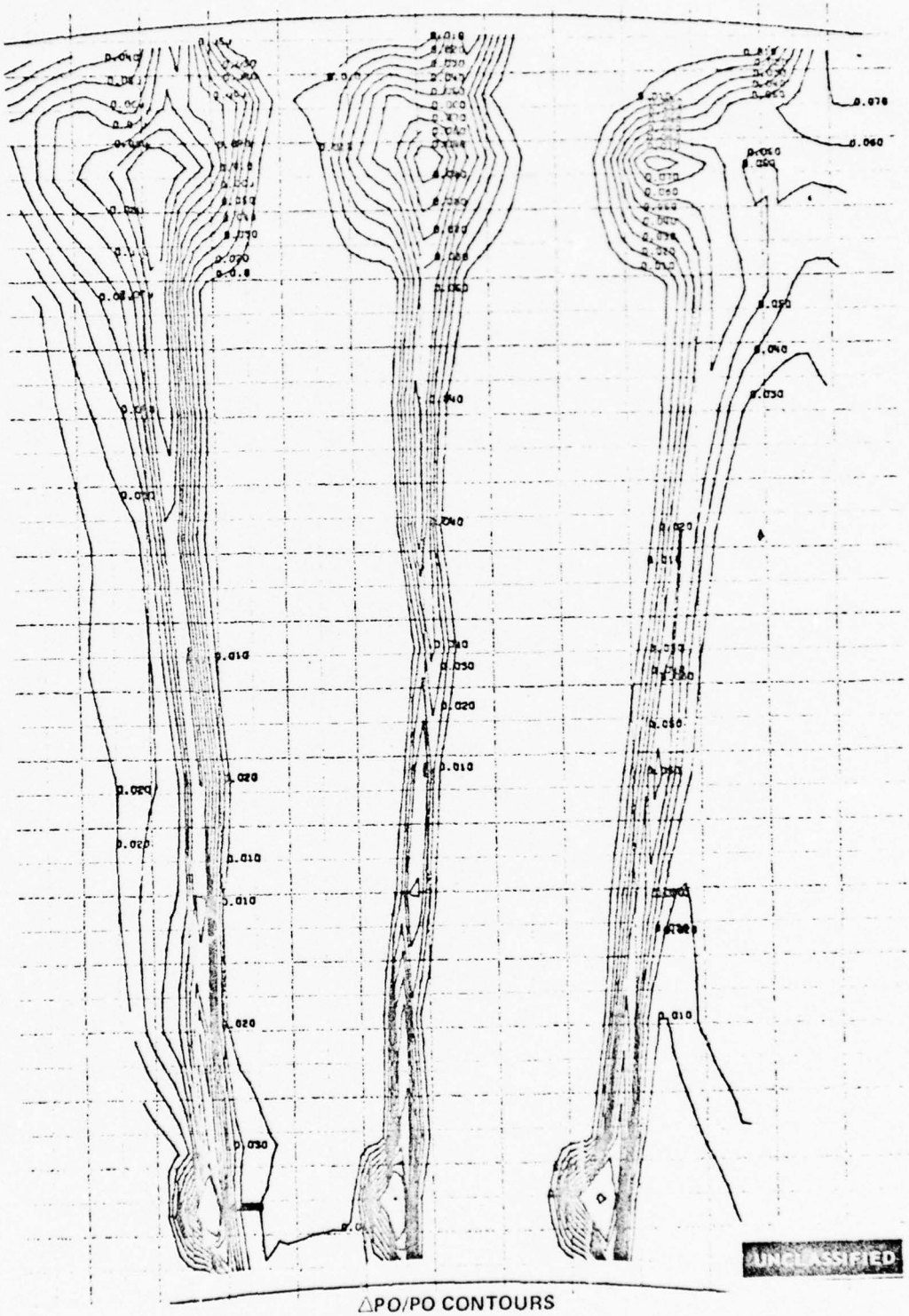

Figure 55 Pressure Loss Contours, Second Vane - Screen Removed. Three Flow Passages. Midspan Exit Mach No. = 0.885. Baseline With Redesigned Inlet Guide Vanes and Optimum Boundary Layer Bleeds

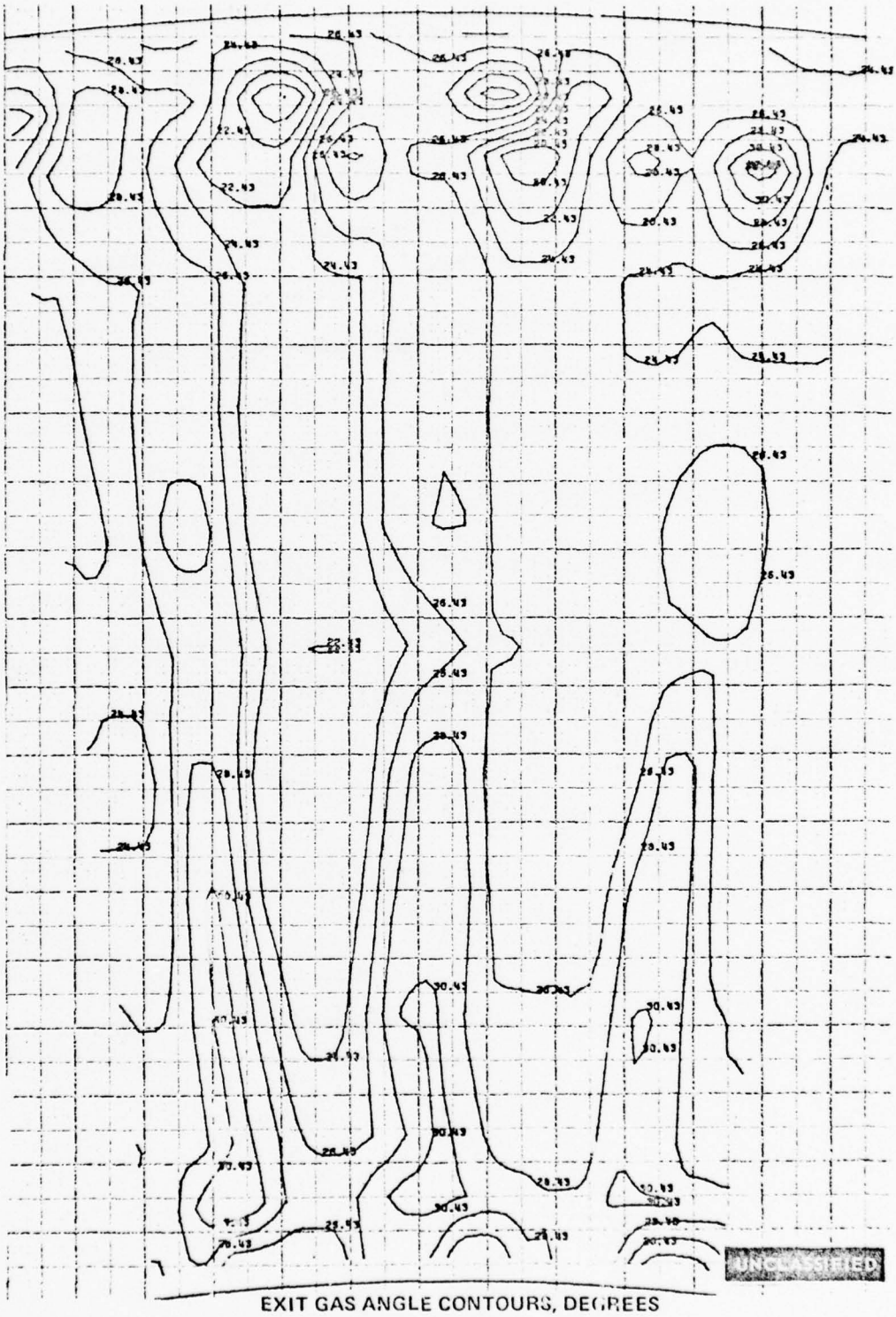

Figure 56 Exit Gas Angle Contours, Second Vane - Screen Removed, Three Flow Passages, Midspan Exit Mach No. = 0.885, Baseline With Redesigned Inlet Guide Vanes and Optimum Boundary Layer Bleeds

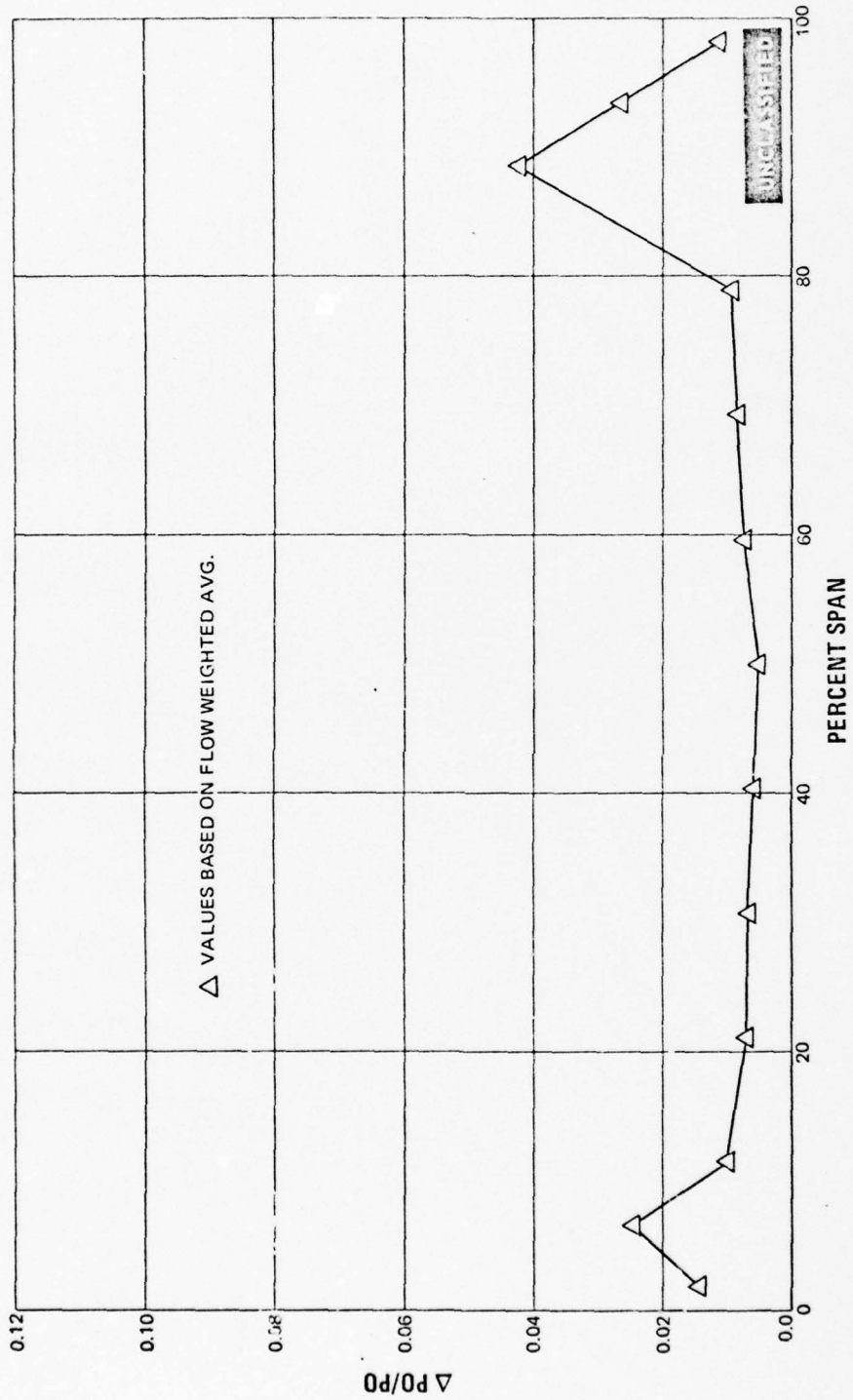

Figure 57 Spanwise Pressure Loss Distribution, Second Vane - Screen Removed, Midspan Exit Mach No. = 0.885, Baseline With Redesigned Inlet Guide Vanes and Optimum Boundary Layer Bleeds

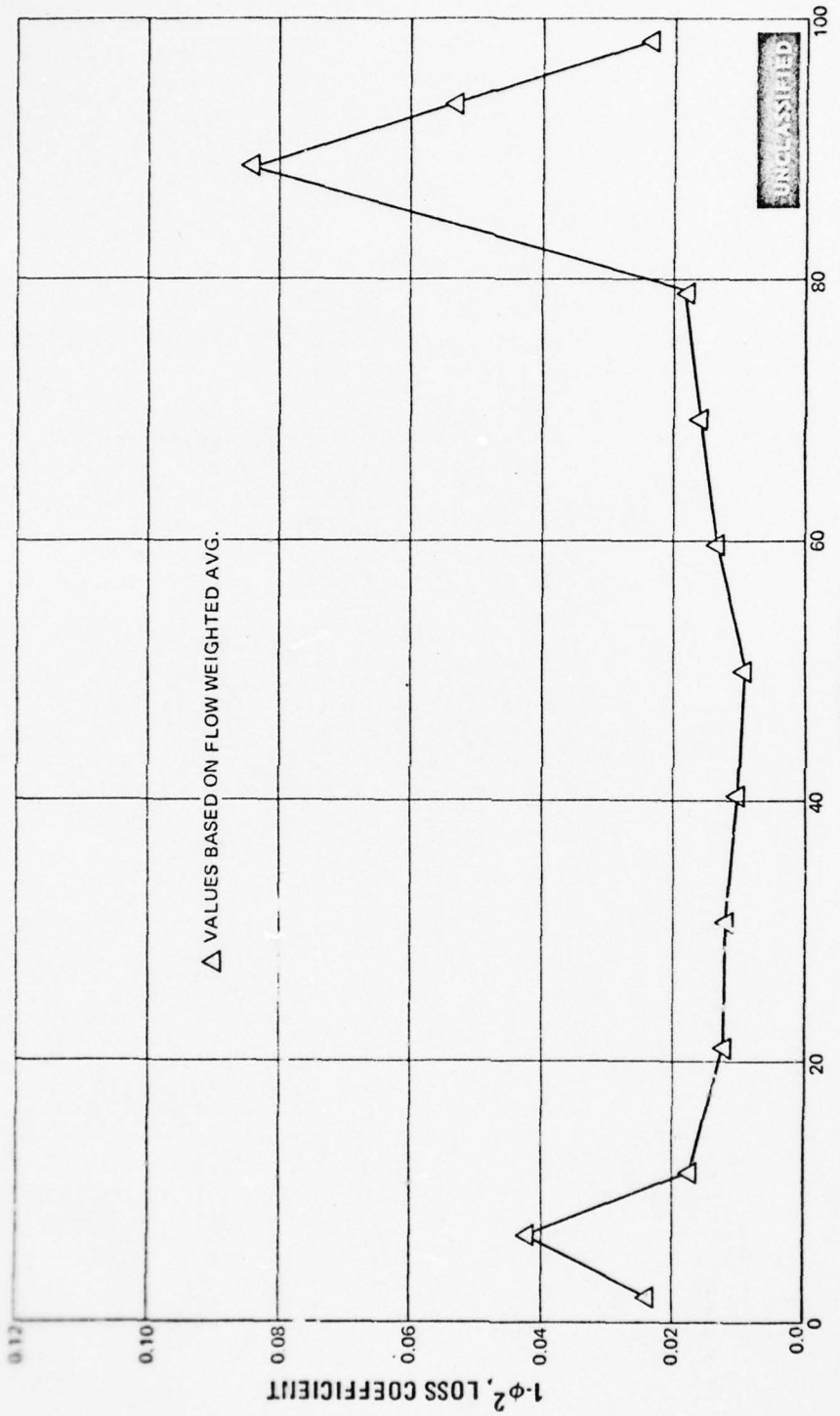

Figure 58 Spanwise Loss Coefficient Distribution, Second Vane - Screen Removed, Mid-span Exit Mach No. = 0.885, Baseline With Redesigned Inlet Guide Vanes and Optimum Boundary Layer Bleeds

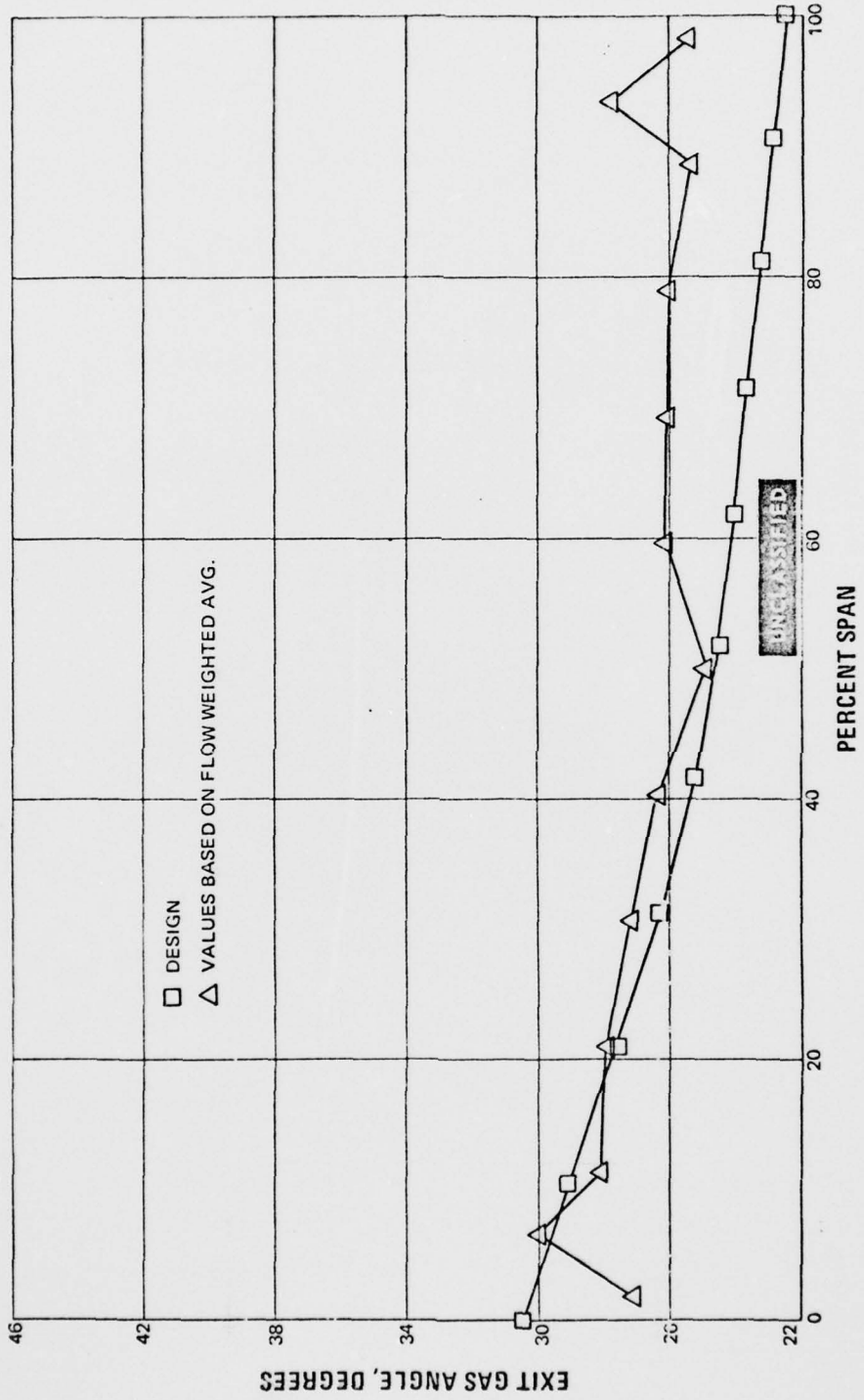

Figure 59 Spanwise Exit Gas Angle Distribution, Second Vane - Screen Removed, Mid-span Exit Mach No. = 0.885, Baseline With Redesigned Inlet Guide Vanes and Optimum Boundary Layer Bleeds

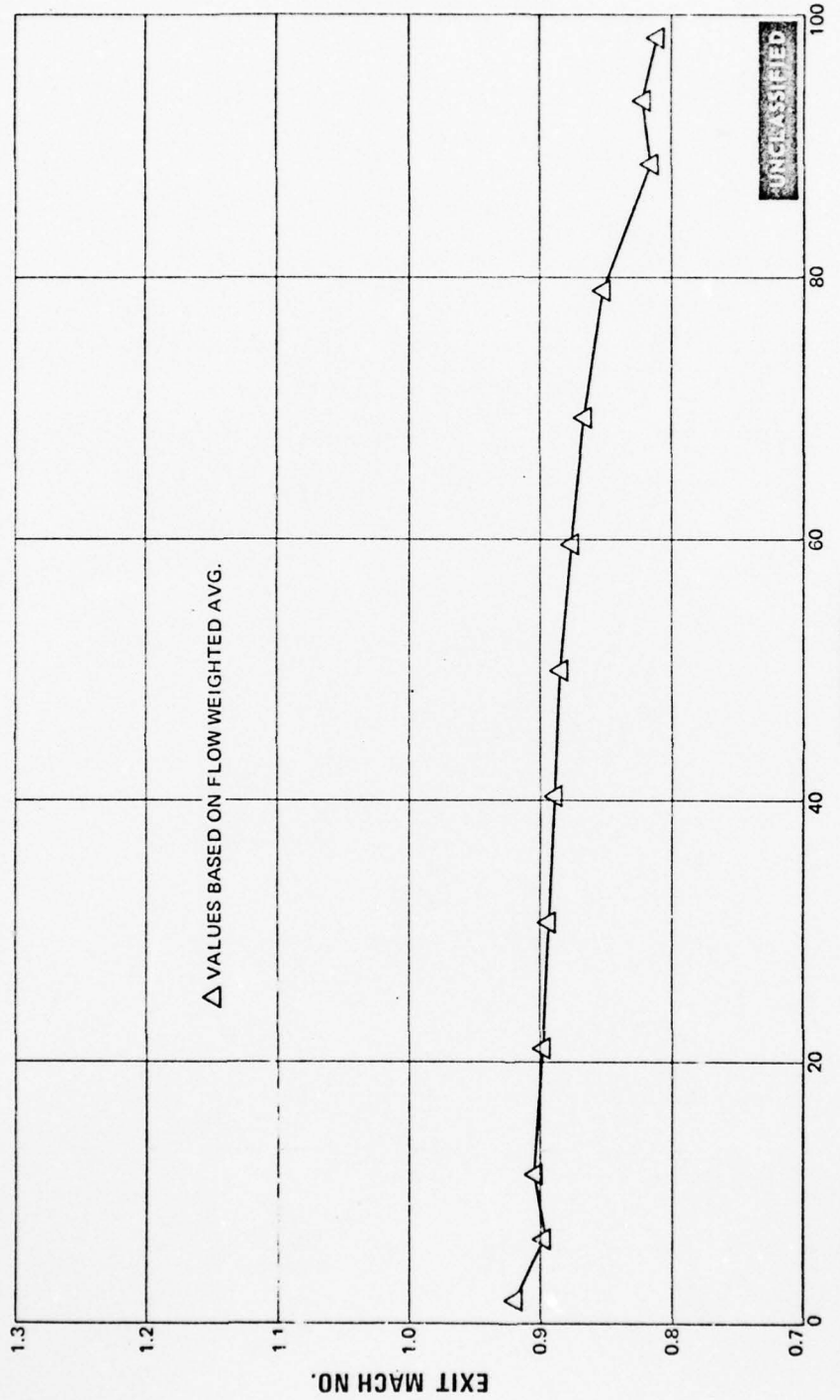

Figure 60 Spanwise Exit Mach Number Distribution, Second Vane - Screen Removed, Midspan Exit Mach No. = 0.885, Baseline With Redesigned Inlet Guide Vanes and Optimum Boundary Layer Bleeds

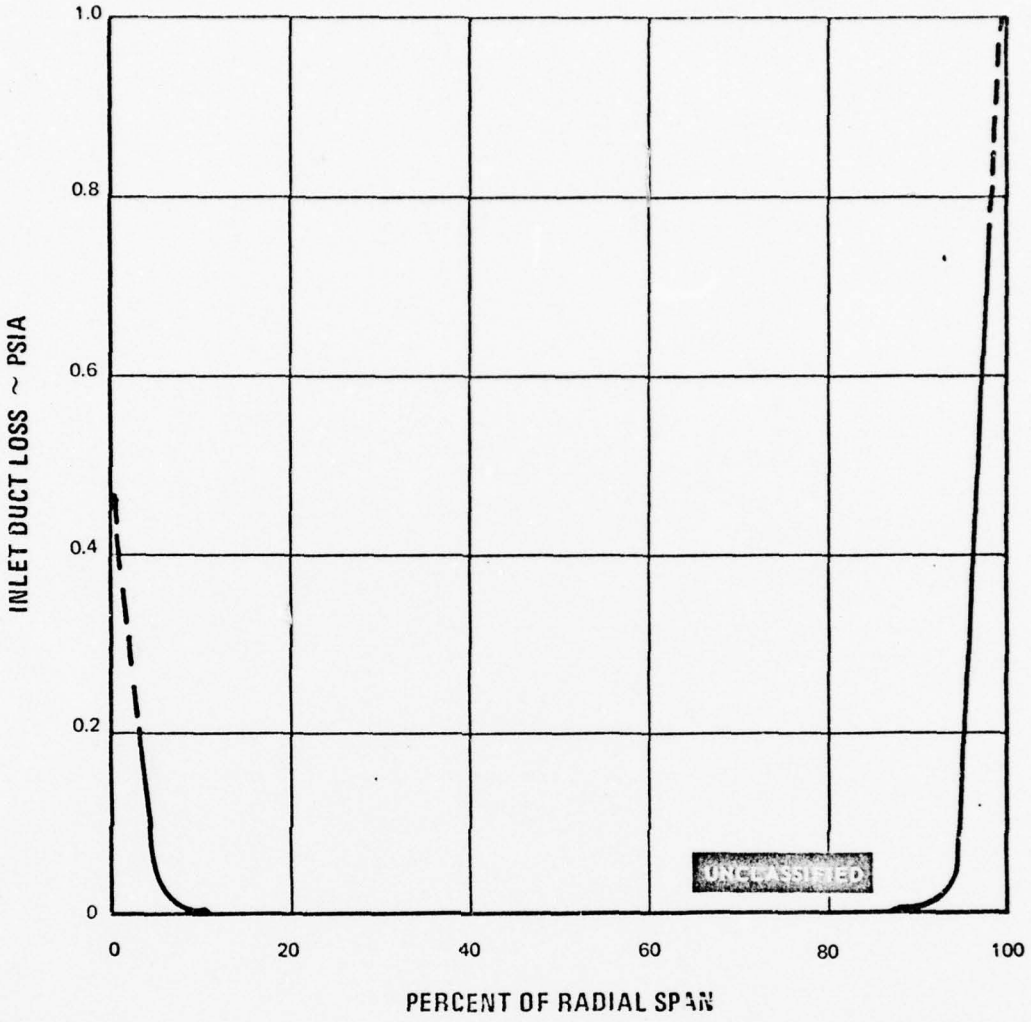

Figure 61 Inlet Duct Loss Versus Percent Radial Span—Second Vane Cascade With Redesigned Inlet Guide Vanes and Optimum Boundary Layer Bleeds

(U) An inlet screen was then installed in the cascade in order to restore a more realistic turbulence intensity level. The performance data of the baseline airfoil with the screen and optimum boundary layer bleeds are shown in Figures 62 through 67. It is important to note that the loss level (0.0326) duplicated the initial baseline value (0.034) within experimental accuracy (± 0.003). Oil and graphite flow visualization tests on these airfoils shown in Figures 68 and 69, indicated uniform, unseparated flow. Based on these results, the recontoured airfoil, contoured end-wall and recambered airfoil cascade packs were tested with the screen in the inlet. After these tests, the baseline evaluation was repeated in order to verify the integrity of these tests. The performance data of the repeated tests are shown in Figures 70 through 75. The airfoil surface static pressures are shown in Figures 76 through 78, and the flow visualization photographs in Figures 79 and 80. The repeated baseline tests (overall loss coefficient of 0.0349) verified the previous baseline (overall loss coefficient of 0.0326) very closely.

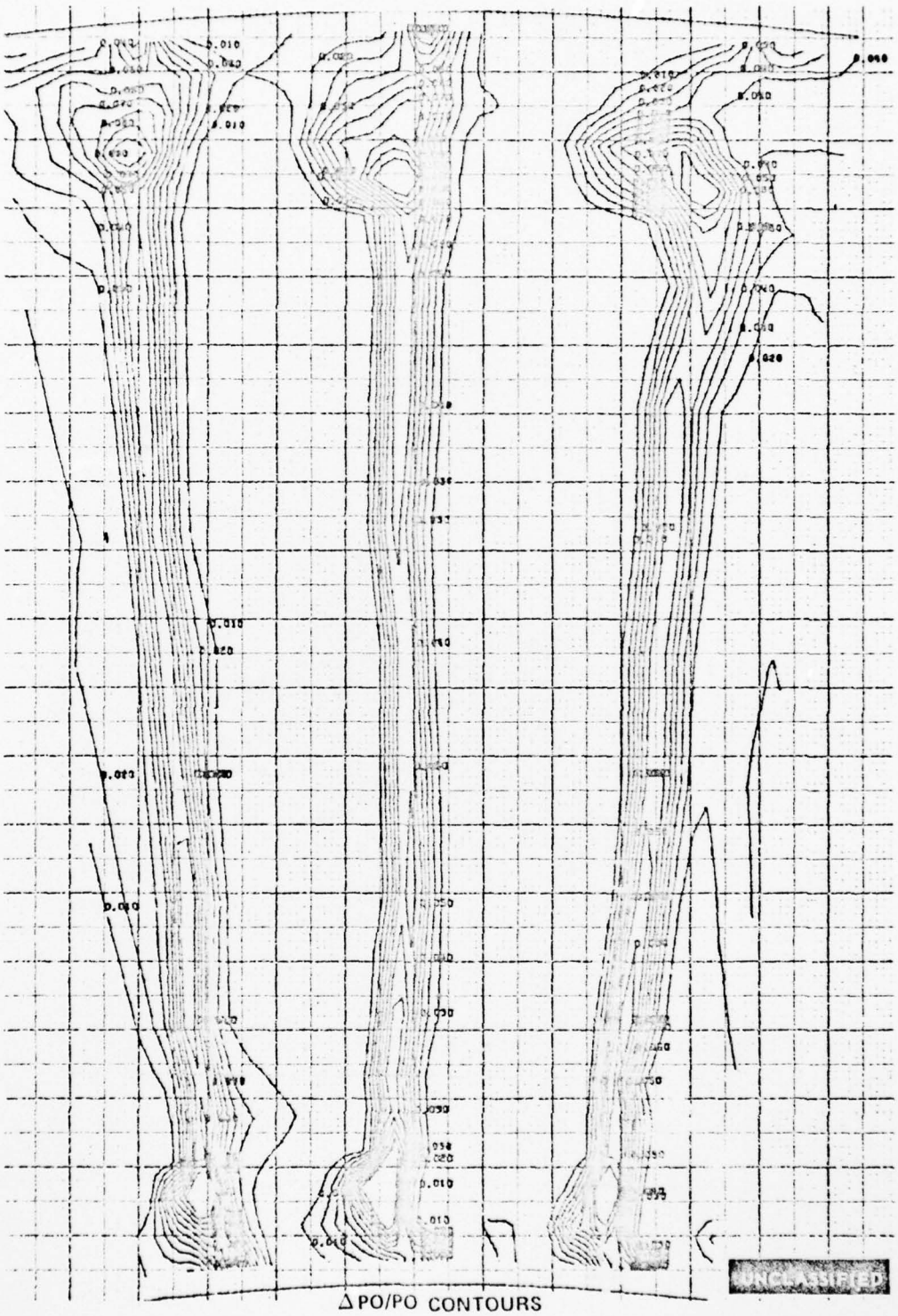

Figure 62 Pressure Loss Contours, Second Vane - Screen Installed, Three Flow Passages, Midspan Exit Mach No. 0.862, Baseline With Redesigned Inlet Guide Vanes and Optimum Boundary Layer Bleeds

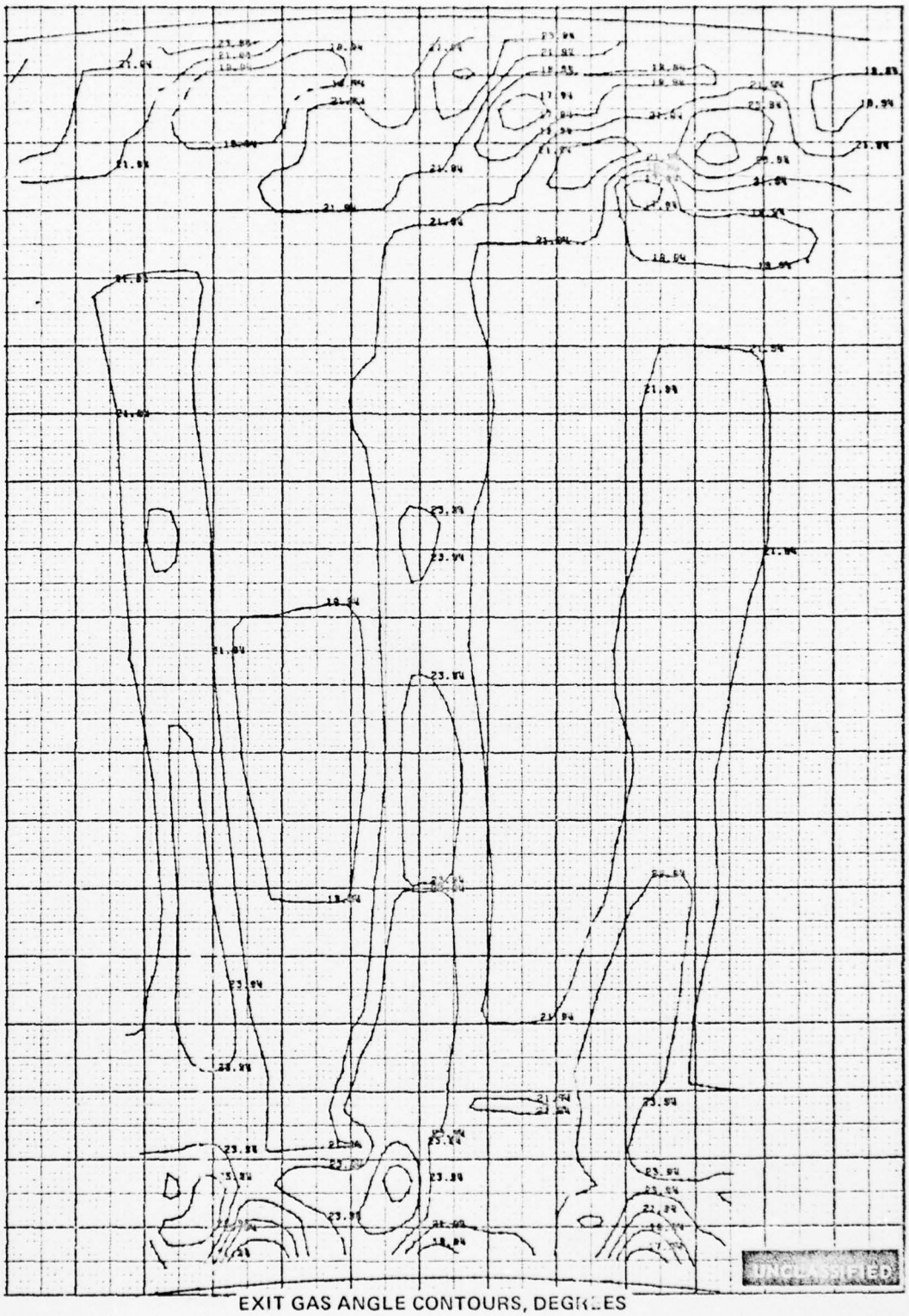

Figure 63 Exit Gas Angle Contours, Second Vane - Screen Installed, Three Flow Passages, Midspan Exit Mach No. = 0.862, Baseline With Redesigned Inlet Guide Vanes and Optimum Boundary Layer Bleeds

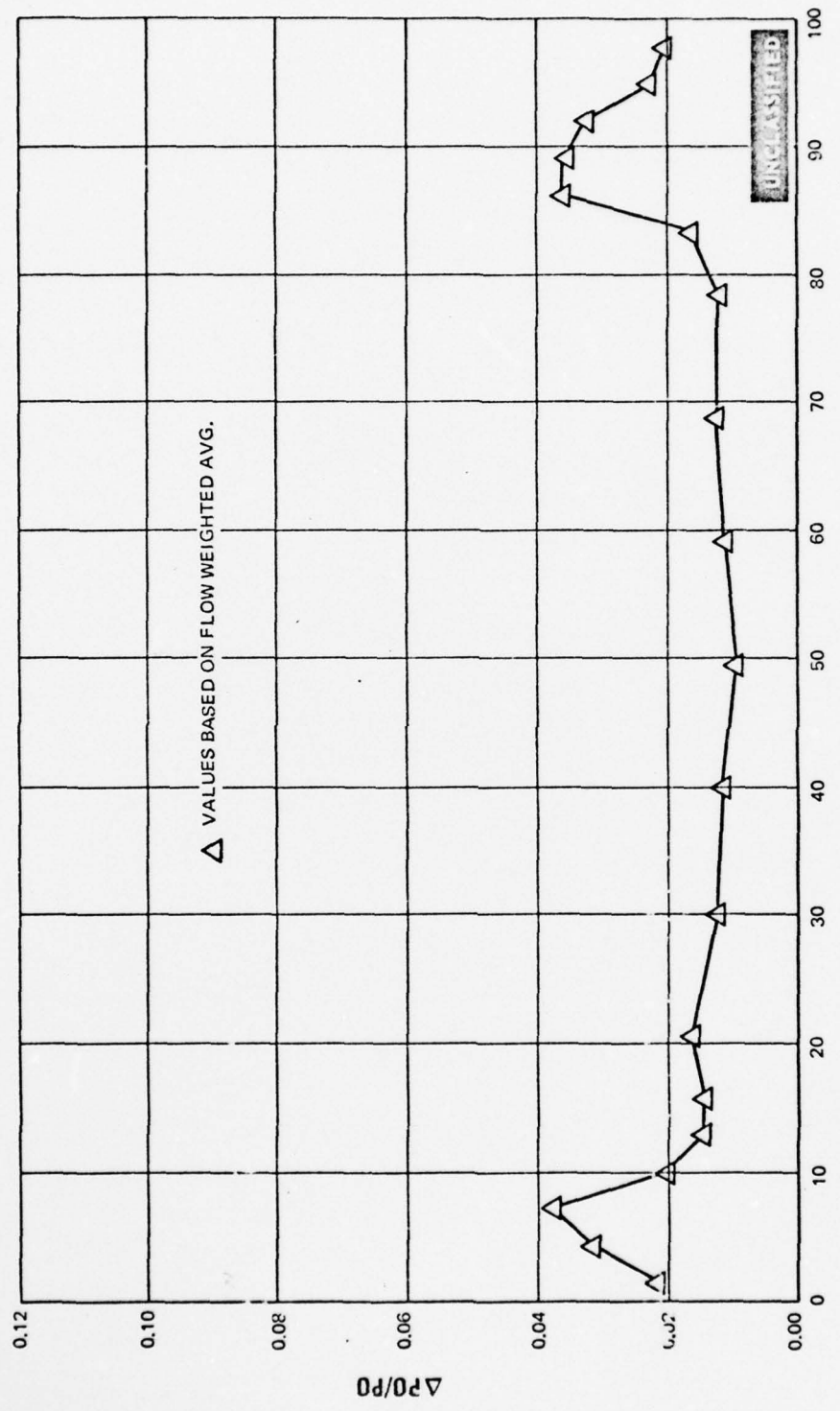

Figure 64 Spanwise Pressure Loss Distribution, Second Vane - Screen Installed, Midspan Exit Mach No. = 0.862, Baseline With Redesigned Inlet Guide Vanes and Optimum Boundary Layer Bleeds

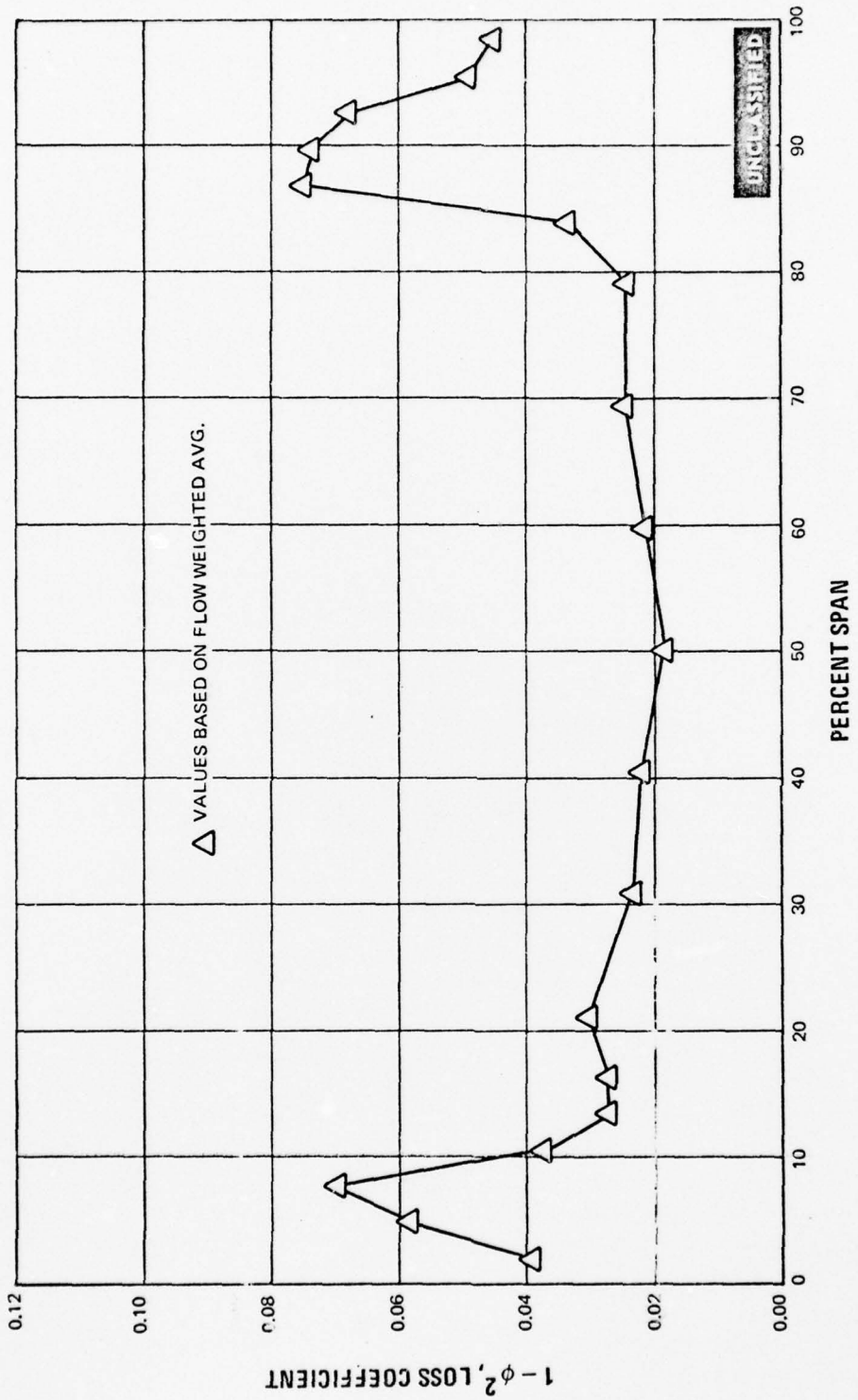

Figure 65 Spanwise Loss Coefficient Distribution, Second Vane - Screen Installed, Mid-span Exit Mach No. = 0.862, Baseline With Redesigned Inlet Guide Vanes and Optimum Boundary Layer Bleeds

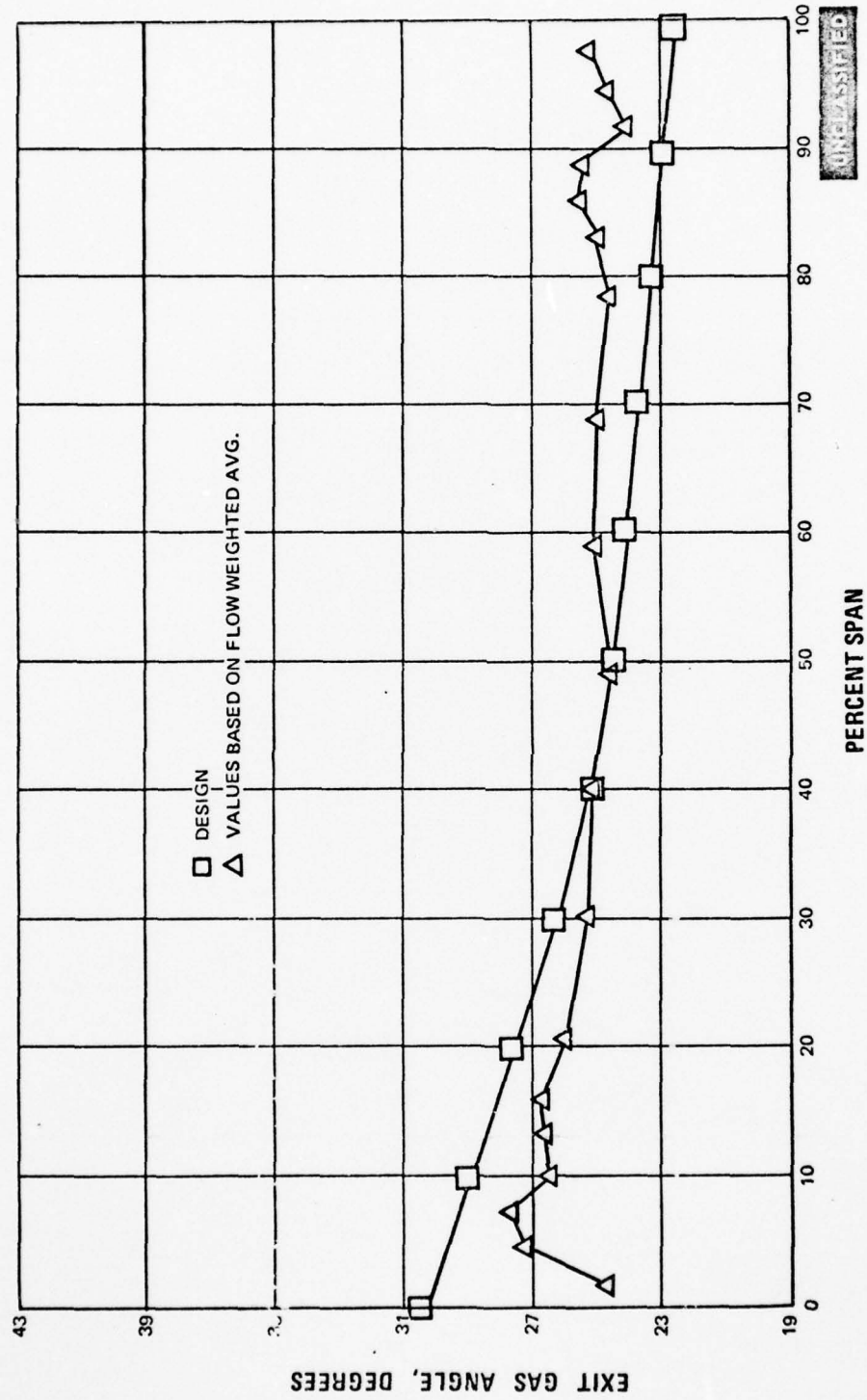

Figure 66 Spanwise Exit Gas Angle Distribution, Second Vane - Screen Installed, Midspan Exit Mach No. = 0.862, Baseline With Redesigned Inlet Guide Vanes and Optimum Boundary Layer Bleeds

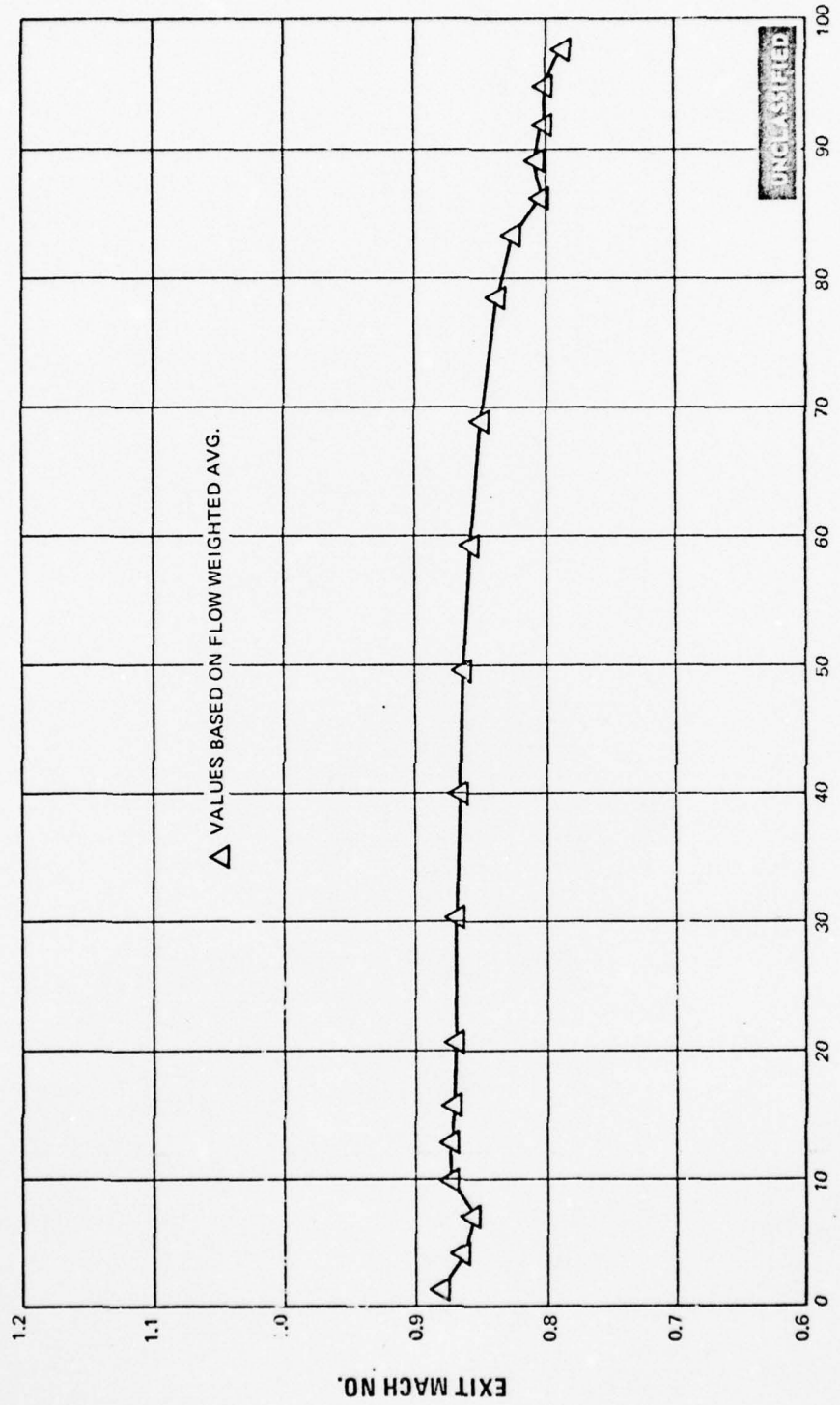

Figure 67 Spanwise Exit Mach Number Distribution, Second Vane - Screen Installed, Midspan Exit Mach No. = 0.862, Baseline With Redesigned Inlet Guide Vanes and Optimum Boundary Layer Bleeds

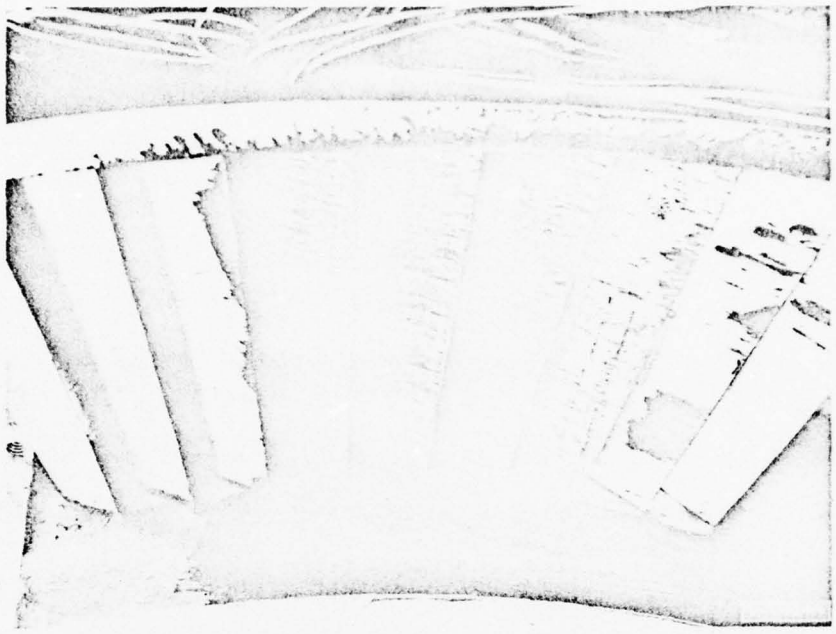

Figure 68 Oil and Graphite Flow Patterns–Second Vane with Redesigned Inlet Guide Vanes, Optimum Boundary Layer Bleeds and Screen Installed; View of Downstream Inside Diameter; Midspan Exit Mach No. =0.862

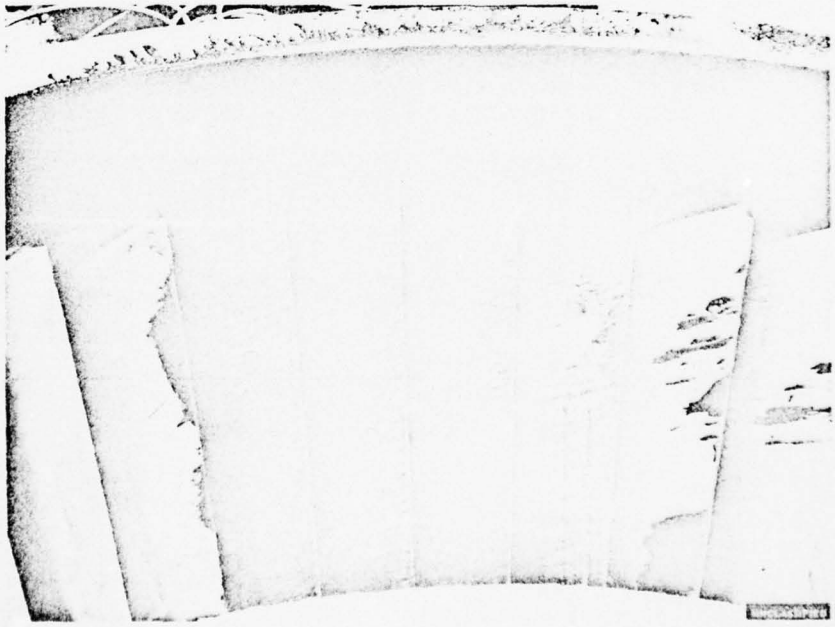

Figure 69 Oil and Graphite Flow Patterns–Second Vane with Redesigned Inlet Guide Vanes, Optimum Boundary Layer Bleeds and Screen Installed; View of Downstream Outside Diameter; Midspan Exit Mach No. =0.862

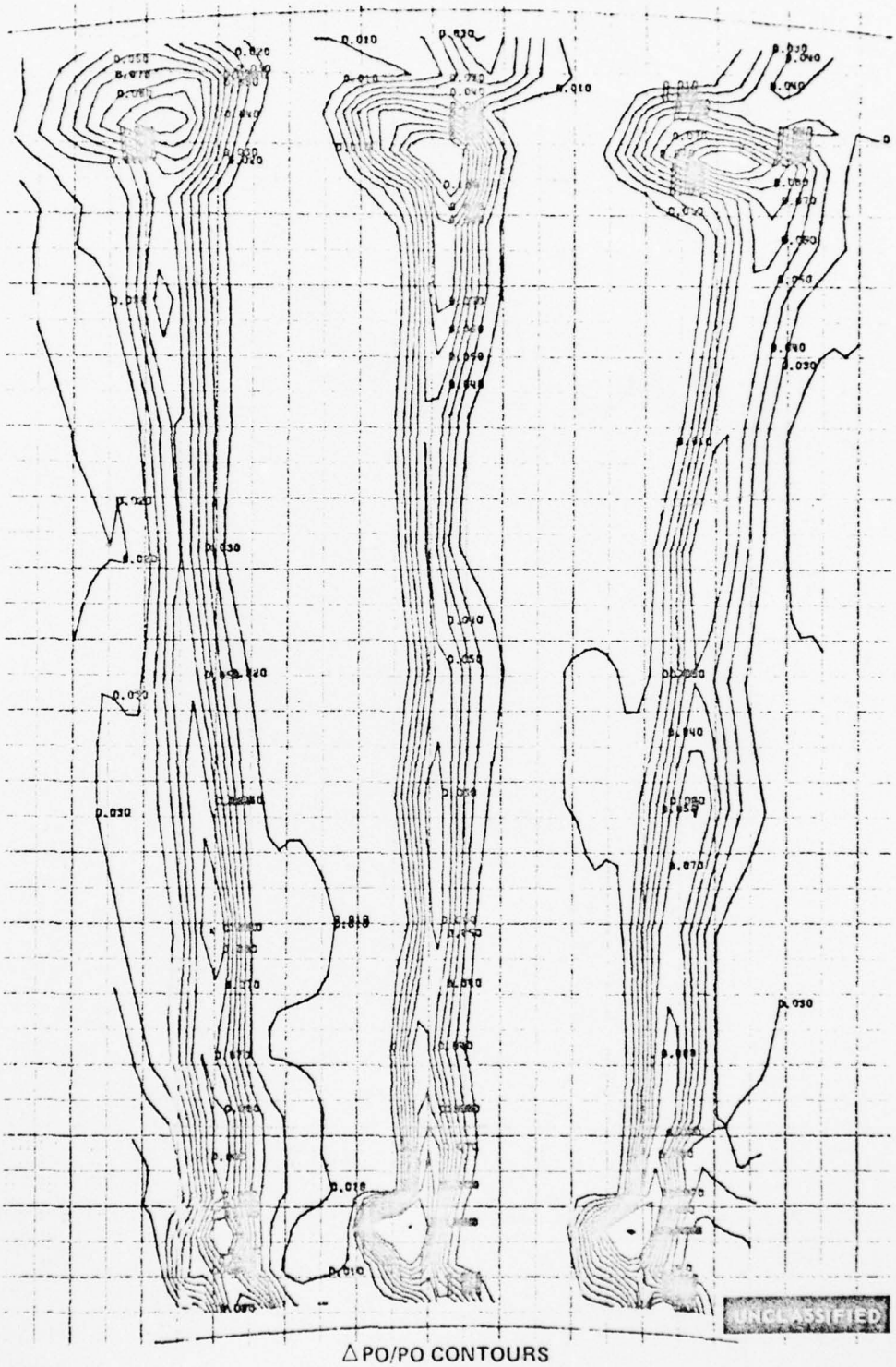

Figure 70 Pressure Loss Contours, Second Vane - Screen Installed, Three Flow Passages, Midspan Exit Mach No. = 0.860, Baseline With Redesigned Inlet Guide Vanes and Optimum Boundary Layer Bleeds

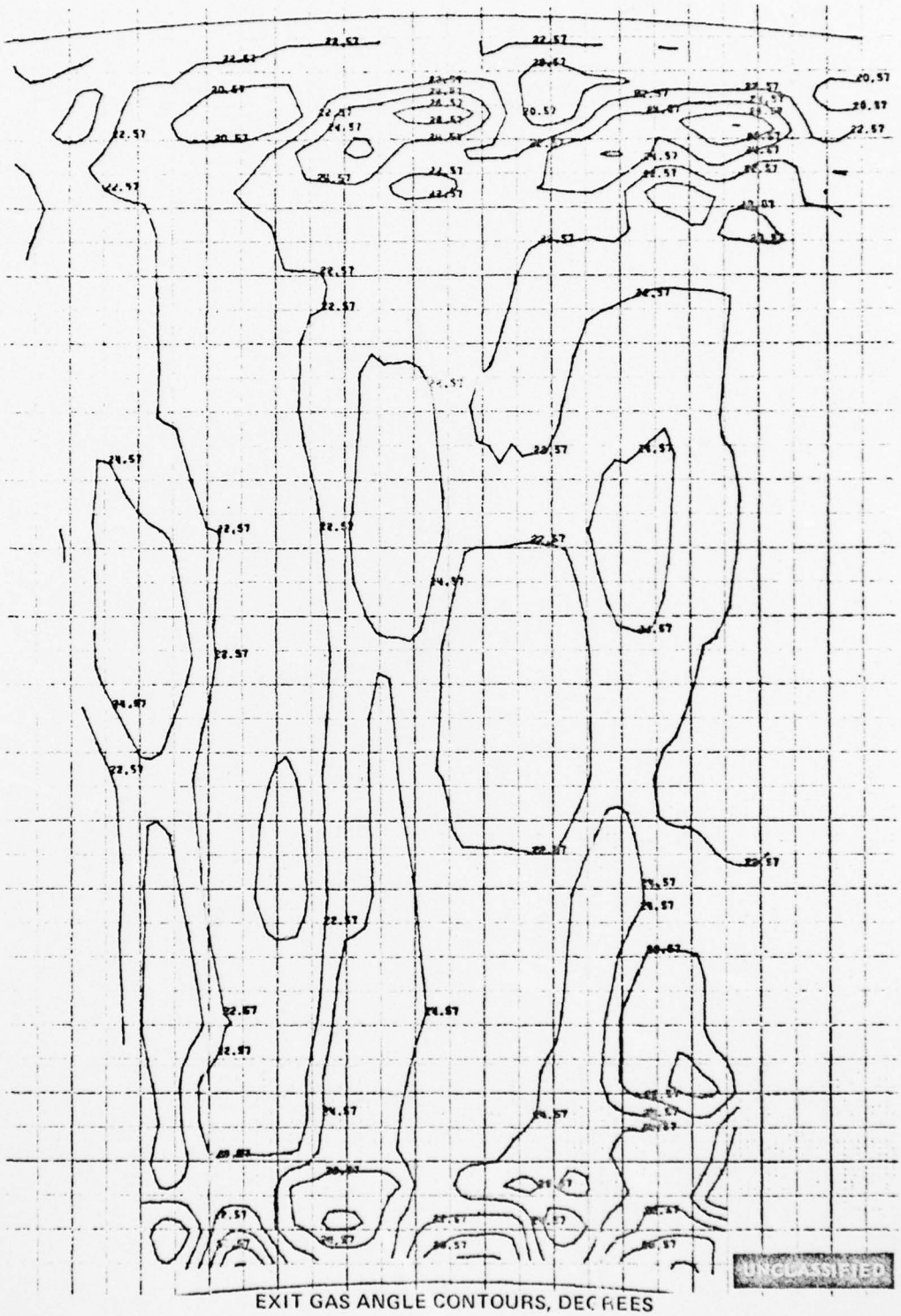

Figure 71 Exit Gas Angle Contours, Second Vane - Screen Installed, Three Flow Passages, Midspan Exit Mach No. = 0.860, Baseline With Redesigned Inlet Guide Vanes and Optimum Boundary Layer Bleeds

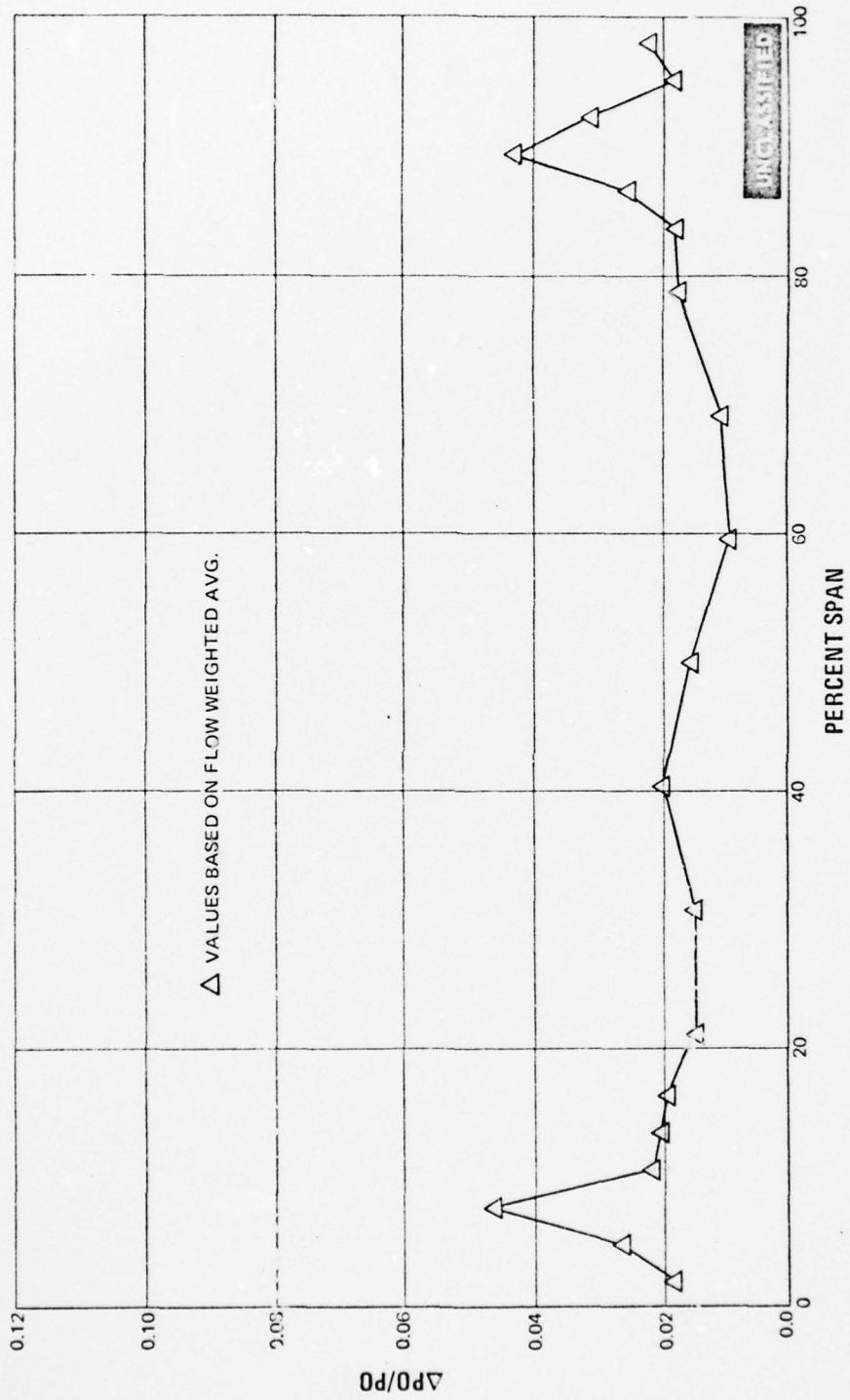

Figure 72 Spanwise Pressure Loss Distribution, Second Vane - Screen Installed, Midspan
Exit Mach No. = 0.860, Baseline With Redesigned Inlet Guide Vanes and
Optimum Boundary Layer Bleeds

AD-A056 285 PRATT AND WHITNEY AIRCRAFT GROUP EAST HARTFORD CONN F/G 21/5
INVESTIGATION OF A HIGHLY LOADED TWO-STAGE FAN-DRIVE TURBINE. V--ETC(U)
DEC 69 H WELNA, D E DAHLBERG, W H HEISER F33615-68-C-1208
UNCLASSIFIED PWA-3827 AFAPL-TR-69-92-VOL-4 NL

2 OF 3
AD
A056285

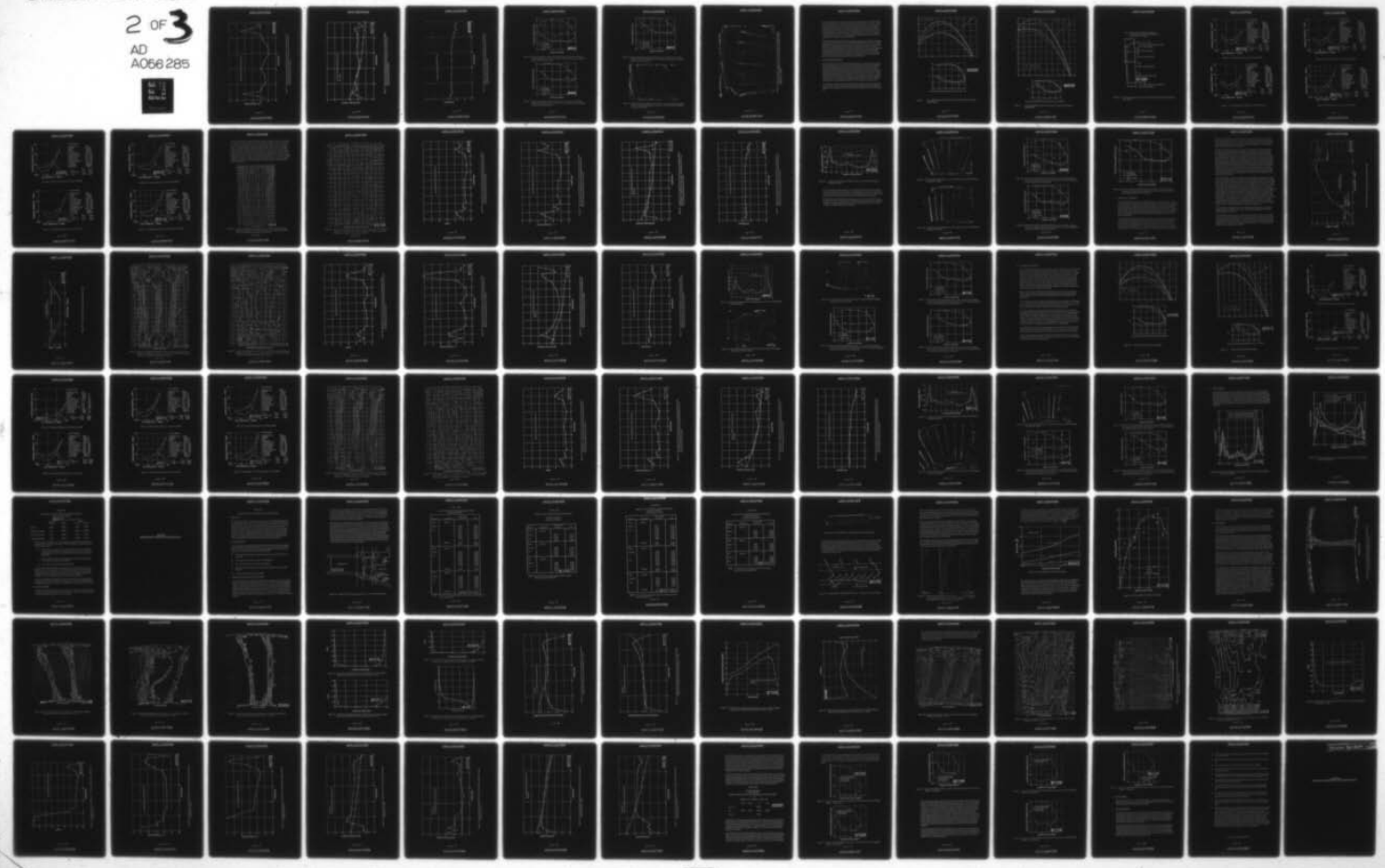

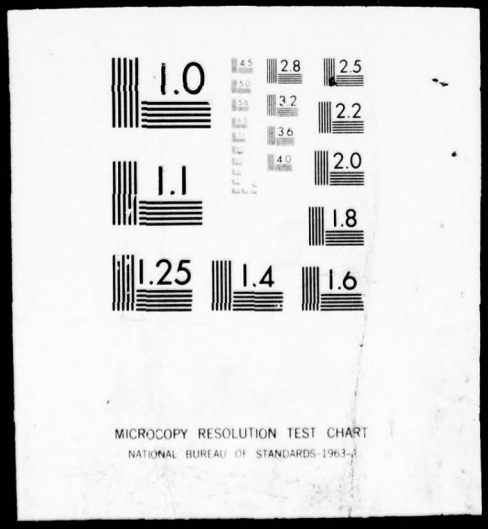

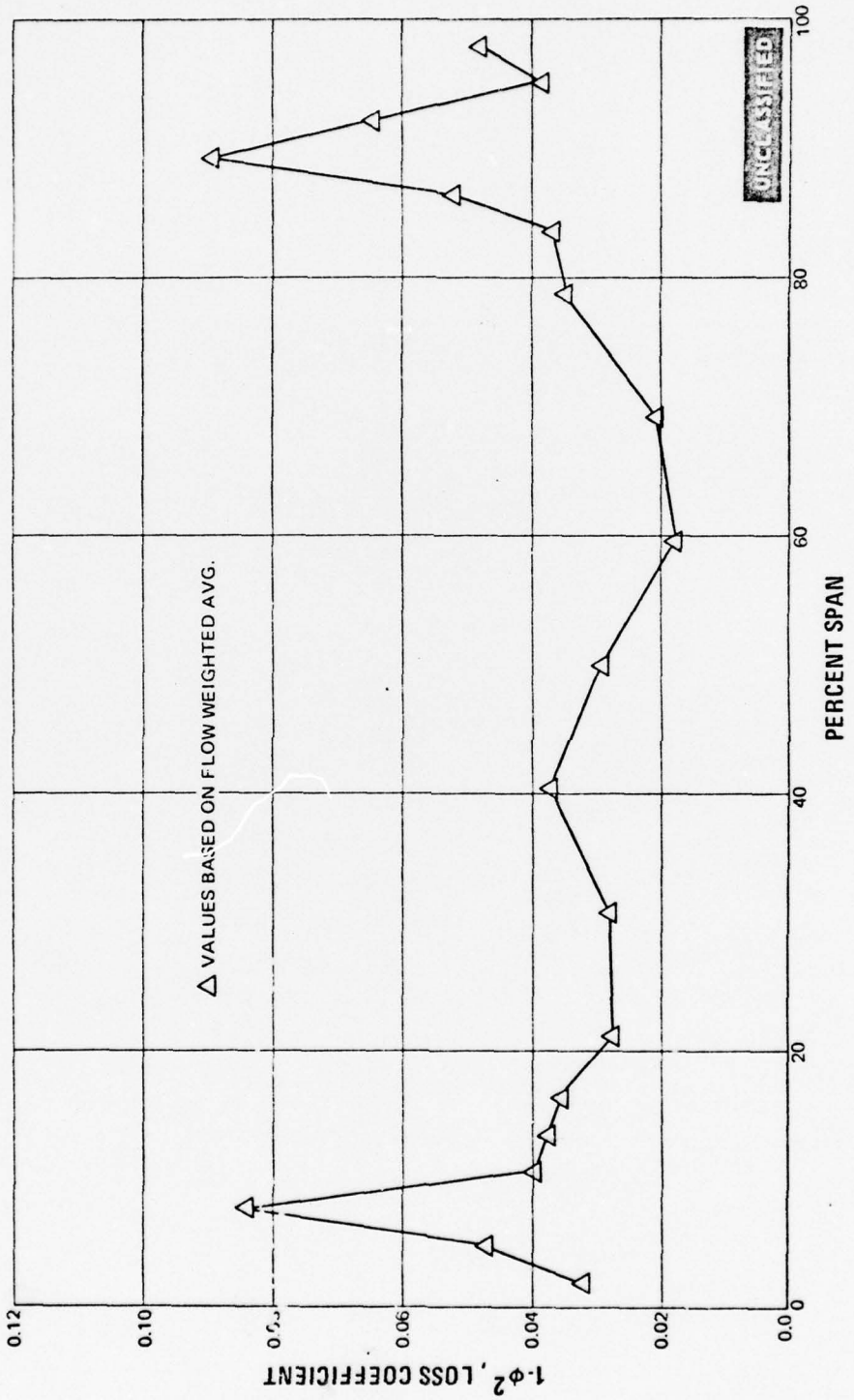

Figure 73 Spanwise Loss Coefficient Distribution, Second Vane - Screen Installed, Mid-span Exit Mach No. = 0.860, Baseline With Redesigned Inlet Guide Vanes and Optimum Boundary Layer Bleeds

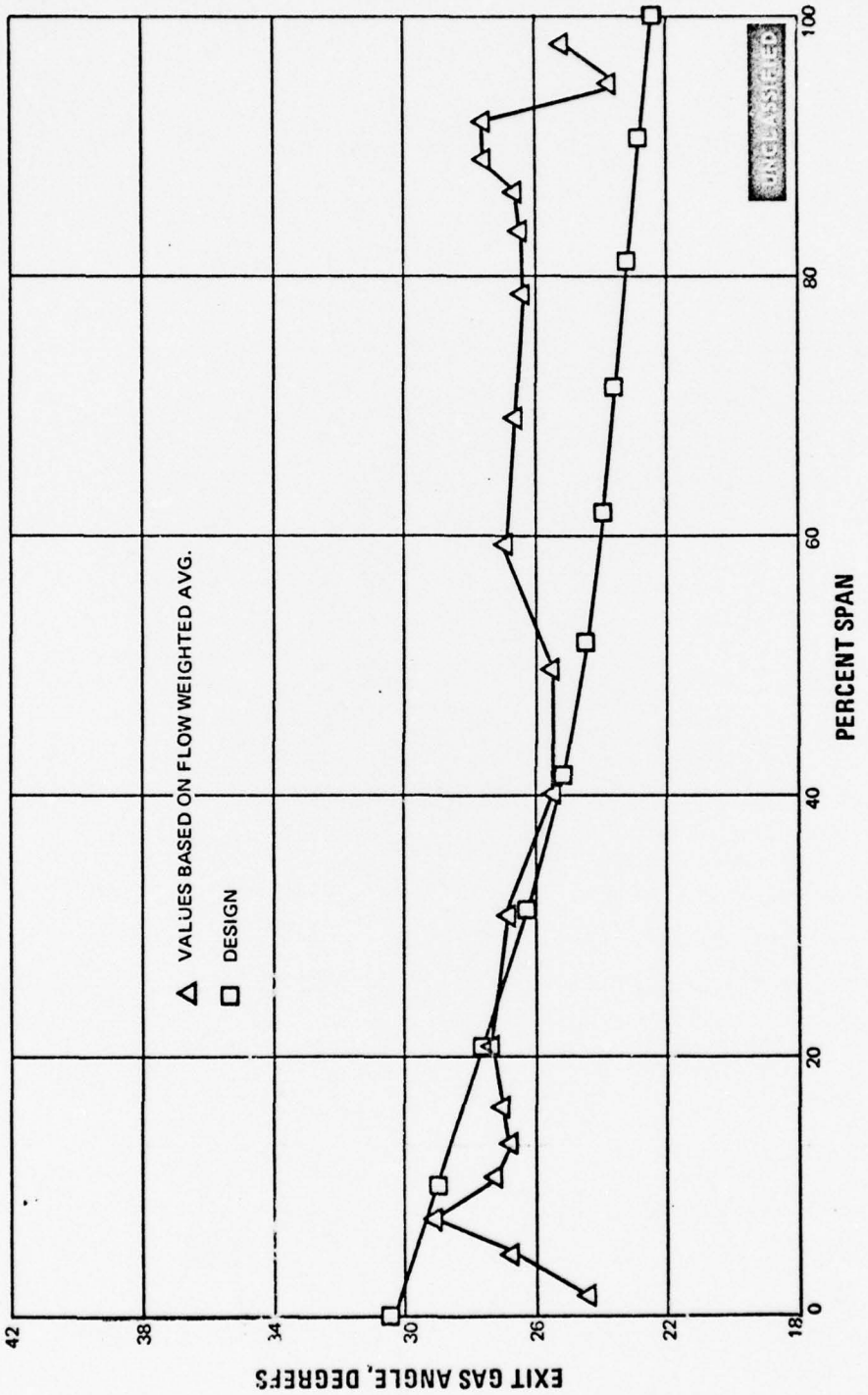

Figure 74 Spanwise Exit Gas Angle Distribution, Second Vane - Screen Installed, Midspan
Exit Mach No.= 0.860, Baseline With Redesigned Inlet Guide Vanes and
Optimum Boundary Layer Bleeds

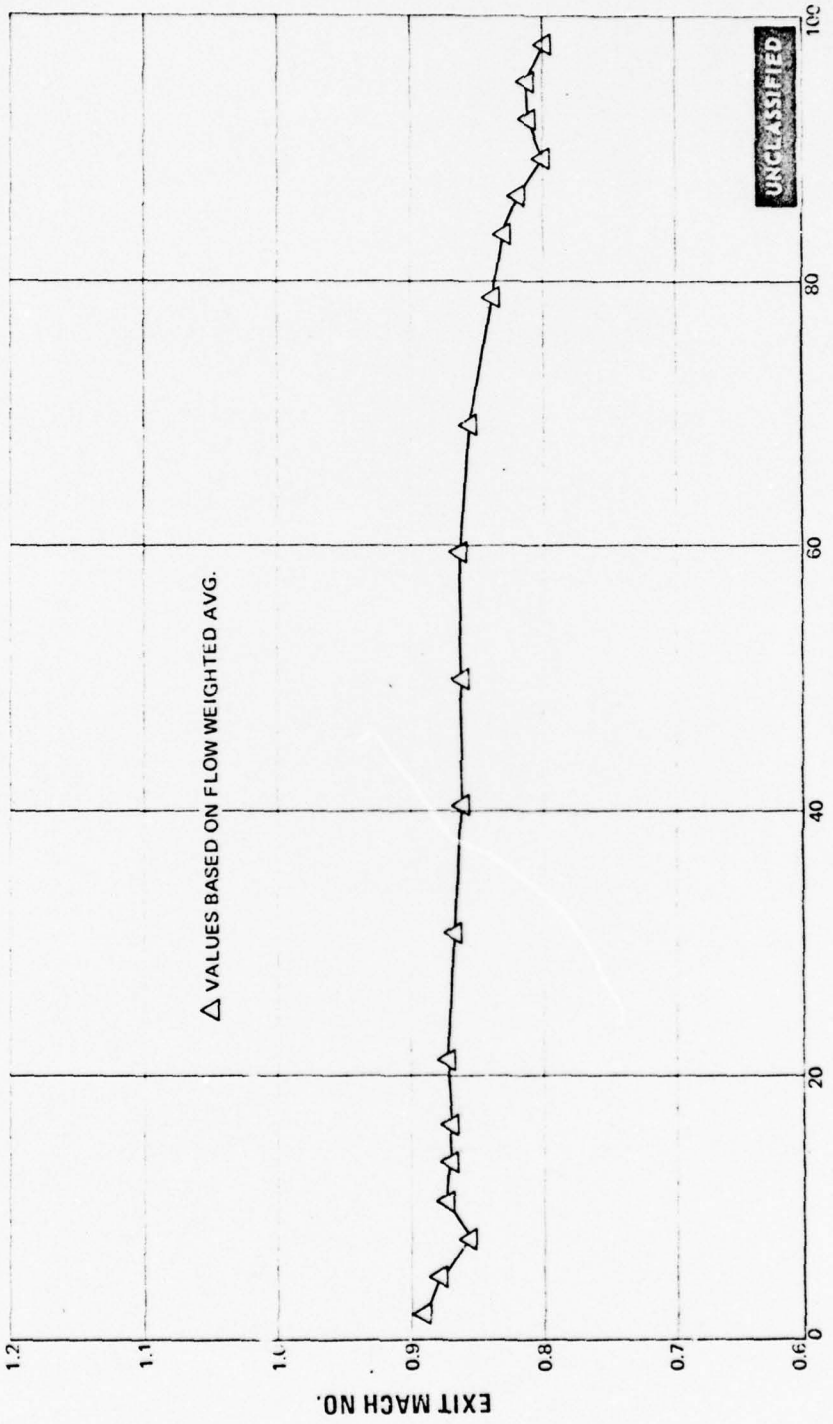

Figure 75 Spanwise Exit Mach Number Distribution, Second Vane - Screen Installed, Midspan Exit Mach No. = 0.860, Baseline With Redesigned Inlet Guide Vanes and Optimum Boundary Layer Bleeds

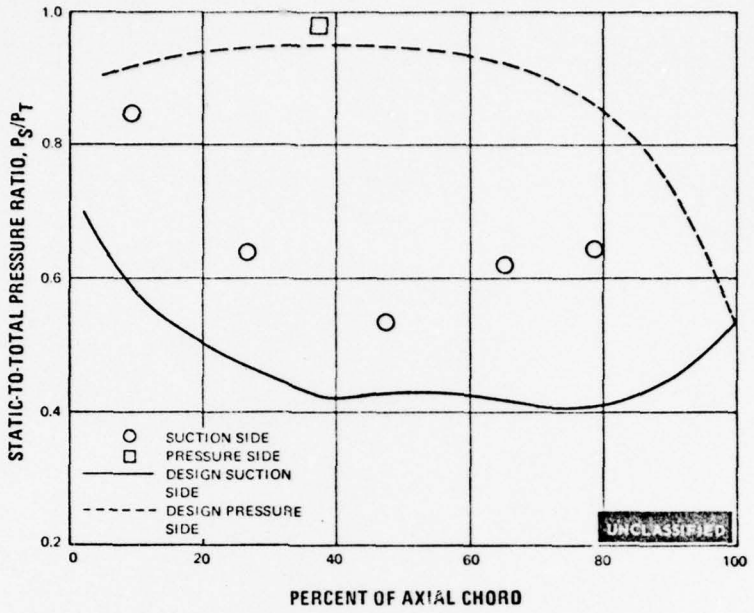

Figure 76 Static-to-Total Pressure Ratio Versus Percent of Axial Chord. Second Vane Baseline With Redesigned Inlet Guide Vanes. Optimum Boundary Layer Bleeds and Inlet Screen—Root Section

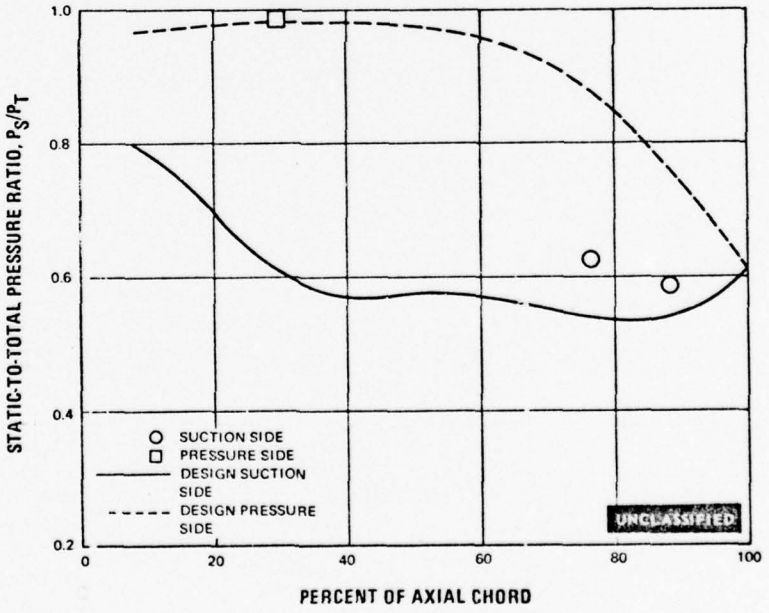

Figure 77 Static-to-Total Pressure Ratio Versus Percent of Axial Chord. Second Vane Baseline With Redesigned Inlet Guide Vanes. Optimum Boundary Layer Bleeds and Inlet Screen—Mean Section

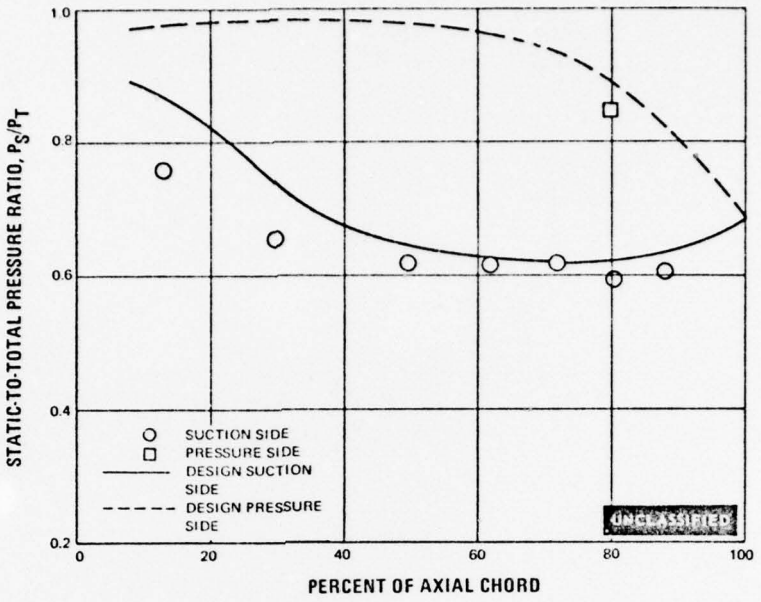

Figure 78 Static-to-Total Pressure Ratio Versus Percent of Axial Chord, Second Vane Baseline With Redesigned Inlet Guide Vanes, Optimum Boundary Layer Bleeds and Inlet Screen—Tip Section

Figure 79 Oil and Graphite Flow Patterns—Second Vane Baseline with Redesigned Inlet Guide Vanes, Optimum Boundary Layer Bleeds and Screen Installed; Midspan Exit Mach No. = 0.860

Figure 80 Oil and Graphite Flow Patterns—Second Vane Baseline with Redesigned Inlet Guide Vanes, Optimum Boundary Layer Bleeds and Screen Installed; Midspan Exit Mach No. = 0.860

(U) Turbine airfoils are, as we know, very sensitive to the location of boundary layer transition, which in turn is strongly affected by the inlet conditions. A good example is seen by the bump at the midspan airfoil loss coefficient in all the data, regardless of the end-wall treatment. The combination of the type of inlet guide vane, inlet duct geometry and inlet turbulence triggered the transition earlier in the middle of the airfoil than anywhere else, causing losses to be slightly higher there. However, since this feature consistently reappeared in all the remaining data, and since even the highest midspan loss coefficient level was comparable to the design value for the second vane, no further note was taken of this flow behavior.

(U) Even though the remainder of this program concentrates on end losses rather than profile losses, it was felt that the most reliable data would be obtained from the closest simulation of turbine conditions in an engine. Therefore, all of our experience indicates that these actual conditions were met with the redesigned inlet guide vane which set the proper test airfoil conditions, the optimized boundary layer bleeds which minimized the effect of the inlet boundary layer effects, and the inlet screen which maintains engine-type turbulence intensity. Therefore, the effects of airfoil recontouring, end-wall recontouring and airfoil recambering were investigated with the redesigned inlet guide vane, optimum boundary layer bleed and an inlet screen.

6. RECONTOURED AIRFOILS

(U) One method of reducing the end wall losses that was investigated was local recontouring of the baseline second vane airfoil. The airfoil surface static pressure gradient over the leading portion was reduced in order to decrease the loading at the airfoil leading edge, while keeping the overall loading constant. A comparison of the baseline root and tip airfoil profiles with the recontoured profiles, along with the predicted airfoil surface static pressure distributions is shown in Figures 81 and 82. These root and tip recontoured sections were faired into the existing midspan contour at approximately the 25 and 75 percent span locations. These changes are intended to delay the onset of strong secondary flow in the upstream portion of the channel and thereby, to reduce the total accumulation of losses near the airfoil suction surface corners.

(U) The elevation of the recontoured second vane is shown in Figure 83, and the profiles of the airfoil section are presented in Figures 84 through 91. The fabrication coordinates for each airfoil profile are tabulated in Tables XIII through XX of the Appendix.

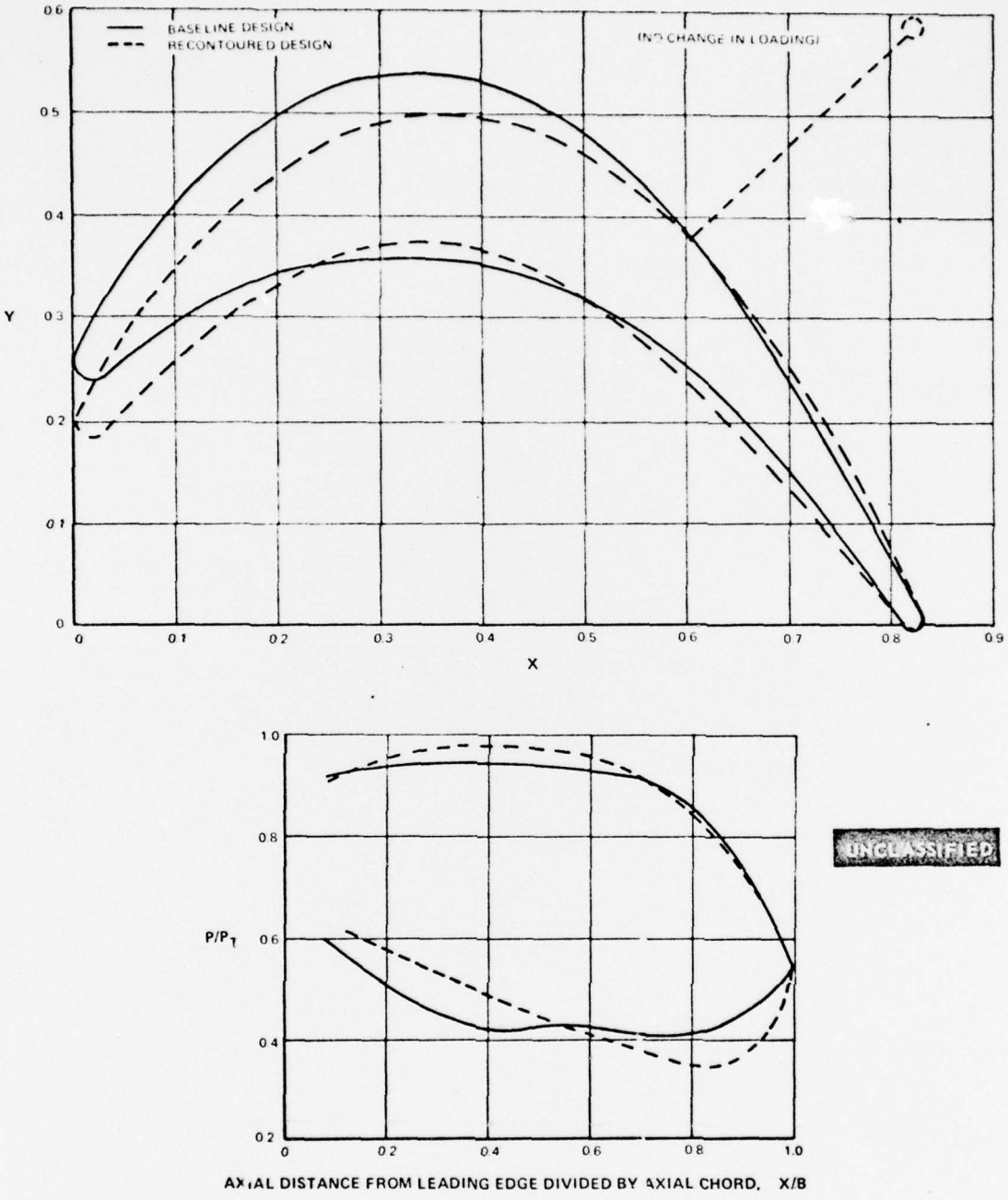

Figure 81 Second Vane Baseline Airfoil Recontouring Root Section Static Pressure Redistribution

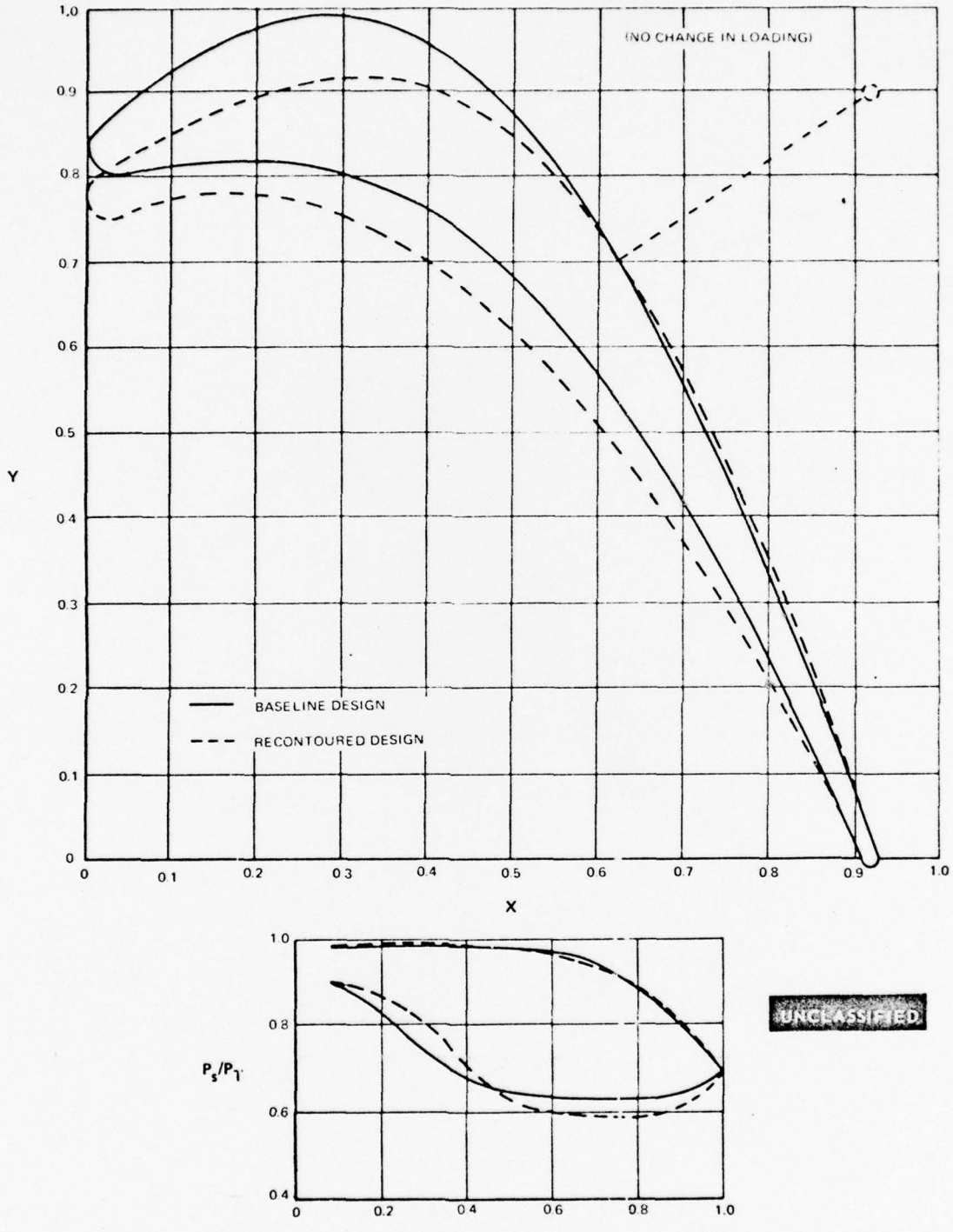

Figure 82 Second Vane Baseline Airfoil Recontouring, Tip Section Static Pressure Redistribution

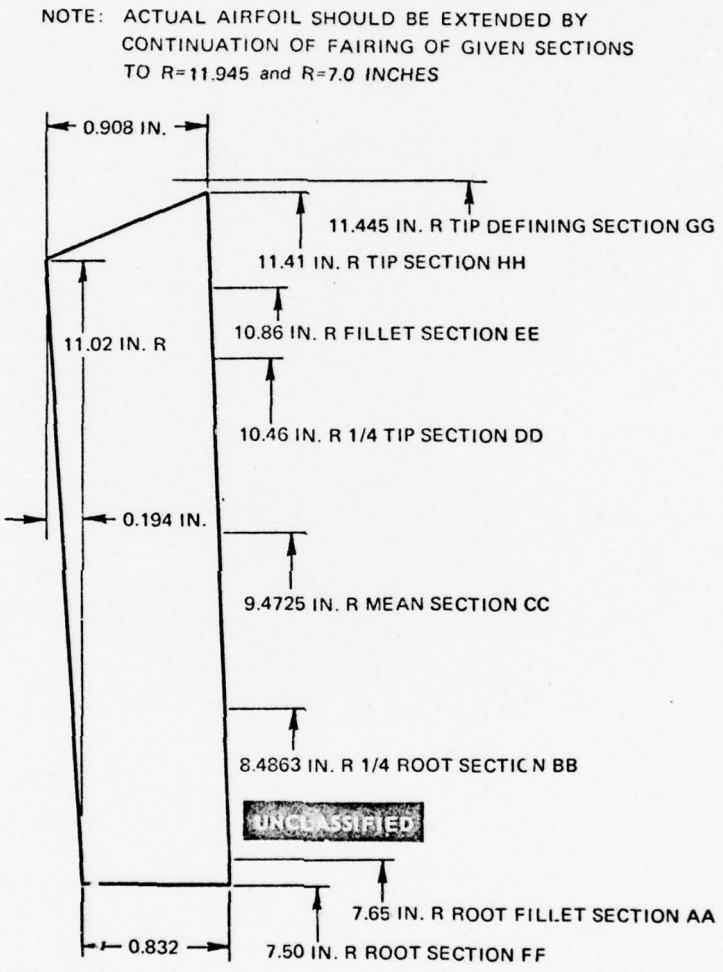

Figure 83 Elevation and Section Location of the Recambered and Recontoured Second Vane Airfoils

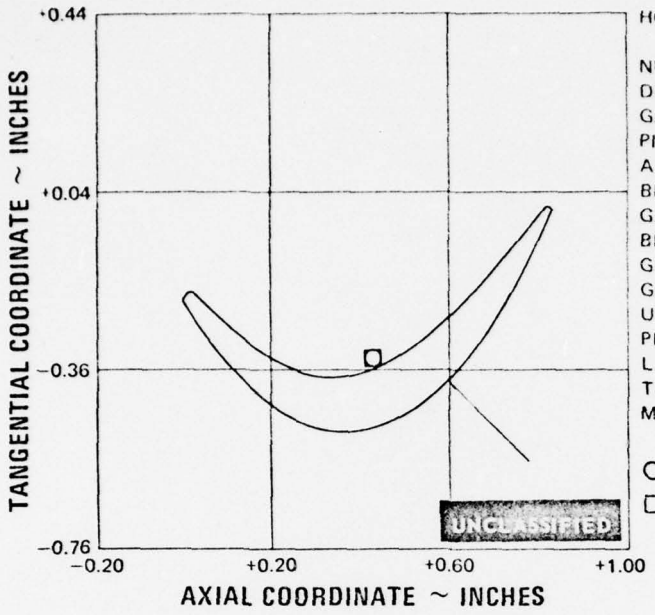

HOT DIMENSIONS

NUMBER OF FOILS	80.00	
DIAMETER	15.0000	IN.
GAGING	0.2941	IN.
PITCH	0.5890	IN.
AXIAL WIDTH	0.8320	IN.
BLADE INLET ANGLE	37.33	DEG.
GAS INLET ANGLE	37.33	DEG.
BLADE EXIT ANGLE	30.57	DEG.
GAS EXIT ANGLE	30.57	DEG.
GAGING ANGLE	29.95	DEG.
UNCOVERED TURNING	20.09	DEG.
PRINCIPAL AXIS	−17.16	DEG.
L. E. RADIUS	0.0175	IN.
T. E. RADIUS	0.0100	IN.
METAL AREA	0.0920	$IN.^2$

	X	Y
○ C. G.	0.4301	−0.3316
□ RADIAL REF.	0.4301	−0.3316
GAGE	0.6024	−0.3787

Figure 84 Recontoured Second Vane, Root Section (FF)

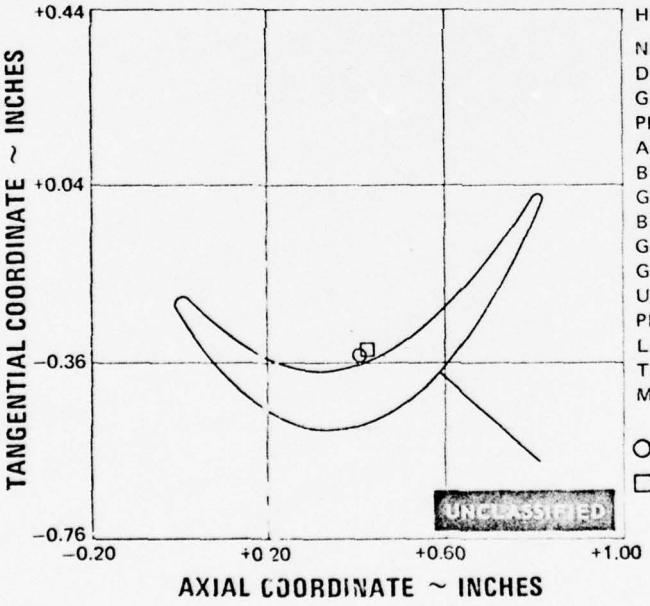

HOT DIMENSIONS

NUMBER OF FOILS	80.00	
DIAMETER	15.3000	IN.
GAGING	0.2962	IN.
PITCH	0.6008	IN.
AXIAL WIDTH	0.8357	IN.
BLADE INLET ANGLE	37.73	DEG.
GAS INLET ANGLE	38.00	DEG.
BLADE EXIT ANGLE	30.02	DEG.
GAS EXIT ANGLE	29.80	DEG.
GAGING ANGLE	29.54	DEG.
UNCOVERED TURNING	18.25	DEG.
PRINCIPAL AXIS	−19.33	DEG.
L. E. RADIUS	0.0185	IN.
T. E. RADIUS	0.0100	IN.
METAL AREA	0.0950	$IN.^2$

	X	Y
○ C. G.	0.4125	−0.3438
□ RADIAL REF.	0.4301	−0.3316
GAGE	0.5916	−0.3820

Figure 85 Recontoured Second Vane, Root Fillet Section (AA)

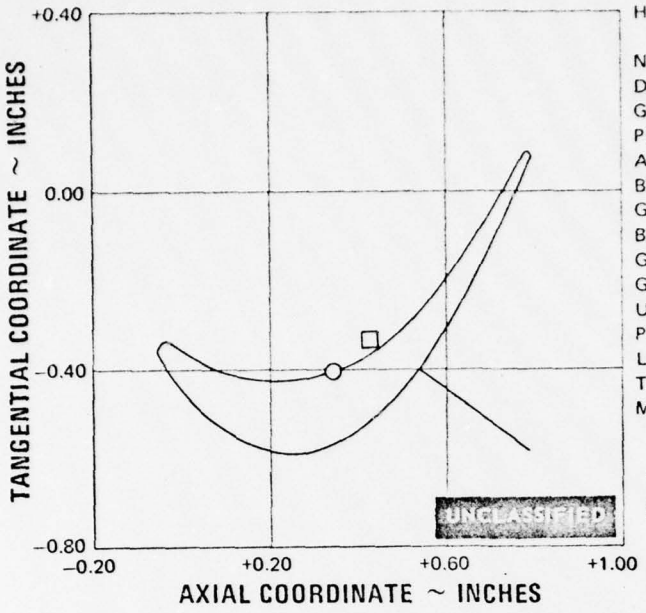

HOT DIMENSIONS

NUMBER OF FOILS	80.00
DIAMETER	16.9726 IN.
GAGING	0.3033 IN.
PITCH	0.6665 IN.
AXIAL WIDTH	0.8565 IN.
BLADE INLET ANGLE	42.10 DEG.
GAS INLET ANGLE	42.10 DEG.
BLADE EXIT ANGLE	27.17 DEG.
GAS EXIT ANGLE	27.17 DEG.
GAGING ANGLE	27.07 DEG.
UNCOVERED TURNING	12.00 DEG.
PRINCIPAL AXIS	−29.78 DEG.
L. E. RADIUS	0.0225 IN.
T. E. RADIUS	0.0100 IN.
METAL AREA	0.1068 IN.^{2}

	X	Y
○ C. G.	0.3464	−0.4008
□ RADIAL REF.	0.4301	−0.3316
GAGE	0.5419	−0.3982

Figure 86 Recontoured Second Vane, ¼ Root Section (BB)

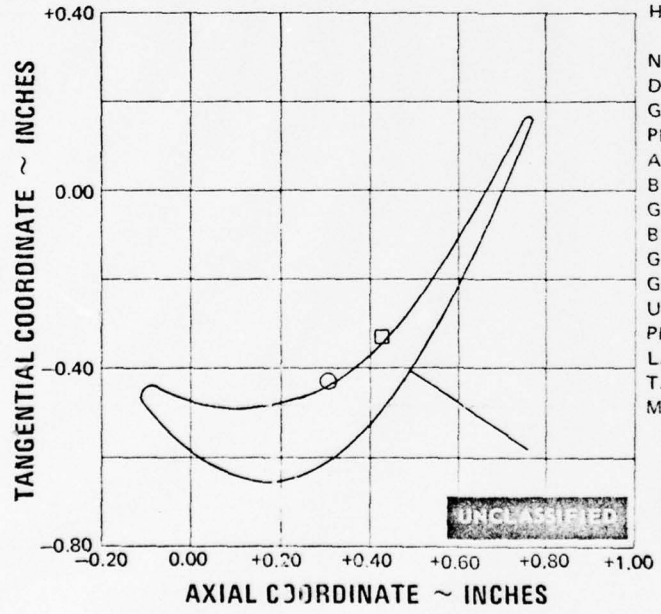

HOT DIMENSIONS

NUMBER OF FOILS	80.00
DIAMETER	18.9450 IN.
GAGING	0.3115 IN.
PITCH	0.7440 IN.
AXIAL WIDTH	0.8810 IN.
BLADE INLET ANGLE	50.50 DEG.
GAS INLET ANGLE	50.50 DEG.
BLADE EXIT ANGLE	24.58 DEG.
GAS EXIT ANGLE	24.58 DEG.
GAGING ANGLE	24.75 DEG.
UNCOVERED TURNING	10.67 DEG.
PRINCIPAL AXIS	−38.90 DEG.
L. E. RADIUS	0.0250 IN.
T. E. RADIUS	0.0100 IN.
METAL AREA	0.1117 IN.^{2}

	X	Y
○ C. G.	0.3086	−0.4308
□ RADIAL REF.	0.4301	−0.3316
GAGE	0.4937	−0.4080

Figure 87 Recontoured Second Vane, Mean Section (CC)

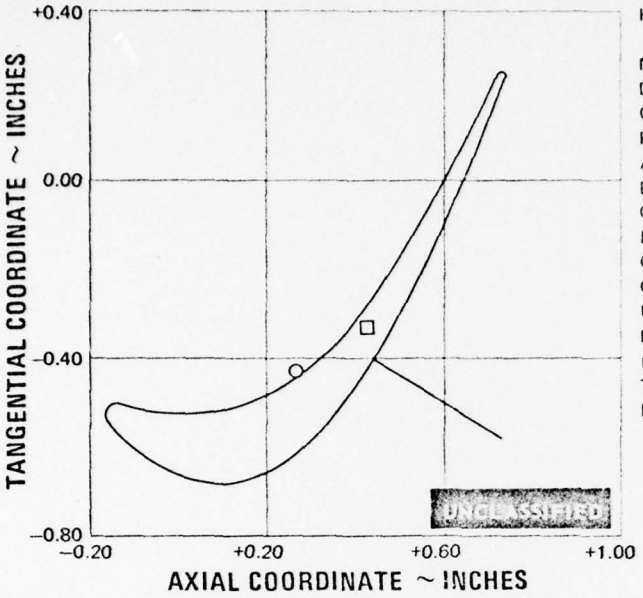

HOT DIMENSIONS

NUMBER OF FOILS	80.00	
DIAMETER	20.9200	IN.
GAGING	0.3307	IN.
PITCH	0.8215	IN.
AXIAL WIDTH	0.9055	IN.
BLADE INLET ANGLE	57.41	DEG.
GAS INLET ANGLE	57.40	DEG.
BLADE EXIT ANGLE	23.60	DEG.
GAS EXIT ANGLE	23.60	DEG.
GAGING ANGLE	23.74	DEG.
UNCOVERED TURNING	9.79	DEG.
PRINCIPAL AXIS	-43.78	DEG.
L. E. RADIUS	0.0275	IN.
T. E. RADIUS	0.0100	IN.
METAL AREA	0.1166	$IN.^2$

	X	Y
○ C. G.	0.2691	-0.4297
□ RADIAL REF.	0.4301	-0.3316
GAGE	0.4425	-0.4034

Figure 88 Recontoured Second Vane, ¼ Tip Section (DD)

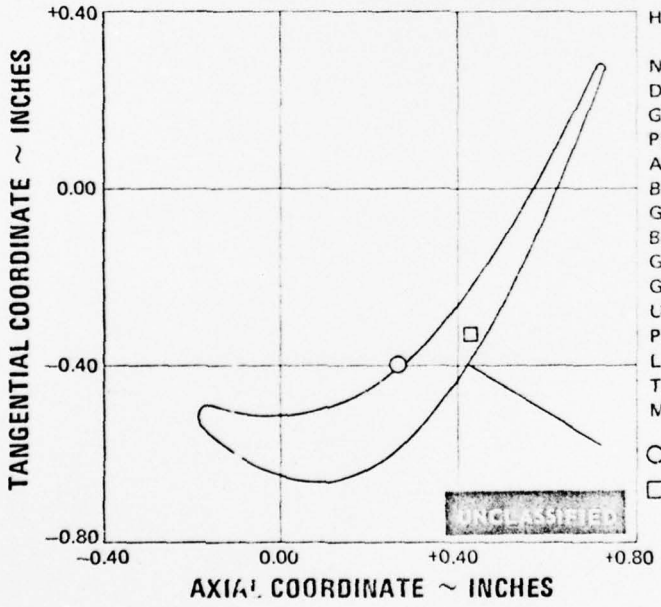

HOT DIMENSIONS

NUMBER OF FOILS	80.00	
DIAMETER	21.7200	IN.
GAGING	0.3378	IN.
PITCH	0.8529	IN.
AXIAL WIDTH	0.9155	IN.
BLADE INLET ANGLE	59.76	DEG.
GAS INLET ANGLE	59.90	DEG.
BLADE EXIT ANGLE	23.25	DEG.
GAS EXIT ANGLE	23.26	DEG.
GAGING ANGLE	23.33	DEG.
UNCOVERED TURNING	10.84	DEG.
PRINCIPAL AXIS	-44.49	DEG.
L. E. RADIUS	0.0279	IN.
T. E. RADIUS	0.0100	IN.
METAL AREA	0.1242	$IN.^2$

	X	Y
○ C. G.	0.2674	-0.3990
□ RADIAL REF.	0.4301	-0.3316
GAGE	0.4248	-0.3980

Figure 89 Recontoured Second Vane, Fillet Section (EE)

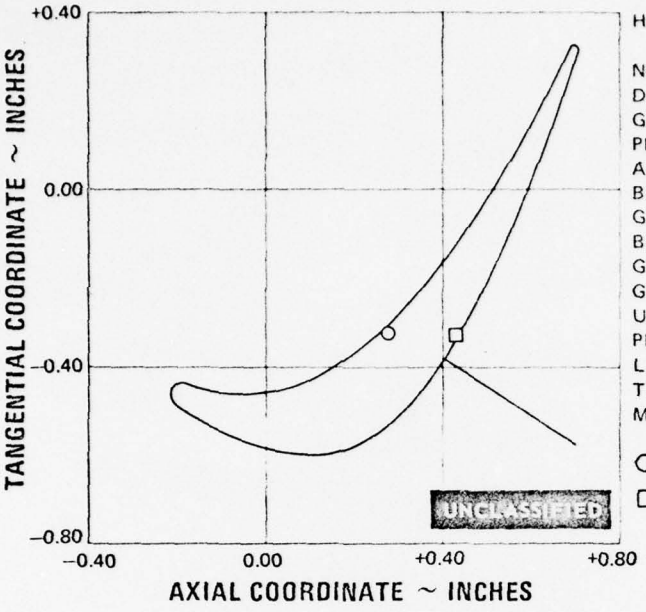

HOT DIMENSIONS

NUMBER OF FOILS	80.00	
DIAMETER	22.8200	IN.
GAGING	0.3455	IN.
PITCH	0.8961	IN.
AXIAL WIDTH	0.9291	IN.
BLADE INLET ANGLE	62.72	DEG.
GAS INLET ANGLE	62.75	DEG.
BLADE EXIT ANGLE	22.62	DEG.
GAS EXIT ANGLE	22.57	DEG.
GAGING ANGLE	22.68	DEG.
UNCOVERED TURNING	14.21	DEG.
PRINCIPAL AXIS	−44.57	DEG.
L. E. RADIUS	0.0276	IN.
T. E. RADIUS	0.0100	IN.
METAL AREA	0.1423	IN.^{2}

	X	Y
○ C. G.	0.2801	−0.3265
□ RADIAL REF.	0.4301	−0.3316
GAGE	0.4061	−0.3857

Figure 90 Recontoured Second Vane, Tip Section (HH)

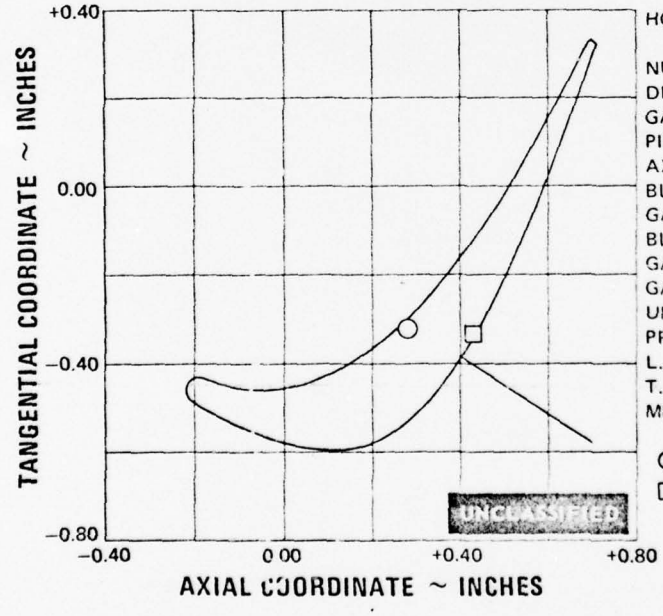

HOT DIMENSIONS

NUMBER OF FOILS	80.00	
DIAMETER	22.8900	IN.
GAGING	0.3459	IN.
PITCH	0.8989	IN.
AXIAL WIDTH	0.9300	IN.
BLADE INLET ANGLE	62.90	DEG.
GAS INLET ANGLE	62.90	DEG.
BLADE EXIT ANGLE	22.57	DEG.
GAS EXIT ANGLE	22.57	DEG.
GAGING ANGLE	22.63	DEG.
UNCOVERED TURNING	14.51	DEG.
PRINCIPAL AXIS	−44.55	DEG.
L. E. RADIUS	0.0275	IN.
T. E. RADIUS	0.0100	IN.
METAL AREA	0.1438	IN.^{2}

	X	Y
○ C. G.	0.2813	−0.3210
□ RADIAL REF.	0.4301	−0.3316
GAGE	0.4050	−0.3849

Figure 91 Recontoured Second Vane, Tip Defining Section (GG)

(U) The performance data of the recontoured airfoils are plotted in Figures 92 through 97. Data is presented at the Mach number nearest to design value, which corresponds to a midspan exit Mach number of 0.863. Data was also taken at midspan exit Mach numbers of 0.806 and 0.969. Analysis of this data indicates that there was a slightly lower loss at both the inside- and outside-diameter walls. The overall integrated loss coefficient for the recontoured airfoils was 0.0336, as compared to the baseline value of 0.0349 at the appropriate test Mach number, indicating essentially no change within experimental accuracy. There was essentially no Mach number effect in the range over which this cascade was evaluated. The spanwise integrated loss, for example, was 0.0356 and 0.0358 at midspan exit Mach numbers of 0.806 and 0.969, respectively. Comparisons of the spanwise recontoured airfoil loss coefficients with the baseline values are shown in Figure 98.

Figure 92 Pressure Loss Contours, Second Vane - Screen Installed, Three Flow Passages, Midspan Exit Mach No. = 0.863, Recontoured Airfoils With Redesigned Inlet Guide Vanes and Optimum Boundary Layer Bleeds

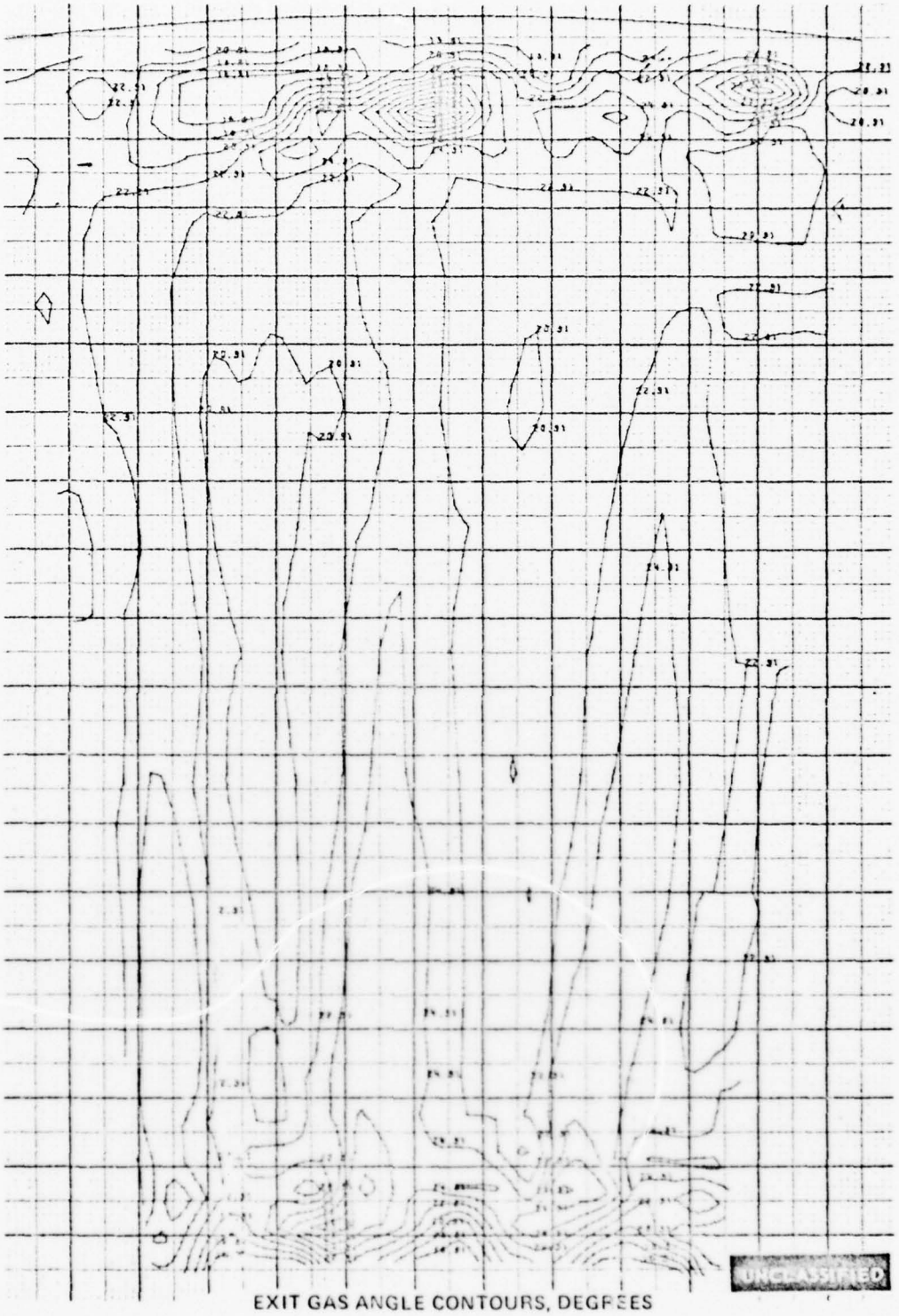

Figure 93 Exit Gas Angle Contours, Second Vane - Screen Installed, Three Flow Passages, Midspan Exit Mach No. = 0.863, Recontoured Airfoils With Redesigned Inlet Guide Vanes and Optimum Boundary Layer Bleeds

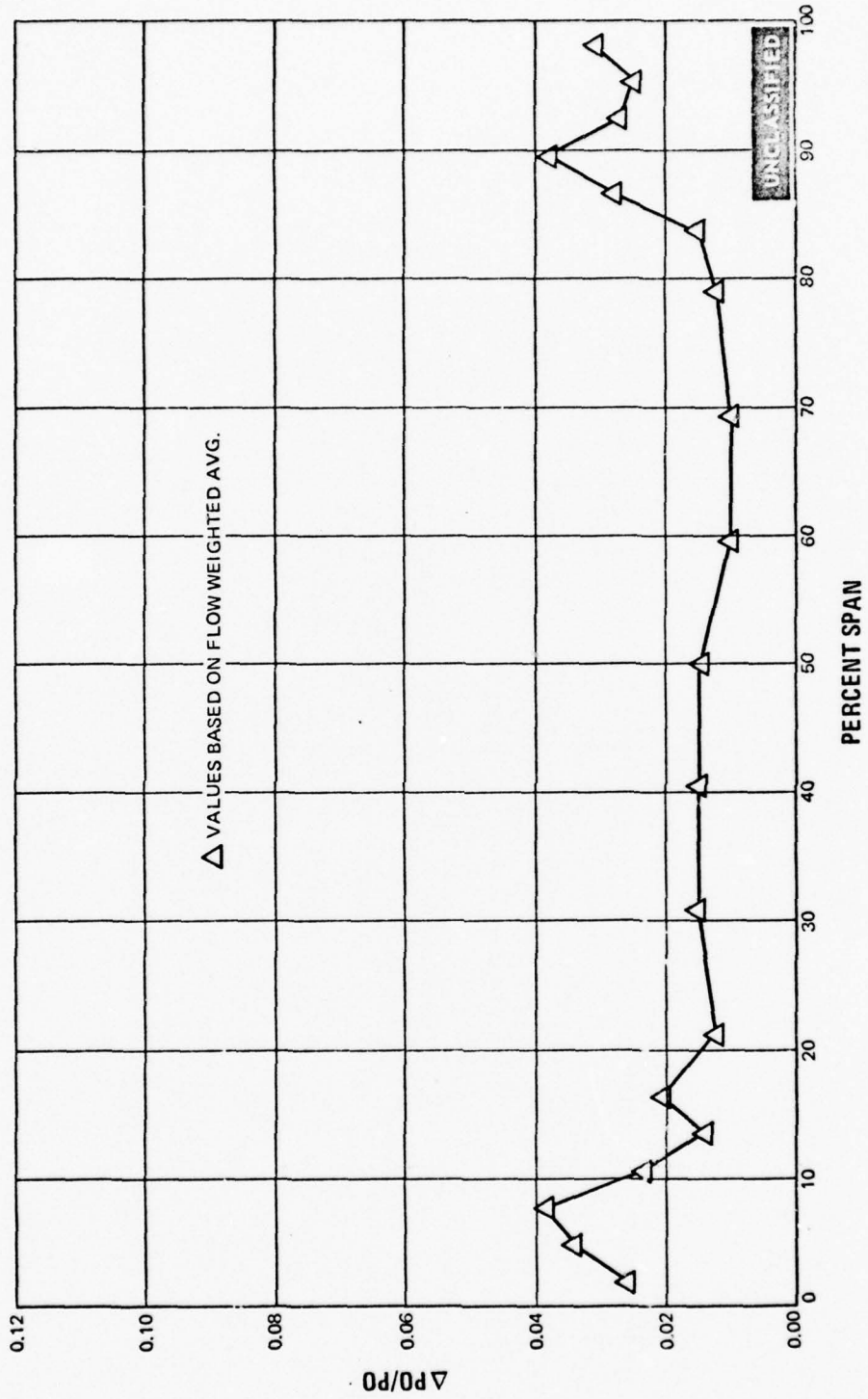

Figure 94 Spanwise Pressure Loss Distribution, Second Vane - Screen Installed, Midspan Exit Mach No. = 0.863, Recontoured Airfoils With Redesigned Inlet Guide Vanes and Optimum Boundary Layer Bleeds

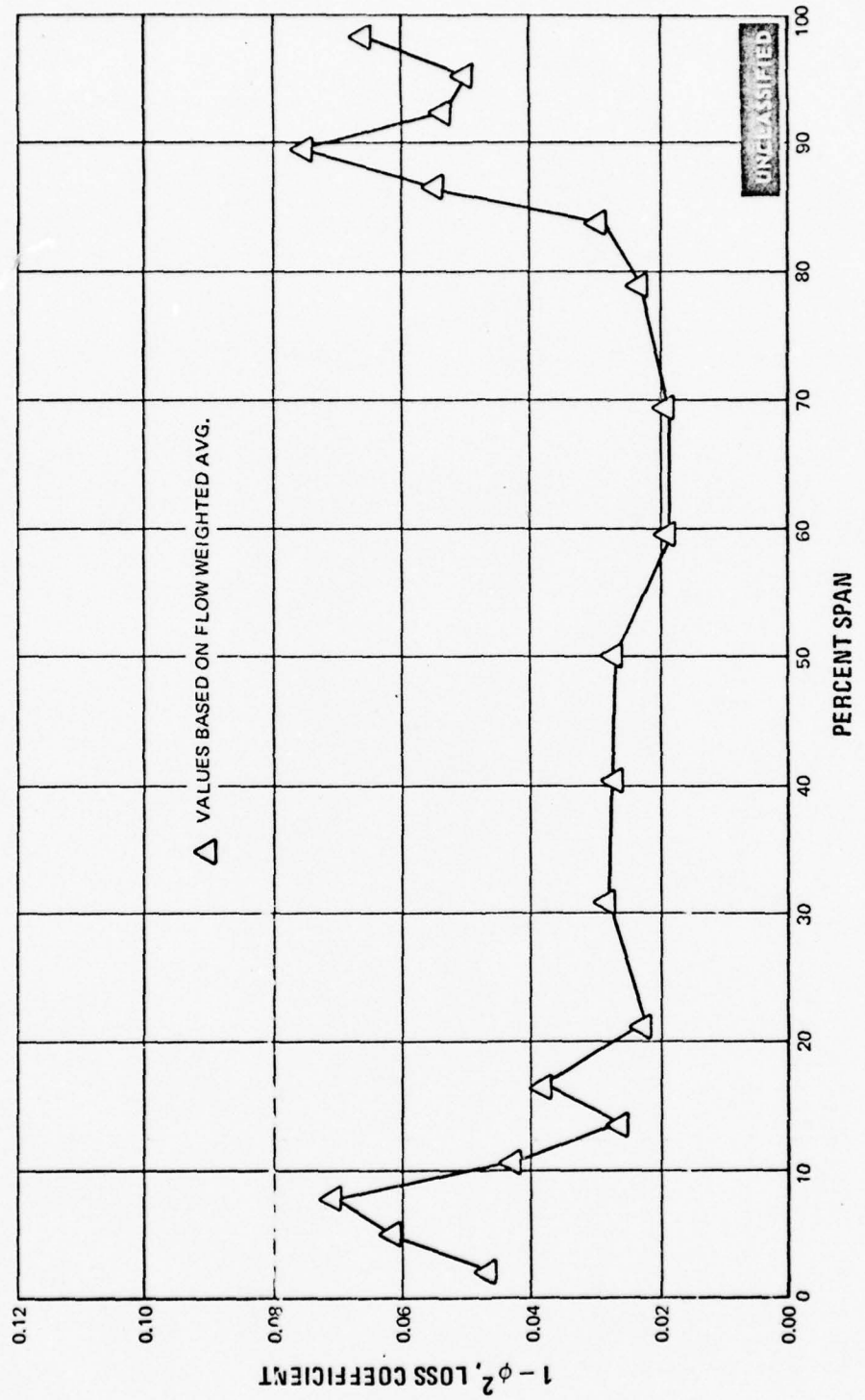

Figure 95 Spanwise Loss Coefficient Distribution, Second Vane - Screen Installed, Mid-span Exit Mach No. = 0.863, Recontoured Airfoils With Redesigned Inlet Guide Vanes and Optimum Boundary Layer Bleeds

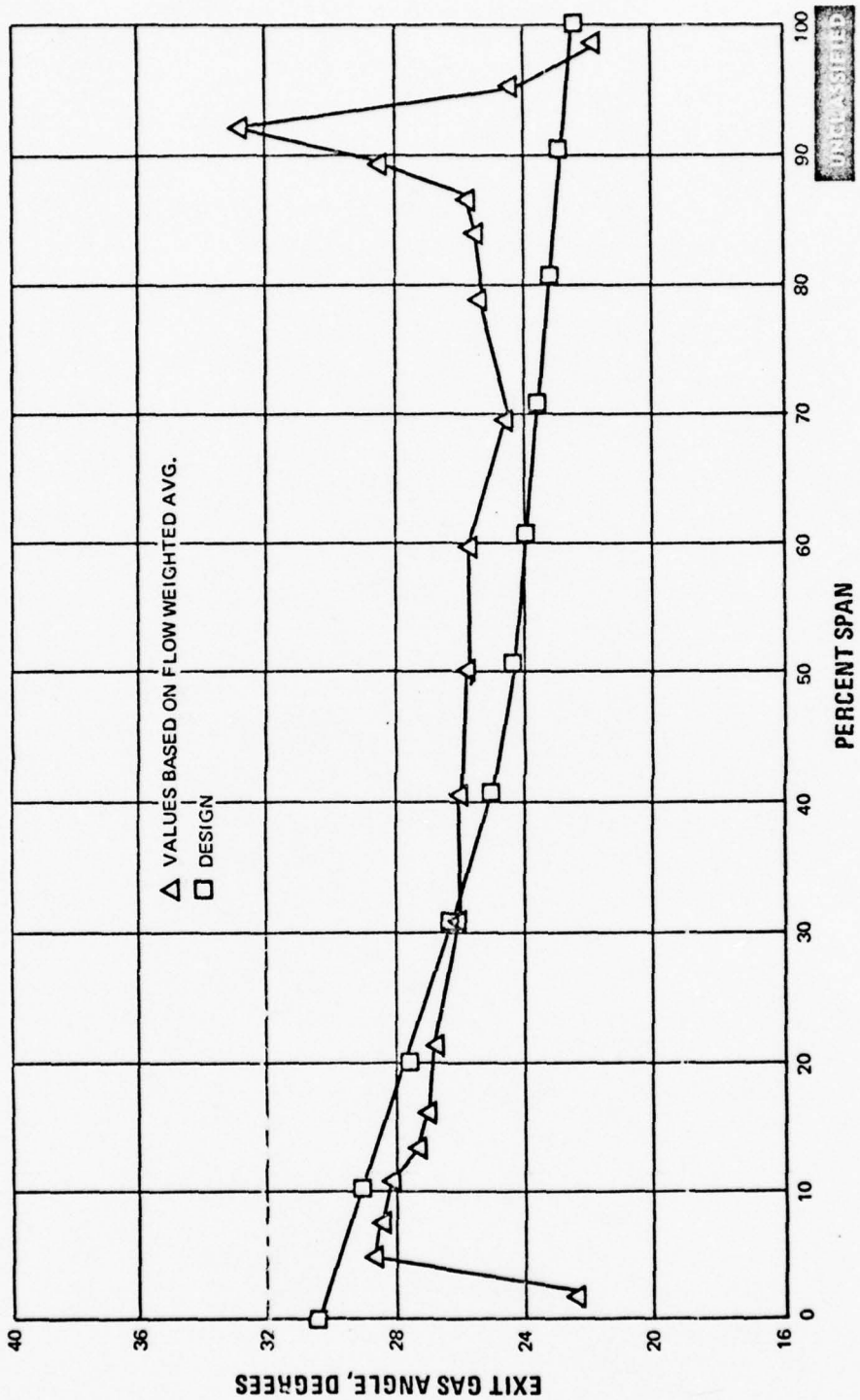

Figure 96 Spanwise Exit Gas Angle Distribution, Second Vane - Screen Installed, Midspan Exit Mach No. = 0.863, Recontoured Airfoils With Redesigned Inlet Guide Vanes and Optimum Boundary Layer Bleeds

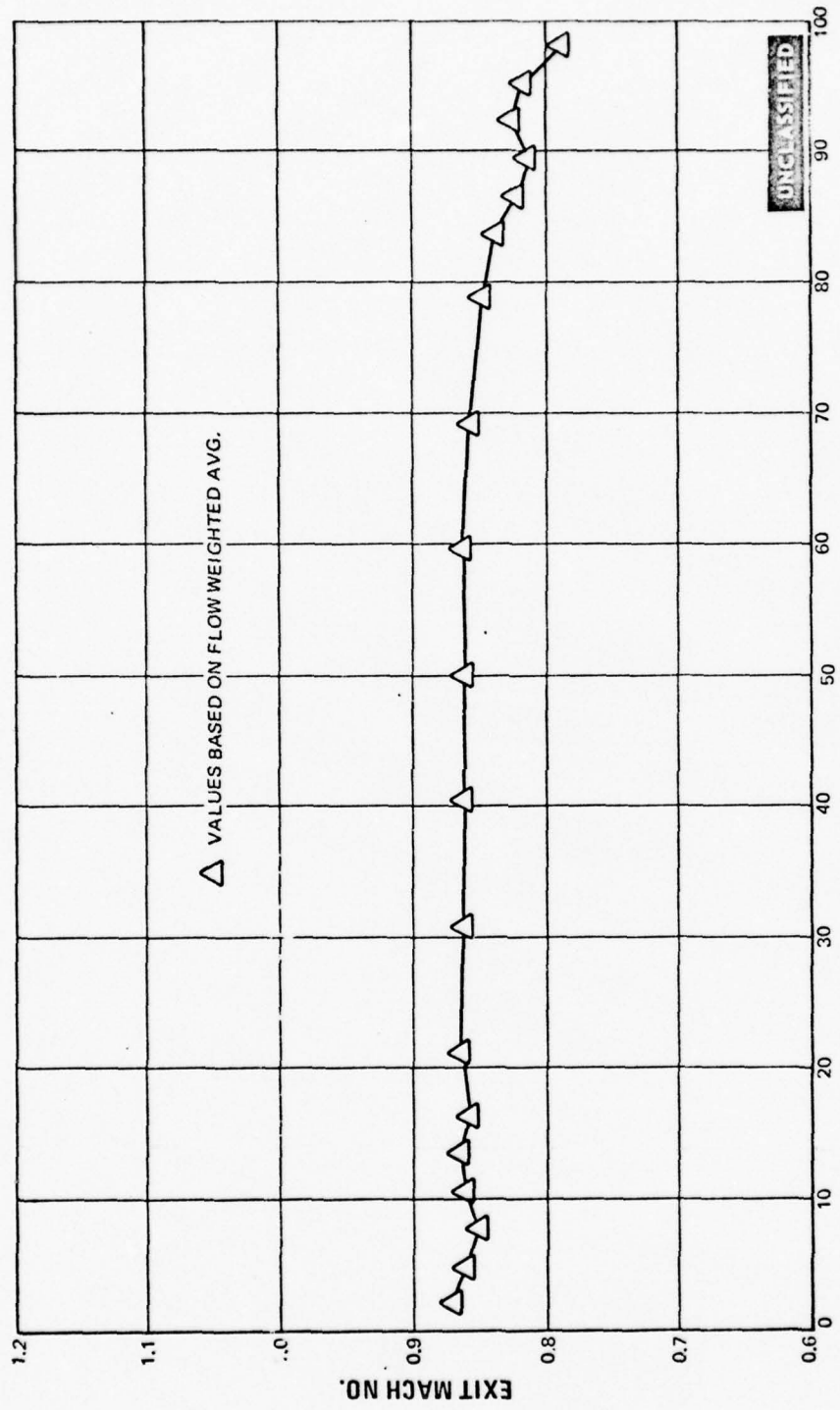

Figure 97 Spanwise Exit Mach Number Distribution, Second Vane - Screen Installed, Midspan Exit Mach No. = 0.863, Recontoured Airfoils With Redesigned Inlet Guide Vanes and Optimum Boundary Layer Bleeds

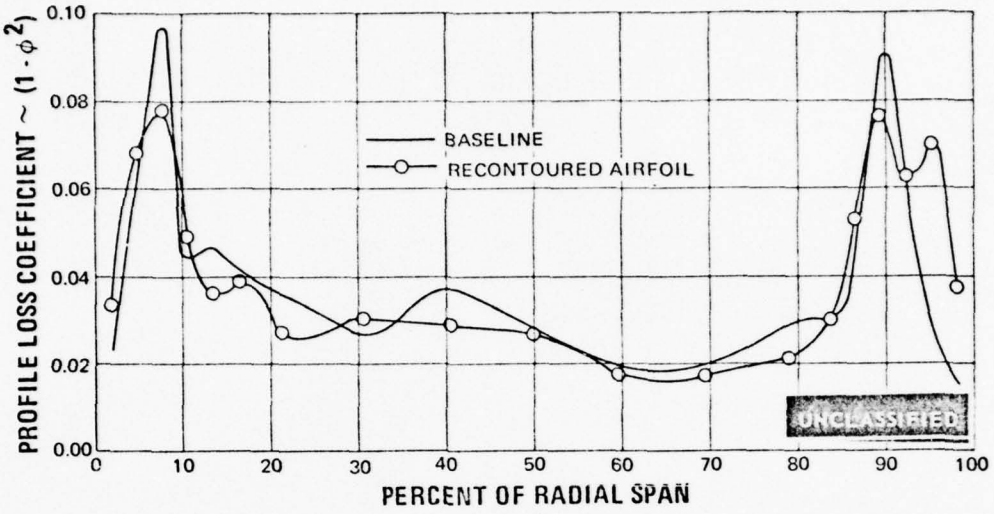

Figure 98 Comparison of Recontoured Airfoil Spanwise Loss Coefficient Distribution with Baseline Values

(U) The measured exit flow angles were almost identical to the baseline values at the root section, while there was an increase in underturning at the tip section. There was no flow separation on either the airfoils, or at the end-wall extensions. The flow visualization test photographs (shown in Figures 99 and 100) verify this conclusion.

(U) The airfoil surface static pressure distributions are shown in Figures 101 through 103 at the root, mean and tip sections. The root section is unloaded and the tip section is slightly more highly loaded than the indicated design predicted values. The reason for this was explained previously in Section II.

Figure 99 Oil and Graphite Flow Patterns–Second Vane Recontoured Airfoils; Midspan Exit Mach No. =0.863

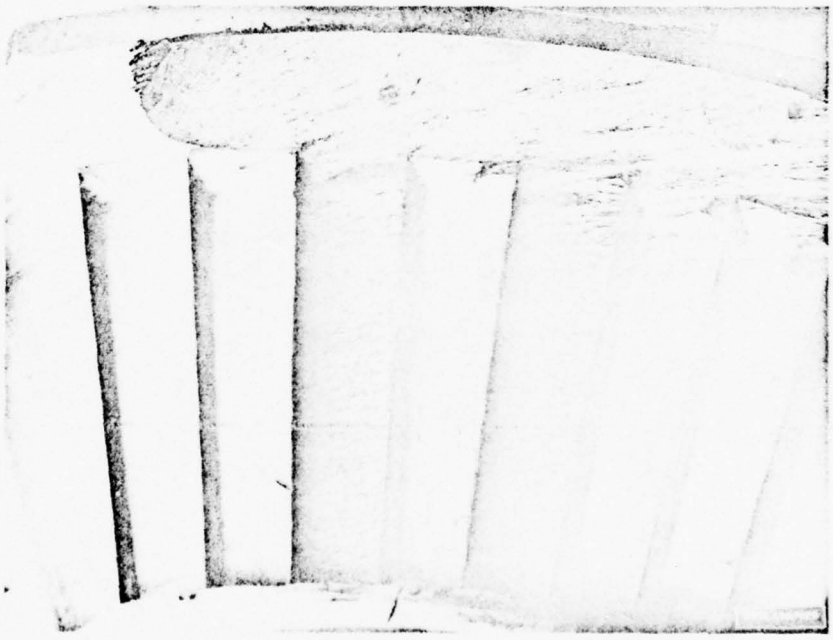

Figure 100 Oil and Graphite Flow Patterns--Second Vane Recontoured Airfoils; Midspan Exit Mach No. =0.863

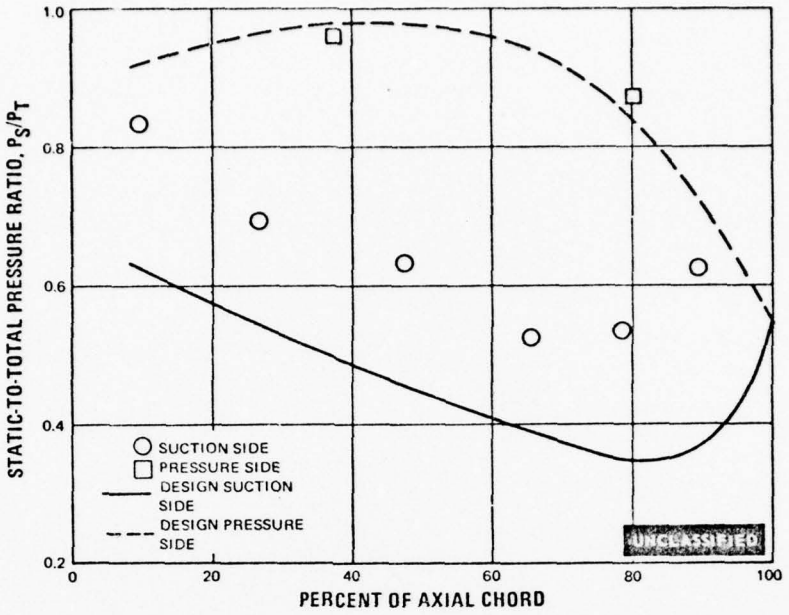

Figure 101 Static-to-Total Pressure Ratio Versus Percent of Axial Chord, Second Vane Recontoured Airfoils With Redesigned Inlet Guide Vanes, Optimum Boundary Layer Bleeds and Screen–Root Section

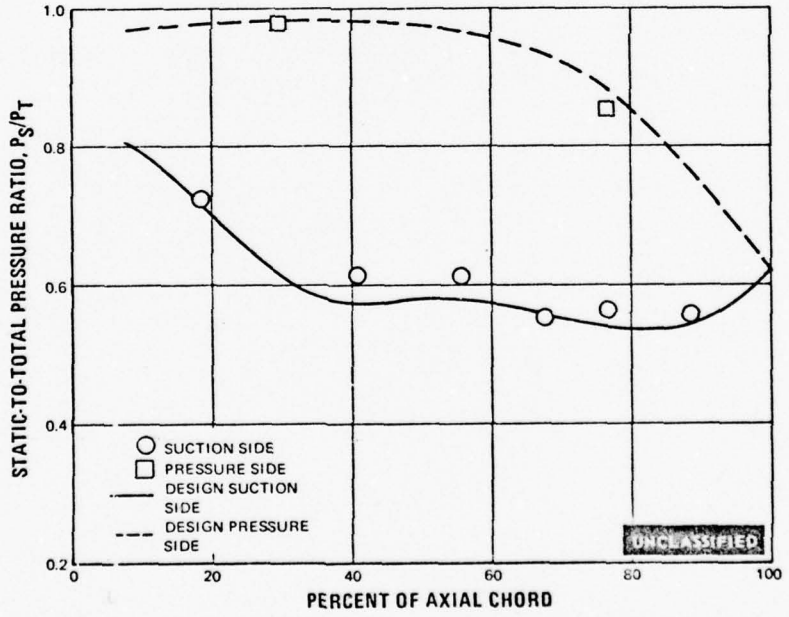

Figure 102 Static-to-Total Pressure Ratio Versus Percent of Axial Chord, Second Vane Recontoured Airfoils With Redesigned Inlet Guide Vanes, Optimum Boundary Layer Bleeds and Inlet Screen–Mean Section

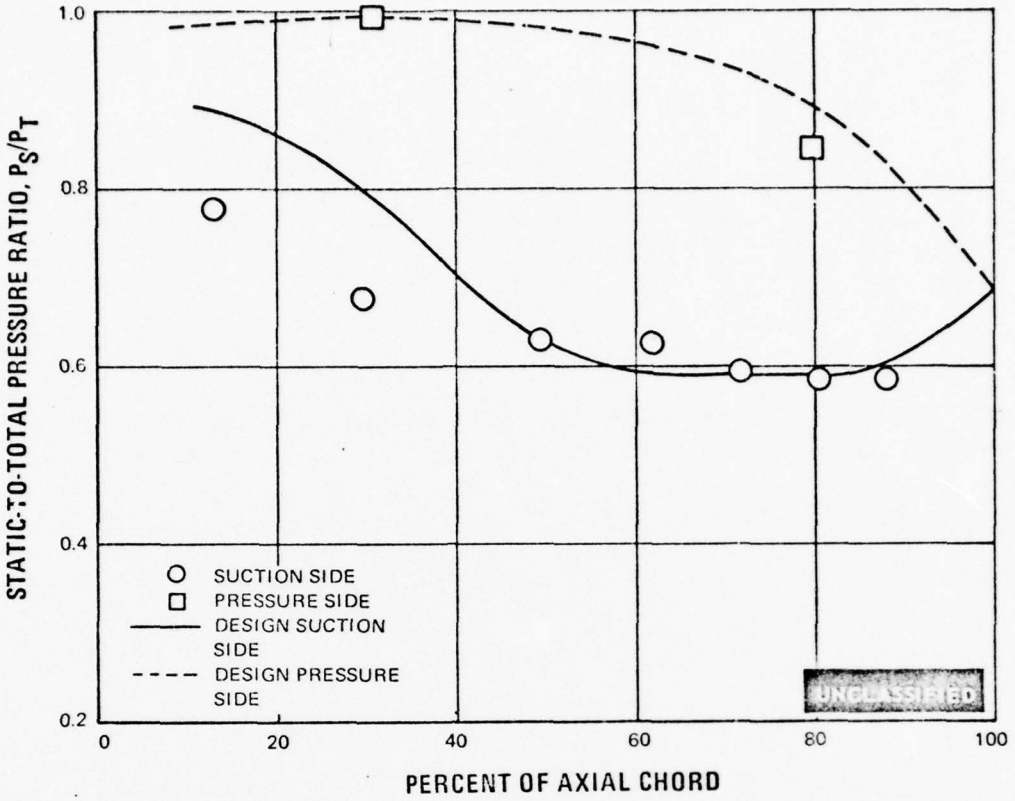

Figure 103 Static-to-Total Pressure Ratio Versus Percent of Axial Chord. Second Vane Recontoured Airfoils With Redesigned Inlet Guide Vanes, Optimum Boundary Layer Bleeds and Inlet Screen–Tip Section

7. END WALL CONTOURING

(U) Another boundary layer control method tested was end-wall contouring. The intent of this design was to reduce the local airfoil loading, and consequently the secondary flow losses, without causing any appreciable disturbance to the flow at other sections of the airfoil or downstream of the airfoil row. Secondary flows occur when the momentum of the fluid near an end-wall has been reduced to a point where it can no longer withstand the pressure-to-suction surface pressure gradient impressed by the potential flow. An attempt was made to reduce the driving pressure gradient forces via a suitable end-wall design.

(U) The design of the end-wall contour was based on two computations. The first was the calculation of the pressure distribution around an airfoil of the desired profile on a plane surface. This program allows streamtube height variations, but is not able to account for radial pressure gradients. The second was the calculation of the axisymmetric, intrablade flow behavior. The guidelines established during the design required that the end-wall contour must decrease the local airfoil loading, must not cause separa-

tion on the end-wall, must not cause an increase of positive incidence by more than 5 degrees, and must not increase the adverse pressure gradient on the uncovered portion of the airfoil suction surface. Each of these could be separately estimated by the application of the two available procedures, although correct solution via a genuine three-dimensional calculation is not yet possible.

(U) The best and final contour was one with sinusoidal inlet and exit wall height distribution, having the leading and trailing edges intersecting at the inflection points. The end-wall contours for both the inner and outer walls of the second vane airfoil are shown in Figures 104 and 105. The inside-diameter wall contour was the one that was actually designed, and the outside-diameter wall contour was scaled from the inside-diameter wall design. The design studies indicated that the end-wall contouring using depths large enough to produce a significant reduction in the tangential pressure difference should not be accomplished by new contours contained completely within the airfoil row. Also, the most acceptable contour was one designed to counteract the airfoil blockage effects by increasing the annulus area in the leading edge region. The inlet and exit sections were connected by a constant area section starting at approximately 24 percent of axial chord and ending at approximately 76 percent of axial chord. The actual manufactured contour is also indicated in these figures, and deviations from the design contour are noted.

(U) The performance data for this airfoil are shown in Figures 106 through 111. These plots are of the same parameter as those shown for the previous tests. The data in these figures is presented at a midspan exit Mach number of 0.843, the value nearest the design point. Data were also taken at midspan exit Mach numbers of 0.79 and 0.988. Analysis of the design point data indicates that there was a negligible increase in loss level at the root section, and a large increase in loss coefficient at the tip section, as compared to the baseline values. The spanwise integrated value from the midspan to the inside-diameter wall was 0.0374, and from the midspan to the outside-diameter wall was 0.0482. The corresponding baseline values were 0.0353 and 0.0345, respectively. The overall integrated spanwise loss coefficient for the end-wall contoured airfoil was 0.0428, as compared to 0.0349 for the baseline tests. A comparision plot of the spanwise loss coefficient for both the end-wall contoured, and the baseline, is shown in Figure 112. The loss coefficient showed a decrease of loss with Mach number, the values decreasing from 0.0444 to 0.0386, as Mach number decreased from 0.79 to 0.988. This effect is mostly due to an increase in Reynolds Number as explained in Part 3 above.

(U) The spanwise integrated exit gas flow angle (Figure 107) indicated a large underturning at the root and tip sections. Flow visualization photographs of this test are shown in Figures 113 and 114.

(U) The airfoil surface static pressure distributions are shown in Figures 115 through 117 at the root, mean and tip sections. The predicted curves shown on these plots are those for the baseline airfoil and not for the contoured end-wall configuration. As previously noted, the tip section wall was not specifically designed. End-wall contouring techniques may well succeed when three-dimensional methods for potential flow and boundary layer calculations are available.

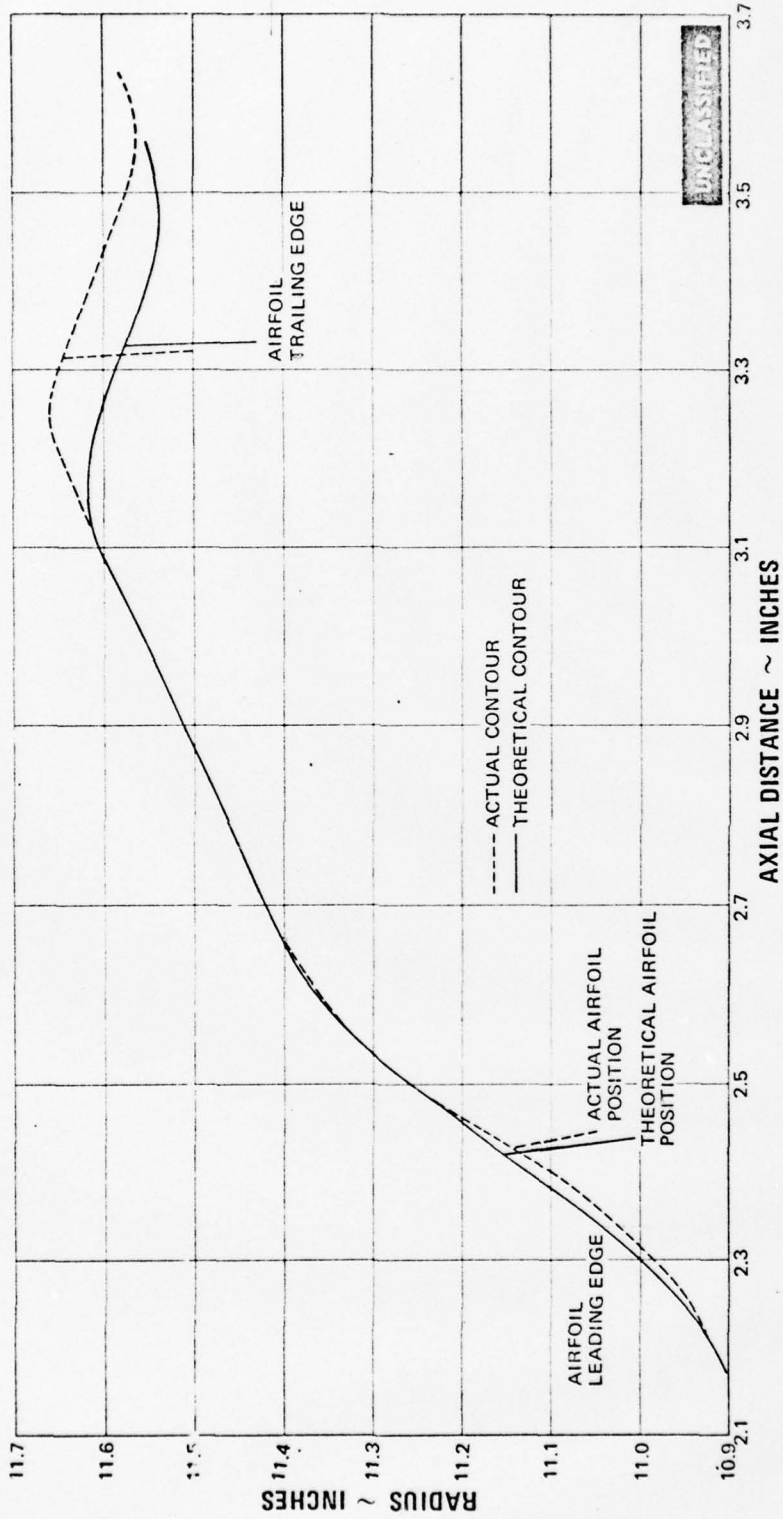

Figure 104 Profile for End Wall Contouring, Inside Diameter Wall

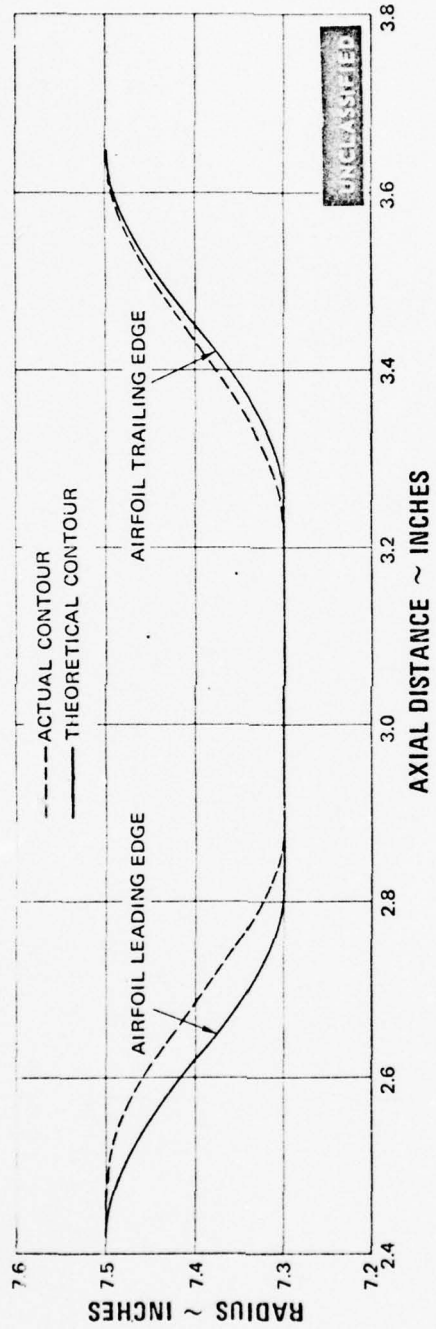

Figure 105 Profile for End Wall Contouring, Outside Diameter Wall

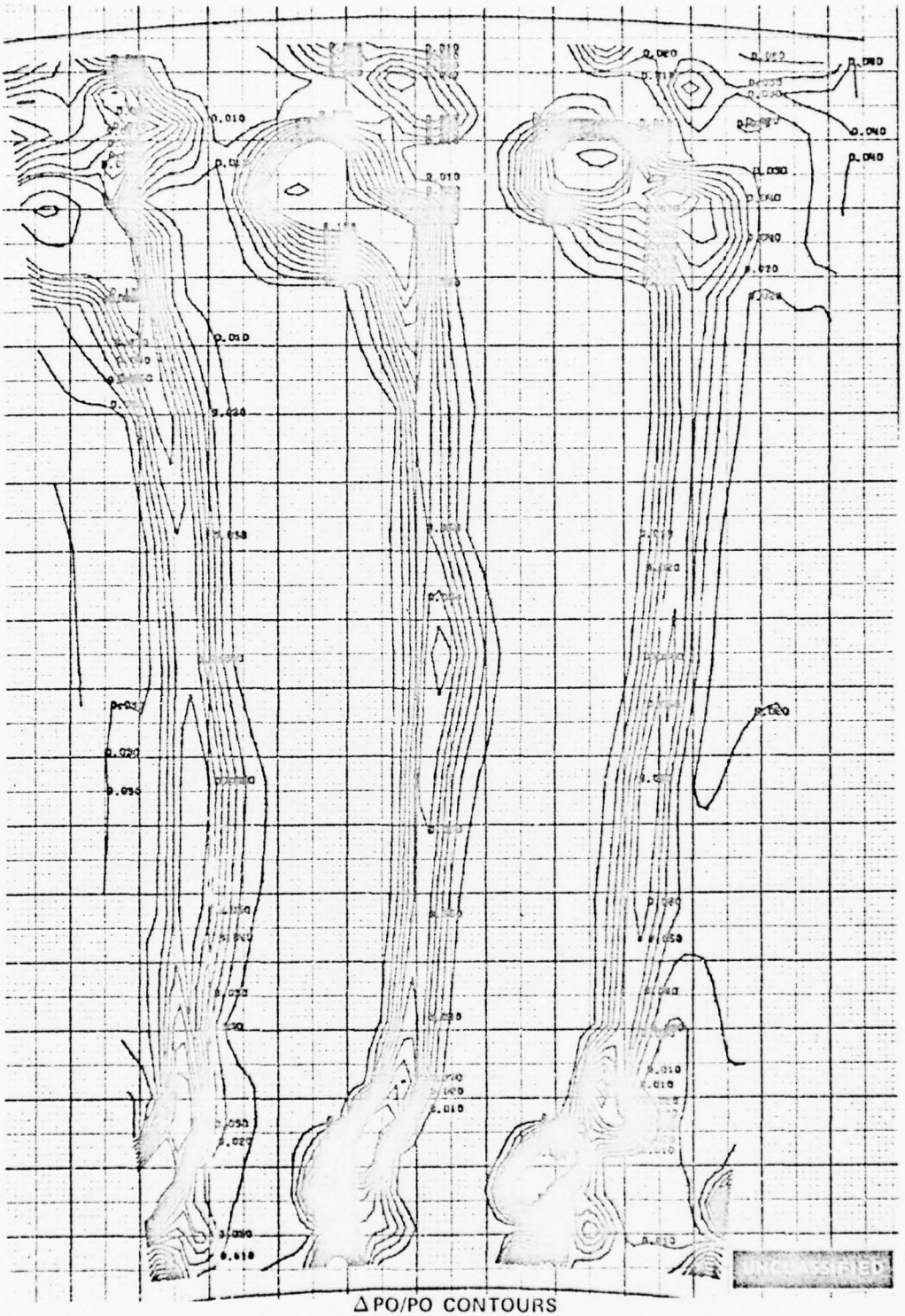

Figure 106 Pressure Loss Contours, Second Vane - Screen Installed, Three Flow Passages, Midspan Exit Mach No. = 0.843, Recontoured Endwalls With Redesigned Inlet Guide Vanes and Optimum Boundary Layer Bleeds

Figure 107 Exit Gas Angle Contours, Second Vane - Screen Installed, Three Flow Passages, Midspan Exit Mach No. = 0.843, Recontoured Endwalls With Redesigned Inlet Guide Vanes and Optimum Boundary Layer Bleeds

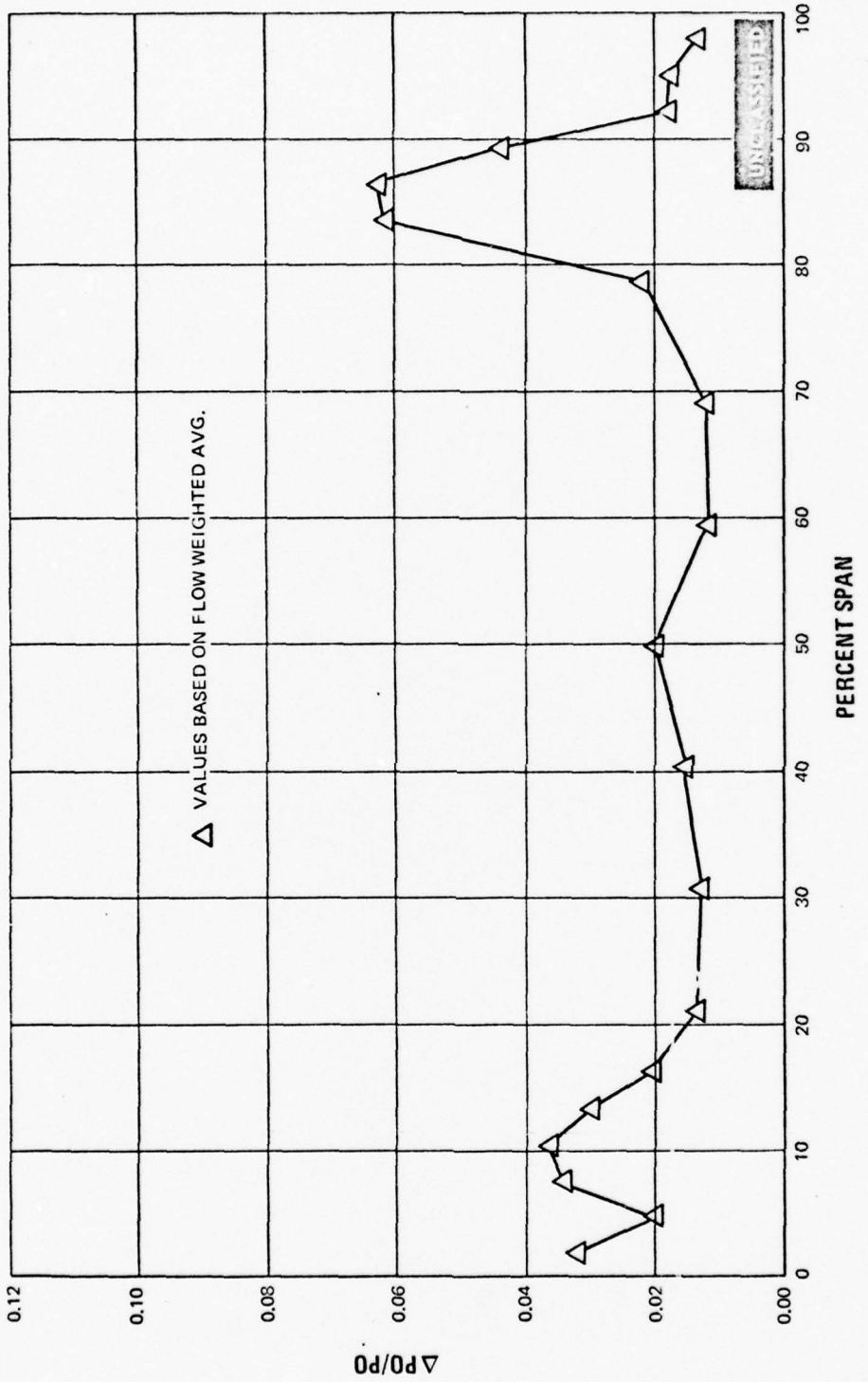

Figure 108 Spanwise Pressure Loss Distribution, Second Vane - Screen Installed, Midspan Exit Mach No. = 0.843, Recontoured Endwalls With Redesigned Inlet Guide Vanes and Optimum Boundary Layer Bleeds

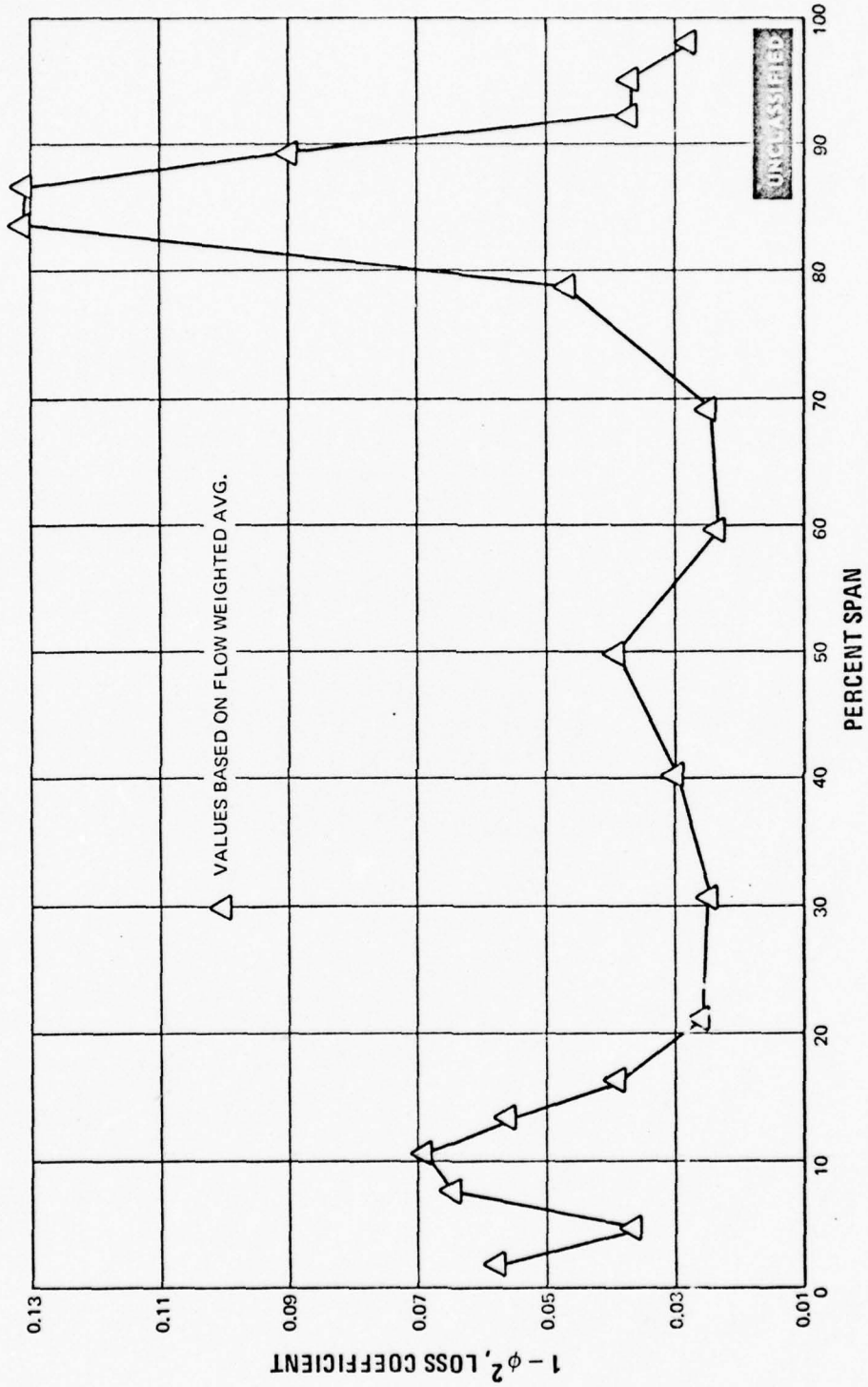

Figure 109 Spanwise Loss Coefficient Distribution, Second Vane - Screen Installed, Mid-span Exit Mach No. = 0.843, Recontoured Endwalls With Redesigned Inlet Guide Vanes and Optimum Boundary Layer Bleeds

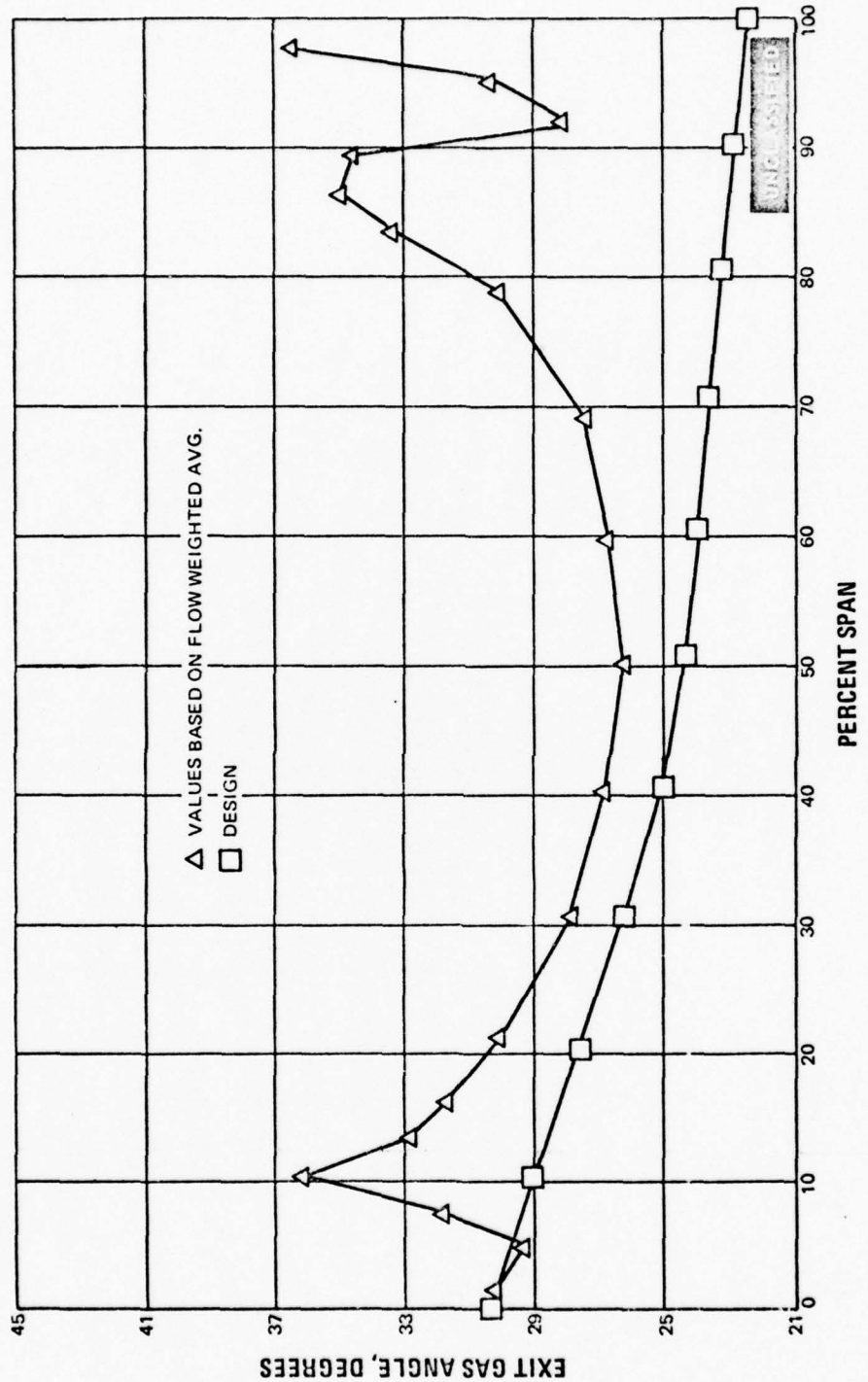

Figure 110 Spanwise Exit Gas Angle Distribution, Second Vane - Screen Installed, Mid-span Exit Mach No. = 0.843, Recontoured Endwalls With Redesigned Inlet Guide Vanes and Optimum Boundary Layer Bleeds

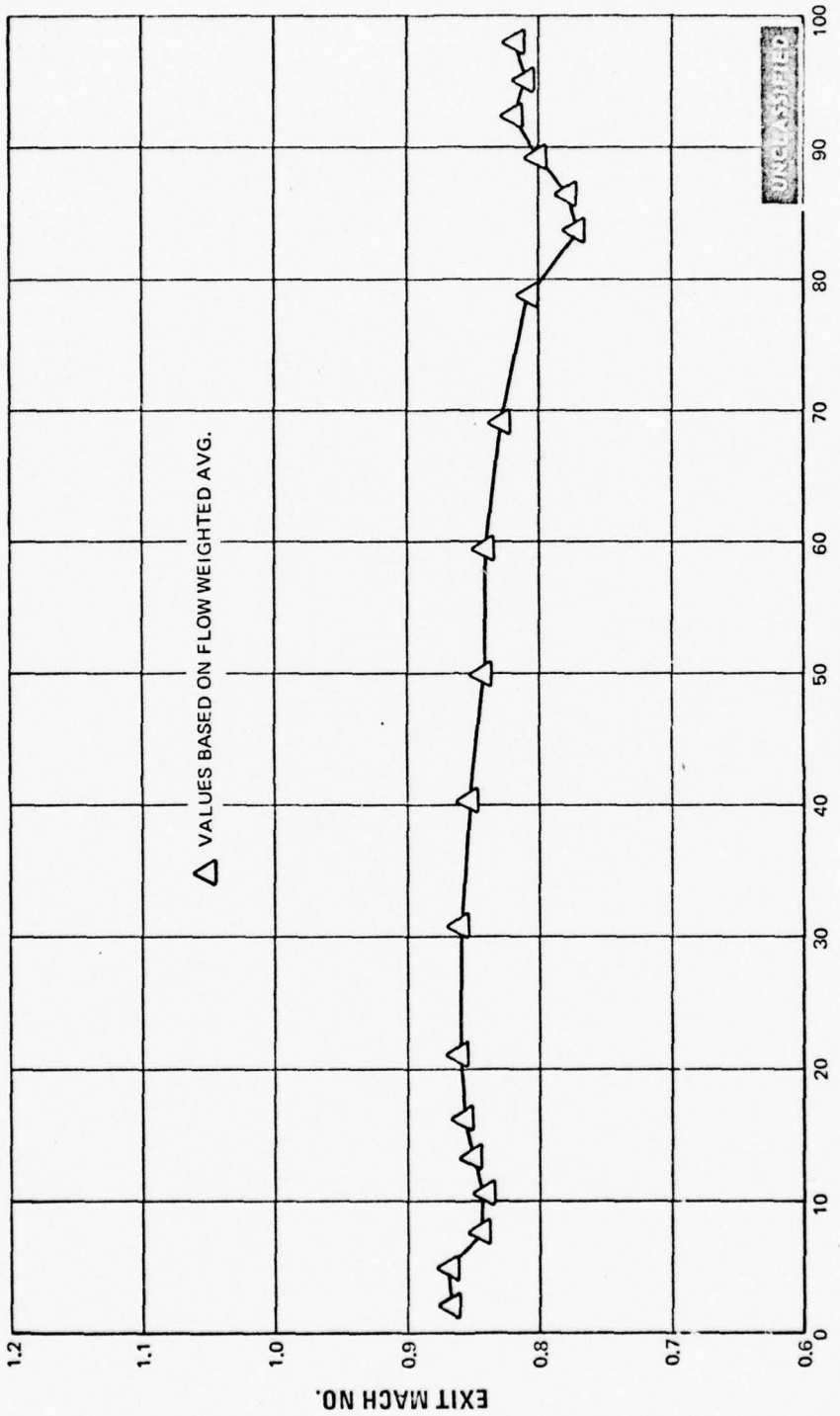

Figure 111 Spanwise Exit Mach Number Distribution, Second Vane - Screen Installed, Midspan Exit Mach No. = 0.843, Recontoured Endwalls With Redesigned Inlet Guide Vanes and Optimum Boundary Layer Bleeds

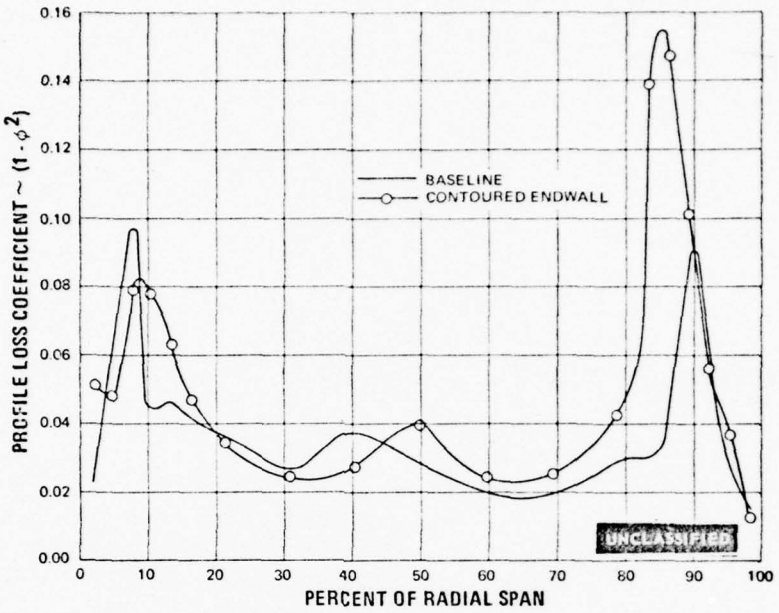

Figure 112 Comparison of Recontoured End Wall Spanwise Loss Coefficient Distribution with Baseline Values

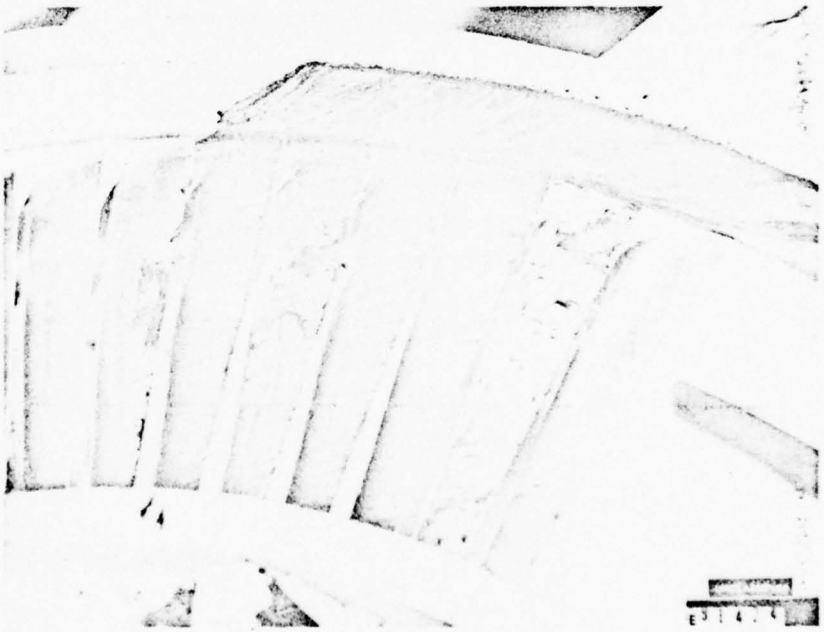

Figure 113 Oil and Graphite Flow Patterns–Second Vane with End Wall Contouring; Midspan Exit Mach No. =0.843

Figure 114 Oil and Graphite Flow Patterns–Second Vane with End Wall Contouring; Midspan Exit Mach No. ≈0.843

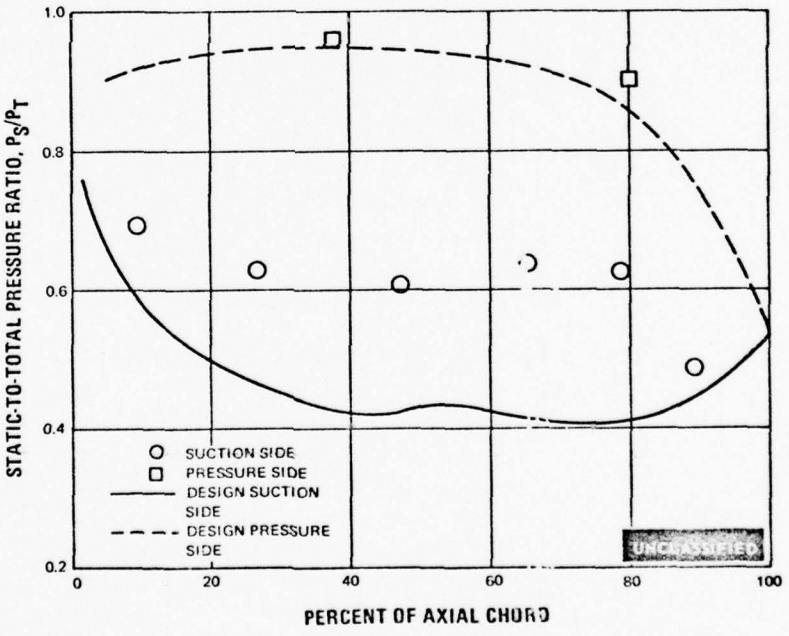

Figure 115 Static-to-Total Pressure Ratio Versus Percent of Axial Chord, Second Vane Recontoured End Walls With Redesigned Inlet Guide Vanes, Optimum Boundary Layer Bleeds and Inlet Screen–Root Section

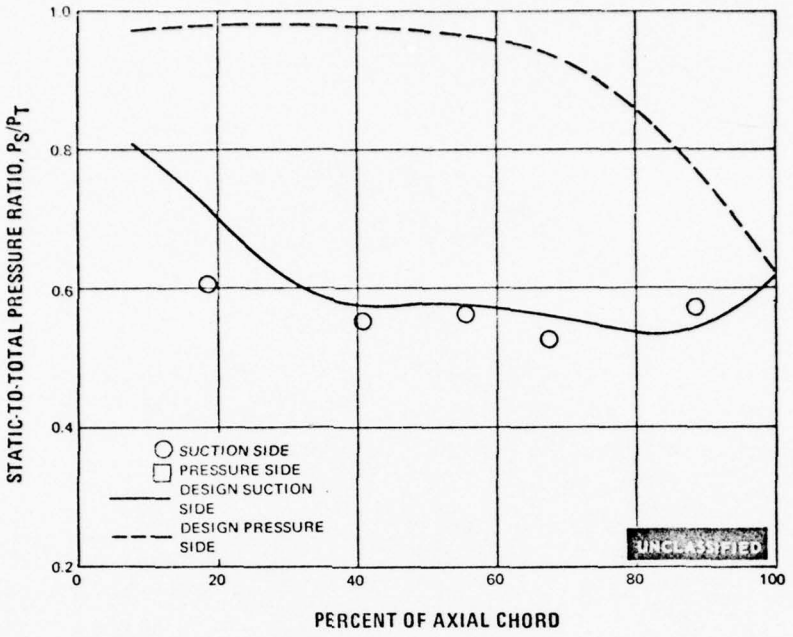

Figure 116 Static-to-Total Pressure Ratio Versus Percent of Axial Chord, Second Vane Recontoured End Walls With Redesigned Inlet Guide Vanes, Optimum Boundary Layer Bleeds and Inlet Screen–Mean Section

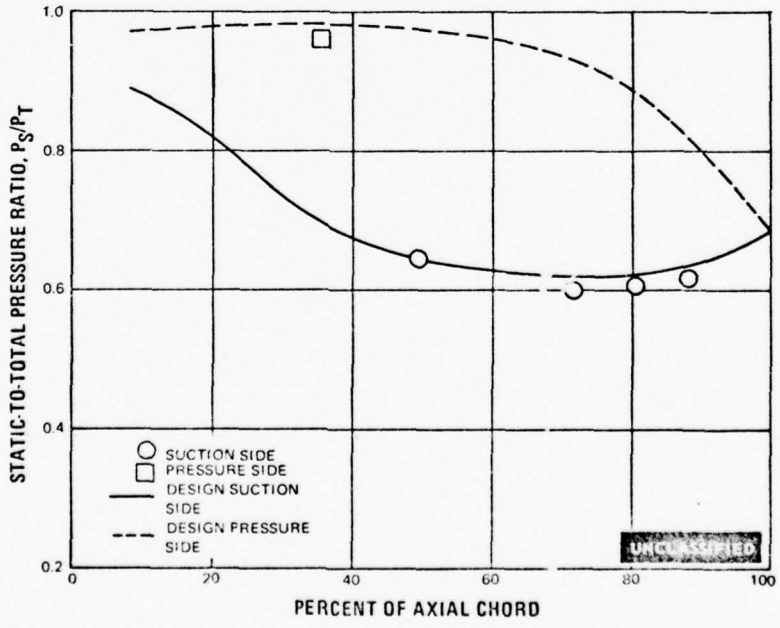

Figure 117 Static-to-Total Pressure Ratio Versus Percent of Axial Chord, Second Vane Recontoured End Walls With Redesigned Inlet Guide Vanes, Optimum Boundary Layer Bleeds and Inlet Screen–Tip Section

8. RECAMBERED AIRFOILS

(U) The final boundary layer control technique tested was the locally recambered second vane airfoil. Local recambering, to reduce secondary losses at the root and tip sections of the second vane, required a streamline analysis of the entire study turbine. The inlet airfoil angles were held constant to allow the use of the same inlet hardware. The tip section was closed or reduced by 5 degrees, while the root section was opened or increased by 5 degrees. This technique was used since the ends behave essentially independently of one another. The camber changes were then curved-line-faired into the original camber at the 25 and 75 percent span sections as reported in the Reference 3 Report. The streamline analysis indicated that, in order to maintain the same stage work and reaction level, the second stage blade would have to be opened by increasing the exit gas angle by 0.5 degree across the span.

(U) Comparison plots with baseline airfoils at the root and tip section are shown in Figures 118 and 119. The elevation of the recambered airfoil with the reference sections are shown in Figure 83 and the section profiles are presented in Figures 120 through 127.

(U) The performance data for the recambered airfoils are given in Figures 128 through 133. This data is shown at a midspan exit Mach number of 0.880. Data were also taken at Mach numbers of 0.823 and 1.033. The resulting spanwise loss coefficients are compared with the baseline values in Figure 134 at the design Mach number.

(U) The overall integrated loss coefficient for the recambered airfoil was 0.0329 as compared to 0.0349 for the baseline value. The root section showed a significant reduction (0.0286 versus 0.0353), while the tip section indicated a slight increase (0.0372 versus 0.0345), compared to baseline values. Flow visualization photographs of these airfoils are shown in Figures 135 and 136. The measured flow angles at the tip section indicate attached flow with only a slight underturning from the design values. The root section data indicate a large increase in underturning over baseline values, but there is no indication of flow separation on the flow visualization photographs.

(U) Airfoil surface static pressure distributions are shown in Figures 137 through 139. The predicted curve for the recambered airfoil section is also shown. The same comments apply to these data as in previous discussions of airfoil surface static pressures.

(U) It is especially comforting that all the observed results of this test are in complete accord with reasonable expectations. In short, the application of this method to turbine design should offer no special difficulities.

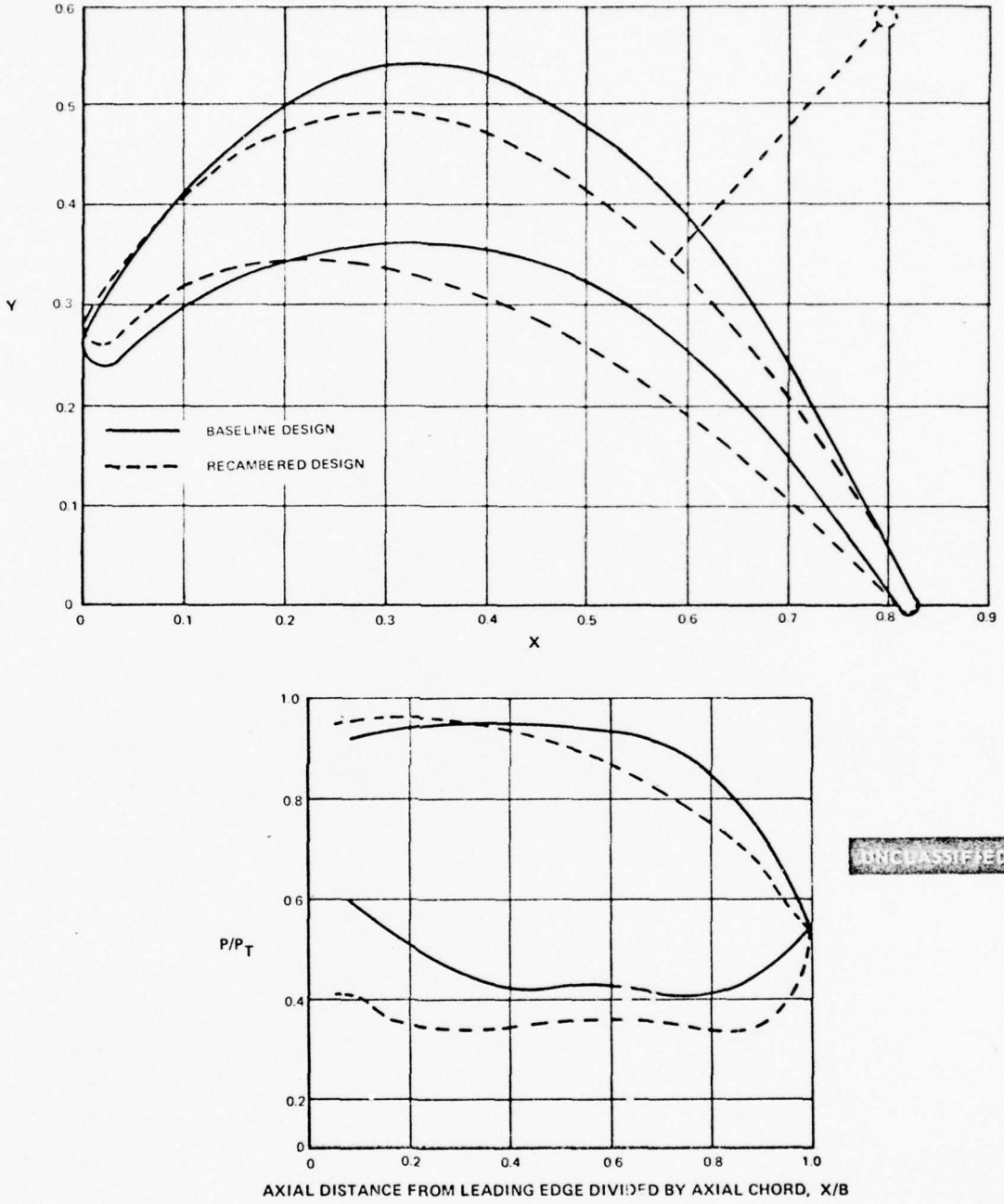

Figure 118 Second Vane Root Section Recambering

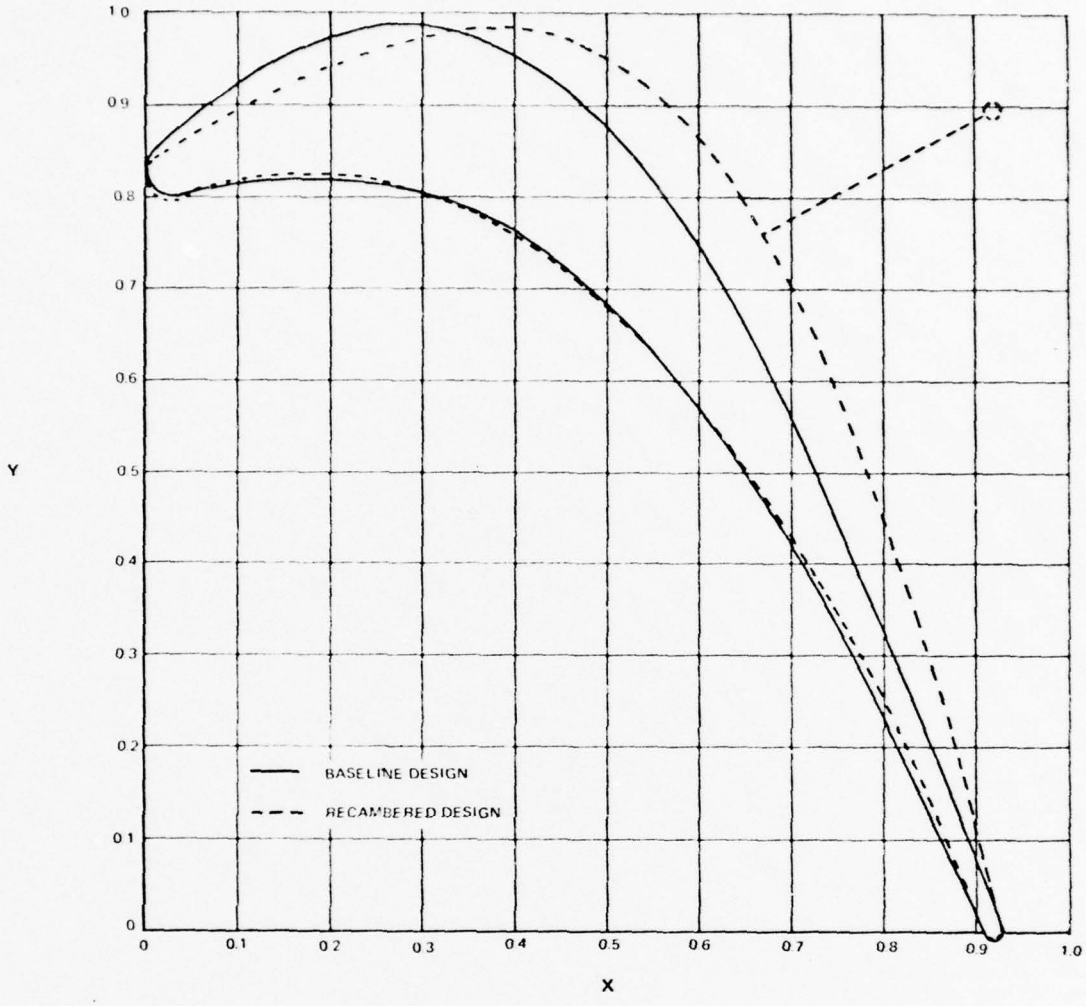

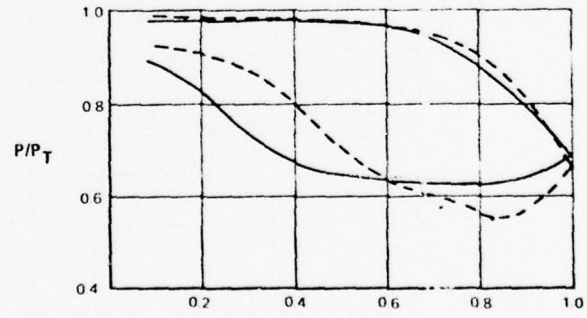

UNCLASSIFIED

Figure 119 Second Vane Tip Section Recambering

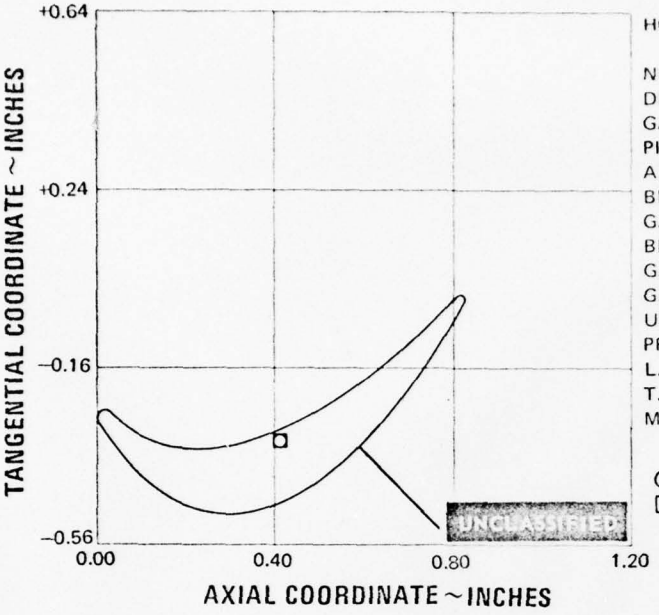

HOT DIMENSIONS

NUMBER OF FOILS	80.00	
DIAMETER	15.0000	IN
GAGING	0.3319	IN
PITCH	0.5890	IN
AXIAL WIDTH	0.8320	IN
BLADE INLET ANGLE	37.33	DEG
GAS INLET ANGLE	37.33	DEG
BLADE EXIT ANGLE	35.57	DEG
GAS EXIT ANGLE	35.57	DEG
GAGING ANGLE	34.29	DEG
UNCOVERED TURNING	17.29	DEG
PRINCIPAL AXIS	−22.84	DEG
L. E. RADIUS	0.0175	IN
T. E. RADIUS	0.0100	IN
METAL AREA	0.0999	IN^2

	X	Y
○ C. G.	0.4125	−0.3248
□ RADIAL REF.	0.4125	−0.3248
GAGE	0.5835	−0.3441

Figure 120 Recambered Second Vane, Root Section (FF)

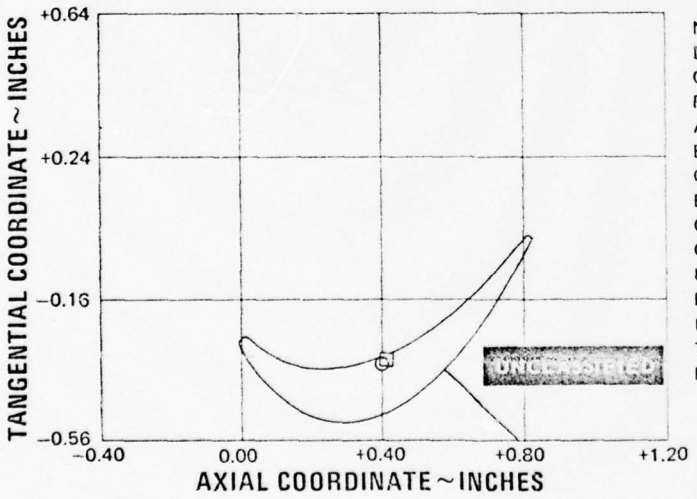

HOT DIMENSIONS

NUMBER OF FOILS	80.00	
DIAMETER	15.3000	IN
GAGING	0.3247	IN
PITCH	0.6008	IN
AXIAL WIDTH	0.8357	IN
BLADE INLET ANGLE	37.73	DEG
GAS INLET ANGLE	38.00	DEG
BLADE EXIT ANGLE	33.88	DEG
GAS EXIT ANGLE	33.88	DEG
GAGING ANGLE	32.71	DEG
UNCOVERED TURNING	16.03	DEG
PRINCIPAL AXIS	−23.51	DEG
L. E. RADIUS	0.0185	IN
T. E. RADIUS	0.0100	IN
METAL AREA	0.1009	IN^2

	X	Y
○ C. G.	0.3996	−0.3394
□ RADIAL REF.	0.4125	−0.3248
GAGE	0.5766	−0.3563

Figure 121 Recambered Second Vane, Root Fillet Section (AA)

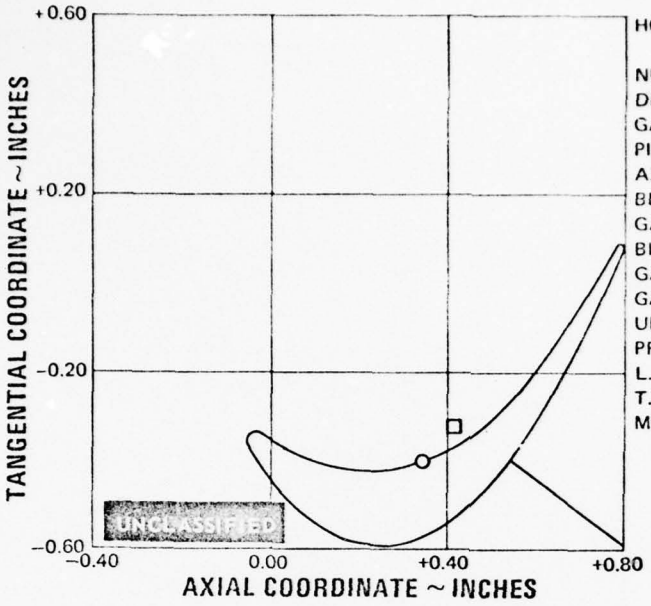

HOT DIMENSIONS

NUMBER OF FOILS	80.00	
DIAMETER	16.9726	IN
GAGING	0.3033	IN
PITCH	0.6665	IN
AXIAL WIDTH	0.8565	IN
BLADE INLET ANGLE	42.10	DEG
GAS INLET ANGLE	42.10	DEG
BLADE EXIT ANGLE	27.17	DEG
GAS EXIT ANGLE	27.17	DEG
GAGING ANGLE	27.07	DEG
UNCOVERED TURNING	12.00	DEG
PRINCIPAL AXIS	-29.78	DEG
L. E. RADIUS	0.0225	IN
T. E. RADIUS	0.0100	IN
METAL AREA	0.1068	IN^2

	X	Y
O C. G.	0.3464	-0.4008
□ RADIAL REF. GAGE	0.4125	-0.3248
	0.5419	-0.3982

Figure 122 Recambered Second Vane, ¼ Root Section (BB)

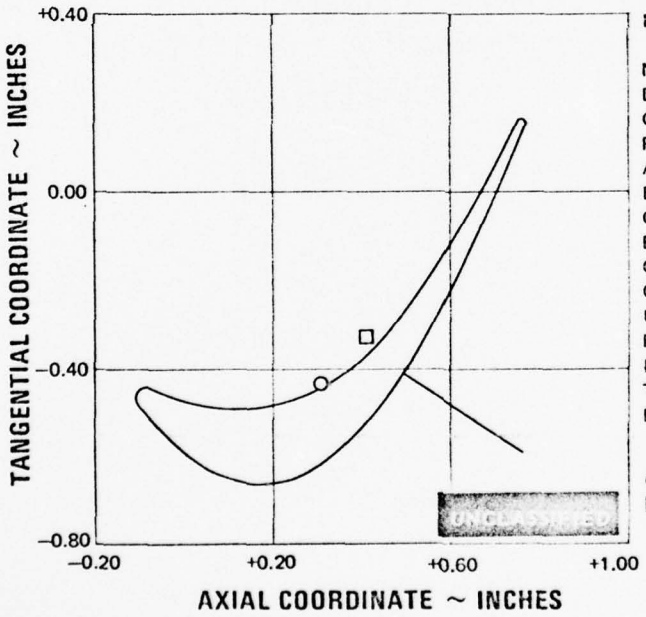

HOT DIMENSIONS

NUMBER OF FOILS	80.00	
DIAMETER	18.9450	IN
GAGING	0.3115	IN
PITCH	0.7440	IN
AXIAL WIDTH	0.8810	IN
BLADE INLET ANGLE	50.50	DEG
GAS INLET ANGLE	50.50	DEG
BLADE EXIT ANGLE	24.58	DEG
GAS EXIT ANGLE	24.58	DEG
GAGING ANGLE	24.75	DEG
UNCOVERED TURNING	10.67	DEG
PRINCIPAL AXIS	-39.90	DEG
L. E. RADIUS	0.0250	IN
T. E. RADIUS	0.0100	IN
METAL AREA	0.1117	IN^2

	X	Y
O C. G.	0.3086	-0.4308
□ RADIAL REF. GAGE	0.4125	-0.3248
	0.4937	-0.4080

Figure 123 Recambered Second Vane, Mean Section (CC)

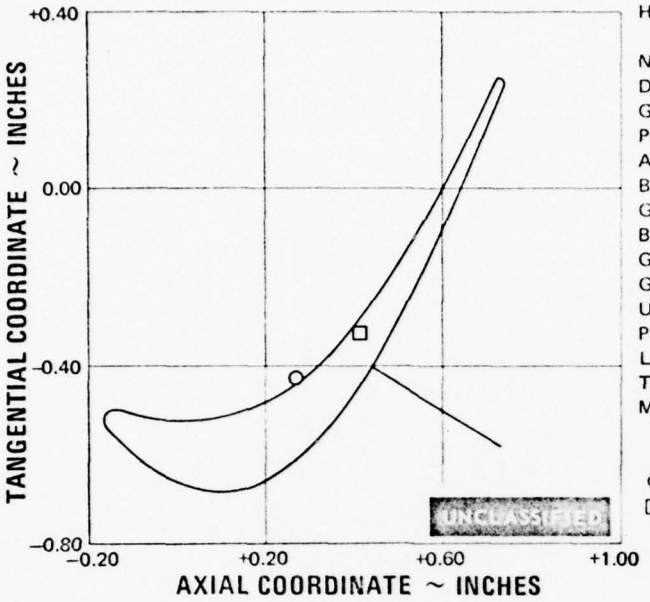

HOT DIMENSIONS

NUMBER OF FOILS	80.00	
DIAMETER	20.9200	IN
GAGING	0.3307	IN
PITCH	0.8215	IN
AXIAL WIDTH	0.9055	IN
BLADE INLET ANGLE	57.41	DEG
GAS INLET ANGLE	57.40	DEG
BLADE EXIT ANGLE	23.60	DEG
GAS EXIT ANGLE	23.60	DEG
GAGING ANGLE	23.74	DEG
UNCOVERED TURNING	9.81	DEG
PRINCIPAL AXIS	-43.79	DEG
L. E. RADIUS	0.0275	IN
T. E. RADIUS	0.0100	IN
METAL AREA	0.1166	IN^2

	X	Y
○ C.G.	0.2691	-0.4297
□ RADIAL REF.	0.4125	-0.3248
GAGE	0.4425	-0.4034

Figure 124 Recambered Second Vane, ¼ Tip Section (DD)

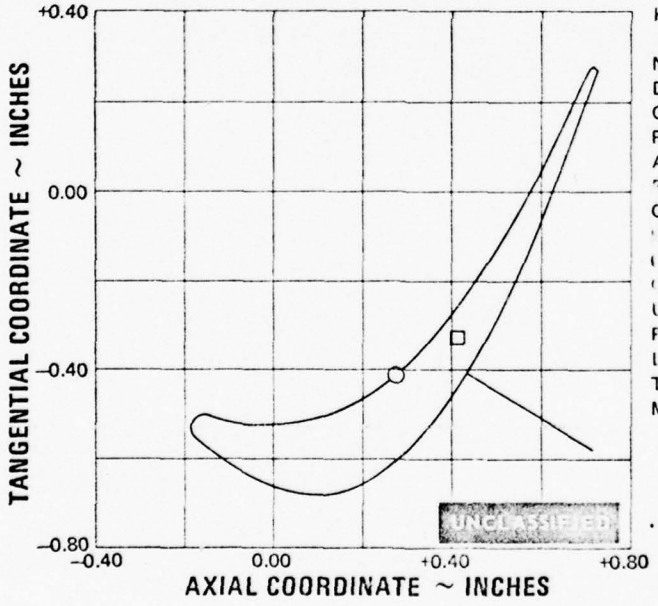

HOT DIMENSIONS

NUMBER OF FOILS	80.00	
DIAMETER	21.7200	IN
GAGING	0.3201	IN
PITCH	0.8529	IN
AXIAL WIDTH	0.9155	IN
BLADE INLET ANGLE	59.76	DEG
GAS INLET ANGLE	59.90	DEG
BLADE EXIT ANGLE	21.94	DEG
GAS EXIT ANGLE	21.94	DEG
GAGING ANGLE	22.04	DEG
UNCOVERED TURNING	11.54	DEG
PRINCIPAL AXIS	-44.85	DEG
L. E. RADIUS	0.0279	IN
T. E. RADIUS	0.0100	IN
METAL AREA	0.1318	IN^2

	X	Y
○ C. G.	0.2774	-0.4079
□ RADIAL REF.	0.4125	-0.3248
GAGE	0.4382	-0.4101

Figure 125 Recambered Second Vane, Fillet Section (EE)

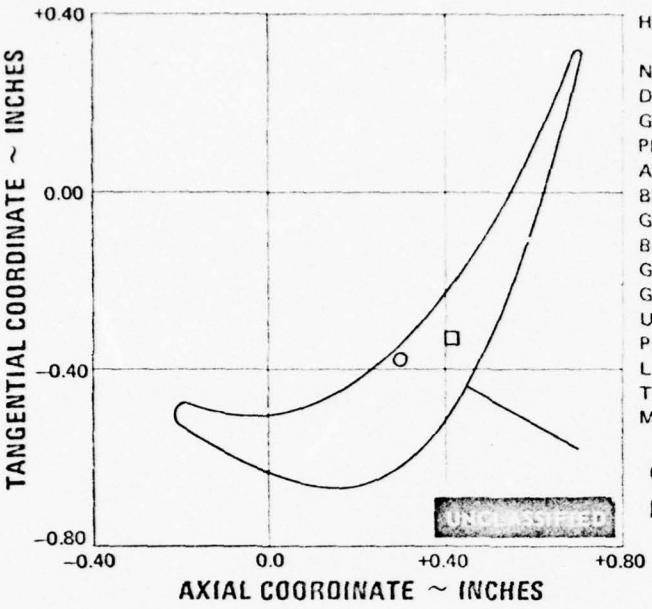

HOT DIMENSIONS

NUMBER OF FOILS	80.00	
DIAMETER	22.8200	IN.
GAGING	0.2799	IN.
PITCH	0.8961	IN.
AXIAL WIDTH	0.9291	IN.
BLADE INLET ANGLE	62.72	DEG.
GAS INLET ANGLE	62.75	DEG.
BLADE EXIT ANGLE	17.90	DEG.
GAS EXIT ANGLE	17.90	DEG.
GAGING ANGLE	18.20	DEG.
UNCOVERED TURNING	15.04	DEG.
PRINCIPAL AXIS	-46.26	DEG.
L. E. RADIUS	0.0276	IN.
T. E. RADIUS	0.0100	IN.
METAL AREA	0.1712	$IN.^2$

	X	Y
○ C. G.	0.3032	-0.3756
□ RADIAL REF.	0.4125	-0.3248
GAGE	0.4510	-0.4380

Figure 126 Recambered Second Vane, Tip Section (HH)

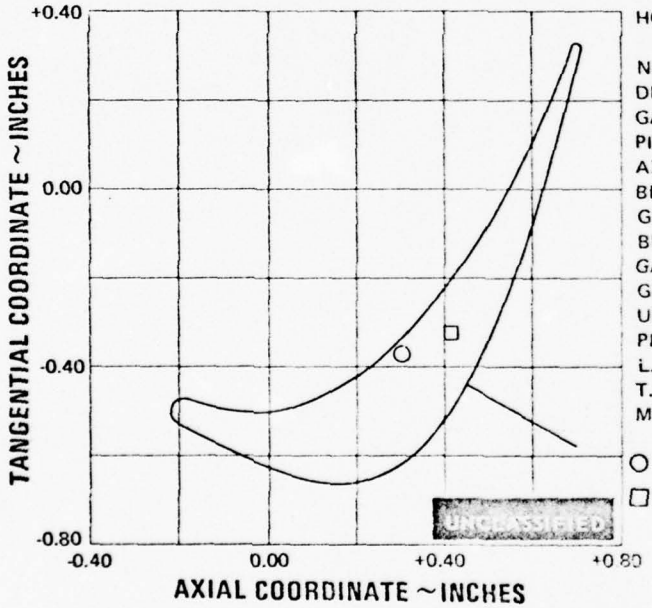

HOT DIMENSIONS

NUMBER OF FOILS	80.00	
DIAMETER	22.8900	IN
GAGING	0.2764	IN
PITCH	0.8989	IN
AXIAL WIDTH	0.9300	IN
BLADE INLET ANGLE	62.90	DEG
GAS INLET ANGLE	62.90	DEG
BLADE EXIT ANGLE	17.57	DEG
GAS EXIT ANGLE	17.57	DEG
GAGING ANGLE	17.91	DEG
UNCOVERED TURNING	15.29	DEG
PRINCIPAL AXIS	-46.39	DEG
L. E. RADIUS	0.0275	IN
T. E. RADIUS	0.0100	IN
METAL AREA	0.1745	$IN.^2$

	X	Y
○ C. G.	0.3049	-0.3742
□ RADIAL REF.	0.4125	-0.3248
GAGE	0.4521	-0.4412

Figure 127 Recambered Second Vane, Tip Defining Section (GG)

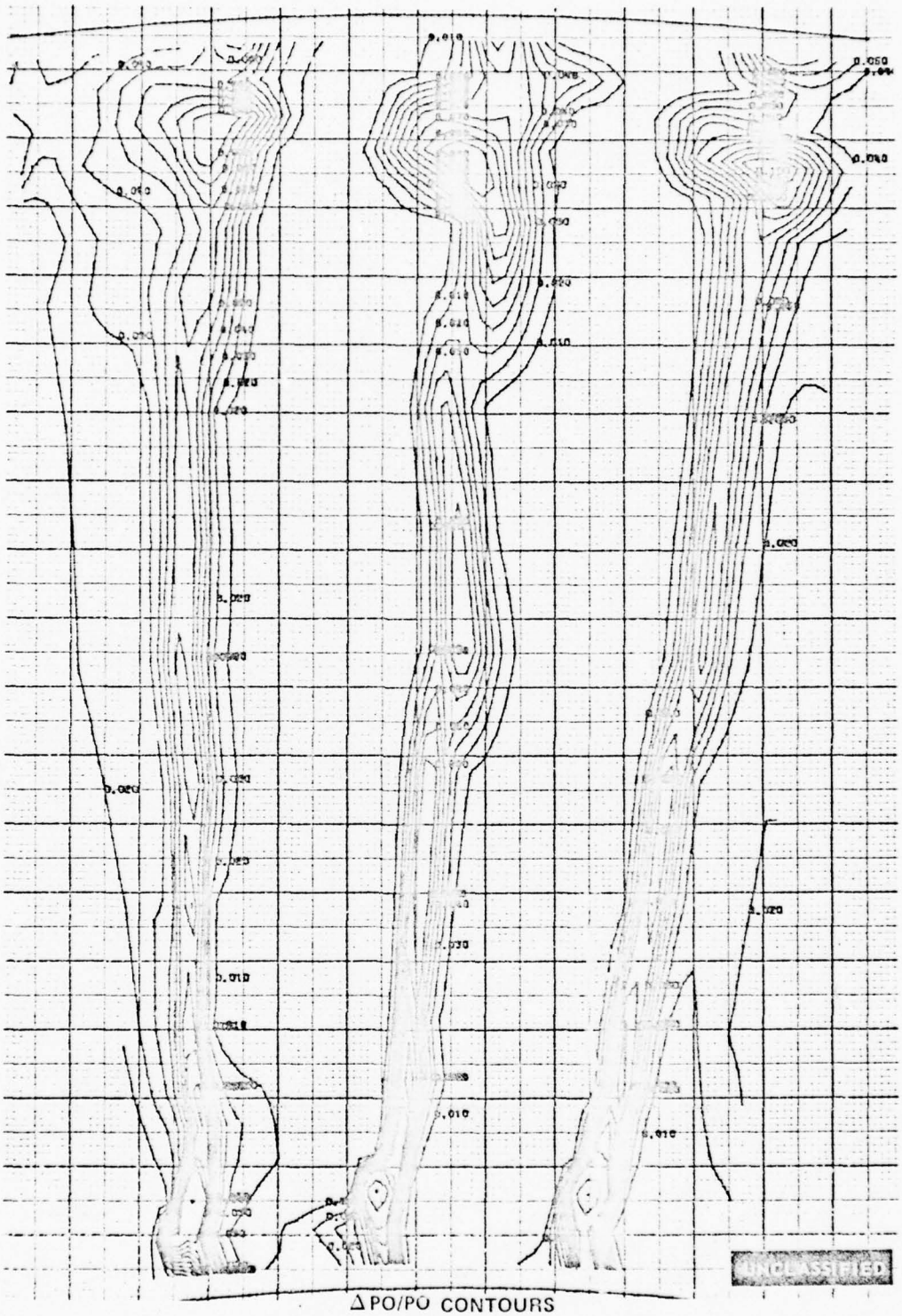

Figure 128 Pressure Loss Contours, Second Vane - Screen Installed, Three Flow Passages, Midspan Exit Mach No. = 0.880, Recambered Airfoils With Redesigned Inlet Guide Vanes and Optimum Boundary Layer Bleeds

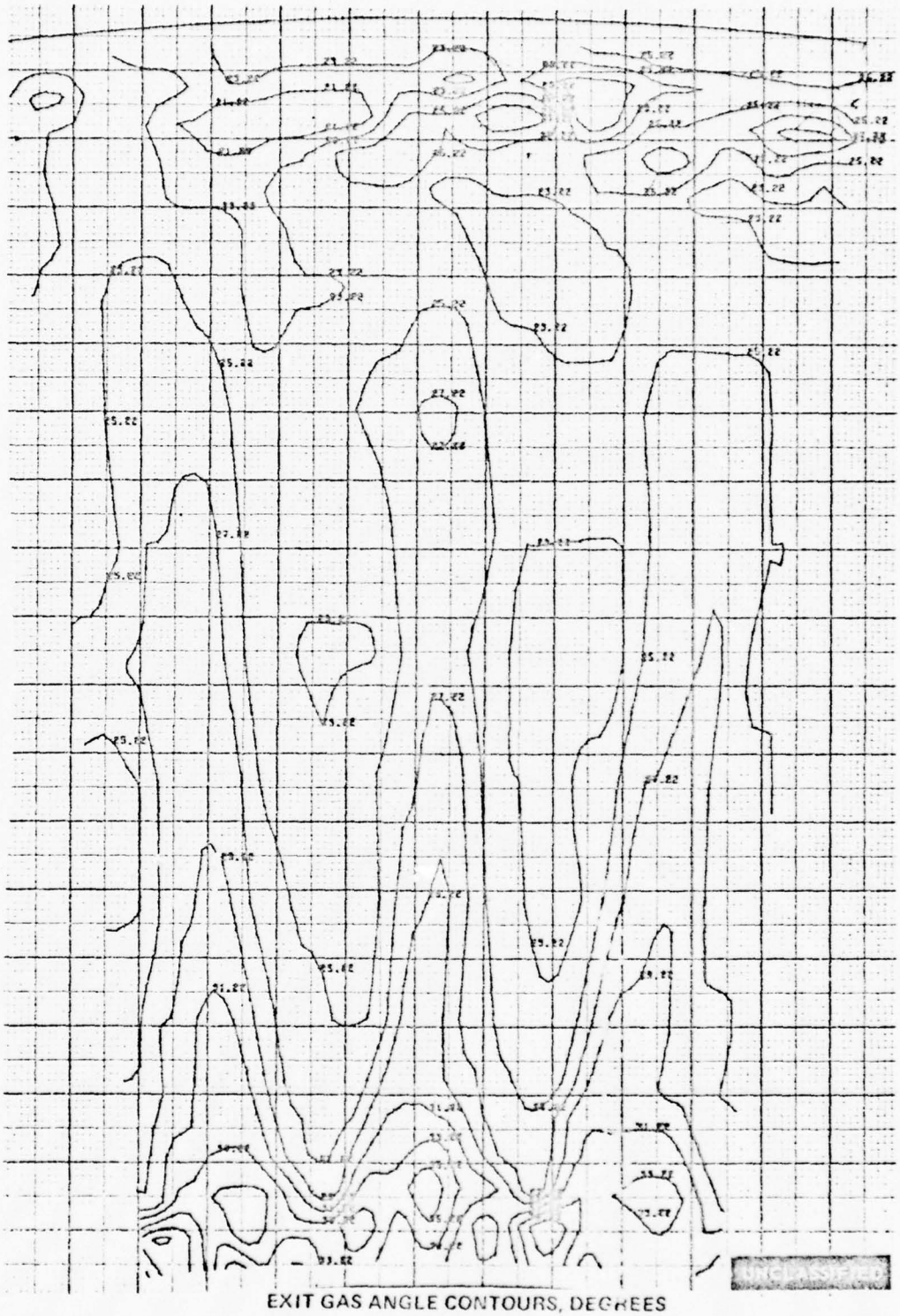

Figure 129 Exit Gas Angle Contours, Second Vane - Screen Installed, Three Flow Passages, Midspan Exit Mach No. = 0.880, Recambered Airfoils With Redesigned Inlet Guide Vanes and Optimum Boundary Layer Bleeds

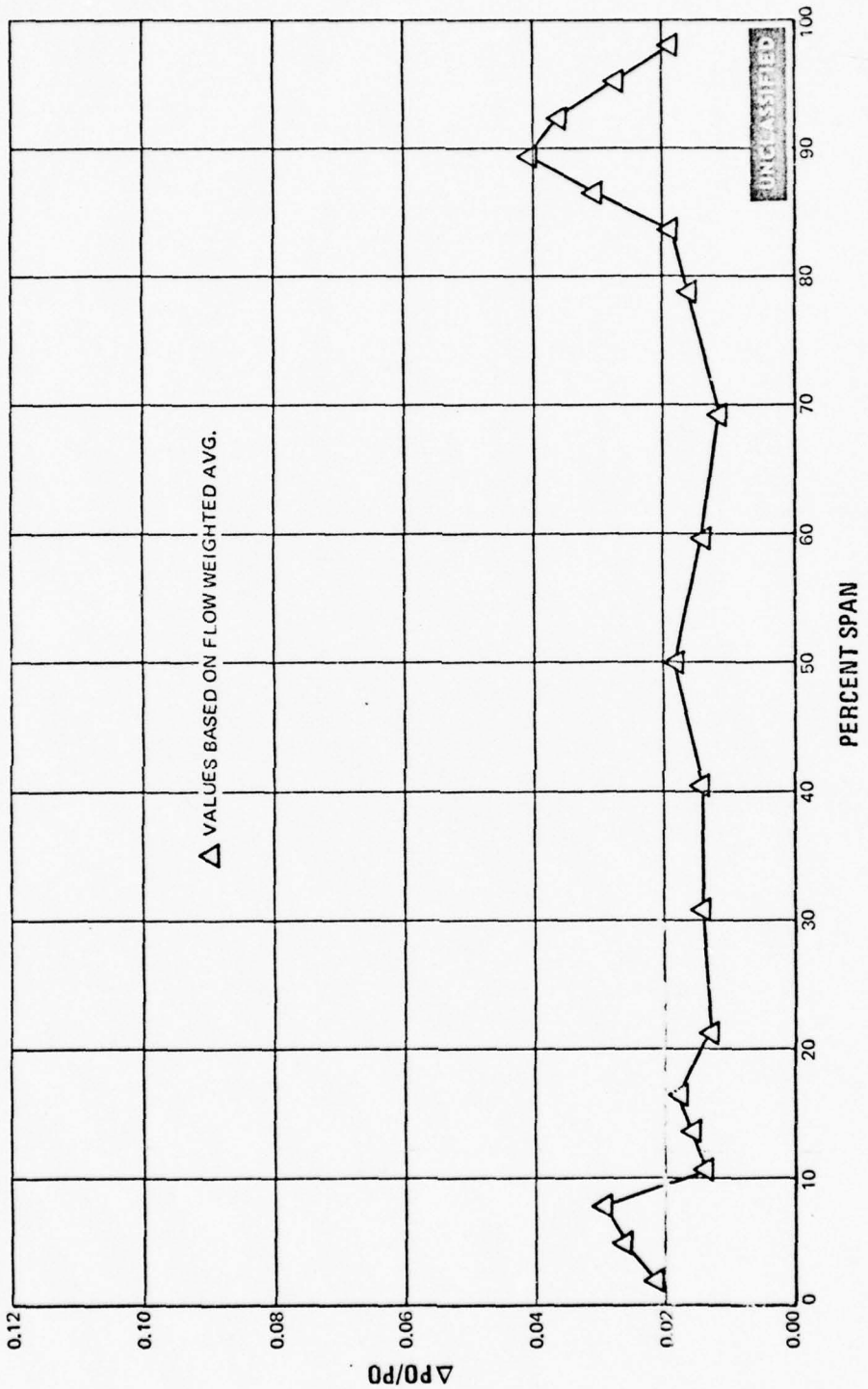

Figure 130 Spanwise Pressure Loss Distribution, Second Vane - Screen Installed, Midspan
Exit Mach No. = 0.880, Recambered Airfoils With Redesigned Inlet Guide
Vanes and Optimum Boundary Layer Bleeds

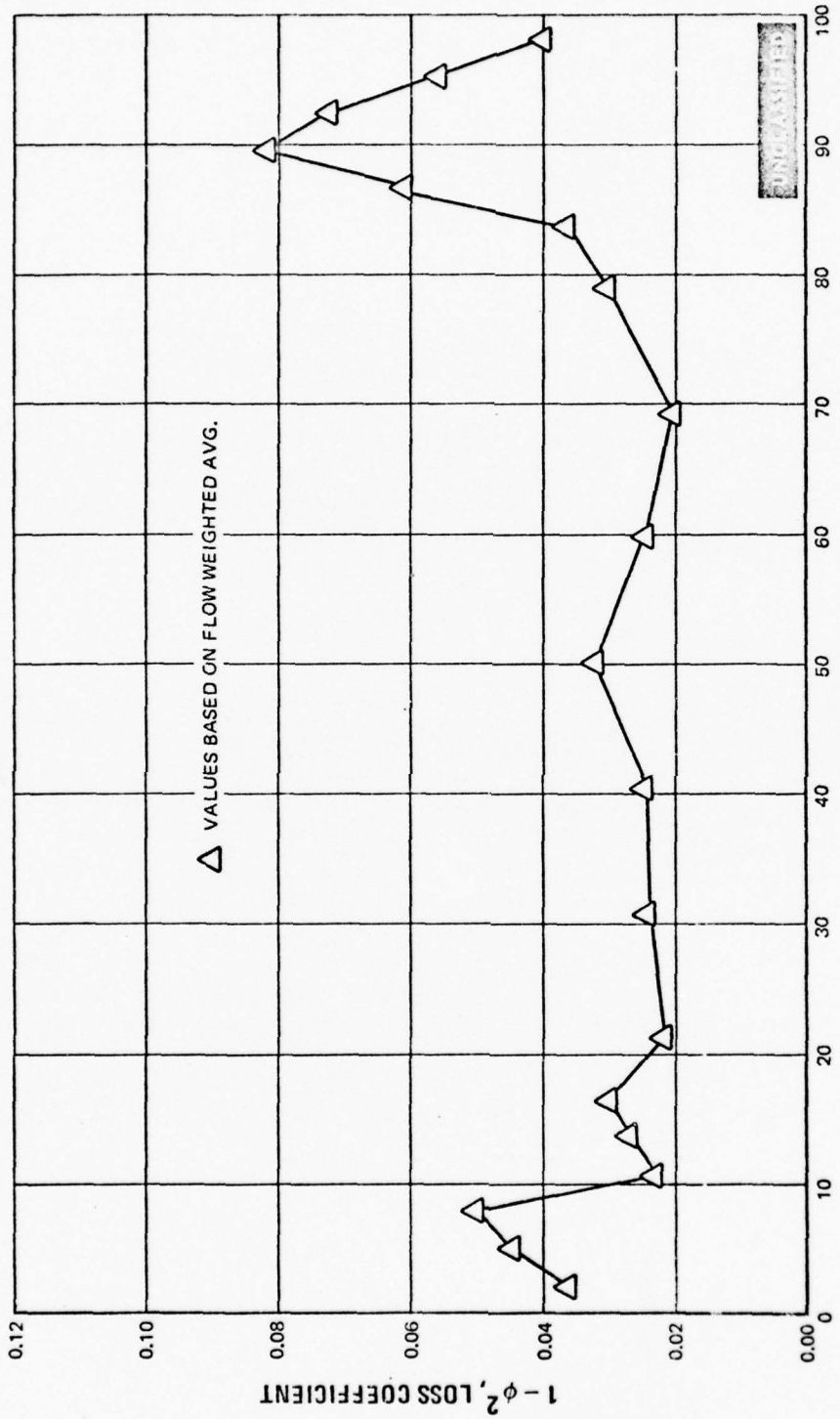

Figure 131 Spanwise Loss Coefficient, Second Vane - Screen Installed, Midspan Exit Mach No. = 0.880, Recambered Airfoils With Redesigned Inlet Guide Vanes and Optimum Boundary Layer Bleeds

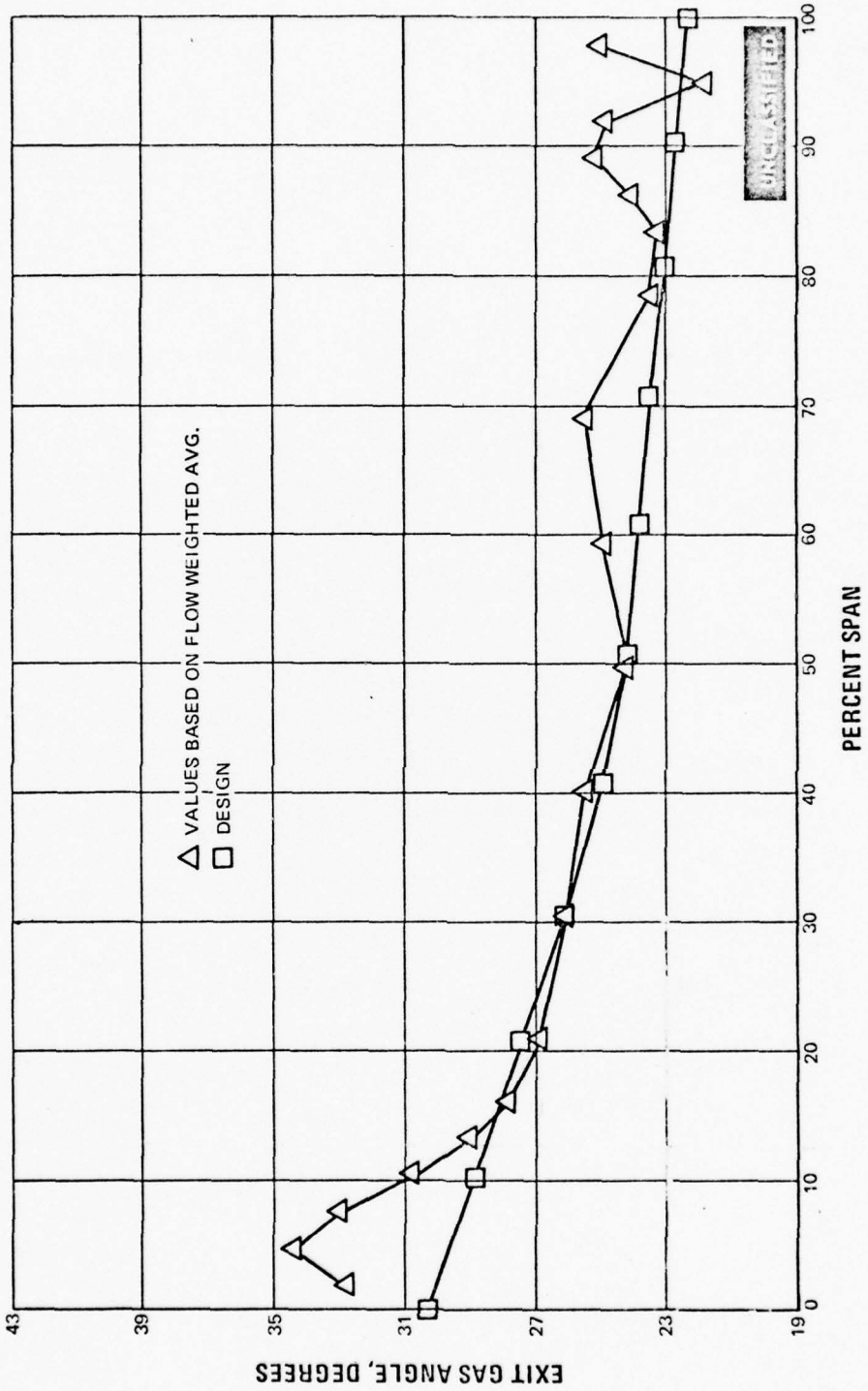

Figure 132 Spanwise Exit Gas Angle Distribution, Second Vane - Screen Installed, Midspan Exit Mach No. = 0.880, Recambered Airfoils With Redesigned Inlet Guide Vanes and Optimum Boundary Layer Bleeds

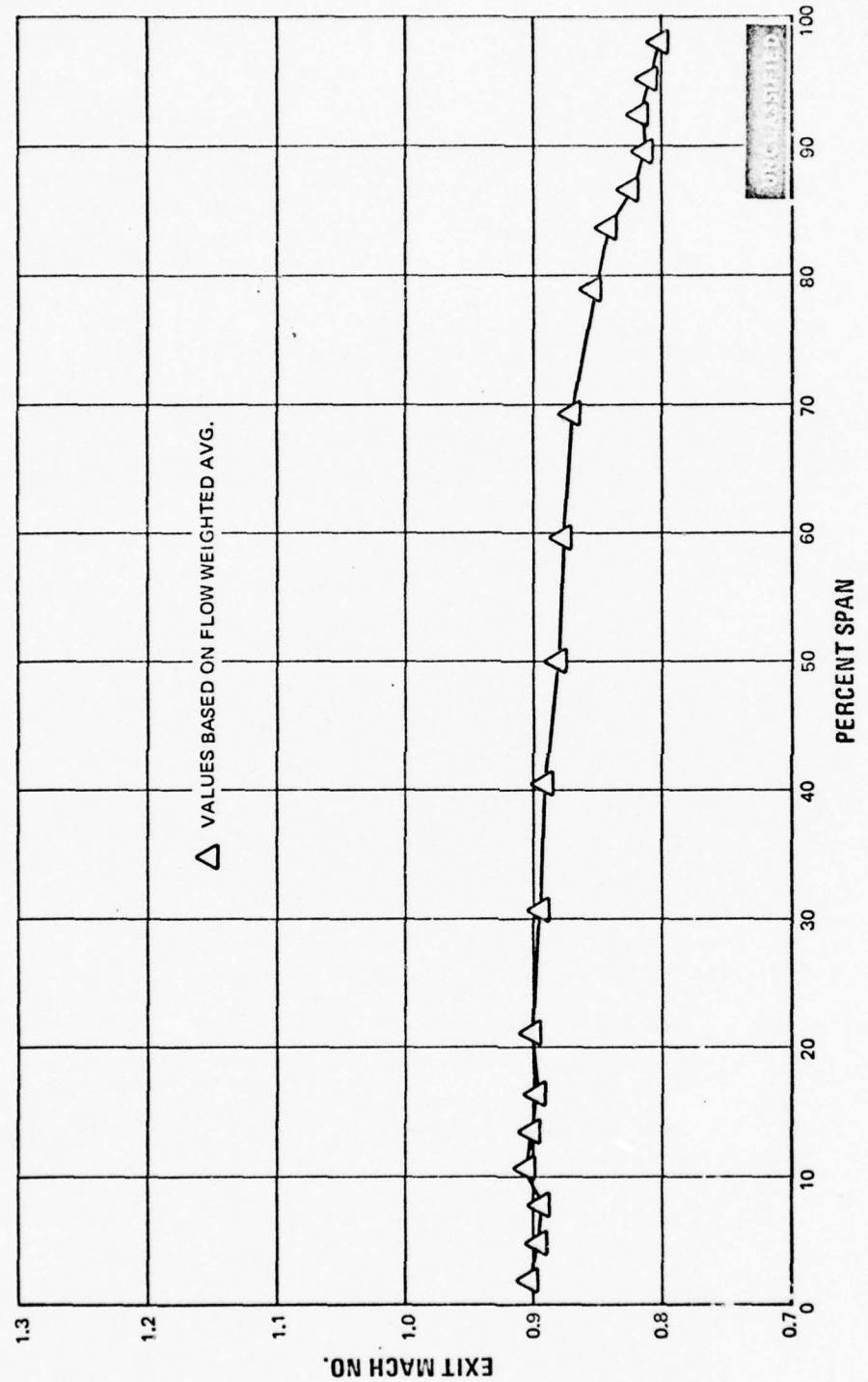

Figure 133 Spanwise Exit Mach Number Distribution, Second Vane - Screen Installed, Mid-span Exit Mach No. = 0.880, Recambered Airfoils With Redesigned Inlet Guide Vanes and Optimum Boundary Layer Bleeds

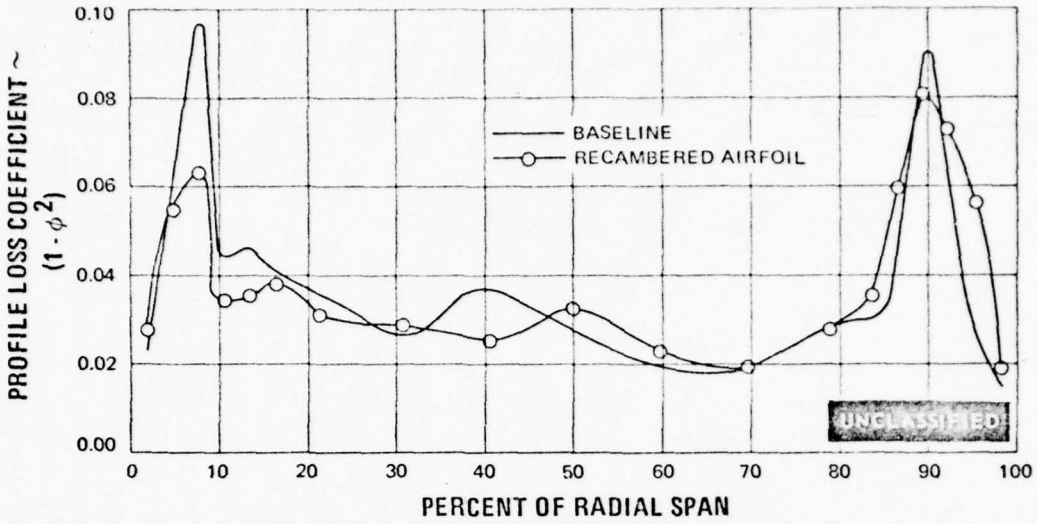

Figure 134 Comparison of Recambered Airfoil Spanwise Loss Coefficient Distribution with Baseline Values

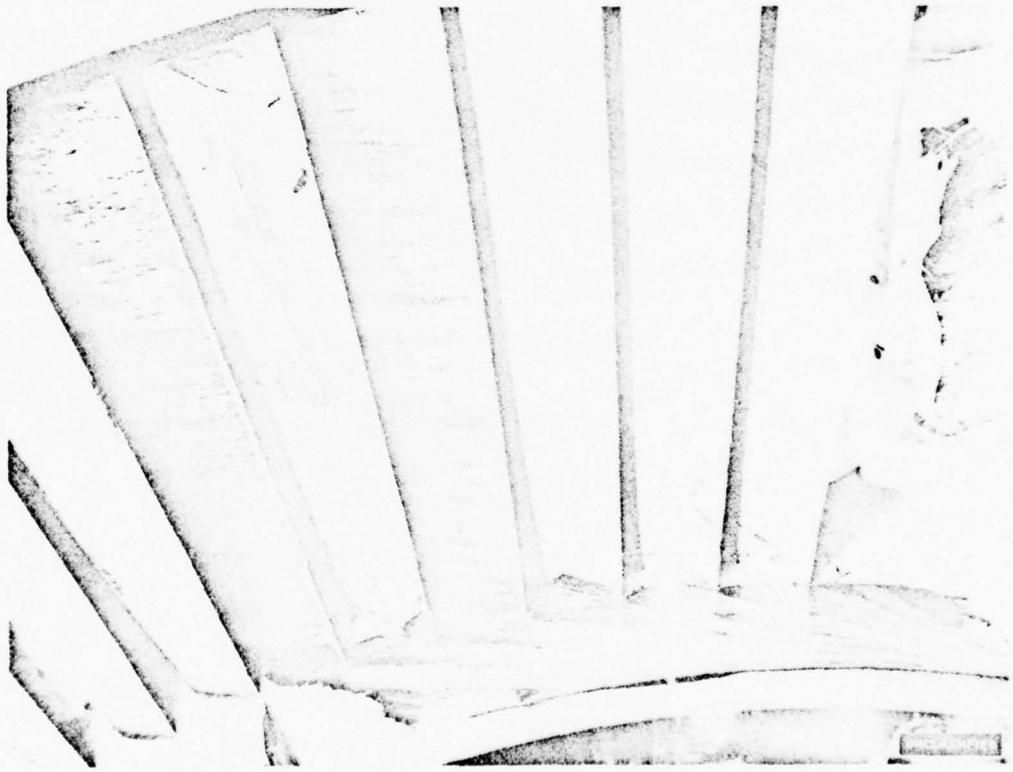

Figure 135 Oil and Graphite Flow Patterns--Second Vane Recambered Airfoils; Midspan Exit Mach No. =0.880

Figure 136 Oil and Graphite Flow Patterns--Second Vane Recambered Airfoils; Midspan Exit Mach No. =0.880

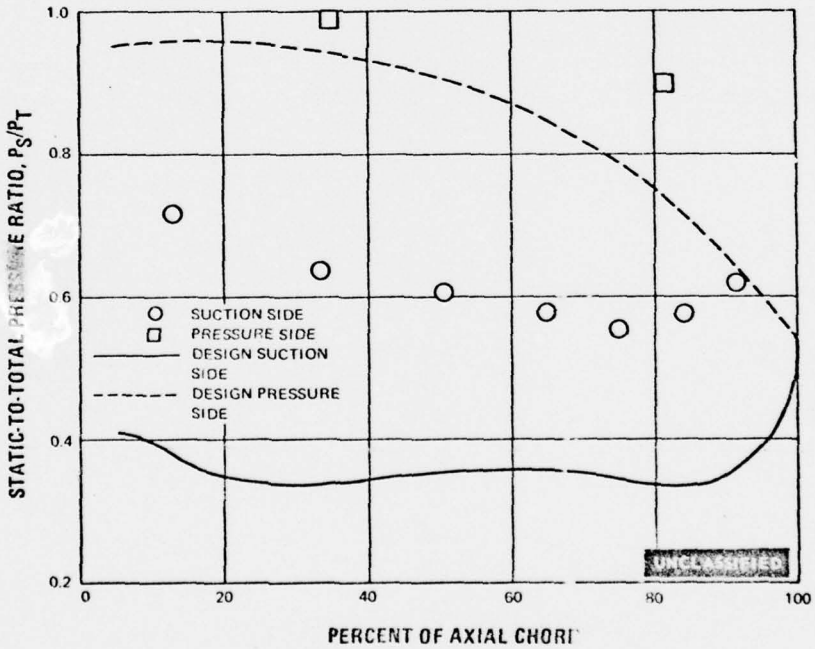

Figure 137 Static-to-Total Pressure Ratio Versus Percent of Axial Chord, Second Vane Recambered Airfoils With Redesigned Inlet Guide Vanes, Optimum Boundary Layer Bleeds and Inlet Screen – Root Section

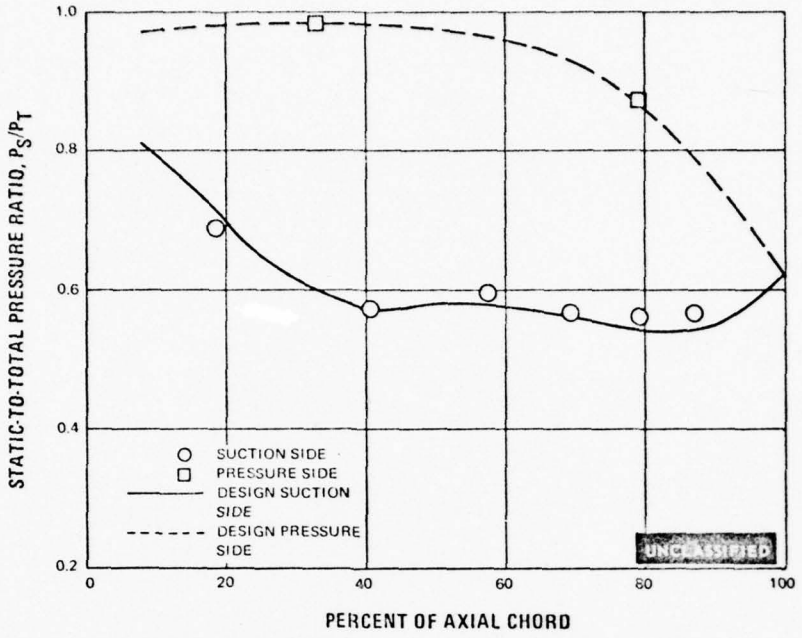

Figure 138 Static-to-Total Pressure Ratio Versus Percent of Axial Chord, Second Vane Recambered Airfoils With Redesigned Inlet Guide Vanes, Optimum Boundary Layer Bleeds and Inlet Screen–Mean Section

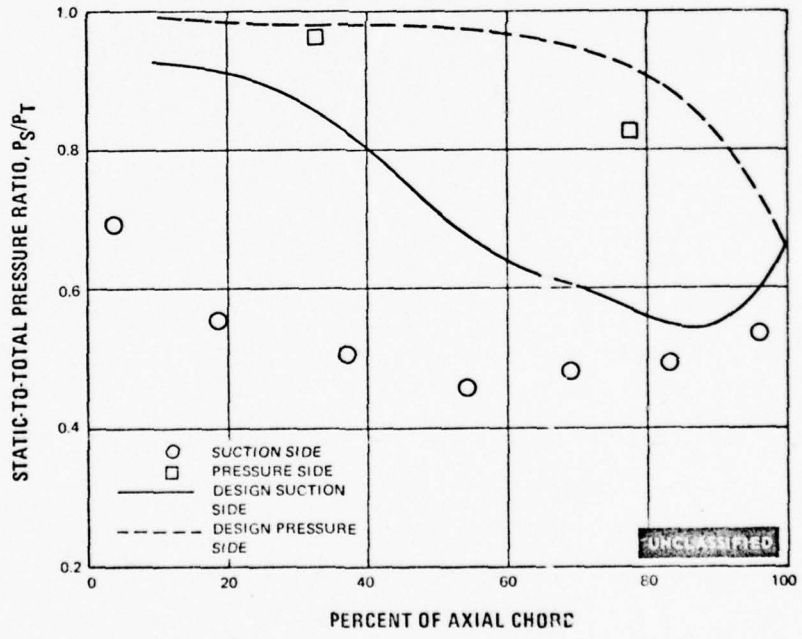

Figure 139 Static-to-Total Pressure Ratio Versus Percent of Axial Chord, Second Vane Recambered Airfoils With Redesigned Inlet Guide Vanes, Optimum Boundary Layer Bleeds and Inlet Screen–Tip Section

9. CONCLUSIONS

(U) Table XXI summarizes the measured loss coefficients for the various boundary layer control techniques, other than the flow fence/increased surface roughness test which showed no promise for future investigation. Overall loss coefficients are shown, as well as integrated values from midspan to each of the end-walls. Also, comparison plots of the average spanwise coefficients and exit gas flow angles are shown in Figures 140 and 141 for the baseline airfoil, the recontoured airfoil, end wall contouring, and recambered airfoil investigation. These plots are at the midspan exit Mach numbers of Table XXI.

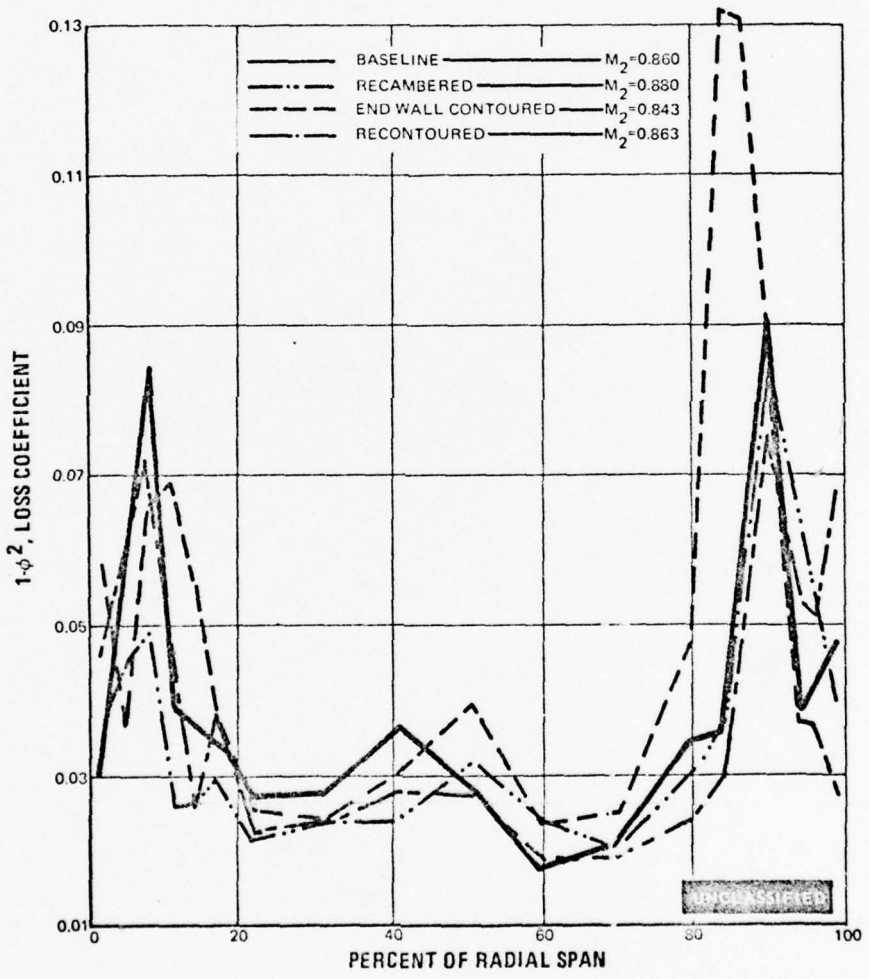

Figure 140 Comparison of Baseline Loss Coefficients With Those of Various Boundary Layer Control Methods

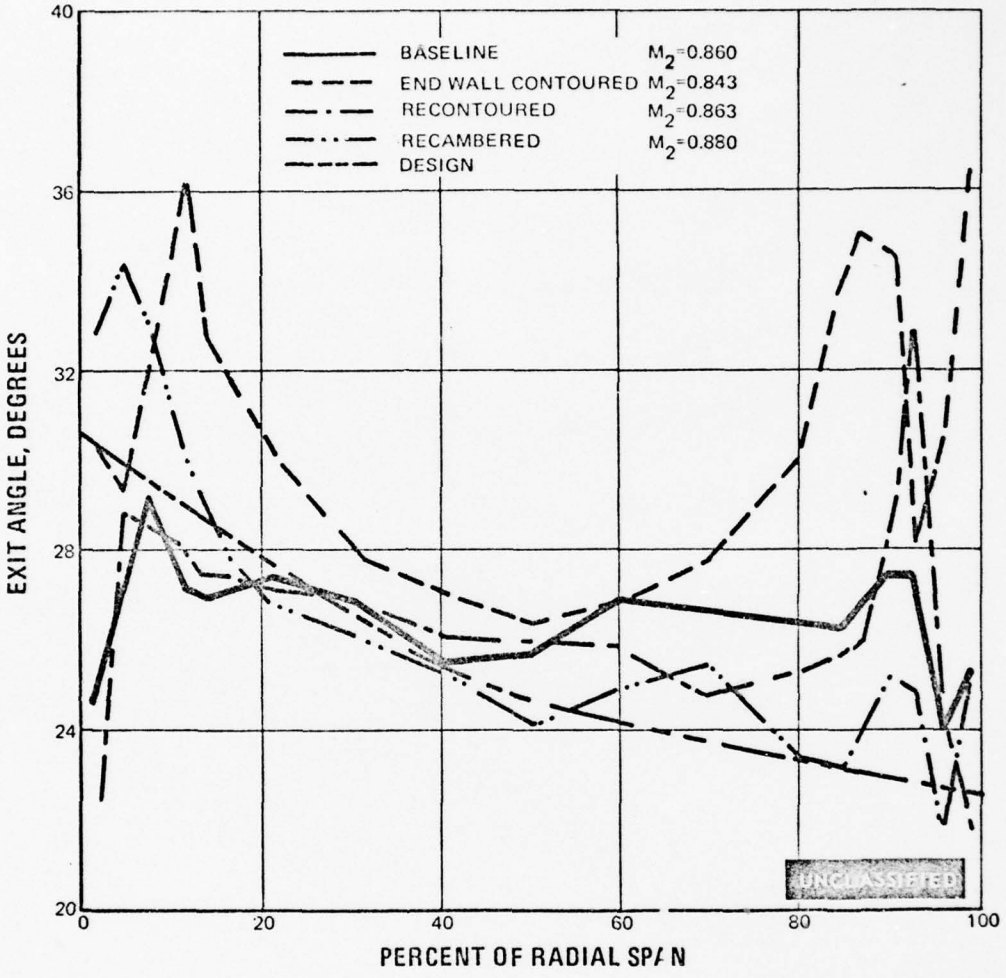

Figure 141 Comparison of Baseline Exit Flow Angles With Those of Various Boundary Layer Control Methods

TABLE XXI

INTEGRATED AVERAGE PROFILE LOSS COEFFICIENTS
SECOND VANE CASCADE

UNCLASSIFIED

	Midspan Mach No.	Loss Coefficient $(1-\phi^2)$ Overall	Midspan To I.D.	To O.D.
Baseline	0.860	0.0349	0.0353	0.0345
Recontoured Airfoil	0.863	0.0336	0.0338	0.0334
End Wall Contoured	0.843	0.0428	0.0374	0.0482
Recambered Airfoil	0.880	0.0329	0.0286	0.0372

(U) Based on these comparisons, it appears that the most promising method for improving turbine performance is that of local airfoil recambering. The reasons for choosing recambering are that:

- This technique was shown to have a strong effect on end losses, including significantly reducing them. It is important to decrease end-wall losses since, proportionally, the end loss per-unit-area is about 2.6 times the profile loss per-unit-area
- This is a technique which is a natural part of the airfoil design optimization if a satisfactory end-wall model is available
- This technique readily lends itself to fabrication.

(U) The other techniques showed no promise of reducing end-wall losses for the configurations that were investigated. Even though a great deal was learned about these other techniques in this program, and even though there may be a successful method of applying them, it is not now clear how this can be done within the scope of this Contract. As a result, recambering is the only practical path available.

(U) It is concluded that the greatest profit lies in the direction of recambering airfoils. Consequently, Phase IIIa will primarily consist of a variety of local recambering tests designed to give us the best qualitative and quantitative information about this method.

10. TEST PROCEDURE

(U) The test procedure employed during the Task IIc boundary layer control technique evaluation was identical to that of the Task IIb baseline evaluation. This procedure was described in complete detail in the Reference 3 Report

SECTION V
MEDIUM SOLIDITY AIRFOIL EVALUATION (TASK IId)

SECTION V

MEDIUM SOLIDITY AIRFOIL EVALUATION (TASK IId)

1. OBJECTIVE

(U) The initial objective of Task IId was to investigate two additional boundary layer control methods, other than the two methods that were investigated under Task IIc, on two different airfoils. Since the performance of the four baseline airfoils was very similar (Reference 3), Task IIc was modified so that four boundary layer control methods were applied only to the second vane (see Section IV of this report), eliminating the need for Task IId as originally conceived. By mutual agreement with the Air Force, the work substituted for the original Task IId was the evaluation of the performance of lower solidity and higher load coefficient airfoils designed for the same velocity triangles as the baseline airfoils of Task IIb. The performance of the first vane and first blade lower-solidity airfoils is reported in this section.

2. TASK OBJECTIVE

(U) Each of the four medium solidity airfoils will be evaluated in an annular segment cascade, exactly as in Task IIb (Reference 3). As of the time of writing this interim report, work on the first vane and blade had been completed; and for these two airfoils, the task objectives were met by the following steps:

- Measurement of all important aerodynamic properties at the cascade inlet and exit planes
- Reconstruction of the entire exit plane loss distribution
- Reconstruction of the entire exit plane flow pattern
- Measurement of the airfoil surface static pressure distributions at three radial locations
- Careful analysis of all data and visual clues.

3. AIRFOIL SECTION AND FACILITY DESIGN

(U) The medium-reaction, medium-solidity airfoils were designed to the same turbine velocity diagrams as the normal solidity airfoils. These were reported in the Reference 1 Report. A summary of the pertinent design values, the airfoil elevations, gaging distribution, airfoil sections, predicted surface pressure distribution, and airfoil radius of curvature for each of the four airfoils was presented at five spanwise locations in the Reference 3 Report. The four airfoils are the first and second vanes, and the first and second blades. The fabrication coordinates of each airfoil were also tabulated in the Reference 3 Report, including the airfoil angles, airfoil areas, axial chords and uncovered turnings.

(U) The test section design for each of the four medium-solidity airfoils is as close as possible to the normal solidity cascades. Since the normal solidity cascade exhausted to atmosphere and the medium solidity cascade rig was connected to the laboratory exhaust system, differences in the exit configurations of these cascades resulted. The inlet guide vane designs were identical for both rigs. The designs of the inlet guide vanes were presented in the Reference 2 Report.

(U) Static pressure instrumentation was installed in order to determine the static pressure distributions on the airfoils, and over both the test airfoil inlet and exit end walls in the medium-solidity cascade rig. The static pressure instrumentation on the airfoils was located at the mean section and at a section 0.1 inch from the outer and inner endwalls. These sections are shown in Figure 142, and the axial chord locations of the pressure taps are listed in Tables XXII through XXV for the four configurations tested. Great care was taken to preserve the contour and smoothness of the suction side of each instrumented airfoil. To this end, all hypodermic tube leads were placed in grooves on the pressure surface, and pressure tap holes were then drilled into these tubes from the suction surface (see Figure 143). The instrumented airfoil was located next to the center channel in each of the four configurations.

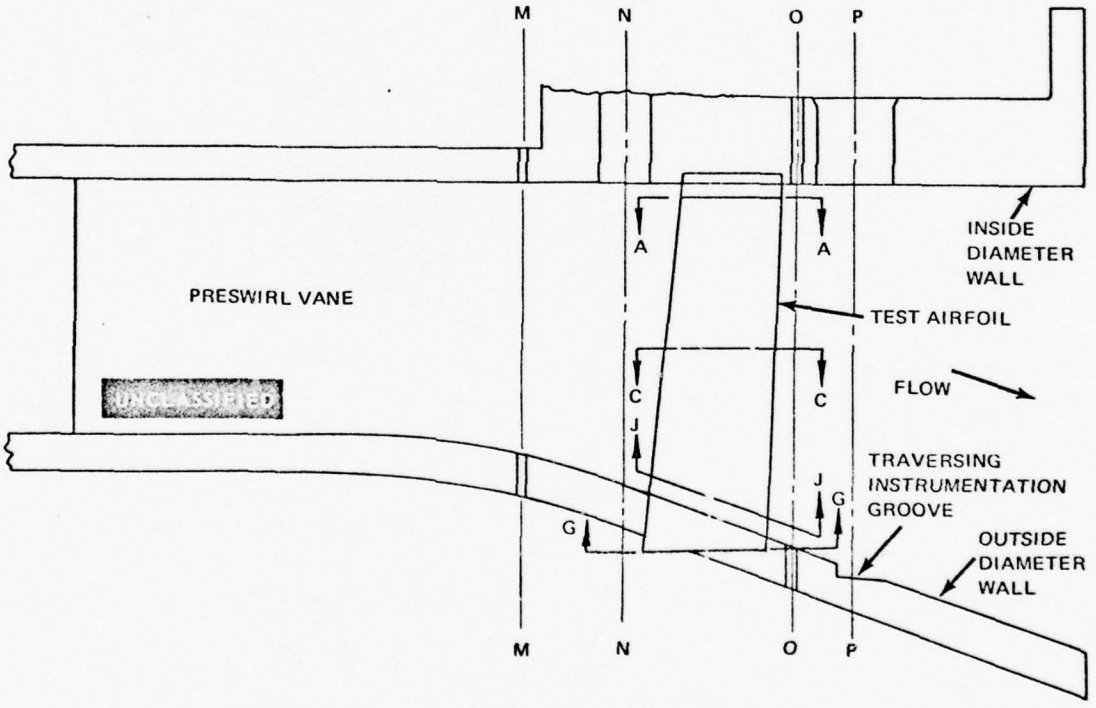

Figure 142 Medium Solidity Annular Segment Cascade – Flowpath Cross-Section

TABLE XXII

AIRFOIL STATIC PRESSURE INSTRUMENTATION
MEDIUM SOLIDITY

Section	Airfoil Side	Axial Length From L. E.	X/bx
Root	Suction		
Section		0.044	0.056
		0.128	0.165
A-A		0.211	0.273
		0.295	0.382
		0.379	0.490
		0.462	0.598
		0.546	0.707
		0.630	0.816
	Pressure	0.520	0.674
		0.265	0.344
Mean	Suction		
Section		0.084	0.100
		0.251	0.299
C-C		0.335	0.400
		0.419	0.500
		0.502	0.599
		0.586	0.700
		0.670	0.799
		0.754	0.899
	Pressure	0.703	0.840
Tip	Suction		
Section		0.100	0.110
		0.309	0.340
G-G		0.499	0.548
		0.574	0.631
		0.655	0.720
		0.710	0.780
		0.792	0.870
	Pressure	0.681	0.747
		0.390	0.429

NOTE: Tip section taps are actually located parallel to wall on section J-J shown in Figure 142.

TABLE XXIII

AIRFOIL STATIC PRESSURE INSTRUMENTATION

MEDIUM SOLIDITY
FIRST STAGE BLADE

Section	Airfoil Side	Axial Length From L.E.	X/bx
Root Section A-A	Suction	0.074 0.276 0.405 0.476	0.124 0.464 0.681 0.800
Mean Section C-C	Suction	0.060 0.150 0.239 0.359 0.419	0.105 0.264 0.421 0.632 0.737
Tip Section G-G	Suction	0.108 0.215 0.323 0.377 0.430	0.201 0.400 0.600 0.700 0.800

NOTE: Tip section taps are actually located parallel to wall on section J-J shown on Figure 142.

TABLE XXIV

AIRFOIL STATIC PRESSURE INSTRUMENTATION
MEDIUM SOLIDITY
SECOND STAGE VANE

Section	Airfoil Side	Axial Length From L.E.	X/bx
Root	Suction		
Section		0.083	0.990
		0.167	0.199
A-A		0.250	0.298
		0.334	0.398
		0.418	0.496
		0.510	0.608
		0.585	0.696
		0.668	0.795
	Pressure	0.561	0.669
		0.191	0.227
Mean	Suction		
Section		0.088	0.100
		0.176	0.200
		0.264	0.300
		0.371	0.421
C-C		0.440	0.500
		0.528	0.600
		0.616	0.700
		0.705	0.800
	Pressure	0.620	0.704
		0.179	0.203
Tip	Suction		
Section		0.256	0.275
		0.473	0.509
G-G		0.544	0.585
		0.618	0.665
		0.674	0.725
	Pressure	0.762	0.819
		0.759	0.816

NOTE: O. D. taps are actually located parallel to wall on section J-J shown on Figure 142.

TABLE XXV

AIRFOIL STATIC PRESSURE INSTRUMENTATION
MEDIUM SOLIDITY
SECOND STAGE BLADE

Section	Airfoil Side	Axial Length From L.E.	X/bx
Root	Suction		
Section		0.081	0.125
		0.200	0.308
A-A		0.342	0.528
		0.530	0.817
Mean	Suction		
Section		0.058	0.100
		0.174	0.300
C-C		0.289	0.500
		0.405	0.700
Tip	Suction		
Section		0.100	0.200
		0.200	0.400
G-G		0.300	0.600
		0.400	0.800

NOTE: Tip section taps are actually located parallel to wall on section J-J shown on Figure 142.

Figure 143 Typical Installation of Airfoil Surface Static Instrumentation

(U) The static pressure instrumentation in the test airfoil exit plane was located on both end walls, 0.1 inch axially downstream from the test airfoils. These taps are located at section 0-0 on Figures 142 and 144. A total of fifteen taps for each end-wall were evenly distributed circumferentially so that two complete channels were surveyed. The static pressure instrumentation for the inlet plane was located downstream of the preswirl vanes at section M-M (Figures 142 and 144). Three taps were placed on each end-wall at the centers of the three channels.

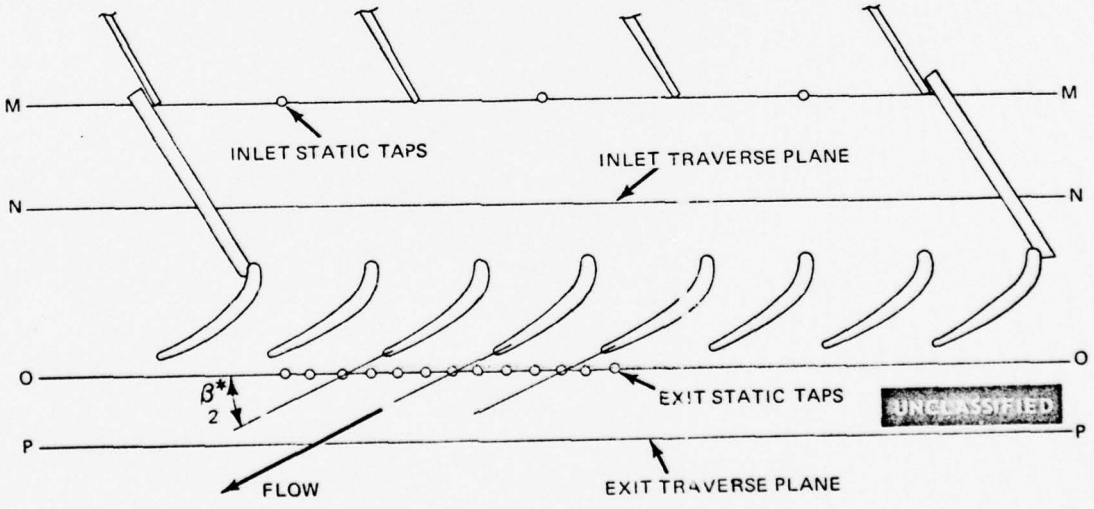

Figure 144 Medium Solidity Annular Segment Cascade -- Unfolded View of Test Section

(U) Four inlet static pressure taps and four total temperature probes were located before and after the inlet plenum screen. Four pressure taps, located in the exit plenum, measured the exit static pressure. A study of these plenum configurations showed the static pressures were equal to the total pressure; therefore, the static taps were used for plenum total pressure readings.

(U) The axial locations of the traverse planes in the medium solidity cascade rig are shown in Figures 142 and 144. Flow quantities necessary for evaluation of the airfoil performance are measured at both these inlet and exit planes. The traversing mechanism moved the probe in circumferential arcs of constant angular extent, and across the flow from the center three channels. The total pressure and gas angle was traversed at nineteen radial locations distributed symmetrically spanwise about the mean. The percents of span for these locations are as follows: 0, 2, 5, 8, 11, 14, 17, 22, 30, 50, 70, 78, 83, 86, 89, 92, 95, 98 and 100. In order to define the end-wall regions more accurately, more traverses were taken in the end regions.

(U) The probe used to measure the total pressure and flow direction was an extended tip yaw angle-seeking cobra probe. This probe has low blockage, operates well at high Mach numbers, and is ideally suited for the traversing mechanism used in this rig. A front view of the cobra probe is shown in Figure 145.

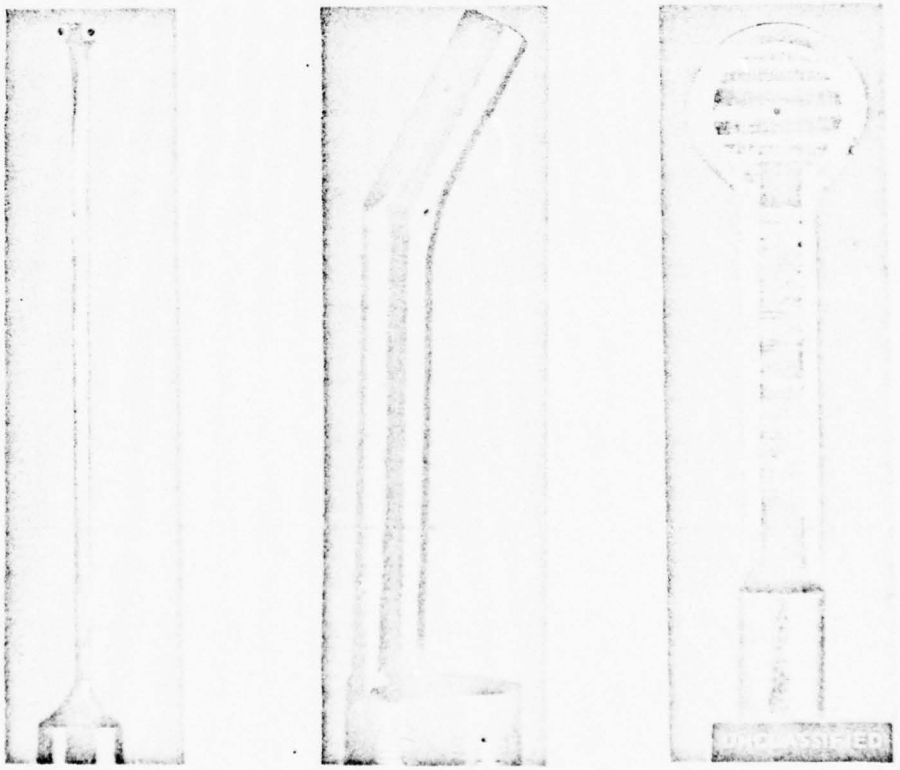

Figure 145 Probes Used in Medium Solidity Annular Cascade – From Left to Right: 1.5 Inch Minimum Blockage "Cobra" Probe (P_{TOTAL} + A/A), "Knee" Probe (Pitch Angle), "Banjo" Probe (P_{STATIC} + A/A)

(U) The slope of the outer wall gives a good indication that significant radial velocities will exist in all the cascade configurations, and stream line calculations using the Turbine Streamline Program proved this to be the case. Therefore, the cobra probe required calibration for pitch angle incidence. A typical example of this pitch angle error is shown in Figure 146. The pitch angle is that angle measured from the shaft axis of the probe, and is equal to the sum of 90°and the arc tangent of the radial velocity component divided by the stream line velocity or $\left[90° + \tan^{-1}\left(\frac{Cr}{C}\right)\right]$.

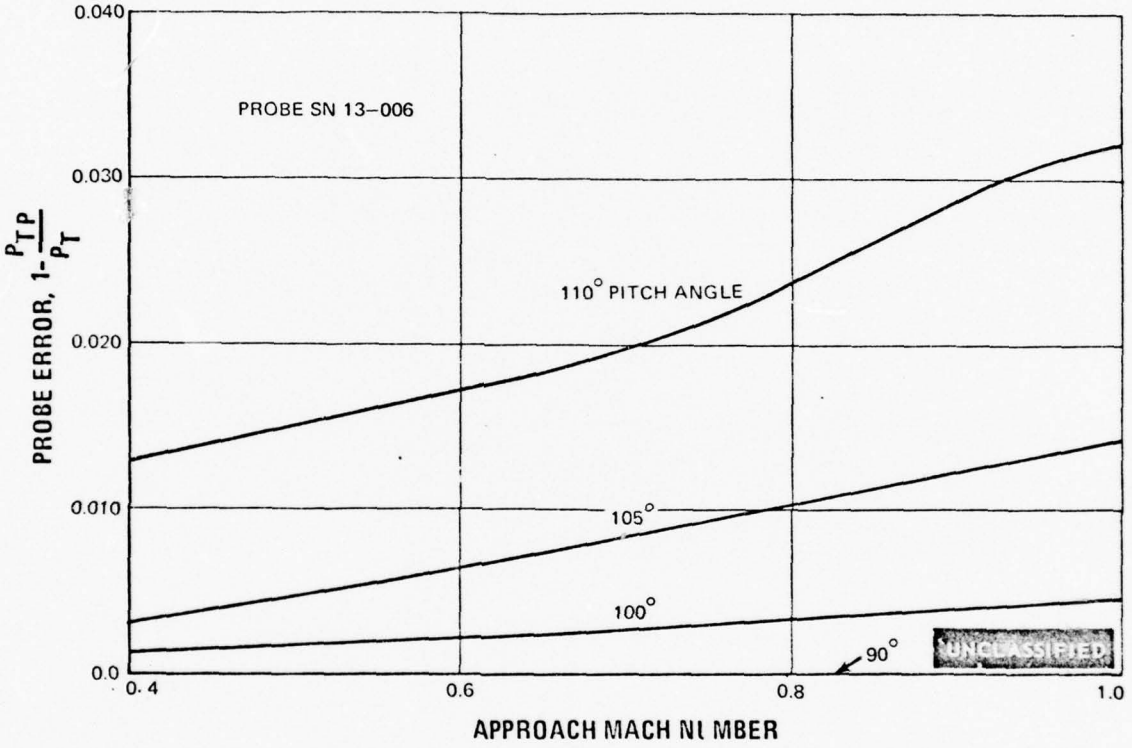

Figure 146 Medium Solidity Cascade Probe Calibration

(U) For the purpose of correcting the total pressure measurements of the cobra probe, the actual pitch angle was measured at the test airfoil exit plane with a pitch angle probe. A picture of this probe is shown in Figure 145 Each cascade test airfoil exit plane was calibrated and a typcial result is shown in Figure 147. Here, the experimental results for the second blade are compared with the analytical prediction. At the test airfoil inlet plane, general agreement with the predicted values made it reasonable to use these values when analyzing the performance of the inlet guide vanes and calculating the test airfoil inlet total pressure profile.

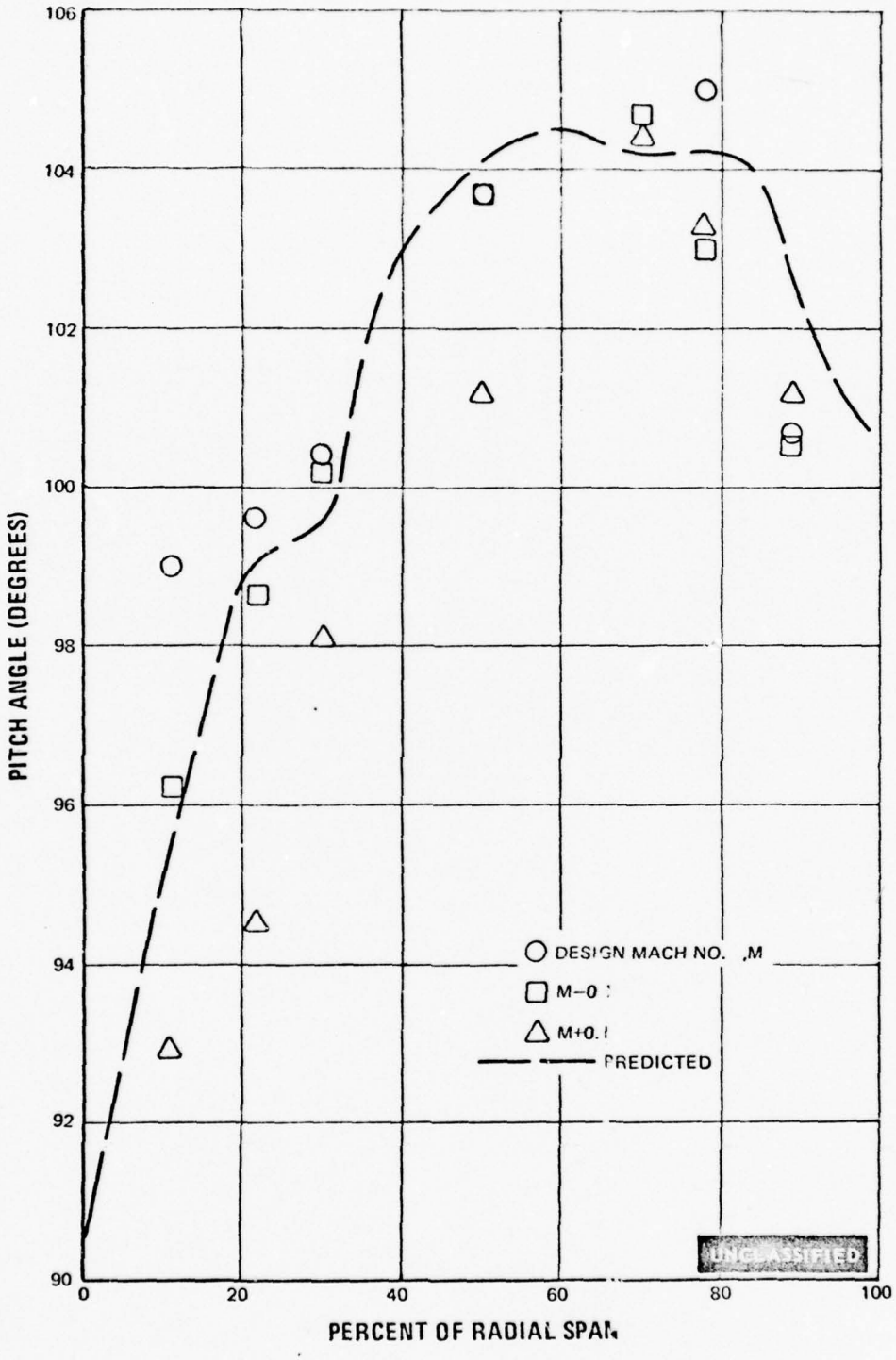

Figure 147 Medium Solidity Second Blade Pitch Angle

(U) Prior to initiating test on the first vane cascade, a banjo probe was used to measure the static pressures at the exit plane. This probe is also shown in Figure 145. Although this probe is difficult to use for measuring static pressure at high design point Mach numbers, it did indicate a smooth static pressure profile at a mean section exit Mach number of 0.6. Experience with previous testing also showed this smooth variation of static pressure at the exit plane.

4. DISCUSSION

(U) The testing and analysis of the data on the medium-reaction, medium-solidity first vane and first blade has been completed. Initial testing of the second vane and second blade has been done, but the data analysis was not completed at the time of writing of this interim report.

(U) For the first vane and first blade, data were taken at the design Mach numbers and at Mach numbers 0.1 below and above the design value, while holding the design Reynolds Number constant. Also, data were taken for the first vane cascade at Reynolds Numbers 50 and 75 percent below the design Reynolds Number and 50 percent above the design Reynolds Number while holding the Mach Number constant at the design value. Except for the 75 percent below design Reynolds Number point, Reynolds Number data were also taken for the first blade. The purpose of taking the test data in this manner was to isolate the Mach number and Reynolds Number effects.

(U) The inlet guide vanes have been calibrated for all four airfoil cascades. Their performance was determined by traversing the inlet to the test airfoils. The measured total pressure loss contours (Figures 148 through 151), the out-of-wake average spanwise loss distribution with probe corrections (Figures 152 through 155) and the inlet guide vane average spanwise exit flow angle (Figures 156 through 159) are presented. The out-of-wake total pressure levels were calculated for the test airfoil inlet conditions since the test airfoil flow channel was not in the path of the inlet guide vane wakes.

(U) Analysis of the inlet guide vane data indicates that the first vane and first blade test airfoils had acceptable inlet pressure loss contours (Figures 148 and 149). Exit gas flow angles from these two guide vanes were also satisfactory (Figures 156 and 157), the incidence on the test airfoils being small over the major portion of the airfoil span. The usual passage secondary flow causes the overturning at the inlet guide vane walls noted in these figures. The second vane inlet guide vane pressure loss contours, however, show excessively large losses and incidence (+5°), indicating that the inlet guide vanes must be corrected before further testing can be justified (Figures 150 and 158). This did not come as a surprise since, as noted in the Reference 3 Report, the normal solidity second vane inlet guide vane of the same design (Task IIb) had to be redesigned for the (Task IIc) boundary layer control evaluation (see Section IV of this Report). This information became known after the guide vanes were fabricated for this medium-solidity test. The second blade cascade also has a drastic positive incidence in the upper half of the span. This inlet guide vane must also be corrected before additional tests are made.

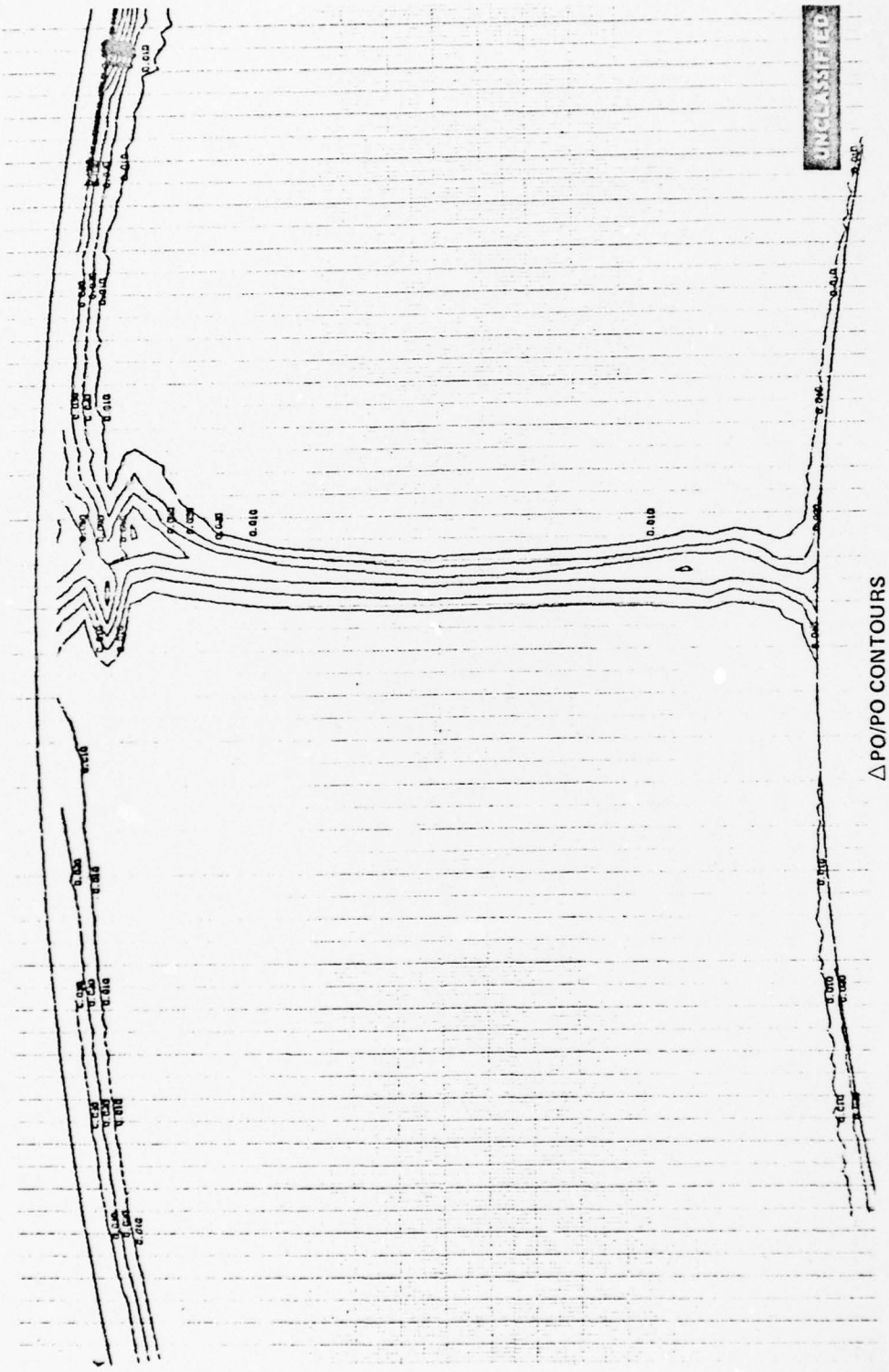

Figure 148 Inlet Guide Vane Pressure Loss Contours, First Vane Medium Solidity Cascade–Midspan Exit Test Airfoil Mach No. = 0.835

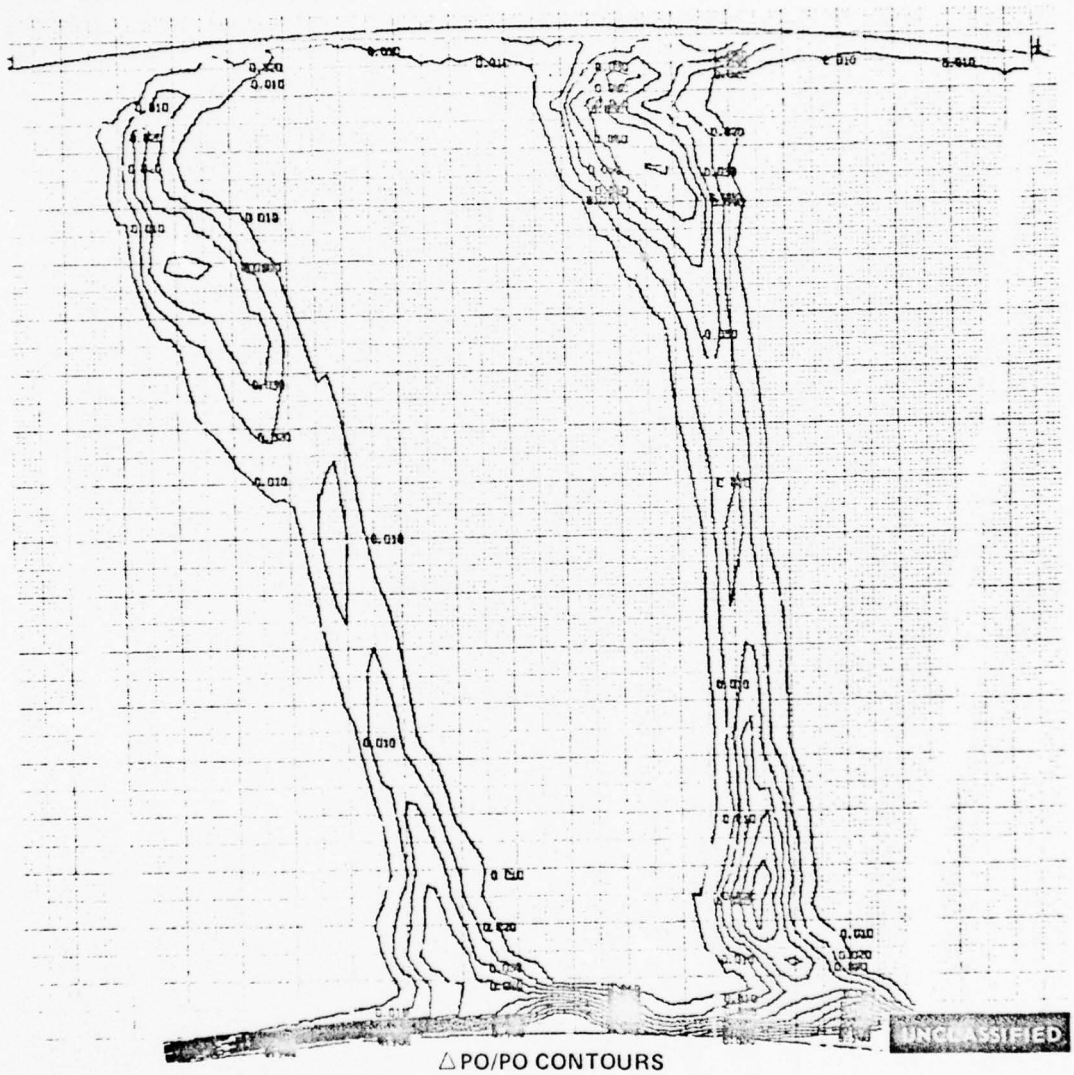

Figure 149 Inlet Guide Vane Pressure Loss Contours, First Blade Medium Solidity Cascade–Midspan Exit Test Airfoil Mach No. = 0.775

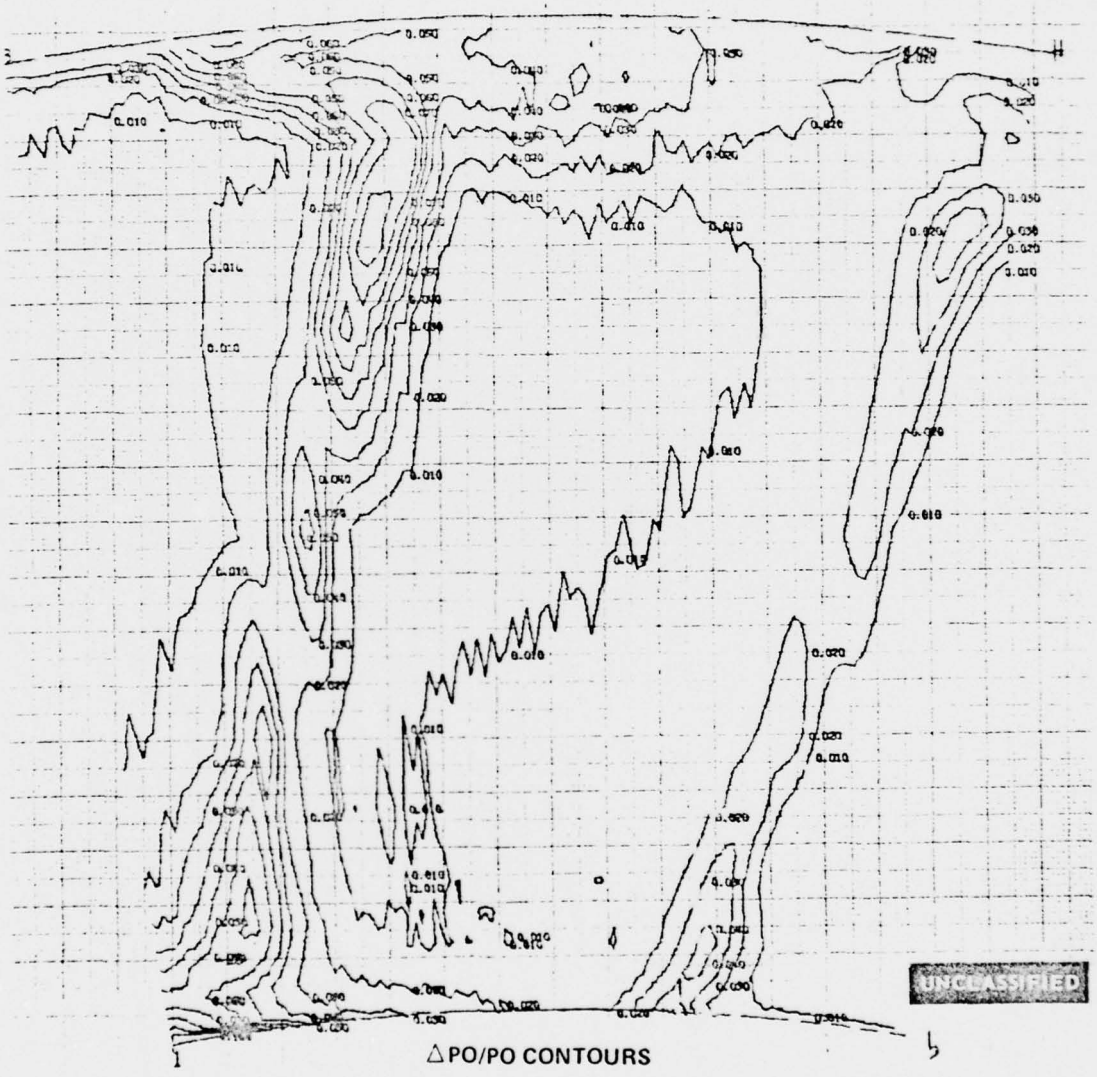

Figure 150 Inlet Guide Vane Pressure Loss Contours, Second Vane Medium Solidity Cascade–Midspan Exit Test Airfoil Mach No. = 0.860

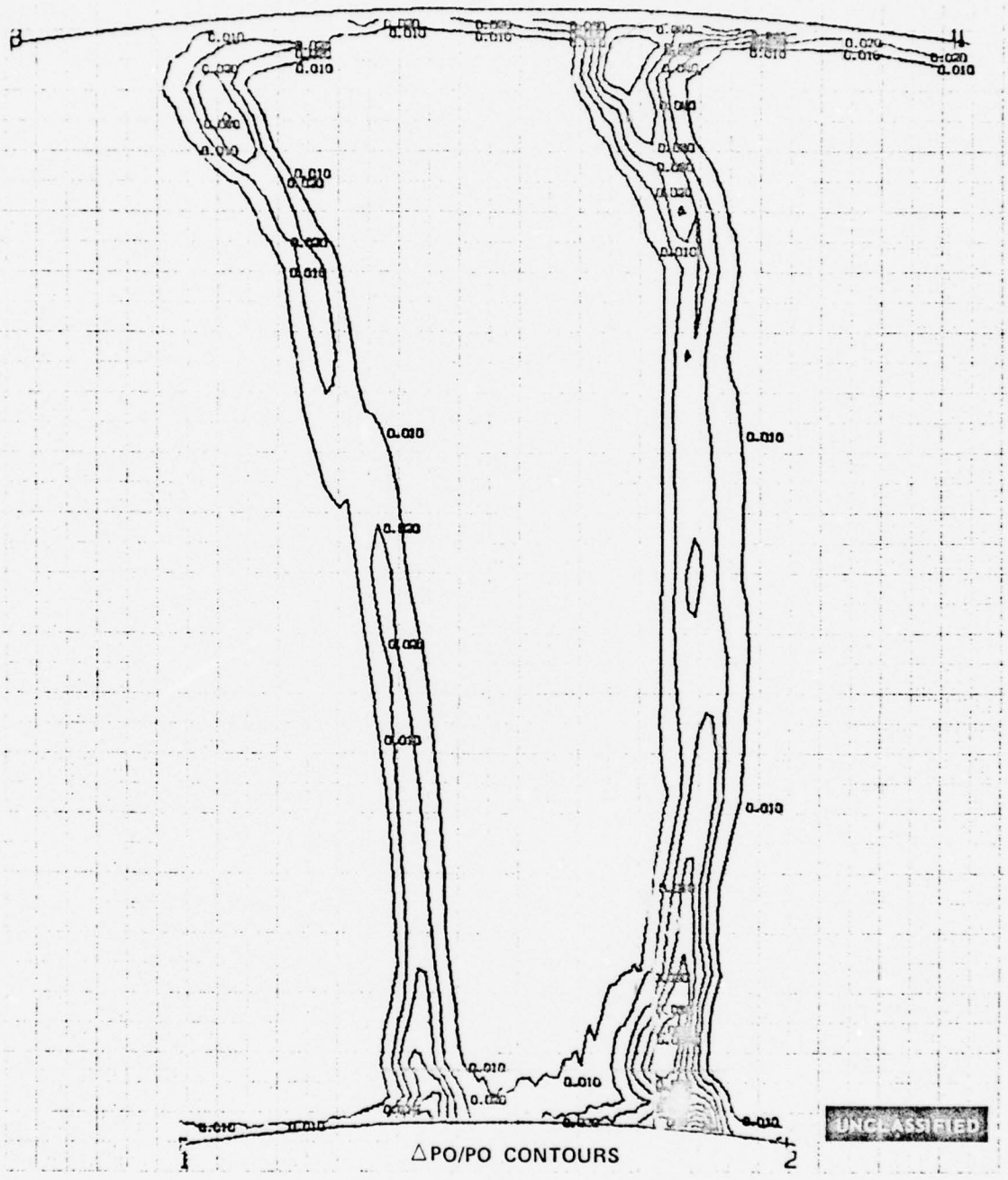

Figure 151 Inlet Guide Vane Pressure Loss Contours, Second Blade Medium Solidity Cascade–Midspan Exit Test Airfoil Mach No. = 0.918

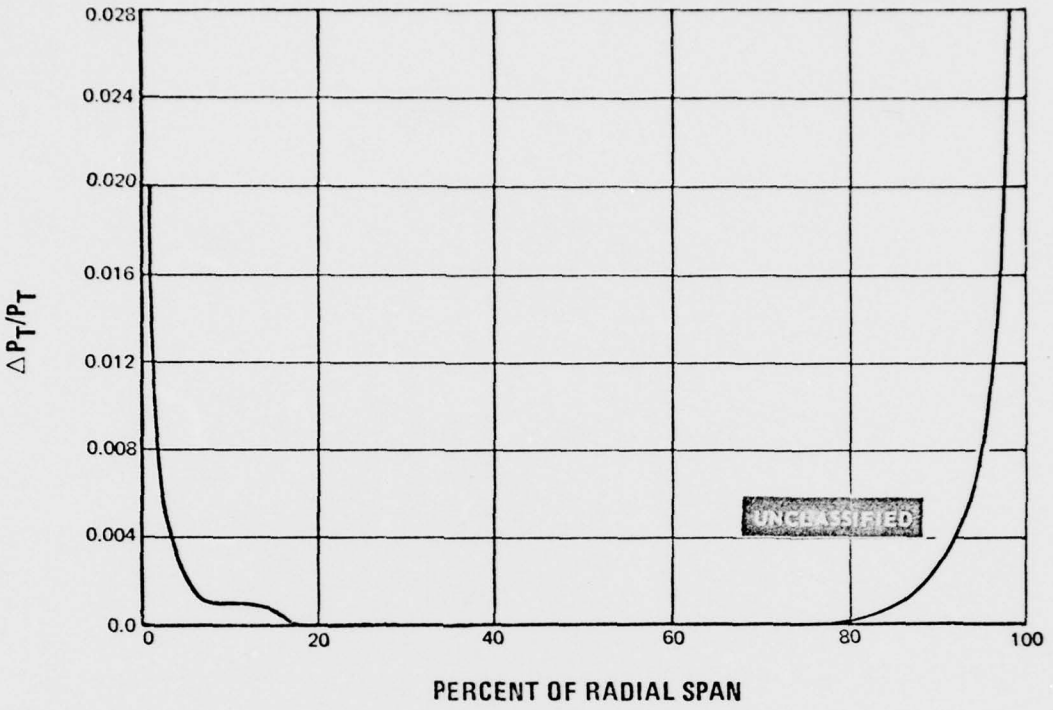

Figure 152 Inlet Guide Vane Spanwise Pressure Loss Distribution, First Vane Medium Solidity Cascade–Midspan Exit Test Airfoil Mach No. = 0.835

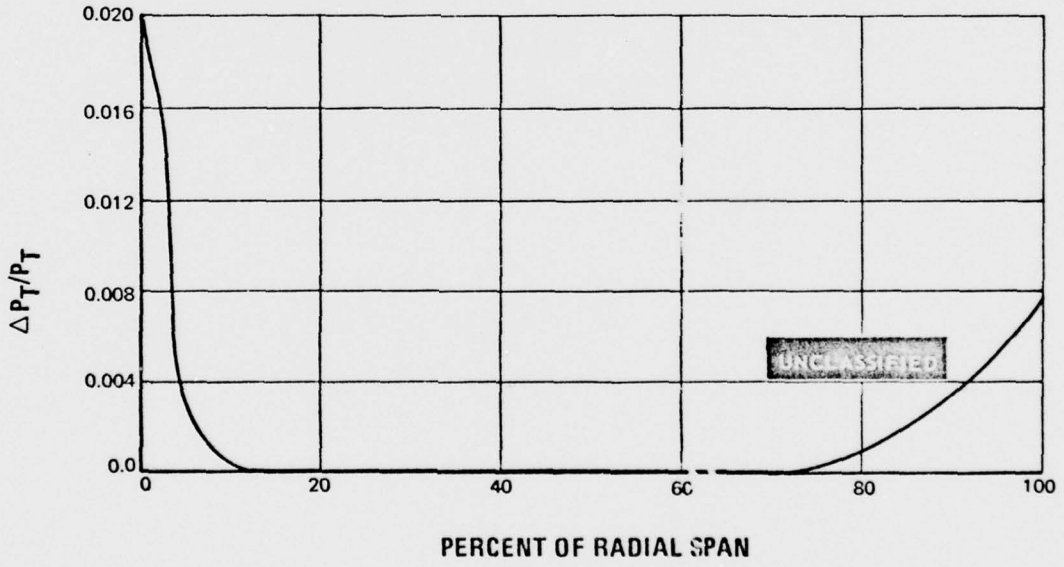

Figure 153 Inlet Guide Vane Spanwise Pressure Loss Distribution, First Blade Medium Solidity Cascade–Midspan Exit Test Airfoil Mach No. = 0.775

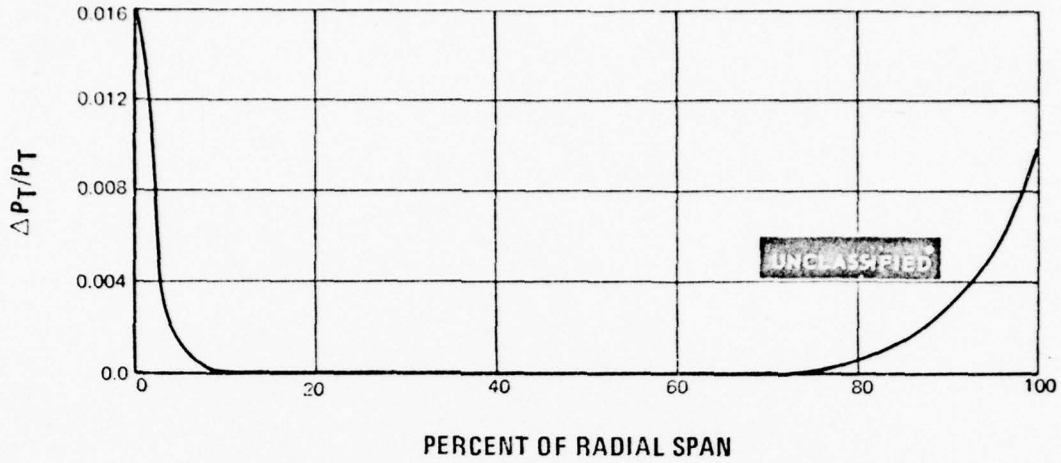

Figure 154 Inlet Guide Vane Spanwise Pressure Loss Distribution, Second Vane Medium Solidity Cascade–Midspan Exit Test Airfoil Mach No. = 0.860

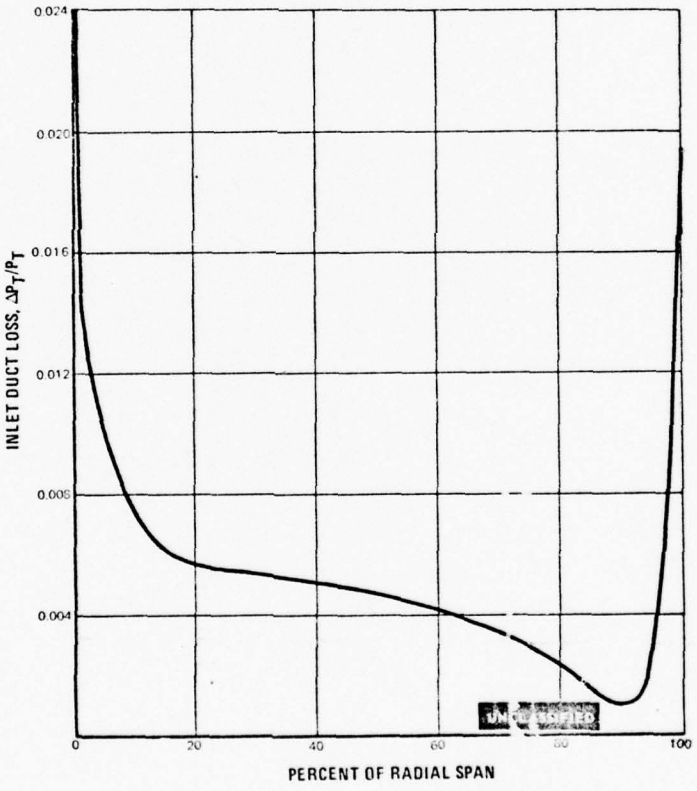

Figure 155 Inlet Guide Vane Spanwise Pressure Loss Distribution, Second Blade Medium Solidity Cascade–Midspan Exit Test Airfoil Mach No. = 0.918

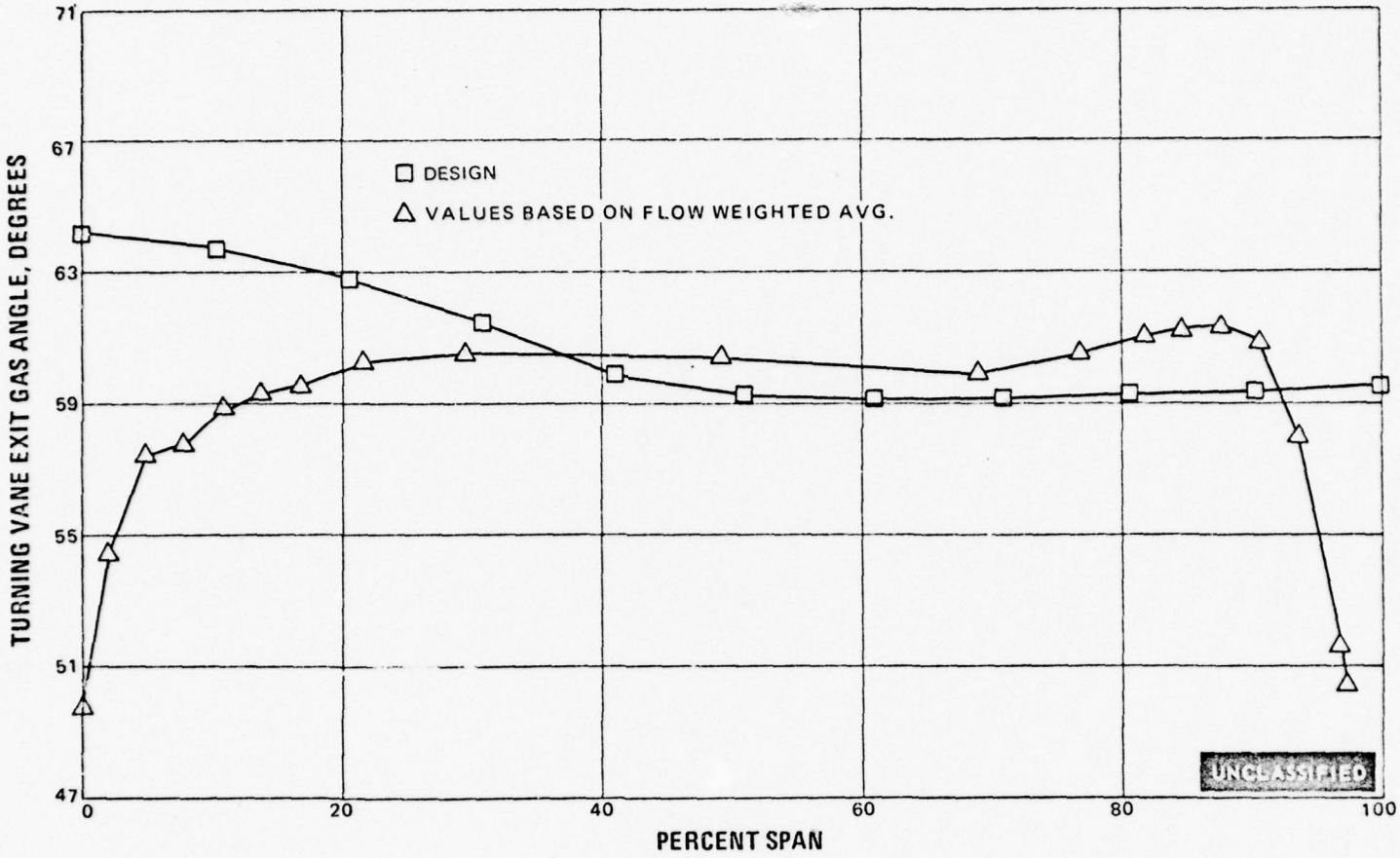

Figure 156 Inlet Guide Vane Spanwise Exit Angle Distribution, First Vane Medium Solidity Cascade--Midspan Exit Test Airfoil Mach No. = 0.835

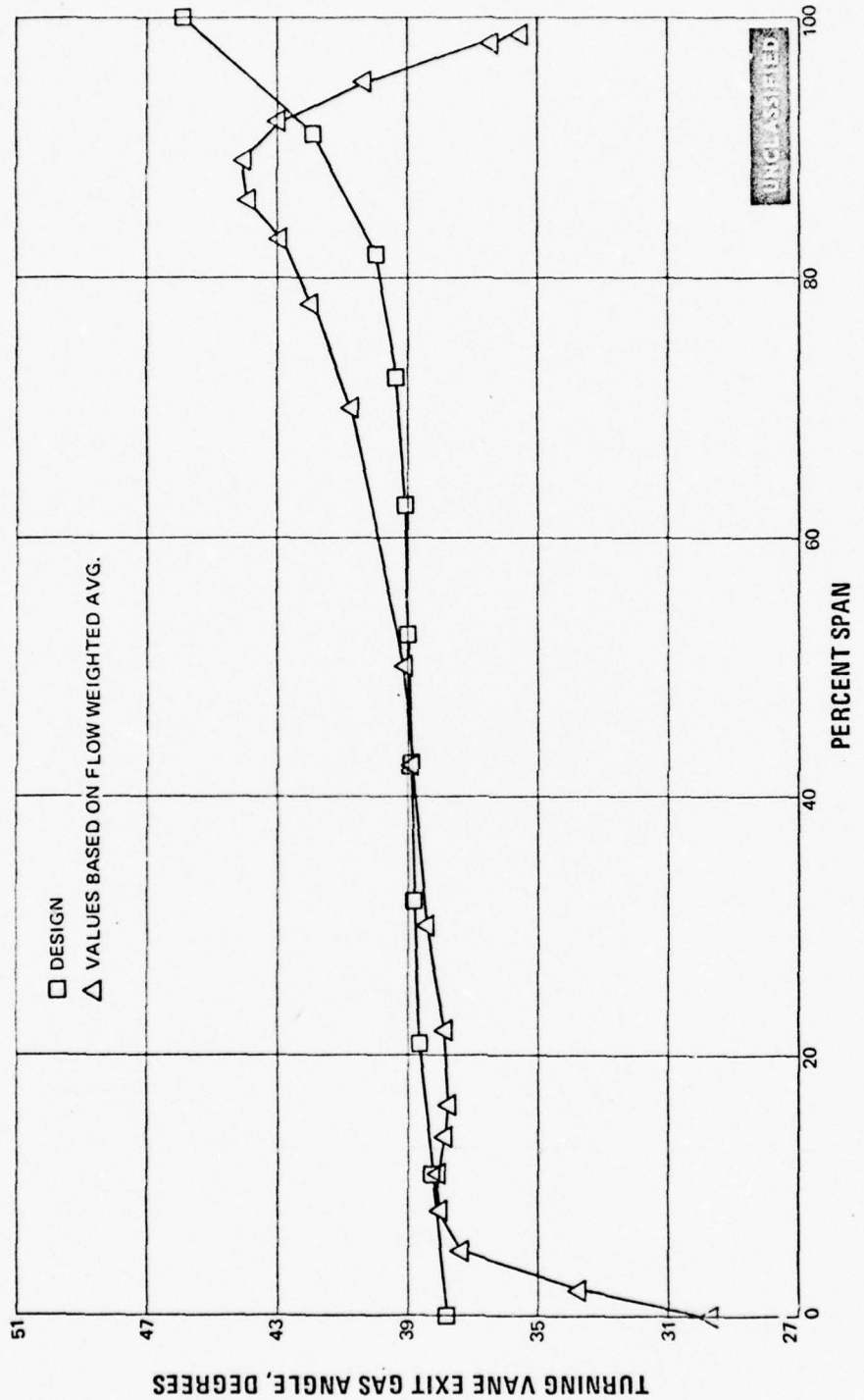

Figure 157 Inlet Guide Vane Spanwise Exit Angle Distribution, First Blade Medium Solidity Cascade–Midspan Exit Test Airfoil Mach No. = 0.775

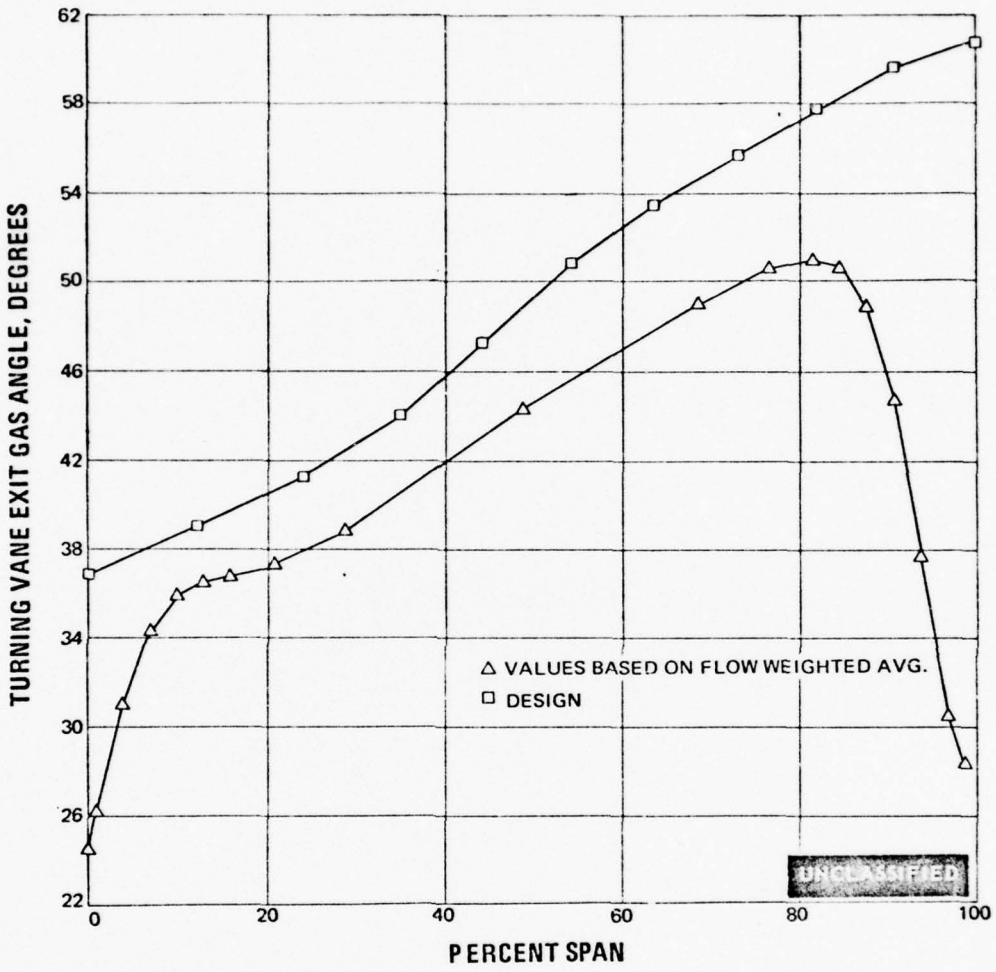

Figure 158 Inlet Guide Vane Spanwise Exit Angle Distribution, Second Vane Medium Solidity Cascade–Midspan Exit Test Airfoil Mach No. = 0.860

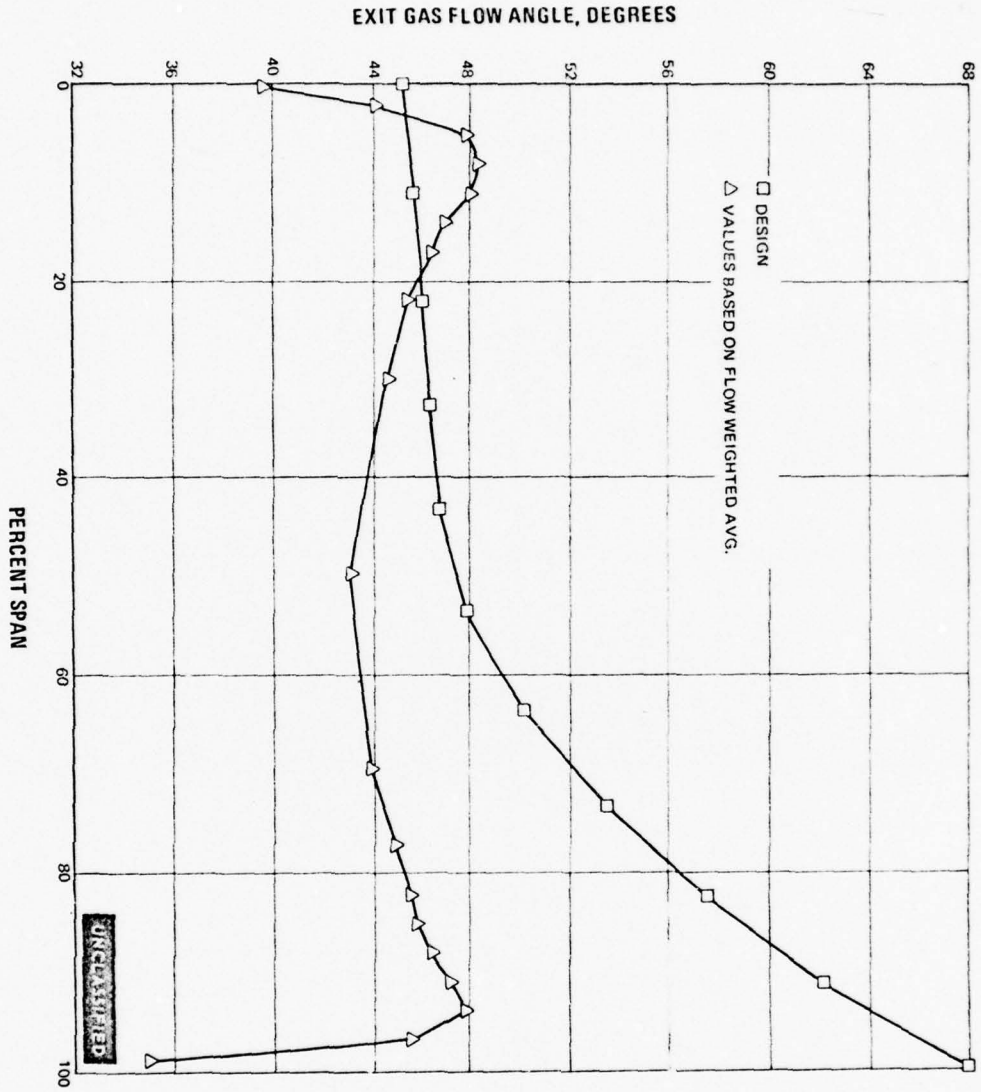

Figure 159 Inlet Guide Vane Spanwise Exit Angle Distribution, Second Blade Medium Solidity Cascade–Midspan Exit Test Airfoil Mach No. = 0.918

(U) The plots of the important aerodynamic quantities based on the inlet and exit plane measurements for the first vane and first blade medium-solidity airfoils are shown in Figures 160 through 171 at the test exit Mach numbers nearest to the design value. These plots are presented for the same parameters and in the same order as the performance data in Section IV.

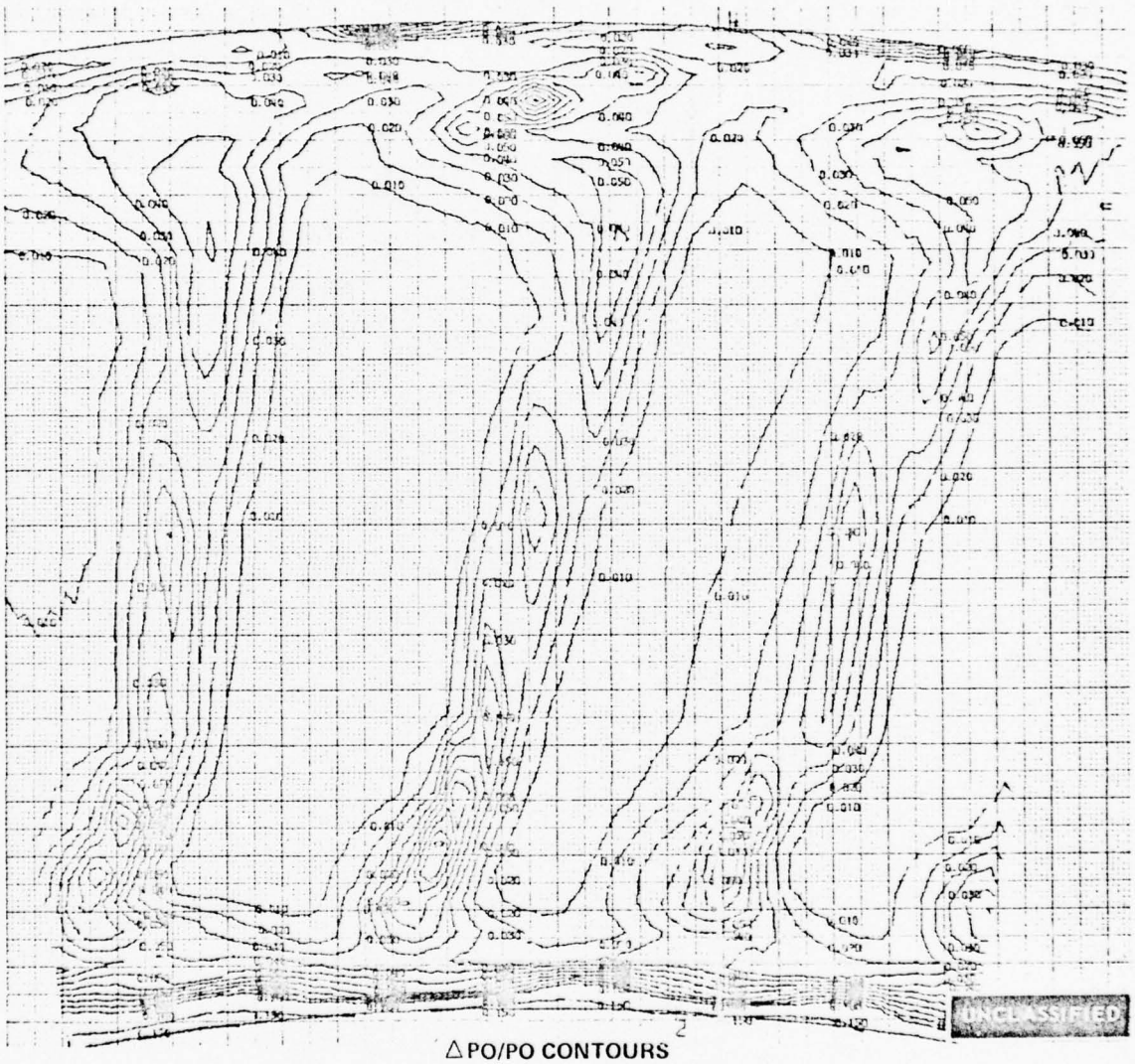

Figure 160 Pressure Loss Contours, First Vane, Medium Solidity, Three Flow Passages, Midspan Exit Mach No. = 0.835

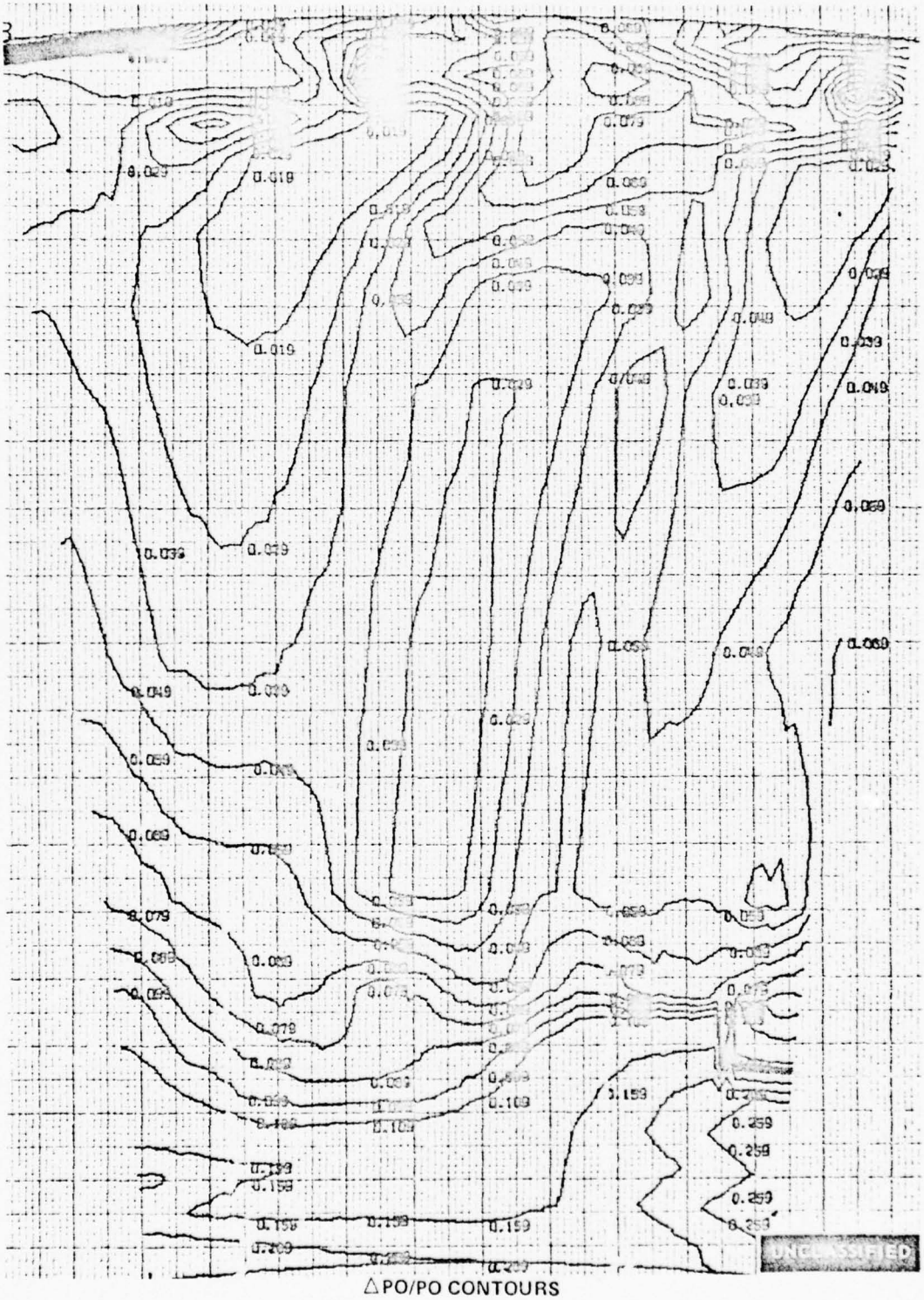

Figure 161 Pressure Loss Contours, First Blade, Medium Solidity, Three Flow Passages, Midspan Exit Mach No. = 0.775

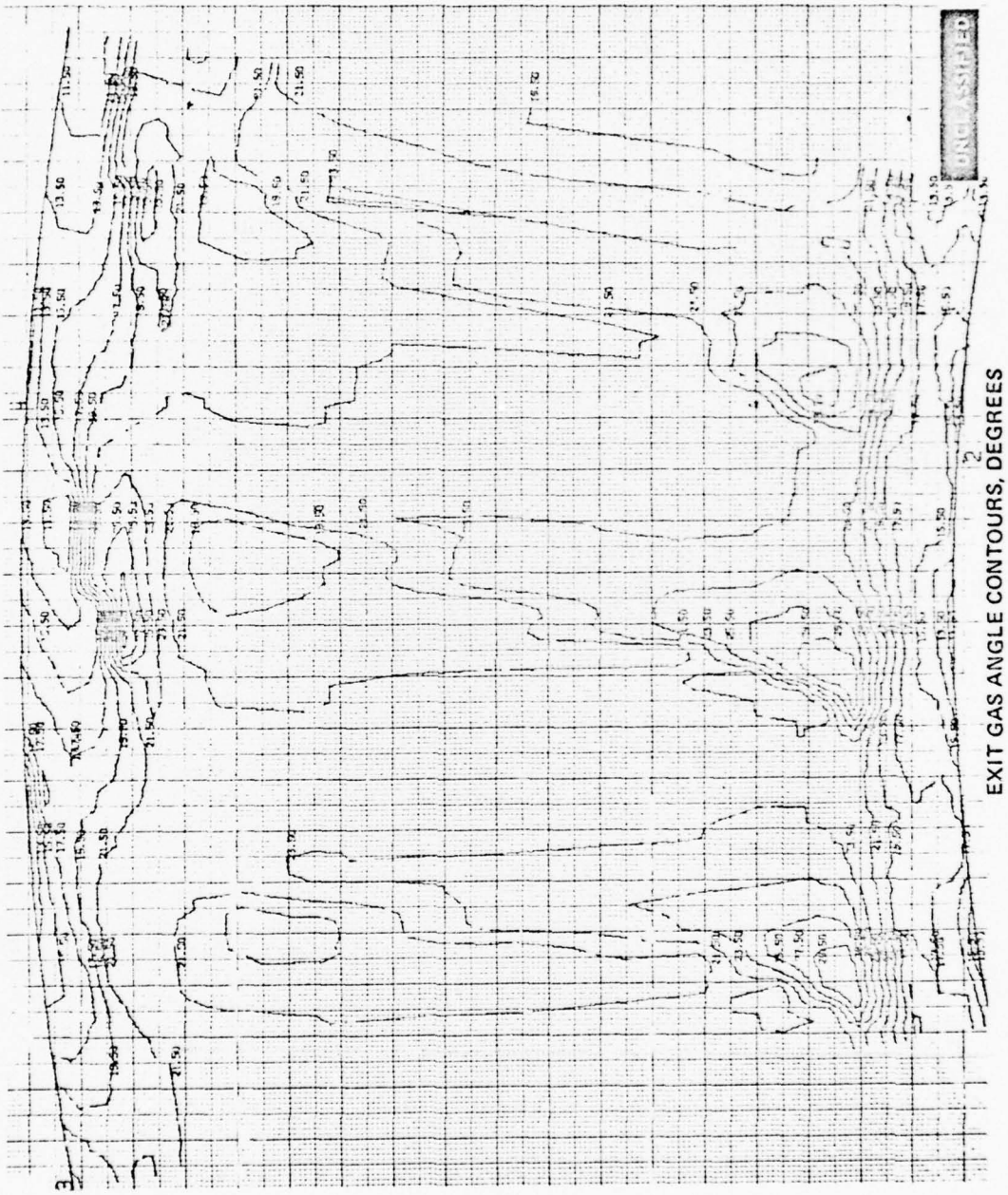

Figure 162 Exit Gas Angle Contours, First Vane, Medium Solidity, Three Flow Passages, Midspan Exit Mach No. = 0.835

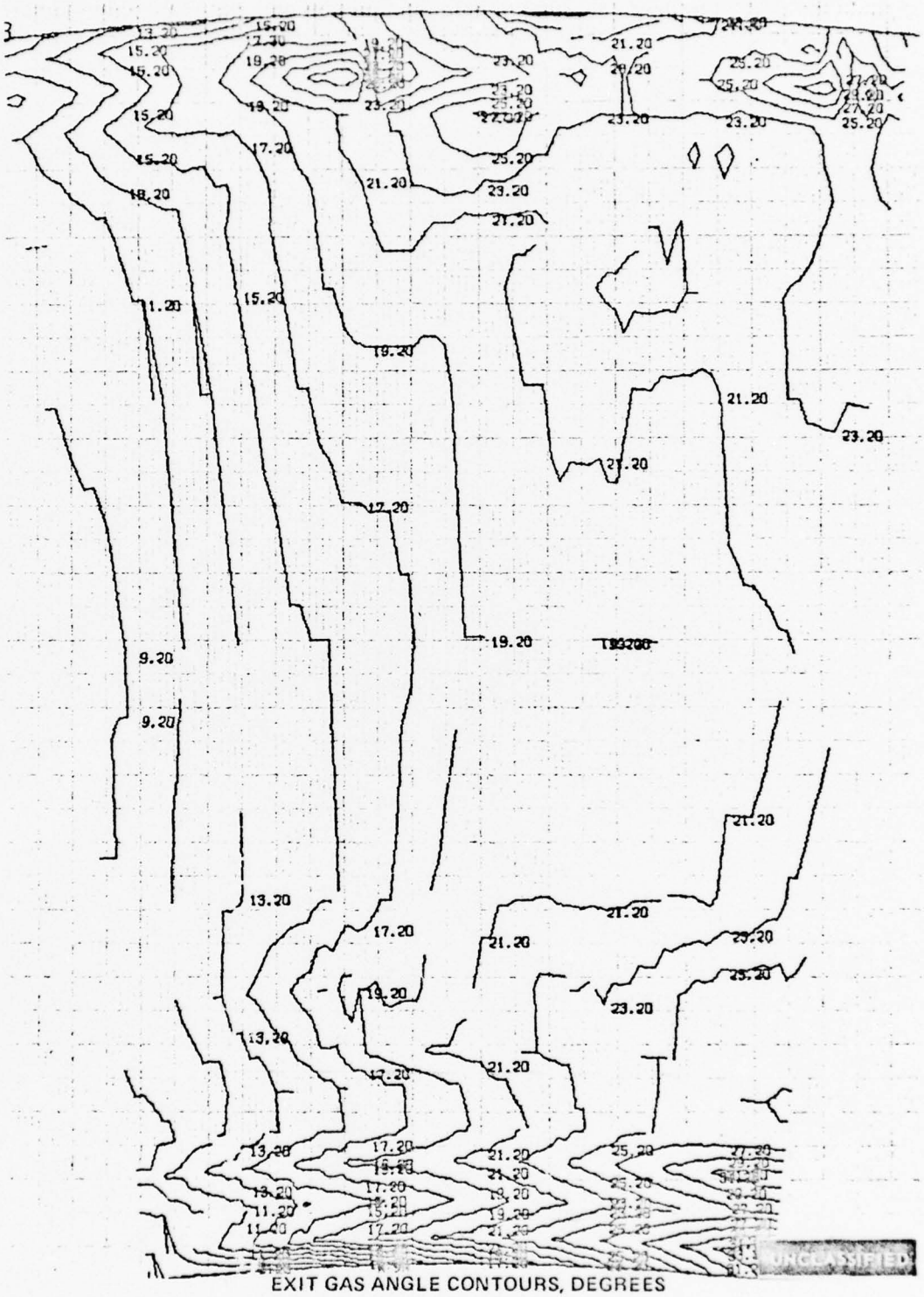

Figure 163 Exit Gas Angle Contours, First Blade, Medium Solidity, Three Flow Passages, Midspan Exit Mach No. = 0.775

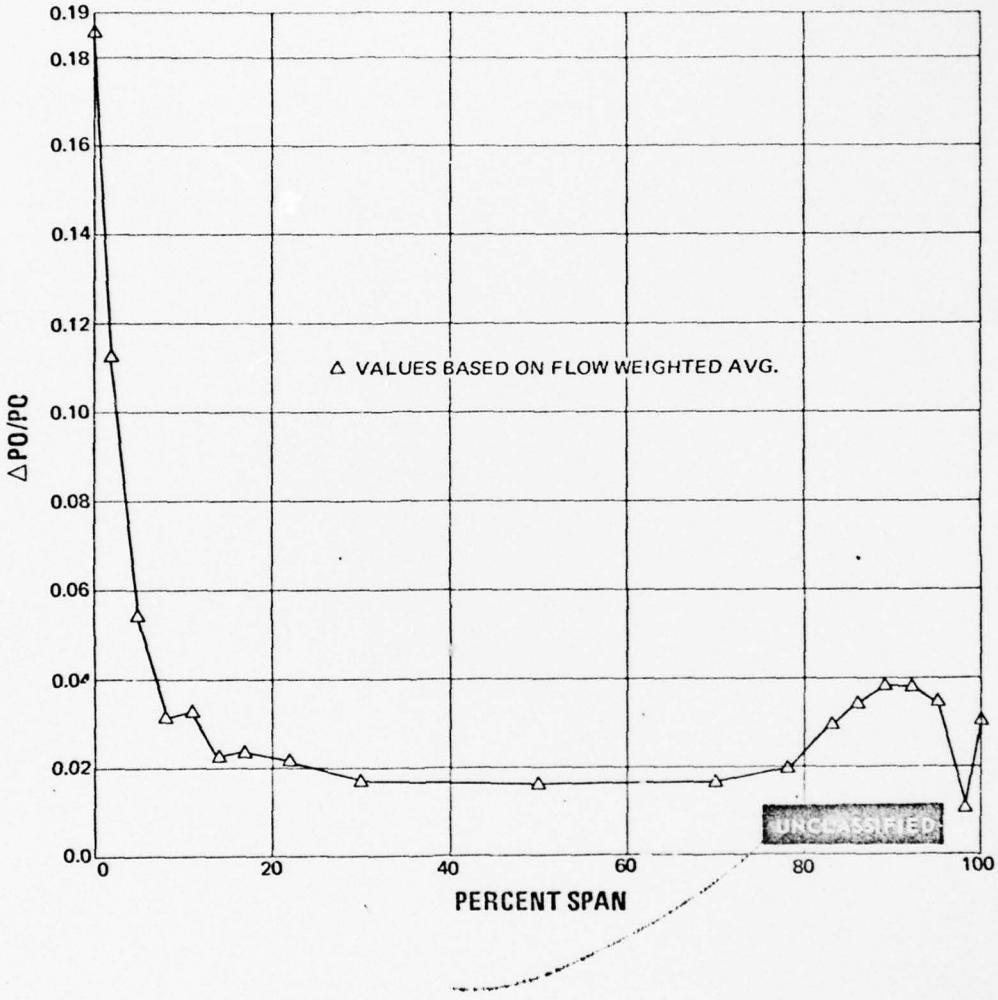

Figure 164 Spanwise Pressure Loss Distribution, First Vane, Medium Solidity, Midspan Exit Mach No. = 0.835

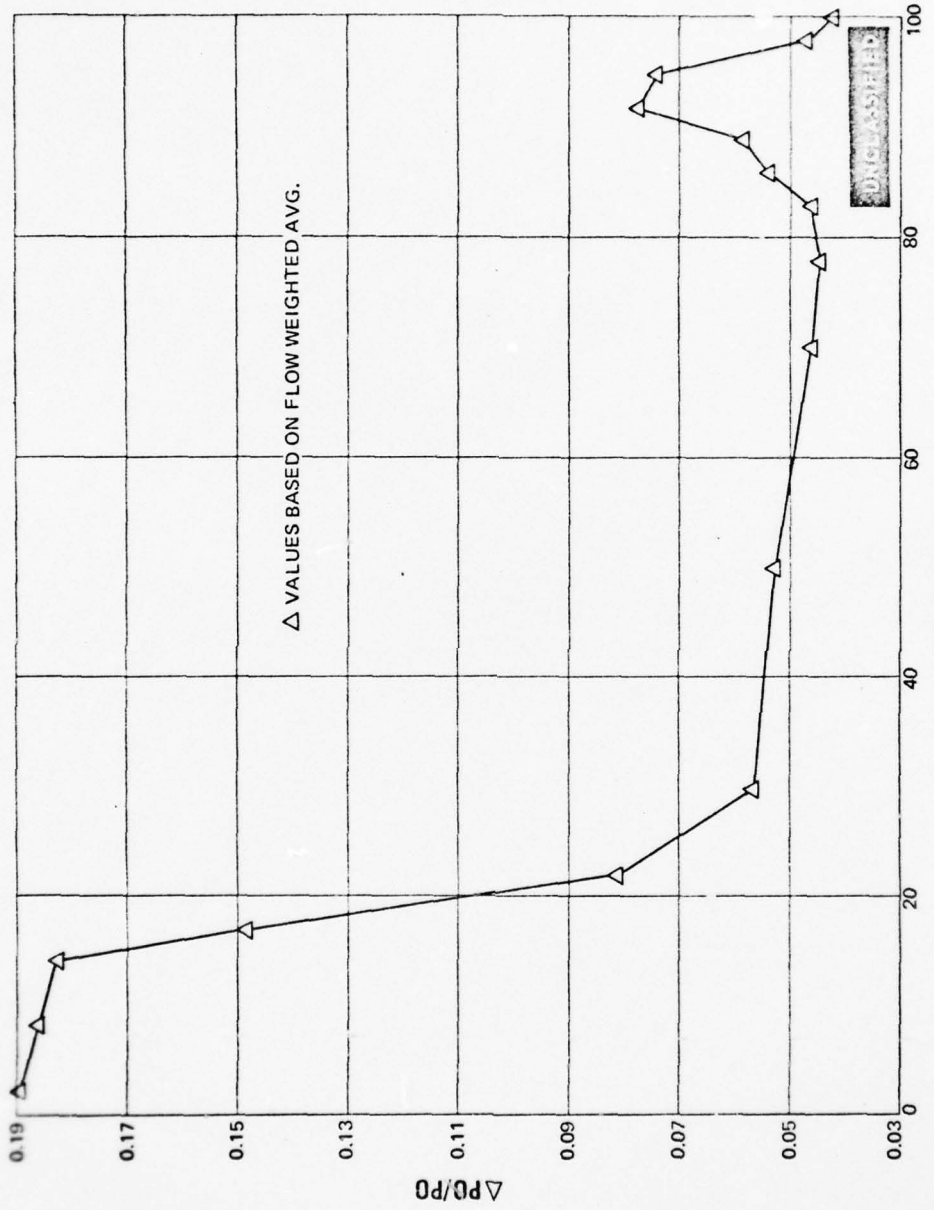

Figure 165 Spanwise Pressure Loss Distribution, First Blade, Medium Solidity, Midspan Exit Mach No. = 0.775

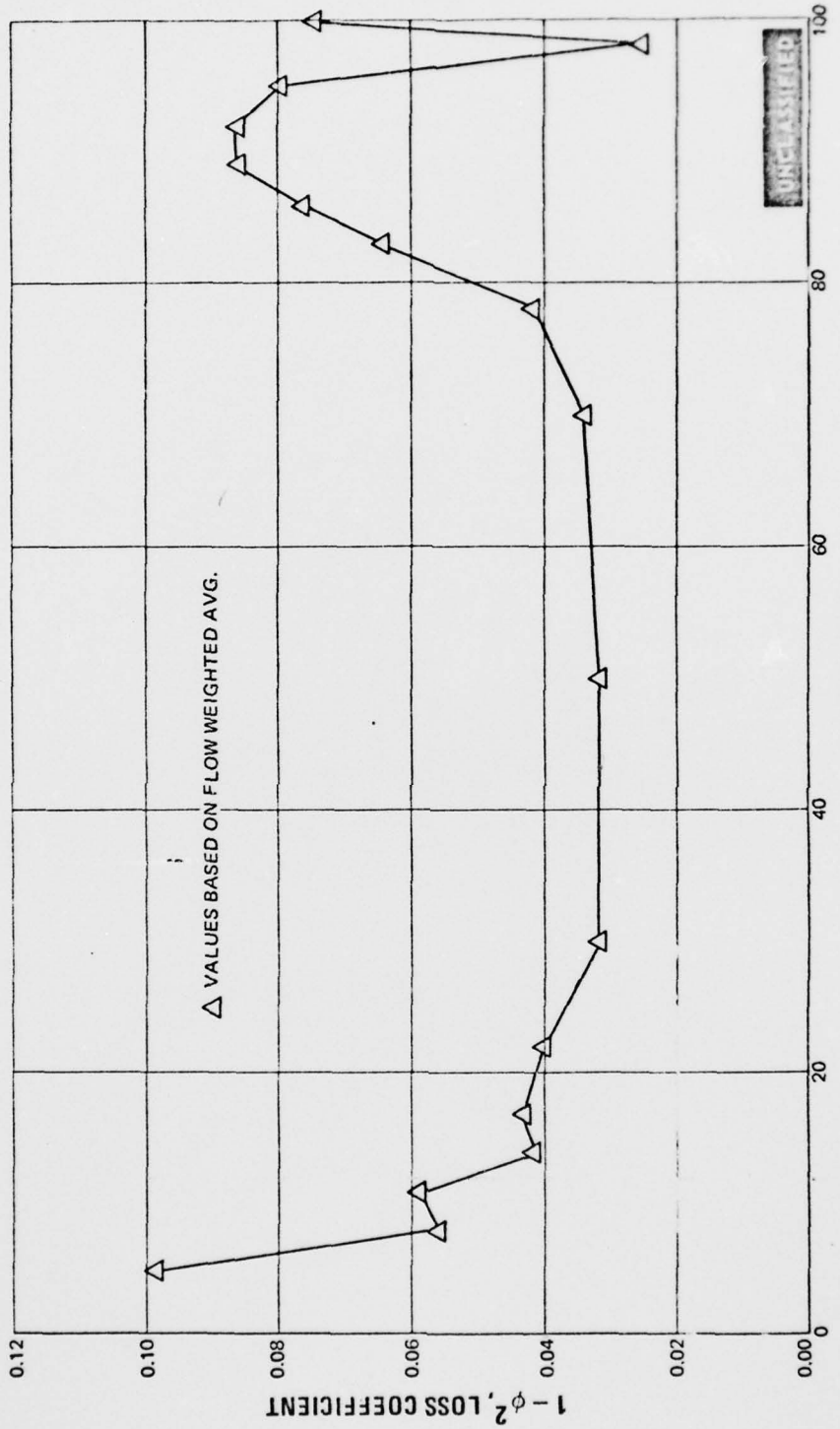

Figure 166 Spanwise Loss Coefficient Distribution, First Vane, Medium Solidity, Midspan
Exit Mach No. = 0.835

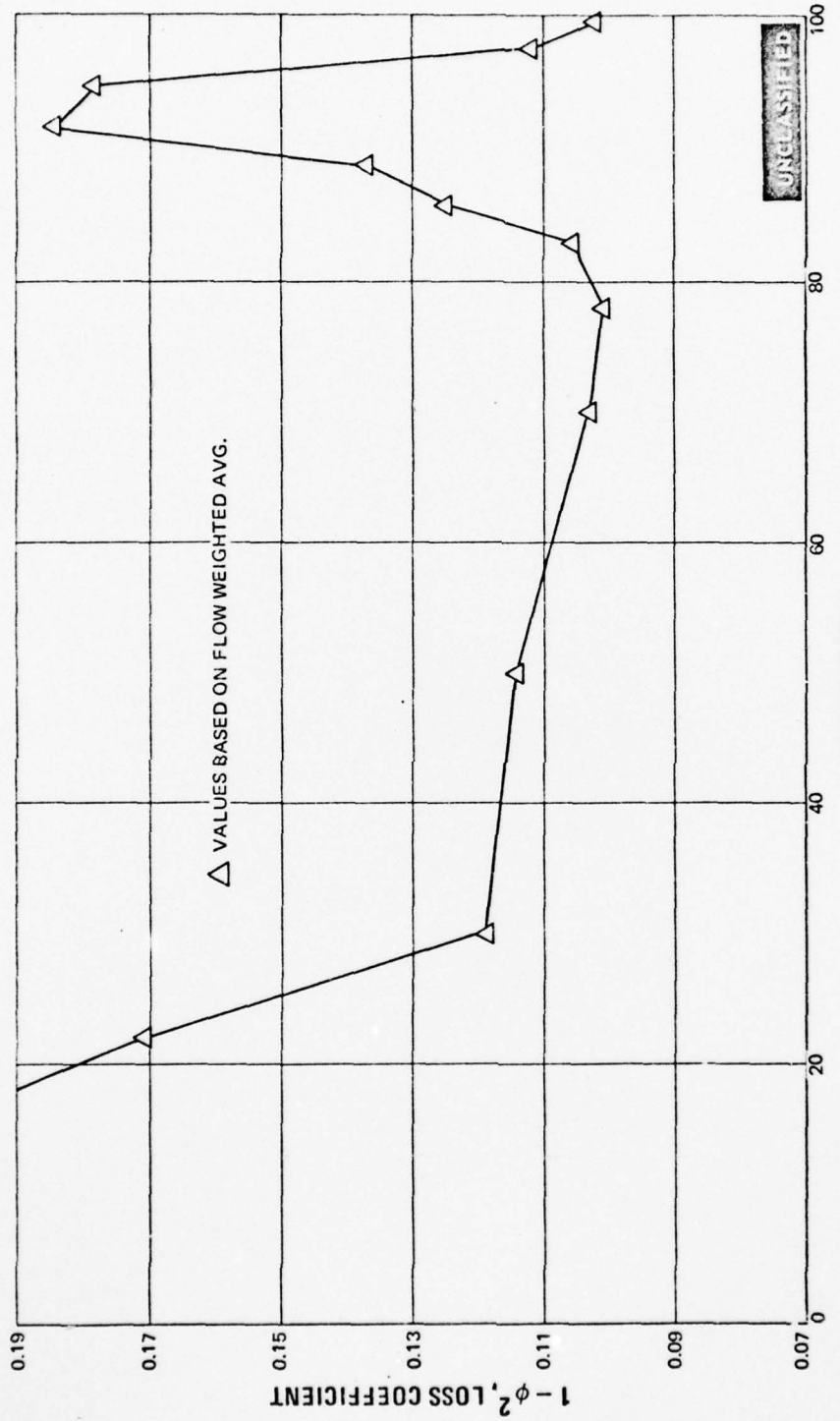

Figure 167 Spanwise Loss Coefficient Distribution, First Blade, Medium Solidity, Midspan
Exit Mach No. = 0.775

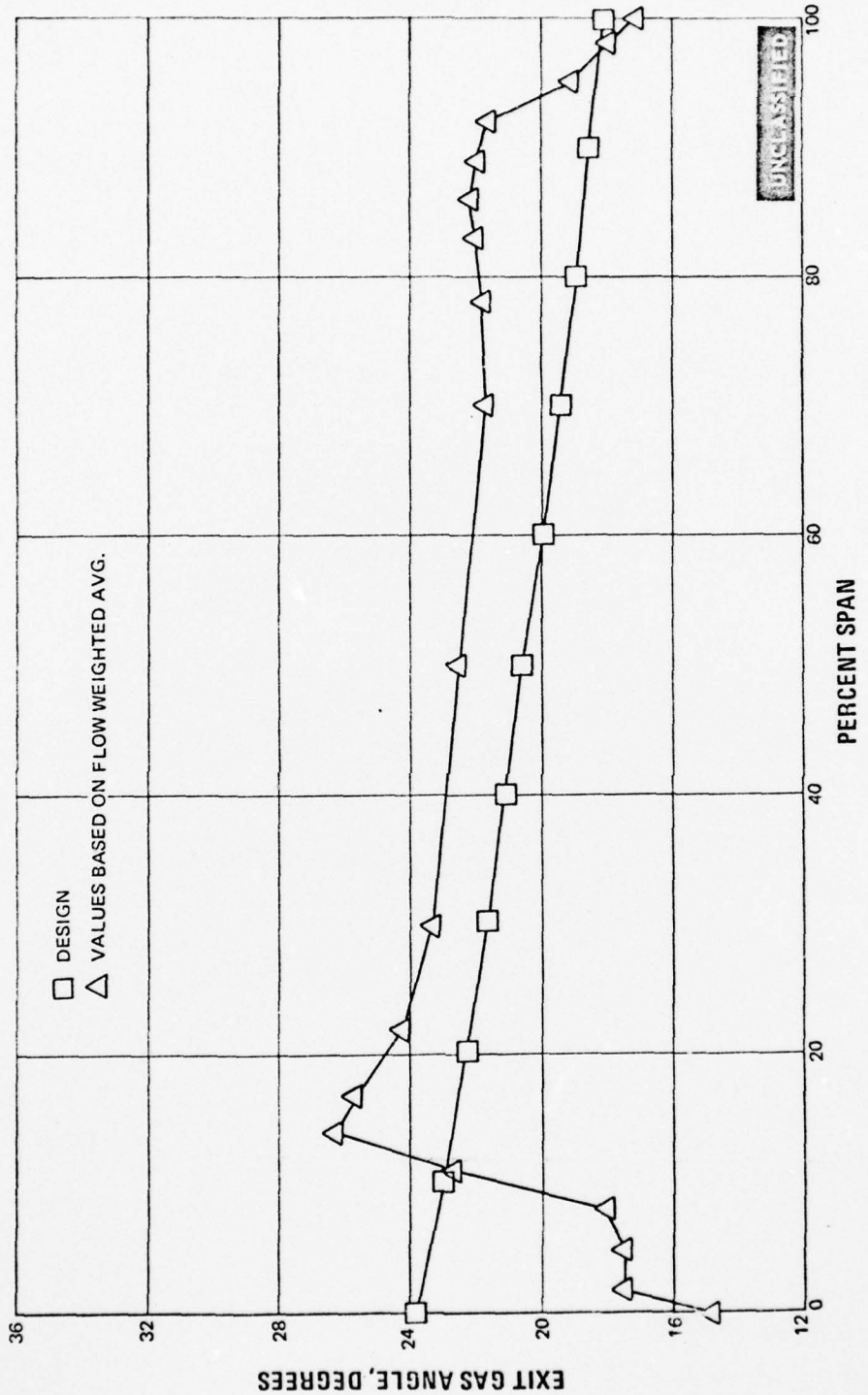

Figure 168 Spanwise Exit Gas Angle Distribution, First Vane, Medium Solidity, Midspan Exit Mach No. = 0.835

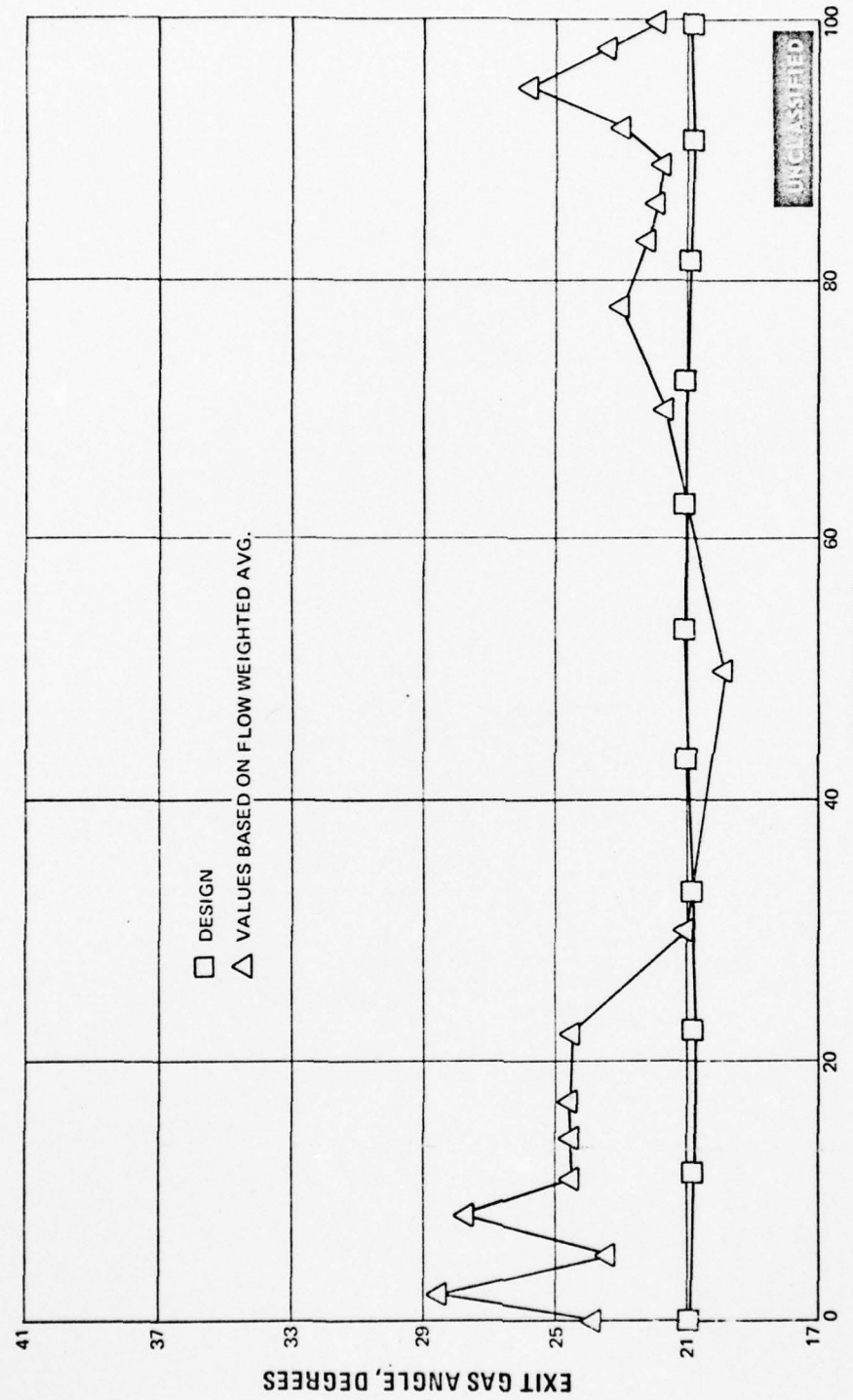

Figure 169 Spanwise Exit Gas Angle Distribution, First Blade, Medium Solidity, Midspan Exit Mach No. = 0.775

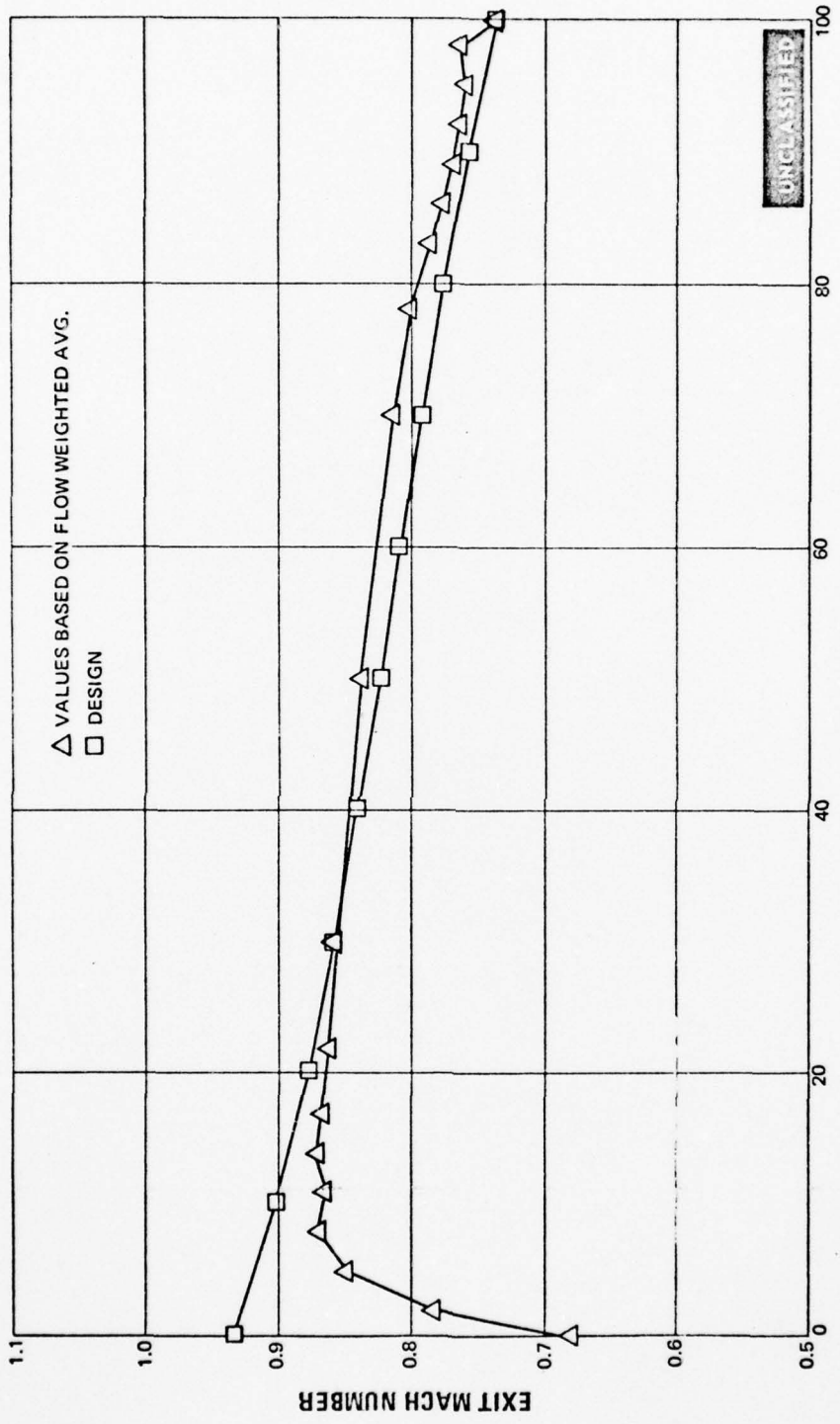

Figure 170 Spanwise Exit Mach Number Distribution, First Vane, Medium Solidity, Mid-span Exit Mach No. = 0.835

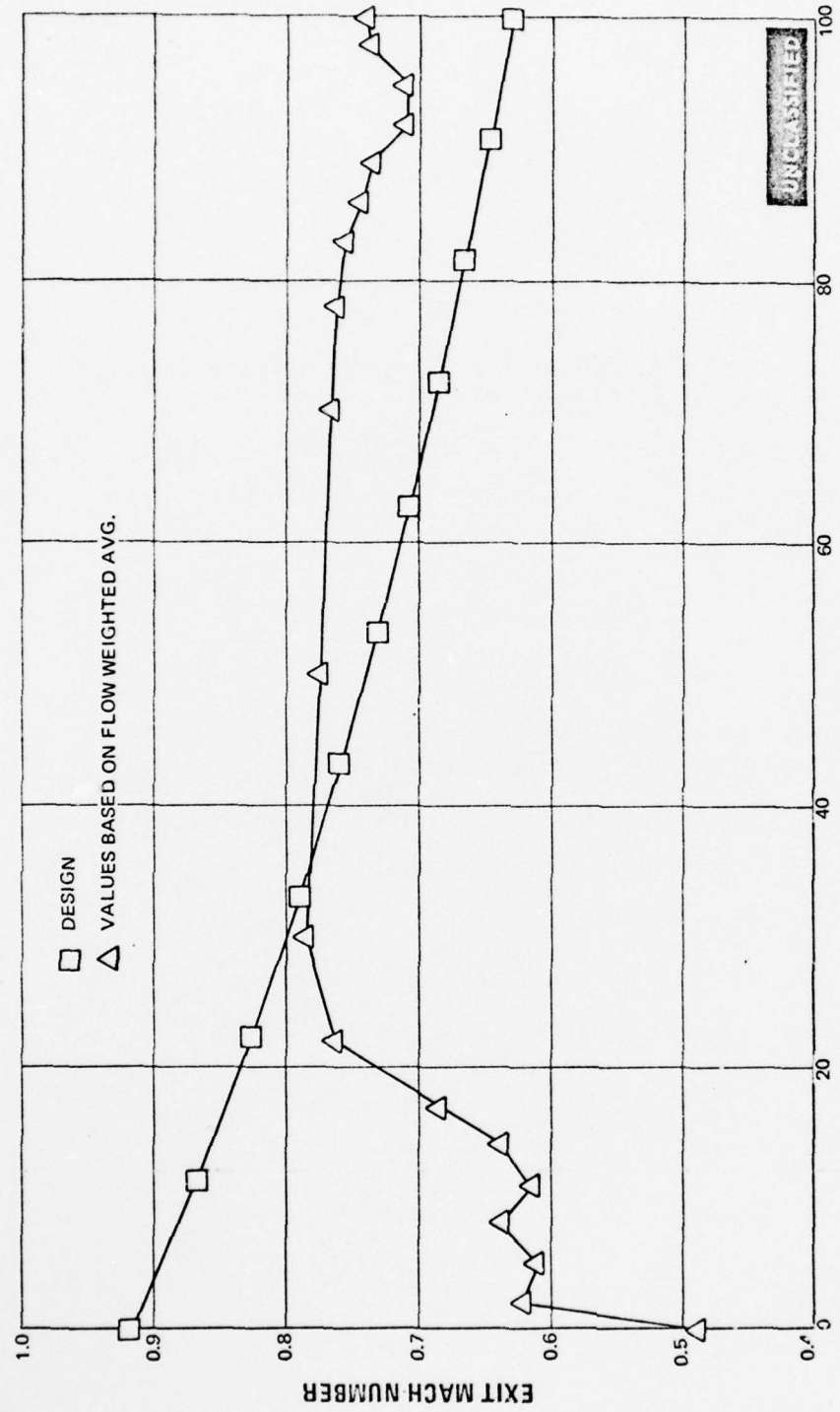

Figure 171 Spanwise Exit Mach Number Distribution, First Blade, Medium Solidity, Mid-span Exit Mach No. = 0.775

(U) The first vane airfoil cascade pressure loss contours (Figure 160) indicate low loss pockets over the midspan areas with the higher loss regions in the airfoil suction surface and end-wall corners. These losses originate at the end-wall and migrate from the pressure surface to the suction surface and accumulate in the corners. This is reflected in the plot of the average spanwise distribution of the total pressure loss (Figure 164) and loss coefficient (Figure 166) where the collection of end-wall loss is evident. The integrated overall loss coefficient for this airfoil is 0.050, and the midspan value is 0.0315 at a midspan exit Mach numbers of 0.835. The midspan loss coefficient predicted by boundary layer calculations is 0.025.

(U) The effect of Mach number and Reynolds Number on the midspan loss coefficient is shown in Table XXVI for the first vane. The loss levels change only within the experimental error with Mach number at constant design Reynolds Number. The loss level at constant Mach number has its lowest value (0.025) at 75 percent of design Reynolds Number, indicating that boundary layer transition point for this Reynolds Number is optimum (i.e., transition takes place just in time to prevent flow separation).

TABLE XXVI

MEDIUM SOLIDITY
FIRST VANE
PROFILE LOSS COEFFICIENT VARIATIONS AT MEAN SECTION
$1 - \phi^2$
DESIGN: M = 0.854, R = 4.38×10^5

	0.5R	0.75R	R	1.5R
M – 0.1			0.035	
M	0.047	0.025	0.0315	0.040
M + 0.1			0.031	

UNCLASSIFIED

(U) The airfoil exit gas angle contours (Figure 152) indicate close agreement with the design angles for the midspan portion of the first vane, with some overturning at the root and tip due to secondary flow. This is more clearly shown on the exit angle spanwise plot on which the design angles are also shown (Figure 158). The data gave no evidence of flow separation, and this was verified by visual observation of the oil and graphite flow patterns.

(U) Airfoil surface static pressure distribution at the root, mean and tip are shown in Figures 172 through 174. The experimental and predicted values are indicated on these plots. As noted from the circumferentially averaged Mach number distribution (Figure 170), the Mach number at the mean was very close to the design value, with a substantially lower Mach number at the root. Consequently, the experimental data dupli-

cated the predicted pressure distribution closely, and the root section indicates an unloaded airfoil. A similar problem, but to a lesser degree, exists at the tip section. As discussed in detail in the Reference 3 Report, the reason for this is the inability of the annular segment cascade to reproduce the desired static pressure gradient at the exit plane.

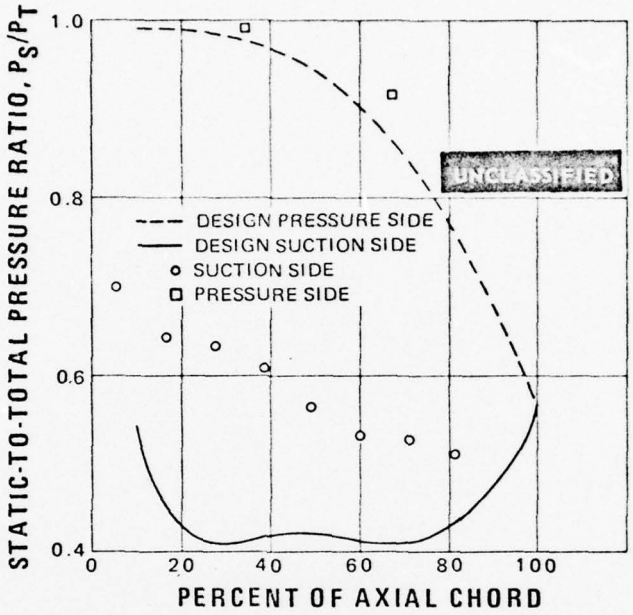

Figure 172 Static-to-Total Pressure Ratio versus Percent of Axial Chord, First Vane Medium Solidity – Root Section

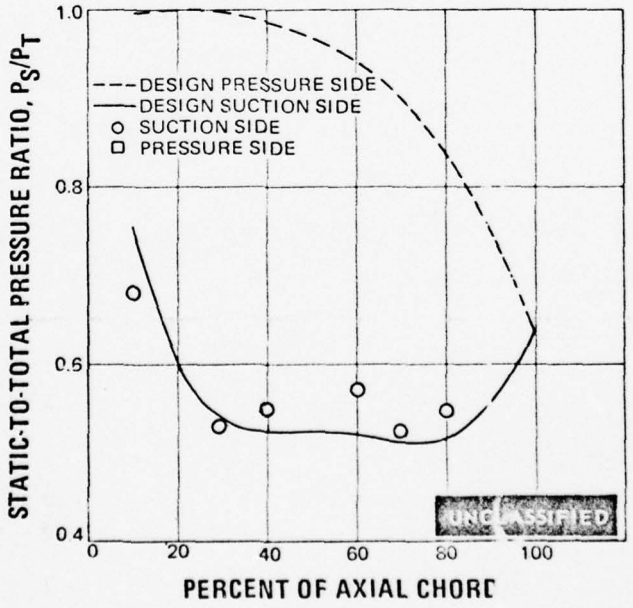

Figure 173 Static-to-Total Pressure Ratio versus Percent of Axial Chord, First Vane Medium Solidity – Mean Section

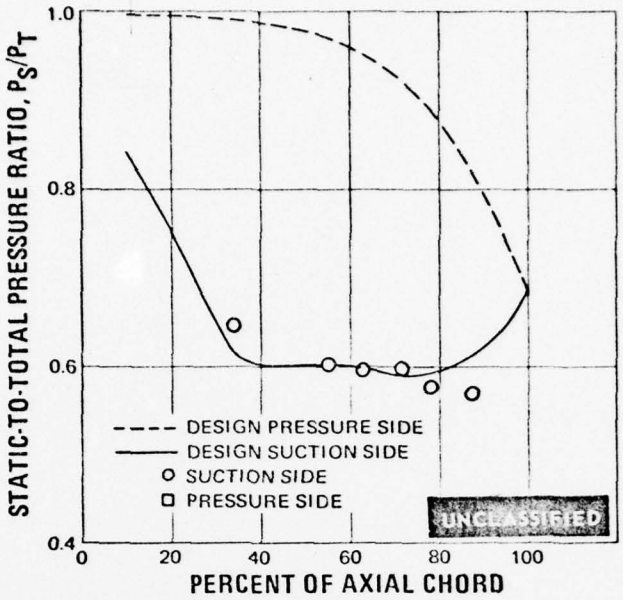

Figure 174 Static-to-Total Pressure Ratio versus Percent of Axial Chord, First Vane Medium Solidity – Tip Section

(U) The first blade airfoil cascade pressure loss contours (Figure 161) show a large loss pocket at the root section, indicating flow separation at the wall. The average spanwise pressure loss distribution (Figure 165) and loss coefficient (Figure 167) also show this to be the case. As noted in the Reference 2 Report, analyses were made to determine if potential problems of flow separation would exist on the inside end-wall extensions downstream of the test airfoil for each cascade design. Unfortunately, the end-wall extension for the first blade cascade was not sufficiently long to maintain a small enough pressure gradient to prevent separation. Some evidence of this was seen in the normal solidity first blade baseline evaluation, reported in the Reference 3 Report. The traverse instrumentation used on that cascade, however, was sufficiently close to the airfoil, so that the performance calibration was not adversely affected. The medium-solidity first blade cascade traverse instrumentation was located further downstream in the wall separated region, giving results which are not indicative of the airfoil performance.

(U) The airfoil surface static pressure distributions are presented for the first blade in Figures 175 through 177. The same comments apply to this data as to the surface pressure distributions for the first vane airfoil. Furthermore, the separated flow at the root section caused a major shift in the flow distribution, causing a large increase in Mach number at the tip section (Figure 171).

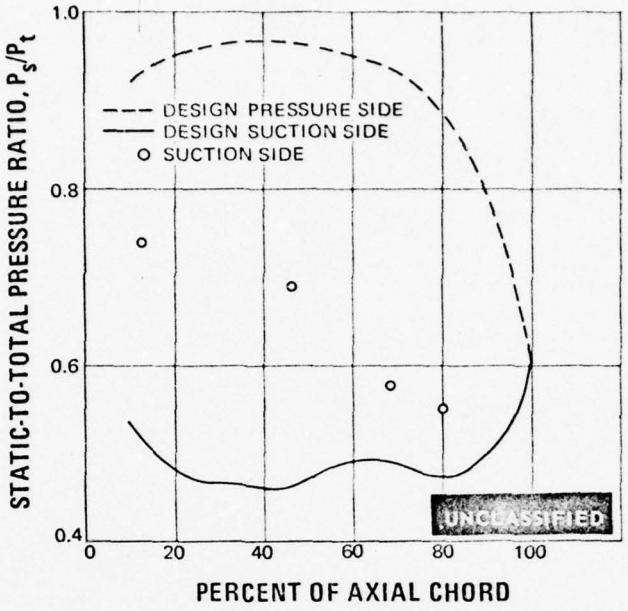

Figure 175 Static-to-Total Pressure Ratio versus Percent of Axial Chord, First Blade Medium Solidity – Root Section

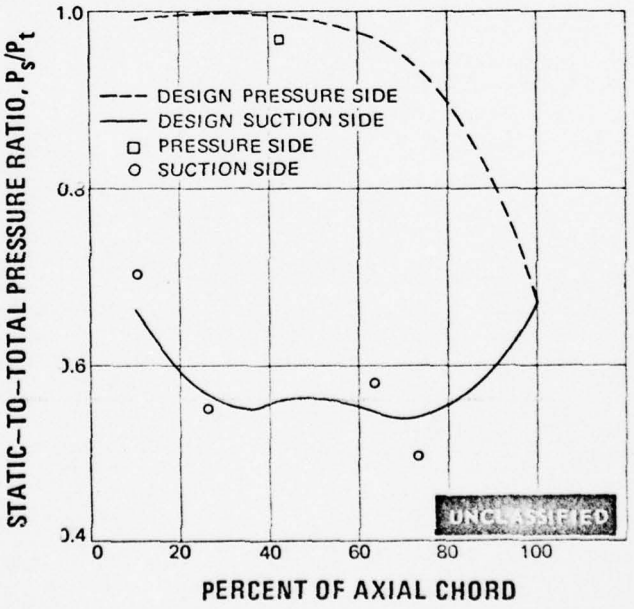

Figure 176 Static-to-Total Pressure Ratio versus Percent of Axial Chord, First Blade Medium Solidity – Mean Section

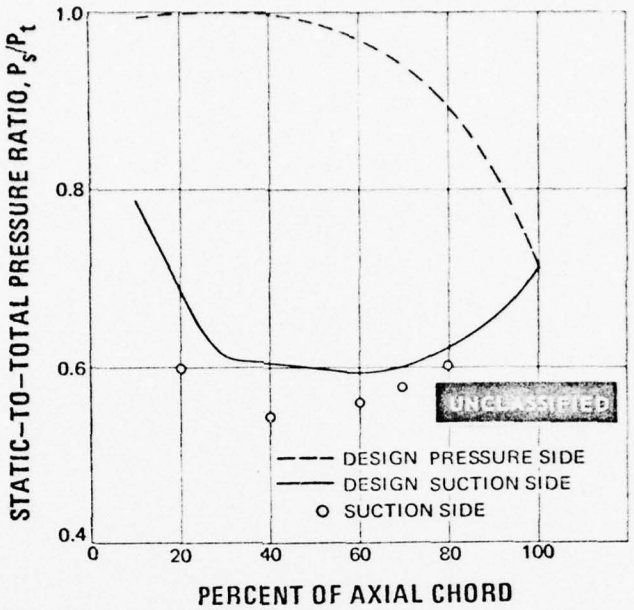

Figure 177 Static-to-Total Pressure Ratio versus Percent of Axial Chord, First Blade Medium Solidity – Tip Section

5. CONCLUSIONS

(U) Conclusions drawn as a result of the performance evaluation of the medium-solidity airfoils and comparisons with the normal solidity results will be reported in the next interim report, after completion of Task IId.

6. TEST PROCEDURE

(U) The annular segment cascade tests of the medium solidity airfoils were performed in the Willgoos Laboratory at East Hartford on X-214A stand. These performance tests required various combinations of compressors and exhausters, as well as the test stand natural gas burner to attain the desired Mach numbers and Reynolds Numbers at the cascade exit plane. Test conditions were always chosen so as to prevent the condensation of atmospheric water vapor.

(U) For each of the four configurations, four tests were required for a complete performance evaluation at any test point. The first and second of these tests were the traversing of the test airfoil inlet and exit planes with the total pressure cobra probe. A third test to determine the pitch angle was conducted by traversing the test airfoil exit plane with the pitch angle probe. Finally, a flow visualization test was conducted. The procedure listed below was used for these tests:

- The cascade test pack was installed on the stand and all of the fixed instrumentation was connected
- The traversing probe was installed either at the inlet or exit plane of the test airfoil
- The traversing probe was correctly located relative to the test airfoil
- The total pressure transducers for the traversing probe and data recording equipment were calibrated
- The laboratory compressors and exhausters which were required for the test were started and allowed to reach steady operating conditions (approximately 2 hrs.)
- Test stand burner was started and the required aerodynamic conditions were set at the cascade exit plane mean section
- Fixed instrumentation readings were recorded with traversing probe removed. This step was repeated after the midspan traverse, and at the conclusion of the test
- The cobra probe was traversed circumferentially at the nineteen required radial locations starting at the outer diameter. Data was simultaneously recorded on plotomat charts and punched onto computer cards
- The test to determine the pitch angle at the cascade exit plane was carried out using the preceeding steps, except that the cobra probe was replaced by the pitch probe
- The flow visualization test was carried out with the exhaust plenum cover removed. For this final test the airfoils and end-walls of the cascade pack were painted with a layer of graphite and heavy oil. The air total temperature was set at about 100°F and the total pressure was set to give the required Mach number. Test stand safety rules prevented dumping of hotter air into the cell with the exhaust cover removed, thus preventing simulation of the design Reynolds Number. Air was allowed to flow through the cascade for one minute and the resulting patterns were observed. In order to determine if removal of this cover affected the cascade performance, a test was made where the cascade was traversed and the performance data obtained with the cover removed. There was no difference between this data, and data taken with the cover in place at the same flow conditions.

(The reverse of this page is blank)

SECTION VI
PRELIMINARY DESIGN MANUAL PREPARATION (TASK IIc)

AD-A056 285 PRATT AND WHITNEY AIRCRAFT GROUP EAST HARTFORD CONN F/G 21/5
INVESTIGATION OF A HIGHLY LOADED TWO-STAGE FAN-DRIVE TURBINE. V--ETC(U)
DEC 69 H WELNA, D E DAHLBERG, W H HEISER F33615-68-C-1208
UNCLASSIFIED PWA-3827 AFAPL-TR-69-92-VOL-4 NL

3 OF 3
AD
A056 285

END
DATE
FILMED
8-78
DDC

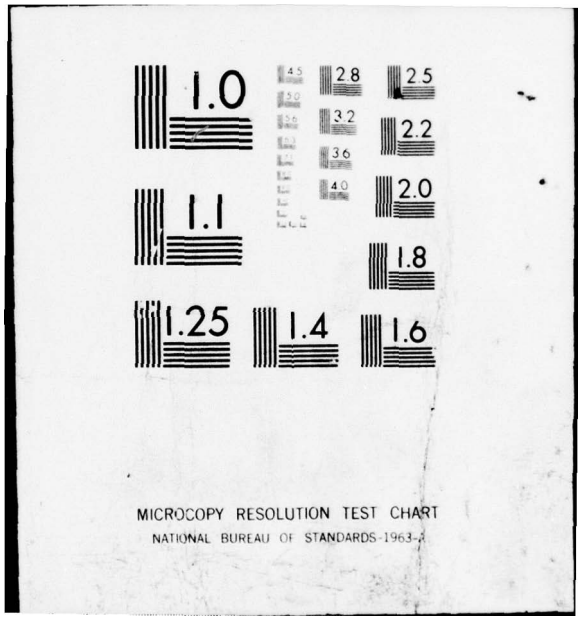
1.0
1.1
1.25
1.4
1.6
1.8
2.0
2.2
2.5
2.8
3.2
3.6
4.0
4.5
5.0
5.6
MICROCOPY RESOLUTION TEST CHART
NATIONAL BUREAU OF STANDARDS-1963-A

SECTION VI

PRELIMINARY DESIGN MANUAL PREPARATION (TASK IIe)

1. RFP OBJECTIVE

(U) Prepare the preliminary draft of the Turbine Design Procedure Manual.

2. TASK OBJECTIVE

(U) The purpose of this task is to do preliminary work on the preparation of a Turbine Design Procedure Manual. This manual will contain the following information for each computer program used to design the Contract turbine: a flow diagram; a listing for all input and output items and their definitions: a list of definitions for each term used in the computer code: a write-up of the pertinent equations: a listing of the computer code in Fortran IV: a copy of the computer program decks in Fortran IV; any necessary test cases for deck check-out.

3. STATUS

(U) All of the decks listed below have been converted to Fortran IV, checked out on an IBM 7094, and a tape containing these decks has been received by the Air Force. In addition, flow diagrams and test cases were also supplied. These decks included:

- Turbine Meanline Design Program
- Turbine Stage-Off Design Program
- Turbine Streamline Analysis Program
- Airfoil Pressure Distribution Program
- Airfoil Boundary Layer Program
- Turbine Airfoil Design and Section Properties Program
- Airfoil Curved Line Fairing Program
- Airfoil Straight Line Fairing Program

This completes the requirements of Task IIe.

(U) Engineering write-up of the above listed decks is in process, and rough drafts have been completed for most of these decks. The Turbine Meanline Design Program write-up has been received by the Air Force. Those remaining will be completed as part of the requirements for Task IId, Design Procedure Manual Preparation.

(The reverse of this page is blank)

APPENDIX

TABLE NOS. IV THROUGH XII

REDESIGNED SECOND VANE
CASCADE TURNING VANE

TABLE NOS. XIII THROUGH XX

RECONTOURED SECOND VANE

TABLE IV

REDESIGNED SECOND VANE CASCADE TURNING VANE

Radius of Root Section = 7.5000 Axial Chord = 3.2500 Actual Chord = 3.7443
Pitch = 1.5708 No. of Foils = 4.

Percent X	Foil X	Foil Y Suction	Foil Y (Circle)
0.0	0.0	1.9060	1.8810
0.01	0.0325	1.9060	1.9060
0.02	0.0650	1.9058	1.9058
0.03	0.0975	1.9052	1.9052
0.04	0.1300	1.9044	1.9044
0.05	0.1625	1.9032	1.9032
0.10	0.3250	1.8926	1.8926
0.15	0.4875	1.8737	1.8737
0.20	0.6500	1.8462	1.8462
0.25	0.8125	1.8098	1.8098
0.30	0.9750	1.7642	1.7642
0.35	1.1375	1.7091	1.7091
0.40	1.3000	1.6443	1.6443
0.45	1.4625	1.5694	1.5694
0.50	1.6250	1.4842	1.4842
0.55	1.7875	1.3885	1.3885
0.60	1.9500	1.2822	1.2822
0.65	2.1125	1.1649	1.1649
0.70	2.2750	1.0367	1.0367
0.75	2.4375	0.8975	0.8975
0.80	2.6000	0.7470	0.7470
0.85	2.7625	0.5854	0.5854
0.90	2.9250	0.4127	0.4127
0.95	3.0875	0.2289	0.2289
0.98	3.1850	0.1101	0.1101
0.99	3.2175	0.0718	0.1718
1.00	3.2500	0.0339	0.0250

Foil L.E. Circle	X = 0.0250,	Y = 1.8810,	R = 0.0250
Foil T.E. Circle	X = 3.2250,	Y = 0.0250,	R = 0.0250
Foil L.E. Tangency Pt. Suction	X = 0.0250,	Y = 1.9060	
Foil L.E. Tangency Pt. Pressure	X = 0.0250,	Y = 1.8560	
Foil T.E. Tangency Pt. Suction	X = 3.2444,	Y = 0.0408	
Foil T.E. Tangency Pt. Pressure	X = 3.2056,	Y = 0.0092	
Foil Nose Point	X = 0.0 ,	Y = 1.8810	
Foil Tail Point	X = 3.2408,	Y = 0.0056	

Foil Area (Less Core) = 0.1968

Gaging	LAMBDA = 1.0214,	X = 2.5142,	Y = 0.8279
Gaging Angle	= 40.561		
Center of Gravity	X = 1.7483,	Y = 1.2100	
Radial Reference	X = 1.7483,	Y = 1.2100	
Inlet Angle	= 90.000,	Delta Beta 1 = 0.001	
Exit Angle	= 39.060,	Delta Beta 2 = 0.001	
Uncovered Turning	= 8.198		

Constant Section Thickness = .050

TABLE V

REDESIGNED SECOND VANE CASCADE TURNING VANE

Radius of 1/8R Section = 7.8905 Axial Chord = 3.2500 Actual Chord = 3.6746
Pitch = 1.6526 No. of Foils = 4.

Percent X	Foil X	Foil Y Suction	Foil Y (Circle)
0.0	0.0	1.4951	1.4701
0.01	0.0325	1.4950	1.4950
0.02	0.0650	1.4949	1.4949
0.03	0.0975	1.4945	1.4945
0.04	0.1300	1.4939	1.4939
0.05	0.1625	1.4930	1.4930
0.10	0.3250	1.4849	1.4849
0.15	0.4875	1.4702	1.4702
0.20	0.6500	1.4485	1.4485
0.25	0.8125	1.4192	1.4192
0.30	0.9750	1.3817	1.3817
0.35	1.1375	1.3353	1.3353
0.40	1.3000	1.2797	1.2797
0.45	1.4625	1.2143	1.2143
0.50	1.6250	1.1384	1.1384
0.55	1.7875	1.0518	1.0518
0.60	1.9500	0.9540	0.9540
0.65	2.1125	0.8449	0 8449
0.70	2.2750	0.7243	0.7243
0.75	2.4375	0.5922	0.5922
0.80	2.6000	0.4489	0.4489
0.85	2 7625	0.2944	0.2944
0.90	2.9250	0.1291	0.1291
0.95	3.0875	−0.0468	−0.0468
0.98	3.1850	−0.1602	−0.1602
0.99	3.2175	−0.1978	−0.1978
1.00	3.2500	−0.2331	−0.2422

Foil L.E. Circle	X = 0.0250,	Y = 1.4701,	R = 0.0250
Foil T.E. Circle	X = 3.2250,	Y = −0.2422,	R = 0.0250
Foil L.E. Tangency Pt. Suction	X = 0.0250,	Y = 1.4951	
Foil L.E. Tangency Pt. Pressure	X = 0.0250,	Y = 1.4451	
Foil T.E. Tangency Pt. Suction	X = 3.2441,	Y = −0.2260	
Foil T.E. Tangency Pt. Pressure	X = 3.2059,	Y = −0.2584	
Foil Nose Point	X = 0.0 ,	Y = 1.4701	
Foil Tail Point	X = 3.2412,	Y = −0.2613	

UNCLASSIFIED

Foil Area (Less Core) = 0.1915

Gaging	LAMBDA = 1.1087,	X = 2.4816,	Y = 0.5545
Gaging Angle	= 42.135		
Center of Gravity	X = 1.7469,	Y = 0.8682	
Radial Reference	X = 1.7483,	Y = 1.2100	
Inlet Angle	= 90.000,	Delta Beta 1 = 0.001	
Exit Angle	= 40.355,	Delta Beta 2 = 0.001	
Uncovered Turning	= 8.737		

Constant Section Thickness = .050

TABLE VI

REDESIGNED SECOND VANE CASCADE TURNING VANE

Radius of 1/4R Section = 8.2810 | Axial Chord = 3.2500 | Actual Chord = 3.6127
Pitch = 1.7344 | No. of Foils = 4.

Percent X	Foil X	Foil Y Suction	Foil Y (Circle)
0.0	0.0	1.1160	1.0910
0.01	0.0325	1.1160	1.1160
0.02	0.0650	1.1159	1.1159
0.03	0.0975	1.1155	1.1155
0.04	0.1300	1.1150	1.1150
0.05	0.1625	1.1143	1.1143
0.10	0.3250	1.1077	1.1077
0.15	0.4875	1.0955	1.0955
0.20	0.6500	1.0772	1.0772
0.25	0.8125	1.0521	1.0521
0.30	0.9750	1.0196	1.0196
0.35	1.1375	0.9791	0.9791
0.40	1.3000	0.9298	0.9298
0.45	1.4625	0.8712	0.8712
0.50	1.6250	0.8026	0.8026
0.55	1.7875	0.7236	0.7236
0.60	1.9500	0.6337	0.6337
0.65	2.1125	0.5328	0.5328
0.70	2.2750	0.4207	0.4207
0.75	2.4375	0.2974	0.2974
0.80	2.6000	0.1633	0.1633
0.85	2.7625	0.0186	0.0186
0.90	2.9250	−0.1362	−0.1362
0.95	3.0875	−0.3010	−0.3010
0.98	3.1850	−0.4063	−0.4063
0.99	3.2175	−0.4412	−0.4412
1.00	3.2500	−0.4753	−0.4850

Foil L.E. Circle	X = 0.0250,	Y = 1.0910,	R = 0.0250
Foil T.E. Circle	X = 3.2250,	Y = −0.4850,	R = 0.0250
Foil L.E. Tangency Pt. Suction	X = 0.0250,	Y = 1.1160	
Foil L.E. Tangency Pt. Pressure	X = 0.0250,	Y = 1.0660	
Foil T.E. Tangency Pt. Suction	X = 3.2435,	Y = −0.4682	
Foil T.E. Tangency Pt. Pressure	X = 3.2065,	Y = −0.5018	
Foil Nose Point	X = 0.0 ,	Y = 1.0910	
Foil Tail Point	X = 3.2418,	Y = −0.5035	

Foil Area (Less Core) = 0.1855

Gaging	LAMBDA = 1.2102,	X = 2.4540,	Y = 0.2843
Gaging Angle	= 44.250		
Center of Gravity	X = 1.7356,	Y = 0.5496	
Radial Reference	X = 1.7483,	Y = 1.2100	
Inlet Angle	= 90.000,	Delta Beta 1 = 0.001	
Exit Angle	= 42.300,	Delta Beta 2 = 0.001	
Uncovered Turning	= 9.080		

Constant Section Thickness = .050

TABLE VII

REDESIGNED SECOND VANE CASCADE TURNING VANE

Radius of 3/8R Section = 8.6715 | Axial Chord = 3.2500 | Actual Chord = 3.5567
Pitch = 1.8162 | No. of Foils = 4

Percent X	Foil X	Foil Y Suction	Foil Y (Circle)
0.0	0.0	0.7617	0.7367
0.01	0.0325	0.7617	0.7617
0.02	0.0650	0.7615	0.7615
0.03	0.0975	0.7613	0.7613
0.04	0.1300	0.7609	0.7609
0.05	0.1625	0.7603	0.7603
0.10	0.3250	0.7541	0.7541
0.15	0.4875	0.7427	0.7427
0.20	0.6500	0.7261	0.7261
0.25	0.8125	0.7029	0.7029
0.30	0.9750	0.6731	0.6731
0.35	1.1375	0.6357	0.6357
0.40	1.3000	0.5905	0.5905
0.45	1.4625	0.5367	0.5367
0.50	1.6250	0.4739	0.4739
0.55	1.7875	0.4015	0.4015
0.60	1.9500	0.3192	0.3192
0.65	2.1125	0.2268	0.2268
0.70	2.2750	0.1241	0.1241
0.75	2.4375	0.0112	0.0112
0.80	2.6000	−0.1115	−0.1115
0.85	2.7625	−0.2440	−0.2440
0.90	2.9250	−0.3859	−0.3859
0.95	3.0875	−0.5368	−0.5368
0.98	3.1850	−0.6299	−0.6299
0.99	3.2175	−0.6641	−0.6641
1.00	3.2500	−0.6966	−0.7069

Foil L.E. Circle: X = 0.0250, Y = 0.7367, R = 0.0250
Foil T.E. Circle: X = 3.2250, Y = −0.7069, R = 0.0250

Foil L.E. Tangency Pt. Suction: X = 0.0250, Y = 0.7617
Foil L.E. Tangency Pt. Pressure: X = 0.0250, Y = 0.7117
Foil T.E. Tangency Pt. Suction: X = 3.2427, Y = −0.6893
Foil T.E. Tangency Pt. Pressure: X = 3.2073, Y = −0.7245

Foil Nose Point: X = 0.0, Y = 0.7367
Foil Tail Point: X = 3.2426, Y = −0.7246

Foil Area (Less Core) = 0.1790

Gaging: LAMBDA = 1.3262, X = 2.4321, Y = 0.0152
Gaging Angle = 46.906

Center of Gravity: X = 1.7155, Y = 0.2492
Radial Reference: X = 1.7483, Y = 1.2100

Inlet Angle = 90.000, Delta Beta 1 = 0.001
Exit Angle = 44.825, Delta Beta 2 = 0.001
Uncovered Turning = 9.303

Constant Section Thickness = .050

TABLE VIII

REDESIGNED SECOND VANE CASCADE TURNING VANE

Radius of Mean Section = 9.0625 Axial Chord = 3.2500 Actual Chord = 3.4991
Pitch = 1.8980 No. of Foils = 4.

Percent X	Foil X	Foil Y Suction	Foil Y (Circle)
0.0	0.0	0.3960	0.3710
0.01	0.0325	0.3960	0.3960
0.02	0.0650	0.3959	0.3959
0.03	0.0975	0.3956	0.3956
0.04	0.1300	0.3952	0.3952
0.05	0.1625	0.3946	0.3946
0.10	0.3250	0.3889	0.3889
0.15	0.4875	0.3787	0.3787
0.20	0.6500	0.3633	0.3633
0.25	0.8125	0.3424	0.3424
0.30	0.9750	0.3154	0.3154
0.35	1.1375	0.2819	0.2819
0.40	1.3000	0.2413	0.2413
0.45	1.4625	0.1931	0.1931
0.50	1.6250	0.1369	0.1369
0.55	1.7875	0.0723	0.0723
0.60	1.9500	−0.0011	−0.0011
0.65	2.1125	−0.0835	−0.0835
0.70	2.2750	−0.1751	−0.1751
0.75	2.4375	−0.2759	−0.2759
0.80	2.6000	−0.3859	−0.3859
0.85	2.7625	−0.5049	−0.5049
0.90	2.9250	−0.6327	−0.6327
0.95	3.0875	−0.7691	−0.7691
0.98	3.1850	−0.8552	−0.8552
0.99	3.2175	−0.8779	−0.8779
1.00	3.2500	−0.9140	−0.9250

Foil L.E. Circle	X = 0.0250,	Y = 0.3710,	R = 0.0250
Foil T.E. Circle	X = 3.2250,	Y = −0.9250,	R = 0.0250
Foil L.E. Tangency Pt. Suction	X = 0.0250,	Y = 0.3960	
Foil L.E. Tangency Pt. Pressure	X = 0.0250,	Y = 0.3460	
Foil T.E. Tangency Pt. Suction	X = 3.2419,	Y = −0.9066	
Foil T.E. Tangency Pt. Pressure	X = 3.2081,	Y = −0.9434	
Foil Nose Point	X = 0.0 ,	Y = 0.3710	
Foil Tail Point	X = 3.2434,	Y = −0.9419	

Foil Area (Less Core) = 0.1736

Gaging	LAMBDA = 1.4514,	X = 2.4249,	Y = −0.2678
Gaging Angle	= 49.880,		
Center of Gravity	X = 1.6977,	Y = −0.0585	
Radial Reference	X = 1.7483,	Y = 1.2100	
Inlet Angle	= 90.000,	Delta Beta 1 = 0.001	
Exit Angle	= 47.550,	Delta Beta 2 = 0.001	
Uncovered Turning	= 9.654		

Constant Section Thickness = .050

TABLE IX

REDESIGNED SECOND VANE CASCADE TURNING VANE

Radius of 1/8T Section = 9.4531 | Axial Chord = 3.2500 | Actual Chord = 3.4371
Pitch = 1.9799 | No. of Foils = 4.

Percent X	Foil X	Foil Y Suction	Foil Y (Circle)
0.0	0.0	−0.0091	−0.0339
0.01	0.0325	−0.0090	−0.0090
0.02	0.0650	−0.0091	−0.0091
0.03	0.0975	−0.0094	−0.0094
0.04	0.1300	−0.0096	−0.0096
0.05	0.1625	−0.0100	−0.0100
0.10	0.3250	−0.0144	−0.0144
0.15	0.4875	−0.0227	−0.0227
0.20	0.6500	−0.0346	−0.0346
0.25	0.8125	−0.0511	−0.0511
0.30	0.9750	−0.0728	−0.0728
0.35	1.1375	−0.0999	−0.0999
0.40	1.3000	−0.1326	−0.1326
0.45	1.4625	−0.1722	−0.1722
0.50	1.6250	−0.2185	−0.2185
0.55	1.7875	−0.2724	−0.2724
0.60	1.9500	−0.3341	−0.3341
0.65	2.1125	−0.4043	−0.4043
0.70	2.2750	−0.4829	−0.4829
0.75	2.4375	−0.5703	−0.5703
0.80	2.6000	−0.6666	−0.6666
0.85	2.7625	−0.7720	−0.7720
0.90	2.9250	−0.8864	−0.8864
0.95	3.0875	−1.0096	−1.0096
0.98	3.1850	−1.0862	−1.0862
0.99	3.2175	−1.1123	−1.1123
1.00	3.2500	−1.1415	−1.1532

Foil L.E. Circle — X = 0.0250, — Y = −0.0339, — R = 0.0250
Foil T.E. Circle — X = 3.2250, — Y = −1.1532, — R = 0.0250

Foil L.E. Tangency Pt. Suction — X = 0.0250, — Y = −0.0089
Foil L.E. Tangency Pt. Pressure — X = 0.0250, — Y = −0.0589
Foil T.E. Tangency Pt. Suction — X = 3.2410, — Y = −1.1340
Foil T.E. Tangency Pt. Pressure — X = 3.2090, — Y = −1.1724

Foil Nose Point — X = 0.0 , — Y = −0.0339
Foil Tail Point — X = 3.2442, — Y = −1.1692

Foil Area (Less Core) = 0.1704

Gaging — LAMBDA = 1.5786, — X = 2.4368, — Y = −0.5699
Gaging Angle = 52.877

Center of Gravity — X = 1.6908, — Y = −0.3909
Radial Reference — X = 1.7483, — Y = 1.2100

Inlet Angle = 90.000, — Delta Beta 1 = 0.001
Exit Angle = 50.133, — Delta Beta 2 = 0.001
Uncovered Turning = 10.405

Constant Section Thickness = .050

TABLE X

REDESIGNED SECOND VANE CASCADE TURNING VANE

Radius of 1/4T Section = 9.8437 | Axial Chord = 3.2500 | Actual Chord = 3.3792
Pitch = 2.0617 | No. of Foils = 4.

Percent X	Foil X	Foil Y Suction	Foil Y (Circle)
0.0	0.0	−0.4270	−0.4520
0.01	0.0325	−0.4270	−0.4270
0.02	0.0650	−0.4271	−0.4271
0.03	0.0975	−0.4272	−0.4272
0.04	0.1300	−0.4274	−0.4274
0.05	0.1625	−0.4277	−0.4277
0.10	0.3250	−0.4305	−0.4305
0.15	0.4875	−0.4358	−0.4358
0.20	0.6500	−0.4439	−0.4439
0.25	0.8125	−0.4551	−0.4551
0.30	0.9750	−0.4699	−0.4699
0.35	1.1375	−0.4889	−0.4889
0.40	1.3000	−0.5125	−0.5125
0.45	1.4625	−0.5413	−0.5413
0.50	1.6250	−0.5761	−0.5761
0.55	1.7875	−0.6176	−0.6176
0.60	1.9500	−0.6662	−0.6662
0.65	2.1125	−0.7228	−0.7228
0.70	2.2750	−0.7878	−0.7878
0.75	2.4375	−0.8615	−0.8615
0.80	2.6000	−0.9443	−0.9443
0.85	2.7625	−1.0362	−1.0362
0.90	2.9250	−1.1373	−1.1373
0.95	3.0875	−1.2477	−1.2477
0.98	3.1850	−1.3201	−1.3201
0.99	3.2175	−1.3455	−1.3455
1.00	3.2500	−1.3676	−1.3800

Foil L.E. Circle — X = 0.0250, — Y = −0.4520, — R = 0.0250
Foil T.E. Circle — X = 3.2250, — Y = −1.3800, — R = 0.0250

Foil L.E. Tangency Pt. Suction — X = 0.0250, — Y = −0.4270
Foil L.E. Tangency Pt. Pressure — X = 0.0250, — Y = −0.4770
Foil T.E. Tangency Pt. Suction — X = 3.2402, — Y = −1.3601
Foil T.E. Tangency Pt. Pressure — X = 3.2098, — Y = −1.3999

Foil Nose Point — X = 0.0 , — Y = −0.4520
Foil Tail Point — X = 3.2449, — Y = −1.3952

Foil Area (Less Core) = 0.1585

Gaging — LAMBDA = 1.7072, — X = 2.4622, — Y = −0.8735
Gaging Angle = 55.900

Center of Gravity — X = 1.6891, — Y = −0.7293
Radial Reference — X = 1.7483, — Y = 1.2100

Inlet Angle = 90.000, — Delta Beta 1 = 0.001
Exit Angle = 52.630, — Delta Beta 2 = 0.001
Uncovered Turning = 11.264

Constant Section Thickness = .050

TABLE XI

REDESIGNED SECOND VANE CASCADE TURNING VANE

Radius of 3/8T Section = 10.2343 | Axial Chord = 3.2500 | Actual Chord = 3.3321
Pitch = 2.1435 | No. of Foils = 4.

Percent X	Foil X	Foil Y Suction	Foil Y (Circle)
0.0	0.0	−0.8247	−0.8497
0.01	0.0325	−0.8247	−0.8247
0.02	0.0650	−0.8248	−0.8248
0.03	0.0975	−0.8248	−0.8248
0.04	0.1300	−0.8249	−0.8249
0.05	0.1625	−0.8251	−0.8251
0.10	0.3250	−0.8266	−0.8266
0.15	0.4875	−0.8294	−0.8294
0.20	0.6500	−0.8340	−0.8340
0.25	0.8125	−0.8403	−0.8403
0.30	0.9750	−0.8489	−0.8489
0.35	1.1375	−0.8602	−0.8602
0.40	1.3000	−0.8748	−0.8748
0.45	1.4625	−0.8934	−0.8934
0.50	1.6250	−0.9166	−0.9166
0.55	1.7875	−0.9455	−0.9455
0.60	1.9500	−0.9810	−0.9810
0.65	2.1125	−1.0244	−1.0244
0.70	2.2750	−1.0763	−1.0763
0.75	2.4375	−1.1373	−1.1373
0.80	2.6000	−1.2074	−1.2074
0.85	2.7625	−1.2860	−1.2860
0.90	2.9250	−1.3733	−1.3733
0.95	3.0875	−1.4697	−1.4697
0.98	3.1850	−1.5344	−1.5344
0.99	3.2175	−1.5583	−1.5583
1.00	3.2500	−1.5769	−1.5899

Foil L.E. Circle	X = 0.0250,	Y = −0.8497,	R = 0.0250
Foil T.E. Circle	X = 3.2250,	Y = −1.5899,	R = 0.0250
Foil L.E. Tangency Pt. Suction	X = 0.0250,	Y = −0.8[illegible]7	
Foil L.E. Tangency Pt. Pressure	X = 0.0250,	Y = [illegible]	
Foil T.E. Tangency Pt. Suction	X = 3.2393,	Y = [illegible]	
Foil T.E. Tangency Pt. Pressure	X = 3.2107,	Y = [illegible]105	
Foil Nose Point	X = 0.0	Y = −0.8497	
Foil Tail Point	X = 3.2455,	Y = −1.6042	

Foil Area (Less Core) = 0.1670

Gaging	LAMBDA = 1.8386,	X = 2.4970,	Y = −1.1620
Gaging Angle	= 59.065		
Center of Gravity	X = 1.6843,	Y = −1.0507	
Radial Reference	X = 1.7483,	Y = 1.2100	
Inlet Angle	= 90.000,	Delta Beta 1 = 0.001	
Exit Angle	= 55.174,	Delta Beta 2 = 0.001	
Uncovered Turning	= 11.840		

Constant Section Thickness = .050

TABLE XII

REDESIGNED SECOND VANE CASCADE TURNING VANE

Radius of Tip Section = 10.6250 Axial Chord = 3.2500 Actual Chord = 3.2963
Pitch = 2.2253 No. of Foils = 4.

Percent X	Foil X	Foil Y Suction	Foil Y (Circle)
0.0	0.0	−1.1953	−1.2203
0.01	0.0325	−1.1953	−1.1953
0.02	0.0650	−1.1953	−1.1953
0.03	0.0975	−1.1953	−1.1953
0.04	0.1300	−1.1954	−1.1954
0.05	0.1625	−1.1954	−1.1954
0.10	0.3250	−1.1959	−1.1959
0.15	0.4875	−1.1969	−1.1969
0.20	0.6500	−1.1985	−1.1985
0.25	0.8125	−1.2008	−1.2008
0.30	0.9750	−1.2041	−1.2041
0.35	1.1375	−1.2087	−1.2087
0.40	1.3000	−1.2150	−1.2150
0.45	1.4625	−1.2238	−1.2238
0.50	1.6250	−1.2358	−1.2358
0.55	1.7875	−1.2523	−1.2523
0.60	1.9500	−1.2751	−1.2751
0.65	2.1125	−1.3057	−1.3057
0.70	2.2750	−1.3456	−1.3456
0.75	2.4375	−1.3952	−1.3952
0.80	2.6000	−1.4534	−1.4534
0.85	2.7625	−1.5191	−1.5191
0.90	2.9250	−1.5917	−1.5917
0.95	3.0875	−1.6726	−1.6726
0.98	3.1850	−1.7288	−1.7288
0.99	3.2175	−1.7544	−1.7544
1.00	3.2500	−1.7662	−1.7800

Foil L.E. Circle	X = 0.0250,	Y = −1.2203,	R = 0.0250
Foil T.E. Circle	X = 3.2250,	Y = −1.7800,	R = 0.0250
Foil L.E. Tangency Pt. Suction	X = 0.0250,	Y = −1.1953	
Foil L.E. Tangency Pt. Pressure	X = 0.0250,	Y = −1.2453	
Foil T.E. Tangency Pt. Suction	X = 3.2383,	Y = −1.7588	
Foil T.E. Tangency Pt. Pressure	X = 3.2117,	Y = −1.8012	
Foil Nose Point	X = 0.0 ,	Y = −1.2203	
Foil Tail Point	X = 3.2462,	Y = −1.7933	

Foil Area (Less Core) = 0.1654

Gaging	LAMBDA = 1.9724,	X = 2.5401,	Y = −1.4311
Gaging Angle	= 62.420		
Center of Gravity	X = 1.6735,	Y = −1.3508	
Radial Reference	X = 1.7483,	Y = 1.2100	
Inlet Angle	= 90.000,	Delta Beta 1 = 0.000	
Exit Angle	= 57.790,	Delta Beta 2 = 0.000	
Uncovered Turning	= 12.139		

Constant Section Thickness = .050

TABLE XIII

RECONTOURED SECOND VANE

Radius of FF Section = 7.5000 | Axial Chord = 0.8320 | Actual Chord = 0.8432
Pitch = 0.5890 | No. of Foils = 80.00

Percent X	Foil X	Foil Y Suction	Foil Y (Circle)	Foil Y Pressure	Foil Y (Circle)
0.0	0.0	−0.2059	−0.2011	−0.1571	−0.2011
0.01	0.0083	−0.2196	−0.2196	−0.1660	−0.1862
0.02	0.0166	−0.2329	−0.2329	−0.1750	−0.1836
0.03	0.0250	−0.2458	−0.2458	−0.1820	−0.1853
0.04	0.0333	−0.2583	−0.2583	−0.1923	−0.1923
0.05	0.0416	−0.2705	−0.2705	−0.2010	−0.2010
0.10	0.0832	−0.3266	−0.3266	−0.2422	−0.2422
0.15	0.1248	−0.3744	−0.3744	−0.2792	−0.2792
0.20	0.1664	−0.4143	−0.4143	−0.3111	−0.3111
0.25	0.2080	−0.4465	−0.4465	−0.3374	−0.3374
0.30	0.2496	−0.4711	−0.4711	−0.3572	−0.3572
0.35	0.2912	−0.4882	−0.4882	−0.3699	−0.3699
0.40	0.3328	−0.4979	−0.4979	−0.3752	−0.3752
0.45	0.3744	−0.5001	−0.5001	−0.3727	−0.3727
0.50	0.4160	−0.4950	−0.4950	−0.3627	−0.3627
0.55	0.4576	−0.4824	−0.4824	−0.3453	−0.3453
0.60	0.4992	−0.4622	−0.4622	−0.3214	−0.3214
0.65	0.5408	−0.4344	−0.4344	−0.2914	−0.2914
0.70	0.5824	−0.3987	−0.3987	−0.2562	−0.2562
0.75	0.6240	−0.3550	−0.3550	−0.2164	−0.2164
0.80	0.6656	−0.3028	−0.3028	−0.1728	−0.1728
0.85	0.7072	−0.2420	−0.2420	−0.1260	−0.1260
0.90	0.7488	−0.1719	−0.1719	−0.0763	−0.0763
0.95	0.7904	−0.0922	−0.0922	−0.0244	−0.0244
0.98	0.8154	−0.0394	−0.0394	0.0074	0.0075
0.99	0.8237	−0.0210	−0.0210	0.0180	0.0099
1.00	0.8320	−0.0022	−0.0	0.294	−0.0

Foil L.E. Circle X = 0.0175, Y = −0.2011, R = 0.0175
Foil T.E. Circle X = 0.8220, Y = −0.0 R = 0.0100

Foil L.E. Tangency Pt. Suction X = 0.0026, Y = −0.2102
Foil L.E. Tangency Pt. Pressure X = 0.0302, Y = −0.1891
Foil T.E. Tangency Pt. Suction X = 0.8312, Y = −0.0040
Foil T.E. Tangency Pt. Pressure X = 0.8141, Y = 0.0061

Foil Nose Point X = 0.0069, Y = −0.1872
Foil Tail Point X = 0.8271, Y = 0.0086

Foil Area = 0.0920

Gaging LAMBDA = 0.2941, X = 0.6024, Y = −0.3787
Gaging Angle = 29.950

Center of Gravity X = 0.4301, Y = −0.3316
Radial Reference X = 0.4301, Y = −0.3316

Inlet Angle = 37.330, DELTA BETA 1 = 12.000
Exit Angle = 30.570, DELTA BETA 2 = 14.000
Uncovered Turning = 20.089

Min. Moment of Inertia = 0.00077115
Max. Moment of Inertia = 0.00450036

Principal Axis Angle = −17.163

Pitch/Axial Chord = 0.7080
Pitch/Actual Chord = 0.6986

TABLE XIV

RECONTOURED SECOND VANE

Radius of AA Section = 7.6500 | Axial Chord = 0.8357 | Actual Chord = 0.8563
Pitch = 0.6008 | *No. of Foils = 80.00*

Percent X	Foil X	Foil Y Suction	Foil Y (Circle)	Foil Y Pressure	Foil Y (Circle)
0.0	−0.0083	−0.2334	−0.2284	−0.1826	−0.2284
0.01	0.0001	−0.2474	−0.2474	−0.1916	−0.2130
0.02	0.0085	−0.2608	−0.2608	−0.2005	−0.2100
0.03	0.0168	−0.2739	−0.2739	−0.2078	−0.2112
0.04	0.0252	−0.2866	−0.2866	−0.2175	−0.2175
0.05	0.0335	−0.2989	−0.2989	−0.2258	−0.2258
0.10	0.0753	−0.3547	−0.3547	−0.2646	−0.2646
0.15	0.1171	−0.4017	−0.4017	−0.2983	−0.2983
0.20	0.1589	−0.4401	−0.4401	−0.3268	−0.3268
0.25	0.2007	−0.4703	−0.4703	−0.3497	−0.3497
0.30	0.2425	−0.4926	−0.4926	−0.3665	−0.3665
0.35	0.2842	−0.5072	−0.5072	−0.3768	−0.3768
0.40	0.3260	−0.5143	−0.5143	−0.3803	−0.3803
0.45	0.3678	−0.5138	−0.5138	−0.3768	−0.3768
0.50	0.4096	−0.5059	−0.5059	−0.3664	−0.3664
0.55	0.4514	−0.4904	−0.4904	−0.3492	−0.3492
0.60	0.4932	−0.4673	−0.4673	−0.3254	−0.3254
0.65	0.5350	−0.4365	−0.4365	−0.2954	−0.2954
0.70	0.5767	−0.3977	−0.3977	−0.2594	−0.2594
0.75	0.6185	−0.3507	−0.3507	−0.2182	−0.2182
0.80	0.6603	−0.2953	−0.2953	−0.1725	−0.1725
0.85	0.7021	−0.2316	−0.2316	−0.1230	−0.1230
0.90	0.7439	−0.1595	−0.1595	−0.0702	−0.0702
0.95	0.7857	−0.0790	−0.0790	−0.0146	−0.0146
0.98	0.8107	−0.0267	−0.0267	-0.0197	0.0195
0.99	0.8191	−0.0085	−0.0085	0.0311	0.0220
1.00	0.8275	0.0099	0.0121	0.0433	0.0121

Foil L.E. Circle X = 0.0102, Y = −0.2284, R = 0.0185
Foil T.E. Circle X = 0.8175, Y = 0.0121, R = 0.0100

Foil L.E. Tangency Pt. Suction X = −0.0056, Y = −0.2379
Foil L.E. Tangency Pt. Pressure X = 0.0234, Y = −0.2155
Foil T.E. Tangency Pt. Suction X = 0.8266, Y = 0.0080
Foil T.E. Tangency Pt. Pressure X = 0.8094, Y = 0.0180

Foil Nose Point X = −0.0011, Y = −0.2138
Foil Tail Point X = 0.8225, Y = 0.0208

Foil Area = 0.0950

Gaging LAMBDA = 0.2962, X = 0.5916, Y = −0.3820
Gaging Angle 29.535

Center of Gravity X = 0.4125 Y = −0.3438
Radial Reference X = 0.4301, Y = −0.3316

Inlet Angle = 37.732, DELTA BETA 1 = 13.749
Exit Angle = 30.022, DELTA BETA 2 = 1..801
Uncovered Turning = 18.155

Min. Moment of Inertia = 0.00077791
Max. Moment of Inertia = 0.00472626

Principal Axis Angle = −19.327

Pitch/Axial Chord = 0.7189
Pitch/Actual Chord = 0.7016

TABLE XV

RECONTOURED SECOND VANE

Radius of BB Section = 8.4863
Pitch = 0.6665

Axial Chord = 0.8565
No. of Foils = 80.00

Actual Chord = 0.9464

Percent X	Foil X	Foil Y Suction	Foil Y (Circle)	Foil Y Pressure	Foil Y (Circle)
0.0	−0.0543	−0.3634	−0.3570	−0.3074	−0.3570
0.01	−0.0458	−0.3771	−0.3771	−0.3156	−0.3393
0.02	−0.0372	−0.3903	−0.3903	−0.3234	−0.3352
0.03	−0.0286	−0.4030	−0.4030	−0.3307	−0.3347
0.04	−0.0201	−0.4152	−0.4152	−0.3376	−0.3378
0.05	−0.0115	−0.4270	−0.4270	−0.3442	−0.3442
0.10	0.0313	−0.4792	−0.4792	−0.3719	−0.3719
0.15	0.0741	−0.5208	−0.5208	−0.3925	−0.3925
0.20	0.1170	−0.5526	−0.5526	−0.4073	−0.4073
0.25	0.1598	−0.5749	−0.5749	−0.4168	−0.4168
0.30	0.2026	−0.5883	−0.5883	−0.4215	−0.4215
0.35	0.2454	−0.5931	−0.5931	−0.4215	−0.4215
0.40	0.2883	−0.5893	−0.5893	−0.4168	−0.4168
0.45	0.3311	−0.5773	−0.5773	−0.4073	−0.4073
0.50	0.3739	−0.5571	−0.5571	−0.3927	−0.3927
0.55	0.4167	−0.5287	−0.5287	−0.3722	−0.3722
0.60	0.4596	−0.4921	−0.4921	−0.3450	−0.3450
0.65	0.5024	−0.4472	−0.4472	−0.3101	−0.3101
0.70	0.5452	−0.3939	−0.3939	−0.2671	−0.2671
0.75	0.5880	−0.3319	−0.3319	−0.2165	−0.2165
0.80	0.6309	−0.2616	−0.2616	−0.1594	−0.1594
0.85	0.6737	−0.1842	−0.1842	−0.0968	−0.0968
0.90	0.7165	−0.1010	−0.1010	−0.0293	−0.0293
0.95	0.7593	−0.0134	−0.0134	0.0425	0.0425
0.98	0.7850	0.0408	0.0408	0.0874	0.0867
0.99	0.7936	0.0591	0.0591	0.1027	0.0896
1.00	0.8022	0.0775	0.0797	0.1182	0.0797

Foil L.E. Circle	X = −0.0318,	Y = −0.3570,	R = 0.0225
Foil T.E. Circle	X = 0.7922,	Y = 0.0797,	R = 0.0100
Foil L.E. Tangency Pt. Suction	X = −0.0509,	Y = −0.3689	
Foil L.E. Tangency Pt. Pressure	X = −0.0181,	Y = −0.3392	
Foil T.E. Tangency Pt. Suction	X = 0.8012,	Y = 0.0755	
Foil T.E. Tangency Pt. Pressure	X = 0.7835,	Y = 0.0846	
Foil Nose Point	X = −0.0469,	Y = −0.3403	
Foil Tail Point	X = 0.7967,	Y = 0.0886	
Foil Area	= 0.1068		
Gaging	LAMBDA = 0.3033,	X = 0.5419,	Y = −0.3982
Gaging Angle	= 27.070		
Center of Gravity	X = 0.3464,	Y = −0.4008	
Radial Reference	X = 0.4301,	Y = −0.3316	
Inlet Angle	= 42.100,	DELTA BETA 1 = 20.250	
Exit Angle	= 27.170,	DELTA BETA 2 = 4.500	
Uncovered Turning	= 12.000		
Min. Moment of Inertia	= 0.00079620		
Max. Moment of Inertia	= 0.00602193		
Principal Axis Angle	= −29.781		
Pitch/Axial Chord	= 0.7782		
Pitch/Actual Chord	= 0.7042		

TABLE XVI

RECONTOURED SECOND VANE

Radius of CC Section = 9.4725
Pitch = 0.7440

Axial Chord = 0.8810
No. of Foils = 80.00

Actual Chord = 1.0660

Percent X	Foil X	Foil Y Suction	Foil Y (Circle)	Foil Y Pressure	Foil Y (Circle)
0.0	−0.1087	−0.4728	−0.4641	−0.4202	−0.4641
0.01	−0.0999	−0.4838	−0.4838	−0.4259	−0.4450
0.02	−0.0911	−0.4945	−0.4945	−0.4313	−0.4402
0.03	−0.0822	−0.5049	−0.5049	−0.4364	−0.4391
0.04	−0.0734	−0.5150	−0.5150	−0.4412	−0.4413
0.05	−0.0646	−0.5247	−0.5247	−0.4458	−0.4458
0.10	−0.0206	−0.5685	−0.5685	−0.4647	−0.4647
0.15	0.0235	−0.6039	−0.6039	−0.4778	−0.4778
0.20	0.0675	−0.6304	−0.6304	−0.4858	−0.4858
0.25	0.1116	−0.6480	−0.6480	−0.4889	−0.4889
0.30	0.1556	−0.6563	−0.6563	−0.4872	−0.4872
0.35	0.1997	−0.6552	−0.6552	−0.4807	−0.4807
0.40	0.2437	−0.6447	−0.6447	−0.4692	−0.4692
0.45	0.2878	−0.6247	−0.6247	−0.4521	−0.4521
0.50	0.3318	−0.5952	−0.5952	−0.4288	−0.4288
0.55	0.3759	−0.5563	−0.5563	−0.3982	−0.3982
0.60	0.4199	−0.5083	−0.5083	−0.3592	−0.3592
0.65	0.4640	−0.4513	−0.4513	−0.3113	−0.3113
0.70	0.5080	−0.3857	−0.3857	−0.2553	−0.2553
0.75	0.5521	−0.3117	−0.3117	−0.1922	−0.1922
0.80	0.5961	−0.2299	−0.2299	−0.1230	−0.1230
0.85	0.6402	−0.1412	−0.1412	−0.0486	−0.0486
0.90	0.6842.	−0.0465	−0.0465	0.0307	0.0307
0.95	0.7283	0.0533	0.0533	0.1144	0.1144
0.98	0.7547	0.1153	0.1153	0.1665	0.1659
0.99	0.7635	0.1363	0.1363	0.1843	0.1693
1.00	0.7723	0.1574	0.1594	0.2021	0.1594

Foil L.E. Circle	X = −0.0837,	Y = −0.4641,	R = 0.0250
Foil T.E. Circle	X = 0.7623,	Y = 0.1594,	R = 0.0100
Foil L.E. Tangency Pt. Suction	X = −0.1032,	Y = −0.4797	
Foil L.E. Tangency Pt. Pressure	X = −0.0720,	Y = −0.4420	
Foil T.E. Tangency Pt. Suction	X = 0.7716,	Y = 0.1556	
Foil T.E. Tangency Pt. Pressure	X = 0.7534,	Y = 0.1639	
Foil Nose Point	X = −0.1030,	Y = −0.4482	
Foil Tail Point	X = 0.7665,	Y = 0.1685	
Foil Area	= 0.1117		
Gaging	LAMBDA = 0.3115,	X = 0.4937,	Y = −0.4080
Gaging Angle	= 24.750		
Center of Gravity	X = 0.3086,	Y = −0.4308	
Radial Reference	X = 0.4301,	Y = −0.3316	
Inlet Angle	= 50.500,	DELTA BETA 1 = 13.500	
Exit Angle	= 24.580,	DELTA BETA 2 = 4.000	
Uncovered Turning	= 10.674		
Min. Moment of Inertia	= 0.00078028		
Max. Moment of Inertia	= 0.00818481		
Principal Axis Angle	= −38.899		
Pitch/Axial Chord	= 0.8445		
Pitch/Actual Chord	= 0.6979		

TABLE XVII

RECONTOURED SECOND VANE

Radius of DD Section = 10.4600 Axial Chord = 0.9055 Actual Chord = 1.1749
Pitch = 0.8215 No. of Foils = 80.00

Percent X	Foil X	Foil Y Suction	Foil Y (Circle)	Foil Y Pressure	Foil Y (Circle)
0.0	−0.1631	−0.5384	−0.5273	−0.4868	−0.5273
0.01	−0.1540	−0.5479	−0.5479	−0.4907	−0.5069
0.02	−0.1450	−0.5570	−0.5570	−0.4945	−0.5015
0.03	−0.1359	−0.5659	−0.5659	−0.4980	−0.4998
0.04	−0.1269	−0.5746	−0.5746	−0.5012	−0.5012
0.05	−0.1178	−0.5829	−0.5829	−0.5043	−0.5043
0.10	−0.0725	−0.6200	−0.6200	−0.5164	−0.5164
0.15	−0.0273	−0.6493	−0.6493	−0.5234	−0.5234
0.20	0.0180	−0.6702	−0.6702	−0.5257	−0.5257
0.25	0.0633	−0.6821	−0.6821	−0.5232	−0.5232
0.30	0.1086	−0.6349	−0.6849	−0.5159	−0.5159
0.35	0.1539	−0.6781	−0.6781	−0.5036	−0.5036
0.40	0.1991	−0.6615	−0.6615	−0.4857	−0.4857
0.45	0.2444	−0.6350	−0.6350	−0.4616	−0.4616
0.50	0.2897	−0.5984	−0.5984	−0.4303	−0.4303
0.55	0.3350	−0.5520	−0.5520	−0.3905	−0.3905
0.60	0.3802	−0.4958	−0.4958	−0.3416	−0.3416
0.65	0.4255	−0.4303	−0.4303	−0.2843	−0.2843
0.70	0.4708	−0.3557	−0.3557	−0.2194	−0.2194
0.75	0.5161	−0.2726	−0.2726	−0.1481	−0.1481
0.80	0.5613	−0.1819	−0.1819	−0.0712	−0.0712
0.85	0.6066	−0.0845	−0.0845	0.0109	0.0109
0.90	0.6519	0.0184	0.0184	0.0977	0.0977
0.95	0.6972	0.1260	0.1260	0.1888	0.1888
0.98	0.7243	0.1924	0.1924	0.2455	0.2451
0.99	0.7334	0.2148	0.2148	0.2647	0.2492
1.00	0.7424	0.2373	0.2392	0.2840	0.2392

Foil L.E. Circle X = −0.1356, Y = −0.5273, R = 0.0275
Foil T.E. Circle X = 0.7325, Y = 0.2392, R = 0.0100

Foil L.E. Tangency Pt. Suction X = −0.1554, Y = −0.5464
Foil L.E. Tangency Pt. Pressure X = −0.1265, Y = −0.5014
Foil T.E. Tangency Pt. Suction X = 0.7417, Y = 0.2355
Foil T.E. Tangency Pt. Pressure X = 0.7234, Y = 0.2435

Foil Nose Point X = −0.1587, Y = −0.5125
Foil Tail Point X = 0.7365, Y = 0.2484

Foil Area = 0.1166

Gaging LAMBDA = 0.3307, X = 0.4425, Y = −0.4034
Gaging Angle = 23.739

Center of Gravity X = 0.2691, Y = −0.4297
Radial Reference X = 0.4301, Y = −0.3316

Inlet Angle = 57.407, DELTA BETA 1 = 26.758
Exist Angle = 23.599, DELTA BETA 2 = 3.500
Uncovered Turning = 9.789

Min. Moment of Inertia = 0.00074674
Max. Moment of Inertia = 0.01048401

Principal Axis Angle = 43.784

Pitch/Axial Chord = 0.9072
Pitch/Actual Chord = 0.6992

TABLE XVIII

RECONTOURED SECOND VANE

Radius of EE Section = 10.8600 Axial Chord = 0.9155 Actual Chord = 1.1982
Pitch = 0.8529 No. of Foils = 80.00

Percent X	Foil X	Foil Y Suction	Foil Y (Circle)	Foil Y Pressure	Foil Y (Circle)
0.0	−0.1851	−0.5304	−0.5179	−0.4776	−0.5179
0.01	−0.1760	−0.5387	−0.5386	−0.4806	−0.4973
0.02	−0.1668	−0.5468	−0.5468	−0.4845	−0.4917
0.03	−0.1577	−0.5548	−0.5548	−0.4879	−0.4900
0.04	−0.1485	−0.5625	−0.5625	−0.4914	−0.4914
0.05	−0.1393	−0.5700	−0.5700	−0.4944	−0.4944
0.10	−0.0936	−0.6034	−0.6034	−0.5061	−0.5061
0.15	−0.0478	−0.6301	−0.6301	−0.5124	−0.5124
0.20	−0.0020	−0.6496	−0.6496	−0.5135	−0.5135
0.25	0.0437	−0.6613	−0.6613	−0.5094	−0.5094
0.30	0.0895	−0.6648	−0.6648	−0.5002	−0.5002
0.35	0.1353	−0.6595	−0.6595	−0.4855	−0.4855
0.40	0.1811	−0.6449	−0.6449	−0.4649	−0.4649
0.45	0.2268	−0.6207	−0.6207	−0.4381	−0.4381
0.50	0.2726	−0.5863	−0.5863	−0.4041	−0.4041
0.55	0.3184	−0.5416	−0.5416	−0.3620	−0.3620
0.60	0.3642	−0.4866	−0.4866	−0.3116	−0.3116
0.65	0.4099	−0.4213	−0.4213	−0.2535	−0.2535
0.70	0.4557	−0.3461	−0.3461	−0.1884	−0.1884
0.75	0.5015	−0.2615	−0.2615	−0.1171	−0.1171
0.80	0.5473	−0.1684	−0.1684	−0.0402	−0.0402
0.85	0.5930	−0.0677	−0.0677	0.0419	0.0419
0.90	0.6388	0.0395	0.0395	0.1289	0.1289
0.95	0.6846	0.1522	0.1522	0.2204	0.2204
0.98	0.7120	0.2222	0.2222	0.2774	0.2771
0.99	0.7212	0.2459	0.2459	0.2972	0.2815
1.00	0.7303	0.2697	0.2716	0.3161	0.2716

Foil L.E. Circle X = −0.1572, Y = −0.5179, R = 0.0279
Foil T.E. Circle X = 0.7203, Y = 0.2716, R = 0.0100

Foil L.E. Tangency Pt. Suction X = −0.1758, Y = −0.5387
Foil L.E. Tangency Pt. Pressure X = −0.1483, Y = −0.4915
Foil T.E. Tangency Pt. Suction X = 0.7297, Y = 0.2680
Foil T.E. Tangency Pt. Pressure X = 0.7113, Y = 0.2759

Foil Nose Point X = −0.1813, Y = −0.5039
Foil Tail Point X = 0.7243, Y = 0.2807

Foil Area = 0.1242

Gaging LAMBDA = 0.3378, X = 0.4248, Y = 0.3980
Gaging Angle = 23.334

Center of Gravity X = 0.2674, Y = −0.3990
Radial Reference X = 0.4301, Y = −0.3316

Inlet Angle = 59.762, DELTA BETA 1 = 23.045
Exit Angle = 23.247, DELTA BETA 2 = 4.366
Uncovered Turning = 10.844

Min. Moment of Inertia = 0.00078773
Max. Moment of Inertia = 0.01155412

Principal Axis Angle = −44.493

Pitch/Axial Chord = 0.9317
Pitch/Actual Chord = 0.7118

TABLE XIX

RECONTOURED SECOND VANE

Radius of GG Section = 11.4450 Axial Chord = 0.9300 Actual Chord = 1.2024
Pitch = 0.8989 No. of Foils = 80.00

Percent T X	Foil X	Foil Y Suction	Foil Y (Circle)	Foil Y Pressure	Foil Y (Circle)
0.0	−0.2173	−0.4729	−0.4577	−0.4169	−0.4577
0.01	−0.2080	−0.4783	−0.4783	−0.4182	−0.4370
0.02	−0.1987	−0.4845	−0.4845	−0.4232	−0.4316
0.03	−0.1894	−0.4902	−0.4902	−0.4272	−0.4302
0.04	−0.1801	−0.4959	−0.4959	−0.4319	−0.4319
0.05	−0.1708	−0.5014	−0.5014	−0.4356	−0.4356
0.10	−0.1243	−0.5274	−0.5274	−0.4500	−0.4500
0.15	−0.0778	−0.5502	−0.5502	−0.4579	−0.4579
0.20	−0.0313	−0.5693	−0.5693	−0.4593	−0.4593
0.25	0.0152	−0.5839	−0.5839	−0.4542	−0.4542
0.30	0.0617	−0.5931	−0.5931	−0.4426	−0.4426
0.35	0.1082	−0.5958	−0.5958	−0.4244	−0.4244
0.40	0.1547	−0.5910	−0.5910	−0.3999	−0.3999
0.45	0.2012	−0.5773	−0.5773	−0.3689	−0.3689
0.50	0.2477	−0.5534	−0.5534	−0.3317	−0.3317
0.55	0.2941	−0.5182	−0.5182	−0.2882	−0.2882
0.60	0.3407	−0.4710	−0.4710	−0.2387	−0.2387
0.65	0.3872	−0.4112	−0.4112	−0.1831	−0.1831
0.70	0.4337	−0.3391	−0.3391	−0.1217	−0.1217
0.75	0.4802	−0.2553	−0.2553	−0.0545	−0.0545
0.80	0.5267	−0.1602	−0.1602	0.0182	0.0182
0.85	0.5731	−0.0548	−0.0548	0.0964	0.0964
0.90	0.6197	0.0604	0.0604	0.1799	0.1799
0.95	0.6662	0.1846	0.1846	0.2685	0.2685
0.98	0.6941	0.2632	0.2632	0.3239	0.3239
0.99	0.7034	0.2900	0.2900	0.3448	0.3288
1.00	0.7127	0.3171	0.3188	0.3616	0.3188

Foil L.E. Circle X = −0.1898, Y = −0.4577, R = 0.0275
Foil T.E. Circle X = 0.7027, Y = 0.3188, R = 0.0100

Foil L.E. Tangency Pt. Suction X = −0.2045, Y = −0.4810
Foil L.E. Tangency Pt. Pressure X = −0.1795, Y = −0.4322
Foil T.E. Tangency Pt. Suction X = 0.7121, Y = 0.3156
Foil T.E. Tangency Pt. Pressure X = 0.6937, Y = 0.3233

Foil Nose Point X = −0.2143, Y = −0.4451
Foil Tail Point X = 0.7065, Y = 0.3281

Foil Area = 0.1438

Gaging LAMBDA = 0.3459, X = 0.4050, Y = −0.3849
Gaging Angle = 22.630

Center of Gravity X = 0.2813, Y = −0.3210
Radial Reference X = 0.4301, Y = −0.3316

Inlet Angle = 62.900, DELTA BETA 1 = 10.000
Exit Angle = 22.570, DELTA BETA 2 = 7.500
Uncovered Turning = 14.5[illegible]

Min. Moment of Inertia = 0.00095658
Max. Moment of Inertia = 0.01280395

Principal Axis Angle = −44.549

Pitch/Axial Chord = 0.9665
Pitch/Actual Chord = 0.7476

TABLE XX

RECONTOURED SECOND VANE

Radius of HH Section = 11.4100 Axial Chord = 0.9291 Actual Chord = 1.2031
Pitch = 0.8961 No. of Foils = 80.00

Percent X	Foil X	Foil Y Suction	Foil Y (Circle)	Foil Y Pressure	Foil Y (Circle)
0.0	−0.2154	−0.4778	−0.4628	−0.4221	−0.4628
0.01	−0.2061	−0.4835	−0.4835	−0.4235	−0.4422
0.02	−0.1968	−0.4898	−0.4898	−0.4284	−0.4368
0.03	−0.1875	−0.4957	−0.4957	−0.4323	−0.4353
0.04	−0.1783	−0.5015	−0.5015	−0.4370	−0.4370
0.05	−0.1690	−0.5072	−0.5072	−0.4406	−0.4406
0.10	−0.1225	−0.5337	−0.5337	−0.4547	−0.4547
0.15	−0.0761	−0.5568	−0.5568	−0.4625	−0.4625
0.20	−0.0296	−0.5758	−0.5758	−0.4638	−0.4638
0.25	0.0169	−0.5901	−0.5901	−0.4587	−0.4587
0.30	0.0633	−0.5988	−0.5988	−0.4472	−0.4472
0.35	0.1098	−0.6009	−0.6009	−0.4293	−0.4293
0.40	0.1562	−0.5952	−0.5952	−0.4050	−0.4050
0.45	0.2027	−0.5806	−0.5806	−0.3743	−0.3743
0.50	0.2491	−0.5559	−0.5559	−0.3372	−0.3372
0.55	0.2956	−0.5199	−0.5199	−0.2938	−0.2938
0.60	0.3421	−0.4720	−0.4720	−0.2440	−0.2440
0.65	0.3885	−0.4117	−0.4117	−0.1882	−0.1882
0.70	0.4350	−0.3393	−0.3393	−0.1264	−0.1264
0.75	0.4814	−0.2553	−0.2553	−0.0589	−0.0589
0.80	0.5279	−0.1603	−0.1603	0.0143	0.0143
0.85	0.5743	−0.0552	−0.0552	0.0928	0.0928
0.90	0.6208	0.0595	0.0595	0.1766	0.1766
0.95	0.6673	0.1829	0.1829	0.2655	0.2655
0.98	0.6951	0.2608	0.2608	0.3212	0.3211
0.99	0.7044	0.2874	0.2874	0.3420	0.3260
1.00	0.7137	0.3143	0.3160	0.3590	0.3160

Foil L.E. Circle X = −0.1879, Y = −0.4628, R = 0.0276
Foil T.E. Circle X = 0.7037, Y = 0.3160, R = 0.0100

Foil L.E. Tangency Pt. Suction X = −0.2028, Y = −0.4860
Foil L.E. Tangency Pt. Pressure X = −0.1776, Y = −0.4372
Foil T.E. Tangency Pt. Suction X = 0.7132, Y = 0.3128
Foil T.E. Tangency Pt. Pressure X = 0.6947, Y = 0.3204

Foil Nose Point X = −0.2124, Y = −0.4502
Foil Tail Point X = 0.7076, Y = 0.3252

Foil Area = 0.1423

Gaging LAMBDA = 0.3455, X = 0.4061, Y = −0.3857
Gaging Angle = 22.676

Center of Gravity X = 0.2801, Y = −0.3265
Radial Reference X = 0.4301, Y = −0.3316

Inlet Angle = 62.722, DELTA BETA 1 = 11.047
Exit Angle = 22.616, DELTA BETA 2 = 7.249
Uncovered Turning = 14.210

Min. Moment of Inertia = 0.00094165
Max. Moment of Inertia = 0.01275547

Principal Axis Angle = −44.566

Pitch/Axial Chord = 0.9645
Pitch/Actual Chord = 0.7448

(The reverse of this page is blank)

REFERENCES

1. H. Welna, D. E. Dahlberg and W. H. Heiser; (Unclassified title) Investigation of a Highly Loaded Two-Stage Fan-Drive Turbine; Technical Report, AFAPL-TR-69-92 Volume 1; Pratt & Whitney Aircraft Division of United Aircraft Corporation; June 1968; Confidential.

2. H. Welna, D. E. Dahlberg and W. H. Heiser; (Unclassified title) Investigation of a Highly Loaded Two-Stage Fan-Drive Turbine; Technical Report AFAPL-TR-69-92 Volume 2; Pratt & Whitney Aircraft Division of United Aircraft Corporation; December 1968; Confidential.

3. H. Welna, D. E. Dahlberg and W. H. Heiser; (Unclassified title) Investigation of a Highly Loaded Two-Stage Fan-Drive Turbine; Technical Report AFAPL-TR-69-92 Volume 3; Pratt & Whitney Aircraft Division of United Aircraft Corporation; June 1969; Confidential.

Unclassified
Security Classification

DOCUMENT CONTROL DATA - R & D

(Security classification of title, body of abstract and indexing annotation must be entered when the overall report is classified)

1. ORIGINATING ACTIVITY (Corporate author)
Pratt & Whitney Aircraft Division
United Aircraft Corporation
East Hartford, Conn. 06108

2a. REPORT SECURITY CLASSIFICATION
[redacted] UNCLASSIFIED

2b. GROUP

3. REPORT TITLE

(U) Investigation of a highly loaded two-stage fan-drive turbine.
Volume IV. Phase II, End Wall Boundary Layer Control Evaluation

4. DESCRIPTIVE NOTES (Type of report and inclusive dates)
Technical Report (July 1, 1969 – December 31, 1969)

5. AUTHOR(S) (First name, middle initial, last name)

Welna, Henry; Dahlberg, Donald E.; Heiser, William H.

6. REPORT DATE	7a. TOTAL NO. OF PAGES	7b. NO. OF REFS
December, 1969	183	3

8a. CONTRACT OR GRANT NO.	9a. ORIGINATOR'S REPORT NUMBER(S)
F33615-68-C-1208	PWA 3827
b. PROJECT NO. 3066	
c. Task No. 306606	9b. OTHER REPORT NO(S) (Any other numbers that may be assigned this report)
d.	AFAPL-TR-69-92, Volume IV

10. DISTRIBUTION STATEMENT

Approved for public release; distribution unlimited

11. SUPPLEMENTARY NOTES	12. SPONSORING MILITARY ACTIVITY
	Air Force Aero Propulsion Laboratory Wright-Patterson AFB, Ohio 45433

13. ABSTRACT

(U) A comprehensive, four-phase, three-year program is in progress to investigate methods of improving the performance of fan-drive turbines. The goals of this program are to develop turbine design procedures and aerodynamic techniques for high work, efficient, low-pressure turbines. The first phase effort of defining the preliminary turbine design has been completed and the results were reported (Reference 1). The second phase consists of an experimental evaluation which includes e tab-lishment of both two-dimensional loss levels and three-dimensional flow behavior for the baseline airfoils and for airfoil utilizing various boundary laye, control methods. The design of the baseline cascade packs was reported in the Referen e 2 Report, and the three-dimensic nal performance of the baseline airfoils was reported in the Reference 3 Report. The test results of the baseline airfoil bo.ndary layer control methods and the performance of the decreased solidity annular cas ades are presented in this report.

DD FORM 1 NOV 1473 REPLACES DD FORM 1473, 1 JAN 64, WHICH IS OBSOLETE FOR ARMY USE.

Unclassified
Security Classification

14. KEY WORDS	LINK A		LINK B		LINK C	
	ROLE	WT	ROLE	WT	ROLE	WT
Turbine Aerodynamic Design						
Boundary Layer Control Survey						

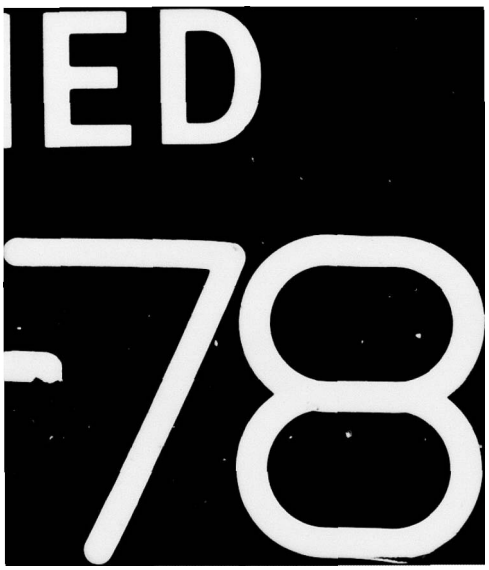
ED
78